September 2012

Relationship between DNA Damage Response and Telomere Maintenance

A thesis submitted for the degree of doctorate of philosophy

By

Maryam Ojani

Division of Biosciences

School of Health Sciences and Social Care

Brunel UNIVERSITY LONDON

Declaration

I hereby declare that the research presented in this thesis is my own work, except where otherwise specified, and has not been submitted for any other degree.

Maryam Ojani

Abstract

Telomeres are regions of repetitive DNA bound with a set of specialized proteins required to protect chromosomes from fusing with each other and from eliciting DNA damage response. Dysfunctional telomere maintenance can lead to premature cellular senescence, premature organismal aging and cancer predisposition.

In the last few years the evidence has emerged indicating a link between dysfunctional maintenance of telomeres and defective DNA damage response.

The objective of this project was to explore further this link by examining effects of some DNA damage response proteins on telomeres that have not been examined before and examining DNA damage response in cells in which telomeres are dysfunctional as a result of alterations in genes not directly involved in DNA damage response.

We have developed a method, termed IQ-FISH, for accurate identification of average telomere length in interphase cells from individuals with defective DNA damage response. By applying IQ-FISH we could successfully measure telomere lengths in cell lines from patients that are heterozygous (+/-) and cell lines from patients or animals that are homozygous (-/-) with respect to mutations in these genes.

We then analysed telomere length and function, as well as DNA damage response, in lymphoblastoid cell lines originating from *BRCA1* and *BRCA2* carriers (+/-) and also a single fibroblast cell line from a patient with bi-allelic mutations in *BRCA2* (-/-). In addition we have analysed a mouse embryonic stem cell line in which *Brca1* was deleted (*Brca1-/-*) by gene targeting. Our results show lack of correlation between DNA damage response and telomere

maintenance in heterozygous cell lines (with the exception of one BRCA1+/- cell line) but a clear positive correlation in the case of cell lines with homozygous mutations.

Finally, as a model for telomere dysfunction we have chosen cell lines from Dyskeratosis Congenita (DC) patients. DC is a rare progressive congenital disorder which results in premature aging. DC is primarily a disorder of dysfunctional telomere maintenance and we used cell lines from patients with mutations in *DKC1,* a gene encoding a protein termed Dyskerin which forms a part of the telomerase enzyme complex. Our results indicate that DC cells with dysfunctional *DKC1* may have a dysfunctional DNA damage response.

Publications

1. Joksic, I., D. Vujic, M. Guc-Scekic, A. Leskovac, S. Petrovic, M. Ojani, J. P. Trujillo, J. Surralles, M. Zivkovic, A. Stankovic, P. Slijepcevic and G. Joksic (2012). "Dysfunctional telomeres in primary cells from Fanconi anaemia FANCD2 patients." Genome Integr 3(1): 6.

Acknowledgments

Foremost, I would like to express my deep and sincere gratitude to my supervisor, Dr. Predrag Slijepcevic for accepting me as his student. His immense knowledge, patience, motivation, enthusiasm and logical way of thinking have been of great value for me. He has always been extremely supportive and has provided me with critical help and guidance throughout the last 4 years.

My deepest gratitude to Dr. Christopher Parris who offered guidance, help and encouragement with his positive thinking and great sense of humour and his invaluable assistance.

I would also like to express special thanks to Dr. Sahar Al-Mahdawi, Dr. Chiranjeevi Sandi and Dr. Hemad Yasaei for their expert advice and those little skills that have made a huge difference in my research.

Additionally, a very big “thank you” must go to my colleagues Yaghoub, Chetana and Parisa for creating such a lively and always cooperative atmosphere and be there for me whenever I needed.

I must say a special thanks to my lovely friends Hiba, Vahid, Sheba, Punam, Azadeh and Gonul who helped me get through the PhD. You have all been great friends.

I would also like to thank my family for their perpetual love and support especially my amazing husband, Mehdi, whose love, support and encouragement was like a scaffold that supported me throughout my entire PhD. Without you, I would have not been able to complete this work. For those reasons and more I dedicate this thesis to my wonderful husband Mehdi Taheri.

Table of Contents

List of Figures

List of Tables

Abbreviations

ALT	Alternative lengthening of telomeres
APB	ALT Promyelocytic leukemia Bodies
APS	Ammonium persulphate
ATM	Ataxia telangastia mutated protein
ATR	ATM-and Rad3-related proteins
BCA	Bicinchoninic acid
BER	Base excision repair
Bp	Base pair
BRCA1	Breast Cancer susceptibility gene 1
BRCA2	Breast Cancer 2 susceptibility protein
BRCT	BRCA1 C-terminal
BSA	Bovine Serum Albumin
CCFL	Corrected Calibrated Fluorescence
cDNA	Complementary DNA
CF	Correction Factor
COD-FISH	Chromosome Orientation and Direction FISH
CO-FISH	Chromosome Orientation Fluorescence in *situ* Hybridization
DDR	DNA damage response
DKC	Dyskeratosis Congenita
DMEM	Dulbecco modified eagle medium
DMSO	Dimethylsulfoxide
DNA-PKcs	DNA-protein kinase catalytic-subunit
dNTP	Deoxynucleotide triphosphate
DSB	Double strand breaks
DTT	Dithiothreitol
DW	Distilled water
ECL	Enhanced chemiluminescence
EDTA	Ethylene diamine-tetra acetic acid
ES	Embryonic stem cells
FA	Fanconi Anemia
FBS	Fetal bovine serum
FCS	Fetal calf serum
FISH	Fluorescence in-*situ* hybridization
FITC	Fluorescein isothiocynate
gDNA	Genomic DNA
Gy	Gray
HR	Homologous recombination
HRP	Horseradish peroxidise
IPA	Isopropyl alcohol
IQ-FISH	Interphase Q-Fish
IR	Ionising Radiation
Kb	Kilobase
KCL	Potassium Chloride
kDa	Kilo Dalton
LOF	Loss of function

LY-R	Radioresistant mouse lymphoma cells
LY-S	Radio-sensitive mouse lymphoma cells
MgCl2	Magnesium chloride
miRNA	MicroRNA
ml	Mililiter
MMEJ	Microhomology-mediated end joining
MRN	MRE11/RAD50/NSB1
NER	Nucleotide Excision Repair
NHEJ	Non-homologous end joining
PAR	Poly ADP-ribose
PBS	Phosphate buffer saline
PCR	Polymerase chain reaction
piRNA	Piwi-interacting RNA
PNA	Peptide nucleic acid
POT1	Protection of telomeres 1
PVDF	Polyvinylidene fluoride
Q-FISH	Quantitative in-situ hybridization
RNA	Ribonucleic acid
RNAi	Ribonucleic acid interference
RPA	Replication protein A
RPM	Rotations per minute
RPMI	Roswell Park Memorial Institute
RS-SCID	Radio sensitive severe combined immunodeficiency
RT	Room Temperature
RT-PCR	Reverse transcriptase-polymerase chain reaction
SCID	Severe-combined immunodeficiency syndrome
SDS	Sodium dodecyl sulphate
siRNA	Short interfering ribonucleic acid
ss	Single stranded
SSB	Single strand breaks
SSC	Sodium chloride sodium citric acid
ssDNA	Single stranded DNA
T	Thymine
TBE	Tris-borate-EDTA
TBST	Tris-buffered saline tween-20
TEMED	Tetramethylethylenediamine
TERT	Telomerase Reverse Transcriptase
TFUs	Telomere fluorescence units
TIF	Telomere dysfunction induced foci
TIN2	TRF1-interacting factor
T-loop	Telomeric-loop
TRF1	Telomeric repeat binding factor 1
TRF2	Telomeric repeat binding factor 2
T-SCEs	telomere Sister Chromatid Exchanges
UV	Ultra violet
H2AX	Histone H2AX phosphorylated on serine-139
µl	Microlitre

Chapter 1 - General Introduction

1.1 - DNA damage: Introduction

Mammalian cells are constantly exposed to a range of agents that cause damage to the genetic material – the DNA molecule. These agents vary from cell's own metabolic products to external agents including various types of radiation and chemicals. As a result of constant exposure to these agents, cells have developed numerous mechanisms to deal with the resulting DNA damage. The current understanding of some of these mechanisms will be outlined below. Furthermore, the interplay between these mechanisms and telomeres, specialized structures at chromosome ends, will be examined. A human disease, Dyskeratosis congenita (DC), will be used as a model to probe the above interplay.

As a result of normal metabolic processes and environmental factors, DNA damage occurs at a rate of 1,000 to 1,000,000 molecular lesions per cell each day (Hoeijmakers 2001). Although this amounts to 0.000165% of the human genome, unrepaired lesions in critical genes (e.g. tumour suppressor genes) could impede a cell's ability to carry out its function and also appreciably increase the likelihood of tumour formation.

There are two ways in which the primary structure of the DNA double helix is affected: a) chemical modification of DNA bases and b) induction of single strand breaks (SSB) or double strand breaks (DSB) in DNA. As these changes occur and repair takes place, the regular DNA structure can be changed by the appearance of non-native chemical bonds that do not fit in the standard size DNA double helix.

Because DNA normally lacks tertiary structure, unlike RNA and proteins, DNA damage cannot affect the tertiary level of DNA organization. However, DNA is super coiled

by histone proteins that package it into chromatin. It is clear that chromatin itself is also vulnerable to the effect of DNA damage (Kimura and Suzuki 2009).

1.1.1 - Source of DNA damage

DNA damage could be separated into two main types. First type is the so called endogenous DNA damage caused by reactive oxygen species resulting from normal metabolic byproducts including products of oxidative deamination. This type of damage also includes replication errors. Second type of DNA damage is caused by external agents, including:

- Ultraviolet [UV 200-300nm] radiation from the sun (Becker and Wang 1989)
- Ionizing radiation (IR) including X and gamma rays (Ward 2000)
- Certain plant toxins (Britt 1996)
- Human-made mutagenic chemicals, in particular aromatic compounds act as DNA intercalating agents (Roulston *et al.* 1999)
- Cancer chemotherapeutic agents (Kim *et al.* 2000)
- Viruses (Roulston *et al.* 1999)

The duplication of damaged DNA in the S-phase of the cell cycle could lead to incorporation of wrong bases opposite damaged ones. These wrong bases are source of mutations and cells do not have the means of removing mutations once they pass through DNA replication process (McGlynn and Lloyd 2002).

1.1.2 - Types of DNA damage

Several forms of DNA damage are caused by endogenous cellular processes. These include:

- Alkylation of bases such as formation of 7-methylguanine, 1-methyladenine and O 6-methylguanine (De Bont and van Larebeke 2004).
- Oxidation of bases and generation of DNA strand interruptions from reactive oxygen species (DNA breaks) (De Bont and van Larebeke 2004).
- Hydrolysis of bases, such as deamination, depurination and depyrimidination.
- Bulky adduct formation (De Bont and van Larebeke 2004).
- Mismatch of bases because of errors in DNA replication where the wrong DNA base is placed in a newly forming DNA strand, or a DNA base is bypassed or mistakenly inserted (De Bont and van Larebeke 2004).

DNA damage occurring as a result of cell exposure to exogenous agents has various forms. Below are some examples:

- UV-B light causes crosslinking between adjacent cytosine and thymine bases creating pyrimidine dimers which is referred to as direct DNA damage (Crespan *et al.* 2010).
- UV-A light creates mostly free radicals. Damages in DNA which are caused by free radicals, is called indirect DNA damage (De Bont and van Larebeke 2004).
- IR causes breaks in DNA strands including SSB and DSB (Ward 1988).
- Thermal disruption at elevated temperature increases the rate of depurination (loss of purine bases from the DNA backbone) and SSB. For example, hydrolytic depurination is seen in the thermophilic bacteria, which grow in hot springs at 85–250 °C (Ohta *et al.*

2006). The rate of depurination (300 purine residues per genome per generation) is too high in these species to be repaired by normal repair processes; hence a possibility of an adaptive response cannot be ruled out.

- Industrial chemicals, vinyl chloride and hydrogen peroxide and environmental chemicals, polycyclic hydrocarbons are found in smoke, soot and tar. This creates a huge diversity of DNA adducts- ethenobases, oxidized bases, alkylated phosphotriesters and cross linking of DNA just to name a few (Brooks 1997).

1.1.3 - Response to DNA damage

Cells exposed to external agents such as IR, UV light or chemicals will suffer various types of DNA damage (Figure 1.1) immediately after the exposure. It is also likely that other biomolecules such as carbohydrates, lipids, RNA and proteins will be damaged. Accumulation of damage in DNA, in particular DSBs or adducts that stall the replication fork, will cause activation of a series of molecular processes in the cell collectively known as DNA damage response (DDR)(Lord and Ashworth 2012).

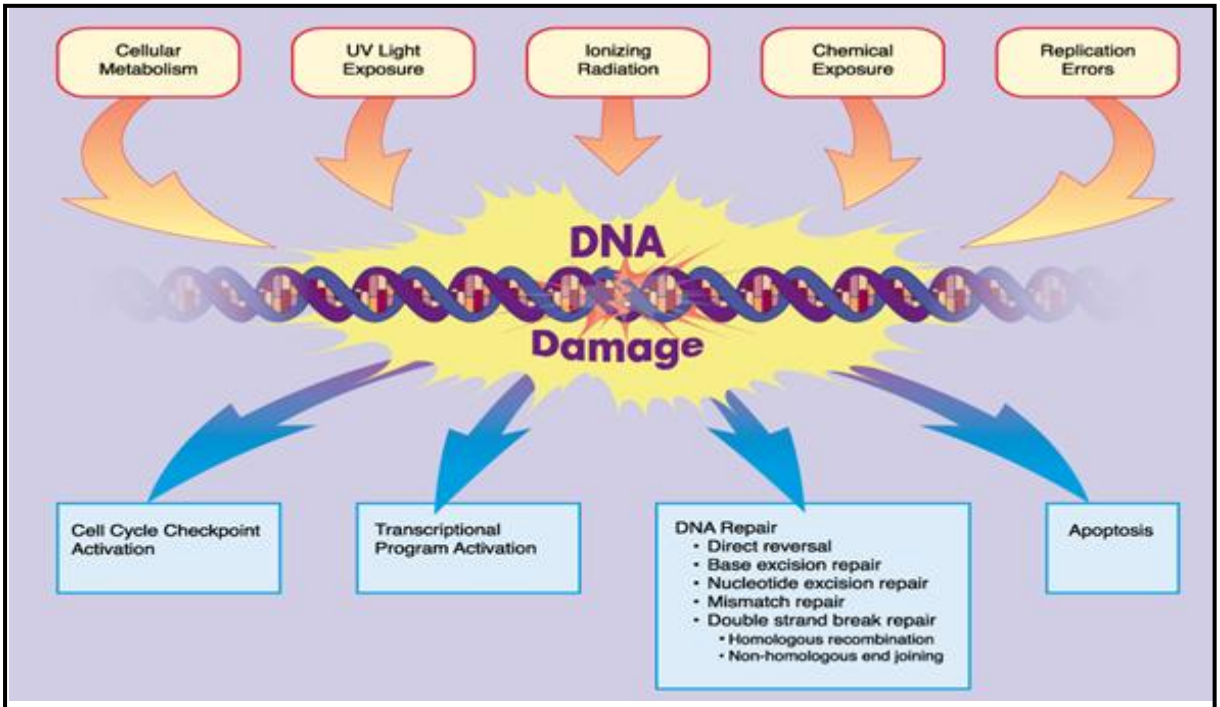

Figure 1.1 - An outline of cellular response to DNA Damage according to (Friedberg *et al.* 1995).

DDR is a process aimed towards the cells own protection and triggers multiple pathways of macromolecular repair. A regular effect of DDR is induction of cell cycle arrest and cell cycle checkpoints the function of which are to allow DNA repair to take place before DNA replication. If repair fails, in particular as a result of high level of DNA damage that a cell cannot cope with, it may be more economical for an organism to eliminate such a cell or cells by a process known as apoptosis (Enoch and Norbury 1995).

1.1.4 - DNA damage checkpoints and DNA repair mechanisms

Cell cycle checkpoints are activated as a result of DDR (Figure 1.2). The cell cycle is paused and this allows the cells to repair DNA damage before the S-phase in which DNA replicates. G1/S and G2/M are the cell cycle boundaries in which DNA damage checkpoints take place. An intra-S checkpoint also exists. Checkpoint activation is controlled by two

master kinases, ATM (Ataxia Telangiectasia Mutated) and ATR (ATM-and Rad3-related proteins). ATM responds to DNA DSB and disruptions in chromatin structure (Bakkenist and Kastan 2003) whereas ATR primarily responds to stalled replication forks (Lopes *et al.* 2001)

These kinases phosphorylate downstream targets in the signal transduction cascade, eventually leading to cell cycle arrest. These include checkpoint mediator proteins such as BRCA1, MDC1, and 53BP1 (Yoo *et al.* 2006). These proteins are required for transmitting the checkpoint activation signal to downstream proteins. P53 is an important downstream target of ATM and ATR, as it is necessary for inducing apoptosis (Roos and Kaina 2006). At the G1/S checkpoint, p53 functions by deactivating the CDK2/cyclin E complex. Similarly, p21 mediates the G2/M checkpoint by deactivating the CDK1/cyclin B complex (Mikule *et al.* 2007). As soon as DNA damage checkpoints are induced this will lead to activation of DNA repair processes. Each DNA lesion is repaired by a different mechanism. For example, when cells are exposed to IR a large number of DNA DSB will be induced and these are repaired by two mechanisms: Non-Homologous End Joining (NHEJ) and Homologous Recombination (HR) (Takata *et al.* 1998)**.** UV induced lesions are usually repaired by Nucleotide Excision Repair (NER)(Wood 1997).

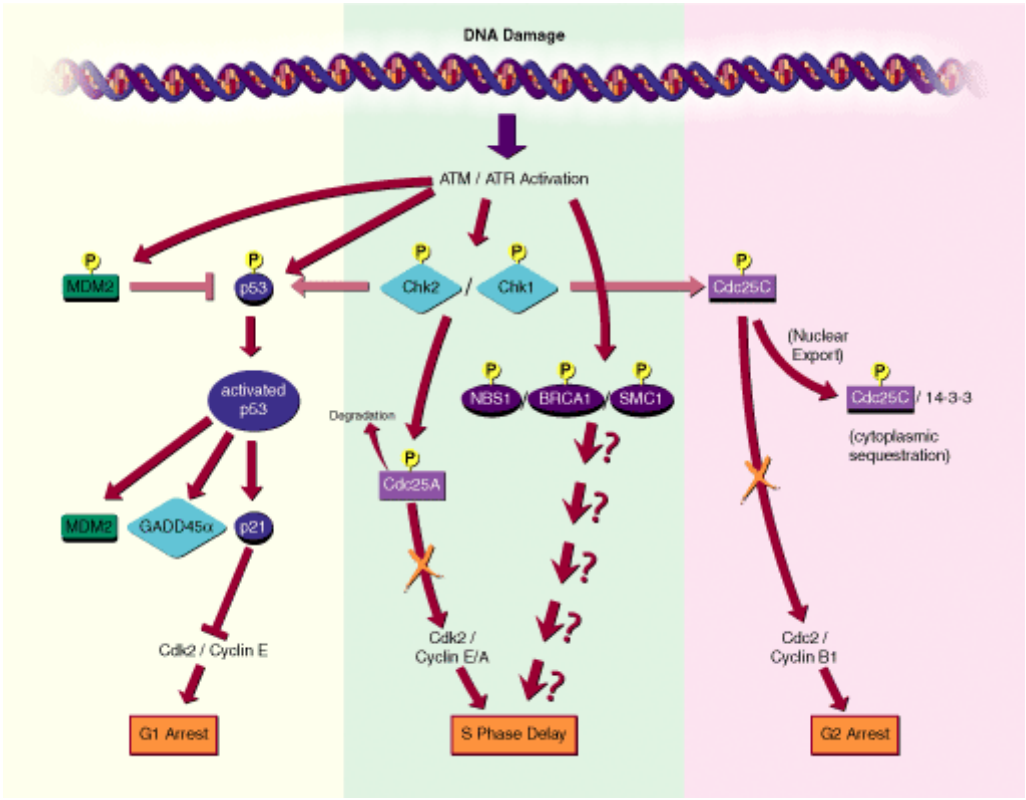

Figure 1.2 - Mammalian Cell Cycle Checkpoint Pathways (Bartek and Lukas 2001).

1.1.5 - DNA repair and cancer

Genetically normal cells or individuals have effective DNA repair mechanisms, which eventually eliminate almost all damage from DNA. However, some people are born with mutations that affect DNA repair mechanisms and these people have high cancer risk. For example, people born with mutations in NHEJ genes are sensitive to IR and have high risk of suffering from leukaemia and solid tumours. There are two well characterized human diseases resulting from mutations in NHEJ genes: Ligase 4 syndrome and RS-SCID (radio sensitive severe combined immunodeficiency) (O'Driscoll *et al.* 2004).

Ligase 4 patients are born with mutations in the gene encoding the Ligase 4, an enzyme that rejoins broken DNA ends. RS-SCID patients have mutations in the gene

encoding Artemis protein which has endonucleolytic activity required for NHEJ (Noordzij *et al.* 2003).

Other examples of mutations in DNA repair genes that predispose to cancer include *BRCA1* and *BRCA2*. These two well-characterized genes, if mutant, confer a significant risk of breast cancer on carriers. Both genes are involved in the repair of DNA DSBs through HR (O'Donovan and Livingston 2010)

1.1.6 - NHEJ pathway

Most DSBs in eukaryotic cells are repaired through either NHEJ or HR. Recent findings indicate a third, less characterized repair mechanism named microhomology-mediated end joining (MMEJ) as another DNA DSB repair pathway (McVey and Lee 2008). HR occurs in late S-G2 phases, while NHEJ takes place throughout the cell cycle, but mainly in the G1 phase (O'Driscoll and Jeggo 2006). Core proteins involved in the NHEJ process include Ku dimers (Ku70-Ku80), DNA-PKcs, XRCC4, Ligase IV, Artemis, and recently discovered cernunnos-XLF (Ahnesorg *et al.* 2006; Buck *et al.* 2006). The Ku complex (Ku70/Ku80) is involved in the initial detection of DNA DSBs due to its high affinity for DNA ends. Attachment of the Ku heterodimmer to the site of DSB attracts DNA-PKcs, a serine/threonine protein kinase. The regulatory Ku70/80/DNA-PKcs complex acts as a DNA damage sensor. A purified Artemis protein has been shown to possess single-stranded 5' to 3'exonuclease activity**.** Artemis is phosphorylated by DNA-PKcs and this induces endonucleotytic activity on 5' and 3' overhangs as well as hairpins (Ma *et al.* 2002). Artemis provides an essential nucleolytic processing activity to prepare DNA ends for re-ligation (Sekiguchi and Ferguson 2006). When ends of the DNA are secured, XRCC4 and Ligase IV seal the break, although another protein complex such as MRE11/RAD50/NSB1 (MRN complex) may be needed for further

processing of the DNA ends before re-ligation. The recently discovered member of NHEJ protein family, Cernunnos-XLF, is understood to play a role in DSB end joining alongside XRCC4 and Ligase IV. The precise role of this new protein is unknown, but Ahnesorg et al (2006) suggested that Cernunnos-XLF might serve as a bridge between XRCC4 and Ligase IV and the other NHEJ factors to facilitate the recruitment of the other factors to the ends of DSB. Alternatively, it might be involved in the regulation of XRCC4-Ligase IV activity via the modulation of active and inactive multimeric states of XRCC4 (Sekiguchi and Ferguson 2006). Interestingly, some of the NHEJ factors are revealed to be involved in telomere maintenance. For example, Ku70, Ku80 and DNA-PKcs associate with telomeric DNA in several human cell types (d'Adda di Fagagna *et al.* 2001). Similar results were seen in mice deficient in Ku86 with increased chromosome end-to-end fusion with strong telomeric signals at point of fusion thus demonstrating important role of Ku86 (Ku86 is the same as Ku80) in telomere end capping in mouse (Samper *et al.* 2000; Espejel and Blasco 2002; Espejel *et al.* 2002). Equally, DNA-PKcs (catalytic subunit of DNA-PK) was shown to be critical in protecting mammalian telomeres (Bailey and Goodwin 2004) and that inhibition of DNA-PKcs leads to increased levels of chromatid fusions (Bailey *et al.* 2001; Bailey and Goodwin 2004). Similar outcomes were observed in DNA-PKcs deficient mice (known as SCID mice) with increased levels of telomere fusions indicative of telomere dysfunction through loss of telomere end capping (rather than telomere shortening since it has been shown that SCID mouse cells have abnormally long telomeres (Hande *et al.* 1999; Samper *et al.* 2000; Goytisolo *et al.* 2001).

1.1.7 - HR

HR is a different form of the DSB repair operating mostly in late S and G2 phases of a cell cycle. HR is a preferred mechanism for DSB repair in simple eukaryotes such as yeast. HR is a great deal more precise than NHEJ, in terms of the original DNA sequence restoration, since it makes use of a sister chromatid as a template in rejoining DSBs. HR is primarily responsible for repairing DSBs that arise as a result of replication fork stalling (in the late S phase) and the HR pathway involves nucleolytic processing, strand invasion, Holliday junction formation, and branch migration.

The proteins involved in HR pathway are: RAD51, RAD52, RPA, CTIP, BRCA1, BRCA2 XRCC2, XRCC3, RAD54, DNA polymerases, DNA ligases etc. The HR repair follows two pathways. A RAD51-dependent pathway, which is an error free and RAD51-independent pathway, which is prone to errors in the DNA sequence (Griffin and Thacker 2004). The RAD51-dependent pathway involves a homology search and strand invasion to allow the restoration of the original DNA sequence based on the undamaged homologous sequence.

The RAD52 protein recognizes the broken DNA ends and processes the DNA into a 3’ single strand by nuecleolytic activities of the MRN complex. Then formations of a nucleoprotein filament onto the 3’ single strand DNA is carried out by RAD51 by polymerization and with the aid of a single strand DNA binding protein, replication protein A (RPA) and RAD52. The RAD51 nucleoprotein filament searches for homologous duplex DNA after which the DNA strand exchange generates a joint molecule between the homologous damaged and undamaged duplex. BRCA2 helps to load RAD51 onto the ssDNA molecule, whereas BRCA1 is required as a regulatory mechanism. After branch migration and holliday junction formation, DNA synthesis takes place where DNA polymerases and accessory

factors fill the gap and DNA Ligase IV, XRCC4 relegate the DSB. BRCA1 deficiency confers sensitivity to ionizing radiation as well as sensitivity to DNA cross-linking agents such as mitomycin C (Powell and Kachnic 2003). Also a BRCA1 deficient human lymphoblastoid cell line shows an elevated level of chromosome end-to-end fusion that suggests a role of BRCA1 in telomere capping (Al-Wahiby and Slijepcevic 2005).

1.1.8 - Senescence and apoptosis

As mentioned above, a high level of DNA damage in a cell can lead to DNA repair failure. In such cases tissues usually activate apoptotic pathway which eliminates cells that carry extensive amount of DNA damage. In addition to apoptosis, tissues use cell senescence mechanisms to eliminate undesired cells. Senescence is a phenomenon in which a cell is not able to divide any longer as a result of activated DNA damage response due to telomere shortening (Blackburn 2000). Telomeres are long regions of repetitive noncoding DNA which cap chromosomes and undergo partial degradation every time a cell divides (Braig and Schmitt 2006). In contrast, quiescence is a state of cellular dormancy which is not related to genome damage.

Cell senescence could serve as a functional alternative to apoptosis when physical presence of a cell, with activated DNA damage response, within a tissue causes a danger to the organism (Lynch 2006). This serves as a last resort to prevent a cell with damaged DNA from replicating in the absence of pro-growth cellular signalling. Formation of tumours as a result of unregulated cell growth could potentially have a lethal effect on the organism.

1.2 - Telomeres

Telomeres are regions of repetitive DNA bound with a set of specialized proteins required to protect chromosomes from fusing with each other. The name comes from Greek words “telos” meaning end and “meros” meaning part. The enzymes which copy DNA cannot carry out DNA replication at the end of chromosome due to the so called “end-replication problem”(Olovnikov 1971). As a result, a small portion of telomeric DNA will be lost after every cell division. Eventually, the loss will become so extensive that the 3D organization of telomeres will be affected and they will lose their function (Figure 1.3). Telomere loss serves as a mechanism that regulates cell senescence.

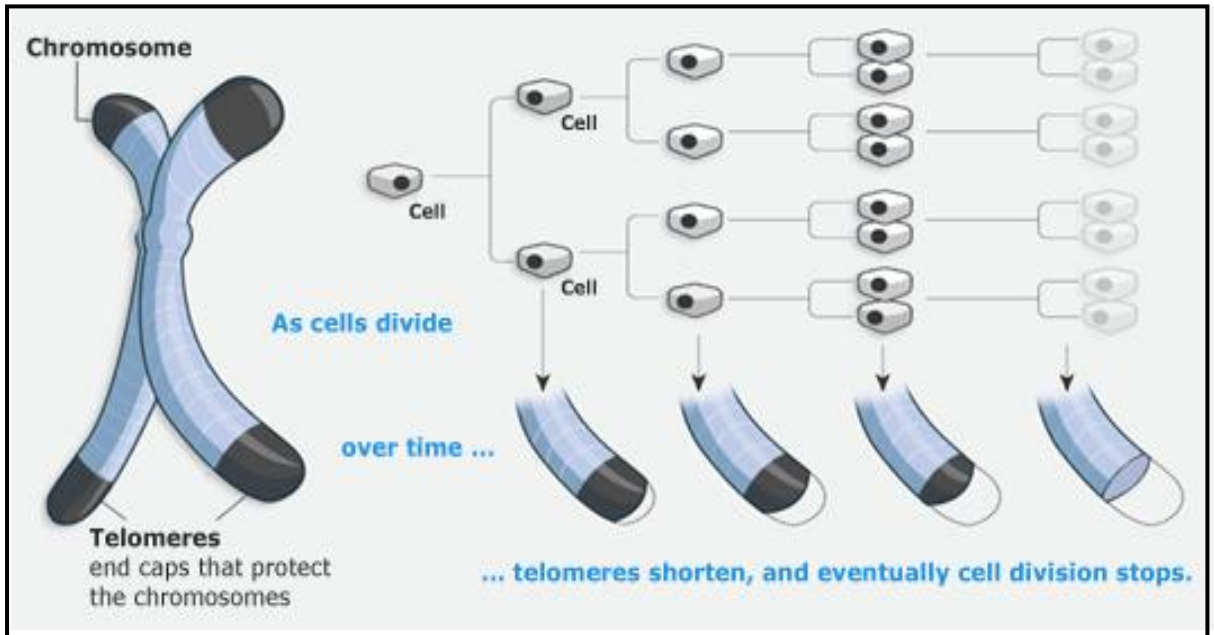

Figure 1.3 - Schematic model of telomeric loss (T.A.Sciences 2010-2012).

When telomeres become critically short this will activate DNA damage response and will cause block in cell proliferation or cell senescence (Satyanarayana *et al.* 2004). However,

a specialized enzyme called telomerase is capable of replicating chromosome ends. This enzyme is active in germ-line and stem cells but not in most somatic cells. Interestingly, a large majority of cancer cells have active telomerase and it has been conclusively demonstrated that telomerase activation gives cells the capacity to proliferate indefinitely (Piatyszek *et al.* 1995).

1.2.1 - Structure of telomeres

Telomeres are composed of repetitive DNA sequences positioned at the termini of linear chromosomes of the majority eukaryotic organisms and a few prokaryotes, bound with a set of specialized proteins. A small portion of bacterial chromosomes (such as those in Streptomyces and Borrelia) are linear and possess telomeres. These are very different from those of the eukaryotic chromosomes in structure and function (Thanbichler *et al.* 2005). Structure of bacterial telomeres take form of proteins bound to the ends of linear chromosomes, or hairpin loops of single-stranded DNA at the ends of the linear chromosomes (de Lange 2004). The length of Telomeres differs greatly amid species, from ~300-600 bp in yeast to many kilobases (Kb) in humans. The telomeric DNA sequence is usually comprised of arrays of 6-8 bp long G-rich repeats. In vertebrates the telomerec DNA repeat is (TTAGGG)n.

Eukaryotic telomeres normally terminate with a 3' ss (single stranded) DNA overhang which is essential for telomere maintenance and capping. Multiple proteins binding single- and double-stranded telomere DNA have been identified (Blackburn 2001). The DNA component of telomeres usually begins with a double-stranded region consisting of repeated sequences of five to nine base pairs, where the number of base pairs varies from species to species (Figure 1.4). It then ends with a single-stranded region rich in guanine (G)

and thymine (T) bases called a 3´ overhang that bends back on itself to facilitate a protective t-loop structure. (Figure 1.4) (Hohensinner *et al.* 2011).

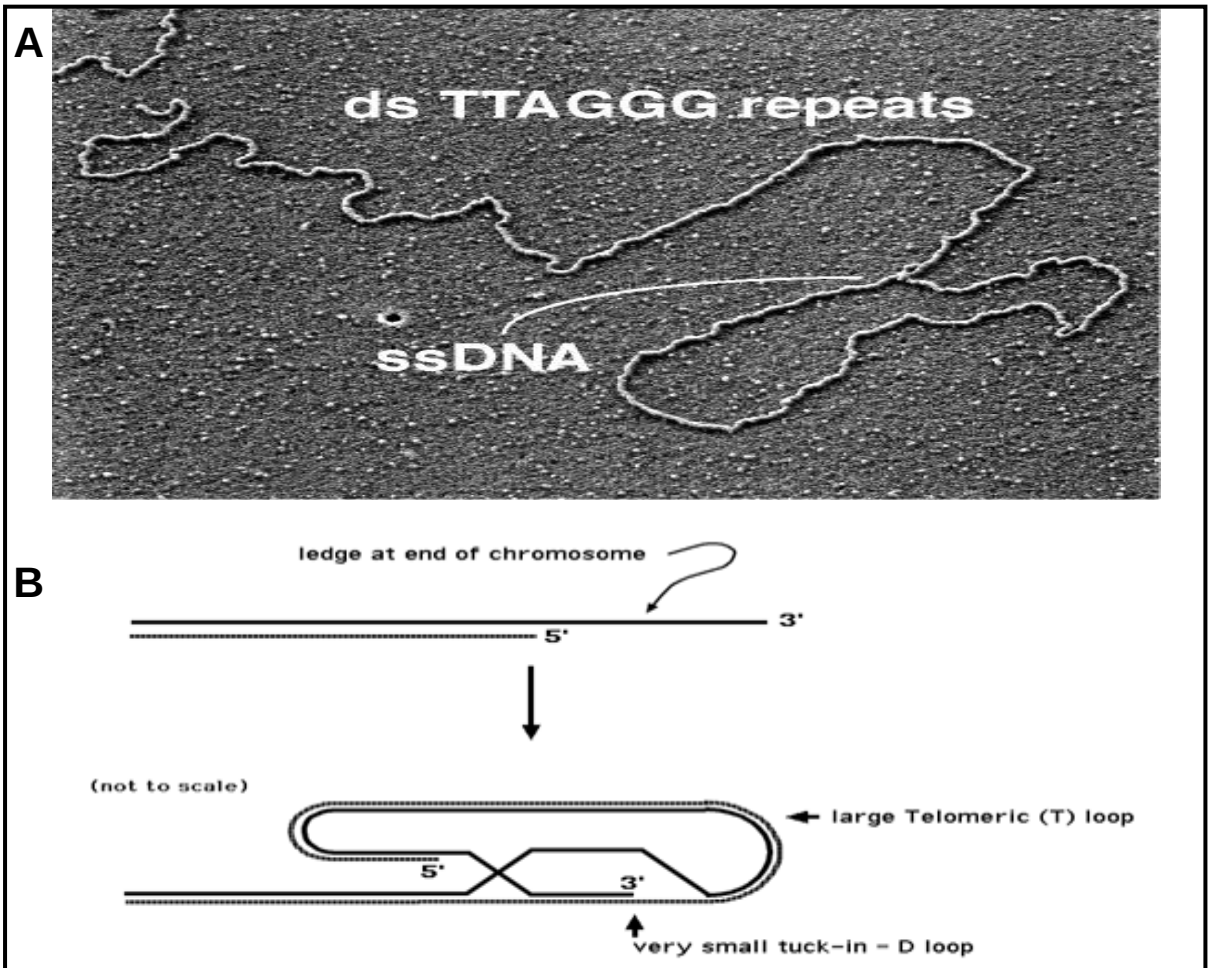

Figure 1.4 - Molecular structure of telomeres. (A) Electron micrograph of a T-loop. (B) A single stranded 3' overhang in linear form which bends on itself to form a T-loop. Images taken from (Greider 1999).

1.2.2 - Telomere proteins

At the very end of the chromosome a T-loop is formed by the action of a single-stranded portion of telomeric DNA and a set of associated proteins (see Figure 1.4). T-loop is

analogous to a 'knot' which stabilizes the telomere thus stopping the telomere ends from being recognized as DNA DSBs by the DNA repair machinery. The T-loop is held together by six known proteins including TRF1, TRF2, Rap1, POT1, TIN1, and TIN2, collectively referred to as the shelterin complex.

Cancer cells escape telomere loss by switching on a gene that expresses telomerase. Telomerase is an enzyme which adds TTAGGG repeats to telomeres in all vertebrates by targeting the 3' end of telomeric single strand. The enzyme is a reverse transcriptase which carries its own RNA template (Greider and Blackburn 1985).

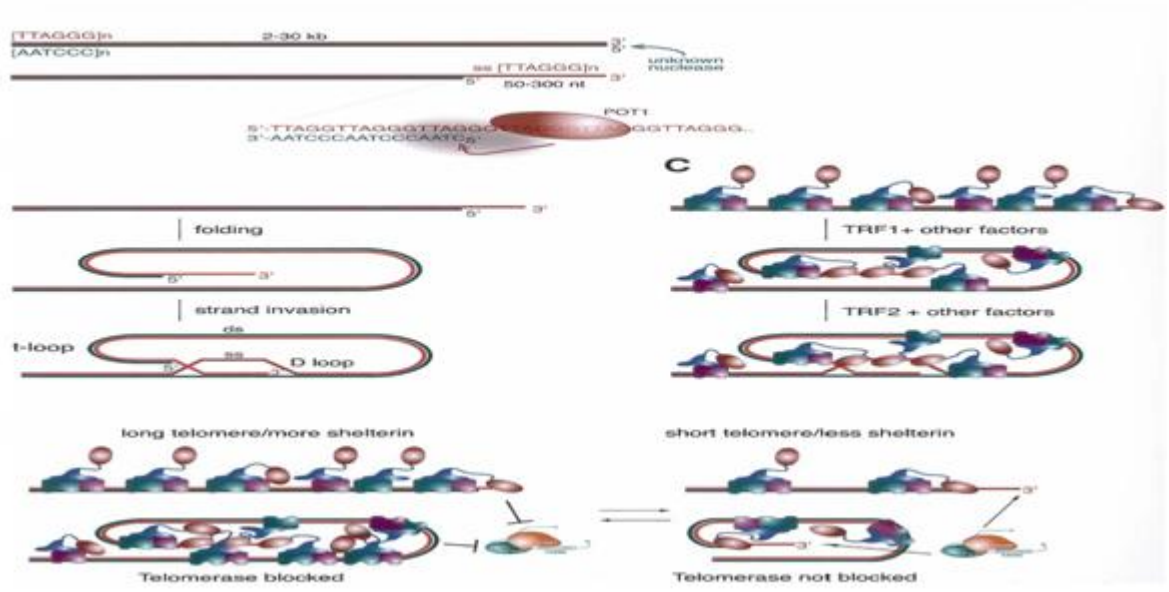

Figure 1.5 - Shelterin and telomerase(de Lange 2005). Telomerase and shelterin interact in the process of telomere length regulation.

Telomerase consists of several molecules including Telomerase Reverse Transcriptase (TERT), Telomerase RNA (hTR or TERC), dyskerin (DKC1) and some others (Cohen *et al.* 2007).

By using TERC, TERT can add a six-nucleotide repeating sequence, 5'-TTAGGG to the 3' telomeric overhang (Figure 1.5). The template region of TERC is 3'-CAAUCCCAAUC-5'. Telomerase usually binds the first few nucleotides of the template to the last telomere sequence on the chromosome, adds a new telomere repeat (5'-GGTTAG-3') sequence, detaches from the telomere, realigns the new 3'-end of telomere to the template. This process is repeated until a desirable length of telomere is achieved (Figure 1.5).

1.2.3 - Telomere function

Telomere length serves as an intrinsic biological clock regulating the life span of the cell. In this scenario, the numbers of underwent cell cycles are “counted” by the cell. This mechanism allows regulation of cell senescence. When telomeres became too short, thus reflecting high number of cell divisions, DDR becomes activated because short telomeres lose a proper T-loop structure and are detected as DNA DSBs by cellular DNA repair machinery (see Figure 1.6). Thus, one of telomere functions is to limit the capacity of a cell to replicate, by inducing senescence as a sort of a tumour-suppressing mechanism (Figure 1.6). It is important to note that induction of senescence is a complex process and a number of pathways are involved, including p53, p21, and the Rb/p16^{INK4A} cell-cycle checkpoint pathway (Reddel 2000).

Another important function of telomeres is to protect chromosome stability. Telomeres act as chromosome “capping” structures that prevent chromosome end-to-end fusions. A number of proteins are identified as important in this “capping” function including components of shelterin but also some proteins involved in DDR (for details see below).

1.2.4 - Telomere dysfunction

Dysfunctional telomeres cause severe clinical symptoms in affected individuals. A human disease Dyskeratosis Congenita is caused by mutations in telomerase genes, or genes encoding some of the shelterin proteins leading to telomere dysfunction (Vulliamy and Dokal 2008). The key consequence of dysfunctional telomeres in an organismal setting is that stem cells, which require telomerase, will not function properly. As a result highly proliferative tissues that depend on a high cell turnover, regulated by tissue specific stem cells, are regularly affected. For example, DC patients typically show bone marrow failure and skin abnormalities (Davidson and Connor 1988). Both failures result from inability of stem cells to replenish/regenerate highly proliferative tissues.

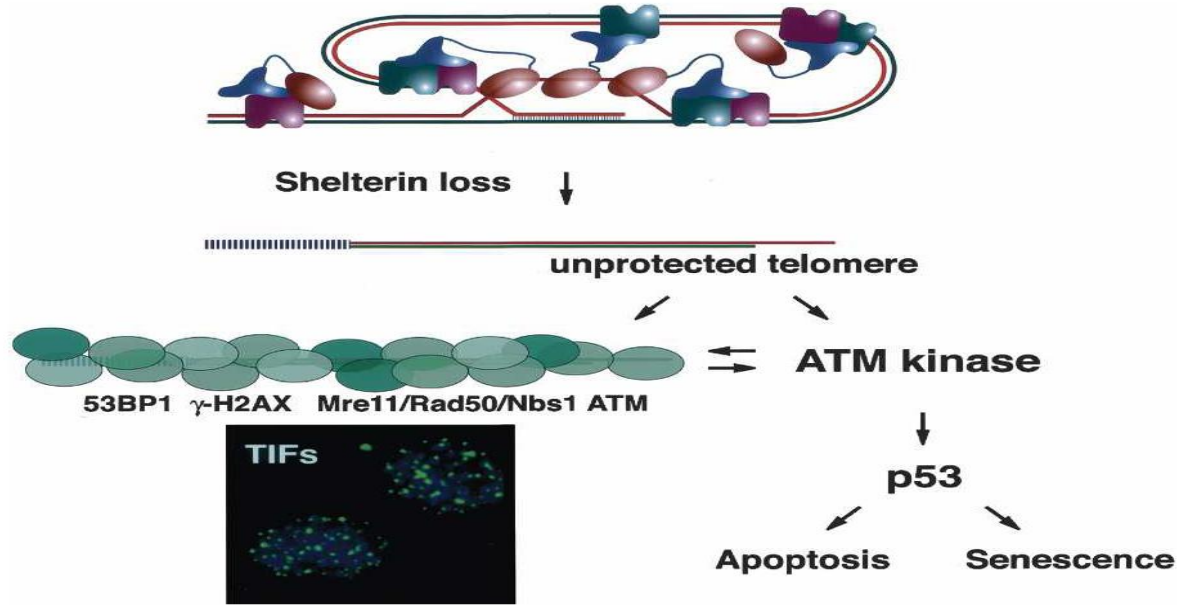

Figure 1.6 - Shelterin and telomere dysfunction (de Lange 2005).

1.3 - Relationship between telomere maintenance and DNA damage response mechanisms

In the life of a cell, DNA damage is common and a possibility exists for it to lead to mutations, cancer or even cellular or organismal death. As a result of DNA damage, a number of cellular responses occur collectively known as DDR (see above). DDR functions to allow the cell to manage and cope with DNA damage by activating appropriate repair processes or activating mechanisms that eliminate from tissues cells with extensive and potentially irreparable DNA damage.

Chromosomal stability is affected regularly by the failure of any component of DDR mechanisms. It should be noted that chromosomal stability is physiologically protected by telomeres as mentioned above. It is becoming increasingly clear that shelterin proteins interact with a number of proteins involved in DDR (Misri *et al.* 2008). Interactions between shelterin and DDR proteins are discussed in detail below.

Changes in a growing number of DDR proteins result in telomere dysfunction leading to chromosomal instability. This signifies extensive functional connections between telomere maintenance and DDR mechanisms. The most likely function of telomere-DDR mechanisms interactions is to enable cells to distinguish the natural chromosome ends from DSBs (Viscardi *et al.* 2007). This is probably achieved by interactions between shelterin proteins and two key NHEJ proteins: DNA-PKcs and Ku. They are normally found at telomeres associated with the shelterin component TRF2 (de Lange 2005). Therefore, telomeres can differentiate themselves from internal DSBs and by doing this they protect genomic stability. It is not surprising that telomeres which become critically short due to either physiological (cell senescence) or pathological (mutations in telomerase, shelterin or

DDR genes) reasons bring out extensive cellular responses including cell cycle checkpoint activation (Maser and DePinho 2004). In addition to the above two NHEJ proteins many more DDR proteins are connected with telomeres and contribute to several aspects of telomere metabolism. One of the first proteins to be associated with telomere dysfunction was ATM (Ju and Lenhard Rudolph 2008). ATM is the key DNA damage signaling molecule (Metcalfe *et al.* 1996). Human or mouse cells that lack functional ATM show accelerated telomere loss, telomeric fusions and appearance of extra chromosomal telomeric fragments (Hande *et al.* 2001) . The importance of ATM in telomere metabolism is illustrated by the observation that one of ATM phosphorylation targets is the shelterin component TRF2 (Demuth *et al.* 2008).

A recent review article focusing on the interplay between telomeres and DDR identified a total of 13 additional mammalian DDR proteins involved in telomere maintenance (Slijepcevic 2006). This includes the MRN protein complex which has been linked to DNA DSB repair. All three MRN components are encoded by essential genes and hypomorphic mutations in any of these genes can result in genome-instability syndromes (van den Bosch *et al.* 2003). MRN is one of the first factors to be localized to the DSBs leading some authors to suggest MRN as DSB sensor (van den Bosch *et al.* 2003) (Figure 1.7).

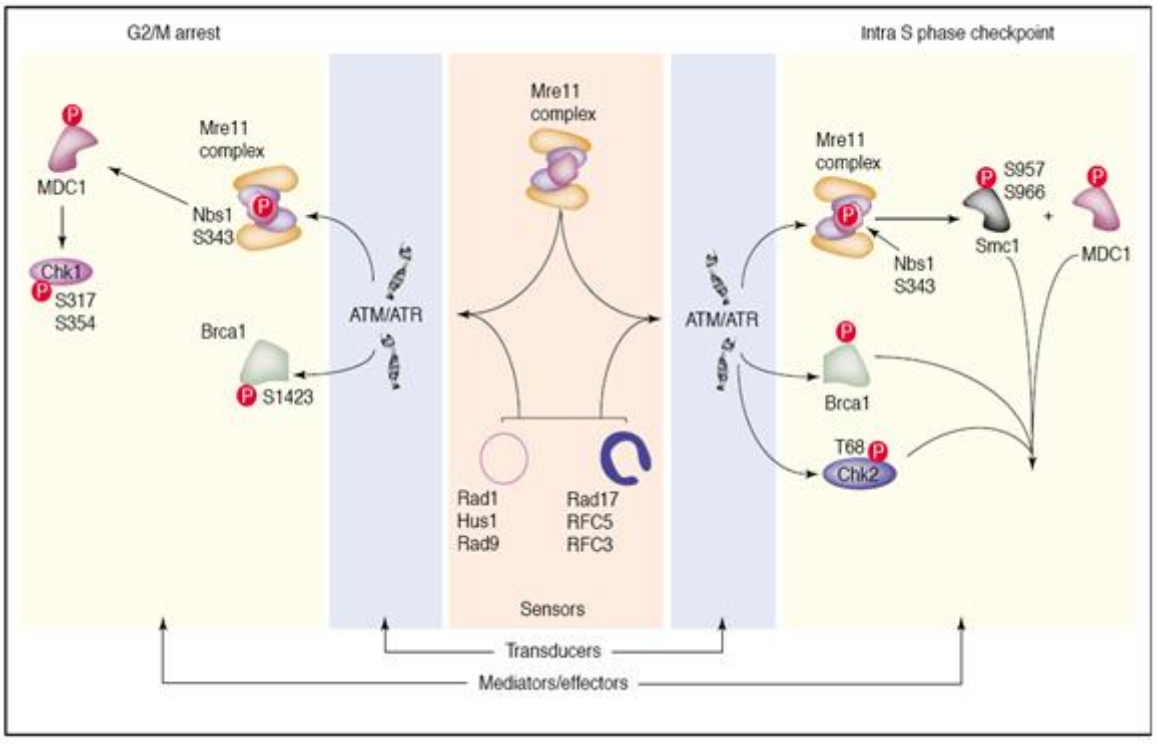

Figure 1.7 - The role of the MRN complex in DDR according to Petrini and Stracker (2003).

Furthermore BRCA1, Rad9 and PARP-1, when dysfunctional, not only affect DDR mechanisms but telomeres as well**,** as exemplified by the presence of telomeric fusions in affected cells or by biochemical associations between shelterin and the above three proteins. BRCA1 confer genetic predisposition to early onset familial breast and ovarian cancer (Moynahan *et al.* 1999; Hartman and Ford 2002; Zhong *et al.* 2002; Slijepcevic 2006). A checkpoint protein hRad9 is a protein that is phosphorylated by ATM following DNA damage. This protein creates a complex with hRad1 and hHus1 proteins which are known as 9-1-1, and is a clamp like complex important in DNA damage induced cell cycle checkpoint response (Chen *et al.* 2001; Slijepcevic 2006).

PARP-1 is a molecule that will detect and signals SSBs. This signalling is mediated by the instantaneous synthesis of poly ADP-ribose (PAR) produced at the lesion site. PARP is

required for the recruitment of XRCC1 which is a critical and important component of the base excision repair (BER) and SSB repair pathways. In addition, PARP-1 is involved in chromatin remodelling and it interacts with DNA-PKcs, ATM and p53 (Herceg and Wang 2001; Ame *et al.* 2004; Slijepcevic 2006).

Another DDR protein that affects telomeres is Apollo. This protein associates with shelterin and it is also known as hSnm1B. Apollo interacts with TRF2 and together they protect chromosome termini from being recognized and processed as DNA damage (Freibaum and Counter 2006; Lenain *et al.* 2006; van Overbeek and de Lange 2006). Finally, a recent paper implicates BRCA2 in telomere maintenance. BRCA2 associates with telomeres during S and G2 phases of the cell cycle and mediates access of RAD51, a homologous recombination protein, to telomeres (Badie *et al.* 2010).

Taken together the above findings demonstrated extensive functional interaction between DDR and telomere maintenance. The objective of my PhD thesis is to explore further this relationship by examining effects of a) some DDR proteins on telomeres that have not been examined before and b) DDR in cells in which telomeres are dysfunctional as a result of alterations in genes not directly involved in DDR. I have chosen BRCA1 and BRCA2 proteins to address a relevant aspect that has not been explored before. Namely, I will focus on the correlation between the degree of DNA damage response defect and telomere dysfunction defect by employing cell lines from patients that are heterozygous (+/-) and cell lines from patients or animals that are homozygous (-/-) with respect to mutations in these genes. As a model for telomere dysfunction I have chosen cell lines from DC patients. DC is a disease caused by mutations in genes that directly affect telomere maintenance. These include genes encoding Dyskerin, TERC, TERT, NOP10, NHP2 and TIN2 (Kirwan *et al.* 2011).

All these proteins are involved in either the telomerase enzyme complex or the shelterin protein complex. It is planned to examine DDR mechanisms in these cells. Given the discussed link between DDR and telomeres our hypothesis is that DC cells should show deficiency in DDR. It is hoped that these studies will shed more light on the mechanisms that regulate interplay between DDR and telomere maintenance. Given the role of both DDR and telomeres in cancer it is possible that these studies will provide useful clues for understanding the process of carcinogenesis. In the final section of this literature review a brief overview of BRCA1 and BRCA2 proteins will be presented, as well as an overview of the current understanding of DC genetics.

1.4 - BRCA1 and BRCA2

Breast Cancer 1 *(BRCA1)* and *BRCA2* are tumor suppressor genes involved in DNA DSB repair through HR and some other DDR pathways (Deng and Wang 2003). The absence of functional *BRCA1* and *BRCA2* is associated with an increased risks of breast and ovarian cancers (Friedenson 2007).

BRCA1 combines with other tumor suppressors, DNA damage sensors, and signal transducers to form a large multi-subunit protein complex known as the BRCA1-associated genome surveillance complex (BASC) (Wang *et al.* 2000). BRCA1 protein associates with RNA polymerase II and it interacts with histone deacetylase complexes through the C-terminal domain. Therefore, this protein plays a role in transcription; repair of DNA DSBs, ubiquitination, transcriptional regulation, as well as in some other molecular pathways (Starita and Parvin 2003; Friedenson 2007).

BRCA2 is a protein primarily involved in the FANC (Fanconi anemia) pathway and it was previously known as FANCD1 until it was established that these are essentially the same proteins (D'Andrea 2003). In the FANC pathway, DNA damage induced by cross-linking agents is repaired by a protein complex that includes several FANC proteins which then ubiquitinate FANCD2 resulting in its transfer to the site of DNA damage. FANCD1 helps the transfer process (Nojima *et al.* 2005). However, BRCA2 is not confined to the FANC pathway as it is also involved in the HR pathway (see below).

It is interesting that both proteins participate in the HR pathway for DSB repair. In this pathway repair proteins utilize homologous intact DNA sequence from a sister chromatid originating from either a homologous chromosome, or the same chromosome (depending on cell cycle phase) as a template (Zhang and Powell 2005). BRCA1 and BRCA2 associate with sites of damaged chromatin in affected parts of the cell nucleus and have a common interacting partner in this process - RAD51, one of the key HR proteins (Boulton 2006). However, BRCA1 and BRCA2 have slightly different roles in HR. BRCA1 is capable of binding DNA directly and it has a high affinity for branched DNA structures which is consistent with its involvement in HR, a pathway that utilizes these branched structures. The DNA binding abilities of BRCA1 contribute to its ability to inhibit the nuclease activity of the MRN complex, which most likely acts as a sensor for DSBs (see above), as well as the nuclease activity of Mre11 alone (Paull *et al.* 2001). This can perhaps explain a role for BRCA1 to promote a higher fidelity DNA repair by NHEJ (Durant and Nickoloff 2005). BRCA1 also colocalizes with γ-H2AX (histone H2AX phosphorylated on serine-139) in DNA DSB repair foci, indicating that it may play a role in recruiting different repair proteins (Ye *et al.* 2001; Starita and Parvin 2003). In contrast, BRCA2 binds single stranded DNA and it helps

the recombinase RAD51 to stimulate strand invasion, a vital step in HR (Genois *et al.* 2012). The localization of RAD51 to the DNA DSBs requires the formation of BRCA1-PALB2-BRCA2 complex (Buisson *et al.* 2010). During repair of DNA cross links DSBs are also generated and it is in this process that BRCA2 can exert its role in the FANC pathway. It is interesting that the BRCA2-RAD51 interaction is also involved in telomere maintenance. A recent study indicates that BRCA2 interacts with telomeres and this interaction is mediated by RAD51 (Badie *et al.* 2010) .

1.5 - DC

DC, also known as Zinsser-Engman-Cole syndrome (Zagorski *et al.* 2001), is a rare, progressive bone marrow failure syndrome. DC is estimated to occur in 1 in 1,000,000 people (Coulthard *et al.* 1998). The key molecular pathway affected in this syndrome is telomere maintenance (Walne and Dokal 2004). Some patients also show ribosome deficiency (Wong and Collins 2006) and protein synthesis dysfunction (Nelson and Bertuch 2012) but this is probably the result of functional links between telomere maintenance and these pathways. Many DC patients die in relatively young age as a result of bone marrow failure, fatal pulmonary complications, infections, or malignancy (Jyonouchi *et al.* 2011).

DC is characterized by a variety of symptoms including bone marrow failure, abnormal skin pigmentation, early greying, leukoplakia of the oral mucosa, dystrophy of the nails, anemia resulting from bone marrow failure, continuous lacrimation due to atresia of the lacrimal ducts, often thrombocytopenia, testicular atrophy in the male carriers, and predisposition to cancer (Buckingham and Klingelhutz 2011).

1.5.1 - Genetics

There are three different types of DC depending of the form of inheritance: autosomal dominant, autosomal recessive and the most common form, X-linked recessive (Dokal 2000).

As stated earlier the 7 affected genes are involved in various processes required for telomere maintenance. Two key protein complexes involved in telomere maintenance include the telomerase enzyme complex and the shelterin protein complex. Telomerase is a reverse transcriptase consisting of several subunits including the RNA component (TERC) and the cataylitic component (TERT). The human telomerase assembles in Cajal bodies when the above two components join each other and require other proteins to function fully (assembly, trafficiking, regulation) including Dyskerin (DKC1) which associates with smaller proteins including NHP2, NOP10 and GAR1, as well as the telomerase Cajal body protein (TCAB1) also known as WRAP53 (Li *et al.* 2011). The shelterin protein complex consists of 6 proteins: TRF1, TRF1, RAP1, TIN2, TPP1 and POT1 (de Lange 2005).

To date mutations in the following genes have been identified in DC patients: *DKC1* (Knight *et al.* 1999), *TERC* (Vulliamy *et al.* 2004), *TERT* (Vulliamy *et al.* 2005; Marrone *et al.* 2007), *TINF2* (Savage *et al.* 2008), *NHP2* (Vulliamy *et al.* 2008), *NOP10* (Walne *et al.* 2007), and *TCAB1* (Zhong *et al.* 2011).

1.5.2 - Autosomal recessive DC

The severity of phenotype in DC individuals may depend upon which protein has incurred a mutation. One documented autosomal recessive mutation in a family that carries DC has been found in the *NOP10* gene (Walne *et al.* 2007). This mutation changes a cytosine

to thymine in a highly conserved region of the *NOP10* sequence leading to a change from arginine to tryptophan. Homozygous recessive individuals show severe DC symptoms including much shorter telomeres compared to age matched control individuals. Given that NOP10 is required for the TERC normal function, the above mutation leads to a reduction in TERC levels resulting in much lower telomerase activity and extremely short telomeres. Since telomerase activity is required for proper functioning of stem cells highly proliferative tissues that depend on tissue specific stem cells for a high cell turnover, including bone marrow and skin, will be highly affected (Walne *et al.* 2007).

Similarly, *NHP2* and *TCAB1* mutations, which also cause autosomal recessive form of DC, will cause similar phenotypic features in patients. This is understandable as both proteins are required for proper functioning of the telomerase RNA component, TERC (Vulliamy *et al.* 2008).

1.5.3 - X-linked recessive DC

The best-characterized and the most common form of DC is the X-linked recessive DC caused by mutations in the *DKC1* gene located in the long arm of the X chromosome (Heiss *et al.* 1998; Vulliamy *et al.* 2001). Before DC was recognised as a disease of dysfunctional telomeres and in the absence of genetic knowledge (i.e. 15 years ago), X-linked recessive DC was clinically diagnosed as a rare bone marrow failure disorder linked to Xq28 (Connor *et al.* 1986; Arngrimsson *et al.* 1993). There are some variations in severity of symptoms in X-linked DC. The most severe form of X-linked DC is also known as Hoyeraal-Hreiderasson syndrome and it was named at the time when there was no knowledge of which genes are affected in DC.

DKC1 or Dyskerin is a protein that is an integral part of the telomerase enzyme complex. It binds the H/ACA box RNA structural motif within TERC and it is required for TERC stability and telomerase activity in vivo (Armanios and Blackburn 2012). Mutations affecting *DKC1* will result in dysfunctional telomerase with all clinical consequences discussed above.

1.5.4 - Autosomal dominant DC

This form of DC is caused by mutations in *TERT, TERC* and *TIN2* genes (Armanios and Blackburn 2012). Given the clinical complexity of DC and the lack of genetic knowledge in the past some of DC patients with *TERC* mutations have been diagnosed as aplastic anemia patients. In addition, there are some patients with *TERC* mutations that would probably be not classified as DC patients clinically (Armanios and Blackburn 2012). In total, approximately 30% of all DC patients have mutations in *TERC* (Armanios and Blackburn 2012). *TERT* and *TIN2* mutations are comparatively lower in frequency.

In terms of its phenotypic effects dysfunctional TERT and TERC will lead to dysfunctional telomerase and relevant clinical features that result from this. It is interesting that *TIN2* is the only gene that do not belong to the telomerase enzyme complex and that leads to DC symptoms. This indicates that shelterin is equally important for telomere maintenance. Given that there are some DC patients that have not been classified genetically it is possible that other shelterin components may be affected in DC.

1.6 - Aims of the study

As indicated above the overal aim of this thesis is to examine further the relationship between DNA damage response and telomere maintenance. Therefore, the work carried out in this project was divided in three parts:

- Development of Interphase Q-FISH (I Q-FISH). In order to be able to accurately assess telomere length in cell lines from individuals with defective DNA damage response and cell lines from DC patients all characterised by poor proliferative phenotype it was necessary to develop a method that can measure telomere length in this type of cells.

- Investigation of DNA damage response and telomere maintenance in cell lines from patients with mutations in *BRCA1* and *BRCA2*, as well as in relevant animal cell lines.
- Investigation of DNA damage response in cell lines from DC patients.

Chapter 2 - Materials and Methods

2.1 - Cell lines and cell culture methodology

2.1.1 - **Primary human fibroblasts**

Primary human fibroblast cell lines GM08399, VU0423-F, GM1787 114 and GM1774 A (Table 2.1), were cultured in Dulbecco's modified eagle medium (DMEM) supplemented with 15% fetal calf serum at 37°C and antibiotics in the atmosphere of 10% CO_2. The VU0423-F cell line, originating from a patient with a biallelic mutation in BRCA2, has been obtained from Dr Hans Joenje, University of Amsterdam. The VU0423-F patient has initially been characterized as a Fanconi anemia patient. All other fibroblast cell lines have been obtained from the Coriell Cell Repository.

2.1.2 - **Human B-lymphocytes**

Human B-Lymphoblast cell lines GM00893, GM13705, GM14090, GM14622 and GM14090 (Table 2.1) were cultured in RPMI 1640 medium (Gibco/invitrogen) and 10 % fetal calf serum and antibiotics at 37^{o}C in the atmosphere of 5 % CO_2. All these cell lines have been obtained from the Coriell Cell Repository.

2.1.3 - **Mouse lymphoma cell lines**

Mouse lymphoma LY-R (radio-resistant) and LY-S (radio-sensitive) cells (Table 2.1) were cultured in RPMI 1640 medium (Gibco/invitrogen) supplemented with 10 % fetal calf serum and antibiotics at 37^{o}C in the atmosphere of 5 % CO_2 and were used as a reference for cytological testing telomeric measurements using interphase Q-FISH (IQ-FISH) technique.

Table 2.1 – Description of cell lines used during the course of this project

Cell Line	Origin and gene affected	Cell Type	Age at sampling	Sex	Clinically affected
GM08399	Healthy individual	Fibroblast	19YR	Female	No
GM1787 114	Dyskeratosis Congenita carrier, X-linked; *DKC1 +/-*	Fibroblast	78YR	Female	No
GM1774 A	Dyskeratosis Congenita carrier, X-linked; *DKC1 +/-*	Fibroblast	7YR	male	Yes
VU0423-F	Patient with biallelic mutation in BRCA2	Fibroblast			Yes
GM00893	Healthy Individual	B-Lymphocyte	32 YR	Female	No
GM13705	BRCA1 carrier *(BRCA1+/-)*	B-Lymphocyte	38 YR	Female	Yes
GM14090	BRCA1 carrier *(BRCA1+/-)*	B-Lymphocyte	43 YR	Female	Yes
GM14622	BRCA2 carrier *(BRCA1+/-)*	B-Lymphocyte	39 YR	Female	Yes
GM14170	BRCA2 carrier *(BRCA1+/-)*	B-Lymphocyte	46 YR	Female	Yes
CB17	Normal Mouse	Fibroblast	Unknown		
SCID	SCID Mouse (DNA-PKcs-/-)	Fibroblast	Unknown		
E14	Normal Mouse embryonic Stem cells	Stem cell	Unknown		No
408	Mouse Embryonic Stem cells with mutation in Brca1 *(Brca1-/-)*	Stem Cells	Unknown		Yes
LY-R	Mouse Lymphoma, Normal radiosensitive	Lymphoma	Unknown		
LY-S	Mouse Lymphoma, radiosensitive	Lymphoma	unknown		
Hela	Human Cervical Carcinoma	Epithelial adherent cells	31 YR	Female	Yes
U2OS	Human Osteosarcoma	Mesnchymal adherent cells	15 YR	Female	Yes
2093, 1823, 1866, 1879	Fannconi Anemia, FANCD2 complementation group	Fibroblast	8±5 YR		Yes
C1,C2,C3,C4	Healthy Individual	Fibroblast			No

2.1.4 - **Mouse fibroblast cell lines**

Mouse fibroblast cell lines CB17 and SCID (Table 2.1) were grown in Wymouth medium (Gibco) and 10% fetal calf serum and antibiotics at 37°C in the atmosphere of 10 % CO_2.

2.1.5 - **Mouse embryonic stem cells**

Mouse embryonic stem cell lines E14 and 408 (Table 2.1), were obtained from Dr Beverly Koller, University of Duke University, US. They represent undifferentiated embryonic stem cells and were cultured at 37°C in the atmosphere of 5% CO2 on gelatine coated dishes in KnockOut DMEM medium supplemented with 20% KnockOut serum replacement, 2 m*M* L-glutamine, 0.001% b-mercaptoethanol (Sigma- Aldrich, St. Louis, MO), 1000 U/ml ESGRO (Chemicon, Temecula, CA), 10 U/ml penicillin, and 10 mg/ml streptomycin (all purchased, except where stated, from Gibco/Invitrogen). Medium was changed every 3 days, and cells were subcultured initially at the ratio 1:2. The ratio progressively increased up to 1:8.

2.1.6 - **Human adherent cell lines**

The U2OS cell line (Table 2.1), originally derived from a 15 years old female with osteosarcoma, exhibit epithelial adherent morphology. U2OS cells were grown in McCoy's 5a medium (Sigma), supplemented with 10% FBS (Gibco/Sigma) and 2mM glutamine (Gibco) at 37˚C in the atmosphere of 10% CO2. In order to avoid contamination, Penicillin and Streptomycin were added (1µl per 100ml medium) to both media. The HeLa cell line (Table 2.1) was originally established from a patient with cervical cancer. HeLa cells were grown in

Dulbecco's modified Eagle medium (DMEM) (Gibco/Sigma), supplemented with 10% foetal bovine serum (FBS) (Gibco/Sigma) at 37°C in the atmosphere of 10% CO2.

2.1.7 - **Tissue culture procedure**

All cell lines were kept frozen in liquid nitrogen. When required vials of frozen cells were thawed (see below) and set up in either a 25cm^2 flask or 75cm^2 flasks with filter head (Nunc) to avoid fungus contamination. All primary fibroblast cell lines were subcultured 1:3 by gentle trypsinization with trypsin-EDTA (Gibco/invitrogen) for five minutes at least every three to four days at 80 percent confluence. Prior to trypsinization the cells were washed with 3ml of D-PBS (Gibco/invitrogen). After trypsinization the cells were spun down in a centrifuge (Megafuge 1.0, Heraeus) at 1200rpm for five minutes. All solutions were brought to room temperature prior to trypsinising using a waterbath (Techne) with a monitor (Tempette Junior TE-8J) to keep the temperature constant 37ºC. The waterbath was constantly cleaned and disinfected alongside the incubator and the hood to avoid spreading of any fungus or bacterial infection.

Supernatants were removed and the cell pellets were re-suspended by gentle flicking in the fresh medium. One ml of suspended cells was then put in a new flask with the fresh medium.

All human and mouse lymphoma cell lines were grown in suspension under tissue culture conditions as mentioned above. Cells were sub-cultured at the ratio of 1:10 every two or three days, preferably before the medium colour changed to yellow.

2.1.8 - **Cryopreservation of cells**

Cells were preserved in liquid nitrogen to avoid aging and contamination. After checking cells for contamination, cells were trypsinized as described above. Cell suspension was mixed with 1ml of freezing medium containing 90 % fetal calf serum (Gibco/invitrogen) and 10 % DMSO (dimethylsulfoxide, Sigma). The cell suspension was aliquoted into cryogenic vials for storage in liquid nitrogen. Prior to storage in liquid nitrogen the vials were kept in a Nalge nunc cooler for 24 hours. This plastic holder was filled with Isopropyl alcohol (IPA). The specific heat of the coolant in the base insulates the container and gives a cooling rate of ~1º/min in the cryotube. Finally the ampoules with cells were transferred into liquid nitrogen for long-term storage.

2.1.9 - **Thawing of cryopreserved cells**

The medium was aliquoted and warmed inside the incubator before the ampoule with frozen cells was taken out of the liquid nitrogen. The cryopreserved cells were handled with great care. The ampoules were thawed for two to three minutes and the content immediately put into the pre-warmed medium. Cells were transferred into appropriate flasks. After 24 hours the medium in flasks was changed to wash away any residual DMSO.

2.1.10 - **Irradiation of cells**

A Cobalt-60 source was used to irradiate cells with ionising radiation. Adherent cells were grown up to 80-90% confluence either in non-filtered tissue culture flasks (Nunc, Fisher) for metaphase preparation, or on polyprep slides (Sigma) for assays that required use of antibodies. Datasheets provided by the physicist in charge of this facility were used to

calculate dosages of radiation measured in Gray (Gy) per minute. In our studies cells were only subjected to relatively low doses of radiation i.e. mostly 0.5 Gy and 1.0 Gy with a maximum dose of 2.0 Gy.

2.2 - Cytogenetic Analysis

2.2.1 - Metaphase Preparation using fibroblast cell lines

A high mitotic index is important in scoring a large number of metaphases in a short time and it is also important to get high quality metaphase spreads. Twenty-four hours after irradiation (i.e. one cell cycle in the case of human cells), a flask with the semi-confluent cells (80-90%) was treated with colcemid (10µg/ml) (Sigma-Aldrich). Colcemid was used to arrest cells in metaphase by inhibiting the mitotic spindle formation. Initially cells were treated for three hours with colcemid (10µg/ml) prior to trypsinization and harvesting. This method gave a low mitotic index when using primary fibroblast cell lines and it was time-consuming if a large number of metaphases were needed for the analysis. The following changes were implemented to yield a higher mitotic index in primary fibroblast cell lines:

1. Colcemid time was increased from three hours to twelve hours of treatment. This ensured that most cells reached M-phase of cell cycle, therefore increasing the mitotic index.

2. A mock flask was used without adding colcemid as a control to check the number of dividing cells. This method gave us a rough idea of when to stop the colcemid's action.

3. During harvesting, culture supernatant were retained to collect mitotic cells in suspension and spun down in a centrifuge at 1000rpm for five minutes and before each spin a fresh fixative solution was added. This ensured that metaphases were not lost.

4. Greater care was taken in handling the cells in the culture. For instance, cells were sub cultured when reaching 60-70**%** confluence rather than 80-90**%** as in previous experiments. This ensured that cells were kept healthy and in the exponential growth phase.

After roughly twelve hours of treatment with colcemid, cells were washed in PBS, trypsinized, and spun down at 1000rpm for five minutes. Cells were then treated with 10ml of hypotonic buffer (75mM of KCl) for 15 minutes in a 37^{o}C water bath and this will cause cells to increase their fluid intake. Cells were then fixed in a solution consisting of methanol and glacial acidic acid (3:1) solution. The process of fixation was carried out two more times and each time 1ml of fresh fixative was added drop wise, followed by the addition of 2ml of extra fixative. The cells were left at room temperature for 10 minutes and 30 minutes respectively. Finally, the cell pellets were re-suspended in fresh fixative and 15µl of cell suspension was dropped onto pre-cleaned slides. The fresh fixative ensured that mitotic cells were spread over the surface of slide effectively. Once the slides were dried they were checked under a phase contrast microscope.

2.2.2 - Metaphase preparation of other cell lines

Preparations of metaphases from other cell lines (mouse embryonic stem cells, mouse LY-R and LY-S cells and human lymphoblasts) were performed as described above (2.2.1) but with maximum colcemid (10µg/ml) (Sigma-aldrich) incubation of 4 h only. These cell lines grow at a faster rate than human primary fibroblasts and therefore did not require changes described above (2.2.1). The remaining protocol was the same as described above.

2.2.3 - Giemsa Staining

Slides were stained with 8% (v/v) Giemsa (Sigma-Aldrich) for ten minutes in 50ml of ddH_20. Giemsa stain was filtered to achieve better purity using standard filter paper (3MM Watman paper). After staining, slides were rinsed quickly with ddH_20 and left to air dry while covered with paper to prevent dust settling onto the slides. Slides were mounted with DPX mountant (BDH laboratories), covered with cover slips, and left overnight to dry. DPX is a neutral solution of Polystyrene Plasticizer in Xylene. By applying this solution the coverslips were permanently attached onto the slides. A clean dust free and evenly stained slide with high mitotic index was selected for analysis using conventional microscopy (Zeiss Axioplan 2) equipped with CCD camera and MetaSystem software (Altlussheim, Germany).

2.3 - Interphase Quantitative Fluorescent *in situ* hybridization (I-QFISH)

2.3.1 - Pre Hybridization washes

Samples for I-QFISH were produced as standard cytogenetic samples (see above) with the exception of colcemid treatment. Microscope slides containing samples were washed with PBS for 5 min on the shaker. After that the samples were treated with 4% formaldehyde for 2 minutes and washed in PBS for 3x5 minutes. In order to remove unwanted proteins, 500 µl of pepsin (10 % pepsin; Sigma Co.) was mixed with 50 ml of acidified dH2O of pH2 (49.5 ml of deionized water added to 0.5 ml HCL) and then added to 50 ml PBS and incubated at 37°C in water bath for 10 minutes. After 2x washing with PBS for 2 minutes on the shaker, the slides were fixed again with 4% Formaldehyde for about 2 minutes. Subsequently, the samples were washed three times with PBS for 5 minutes and

then dehydrated in the ethanol series (70%, 90%, 100%) and left to dry at room temperature.

2.3.2 - Hybridization

A total of 20µl of the synthetic oligonucleotide PNA (peptide nucleic acid) specific for the telomeric DNA sequence $(CCCTAA)_3$, labeled with FITC, was added to the slides. The slides were then placed on the heating block for 2 minutes at 70-75^{o}C. Samples were left in a dark humidified chamber for 2 hours to allow for hybridization.

2.3.3 - Post Hybridization Washes

The samples were washed twice in 70% Formamide solution for 15 minutes, followed by washing the slides 3 x with PBS for 5 minutes each time. Samples were then dehydrated in ethanol series (70%, 90%, and 100%). A total of 15µl of Vectra-shield anti-fade (DAPI) mounting medium was added to each slides before they were sealed with a clear nail varnish.

2.3.4 - Image Capture and Telomere length analysis

Images of interphase cells have been acquired using the Smart Capture software (Digital Scientific, Cambridge, UK) and telomere fluorescence analyzed using the IP Lab software adapted for this purpose by Digital Scientific. Details of this procedure (Figure 2.1) are described in Chapter 3.

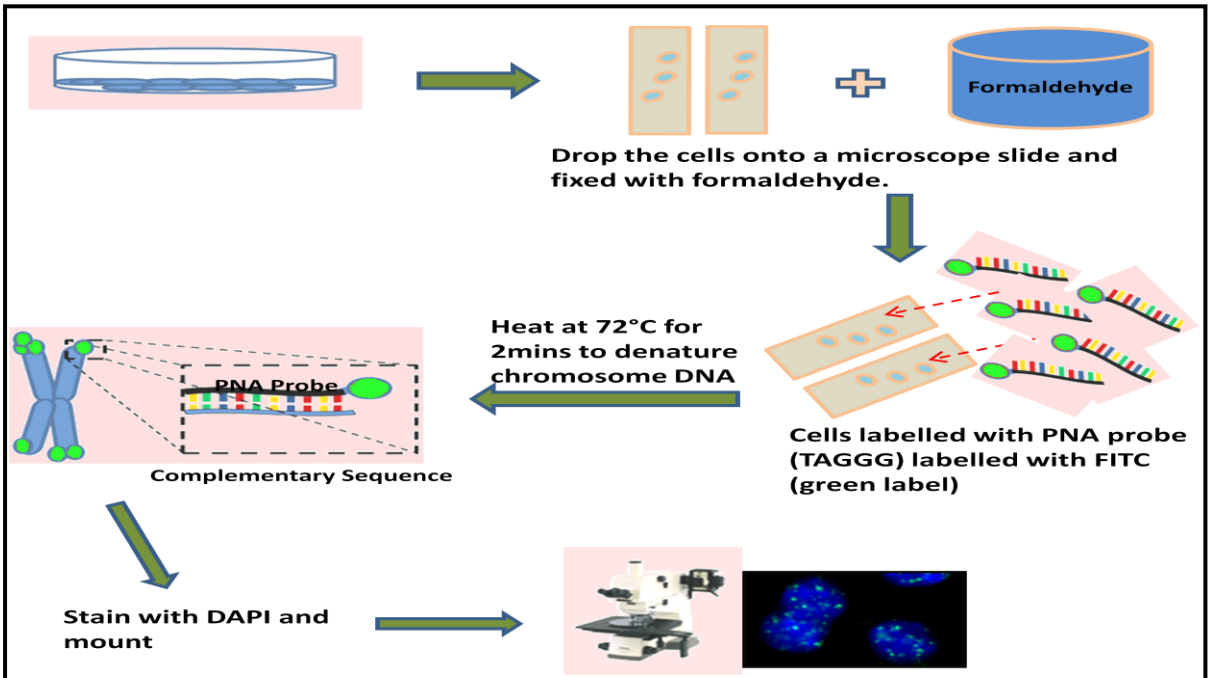

Figure 2.1 - An overview of Q-FISH (Authors' own adaptation)

2.4 - Chromosome Orientation Fluorescence in situ Hybridization (CO-FISH)

CO-FISH technique is based on standard FISH which also has further ability to determine the absolute 5`- to -3` orientation of DNA sequence relative to the short arm(q) to long arm(p) of the chromosome. This technique was originally termed COD-FISH (Chromosome Orientation and Direction FISH). Basically, the various applications of CO-FISH include: distinction between telomeres produced by leading-versus lagging- strand DNA synthesis, detection of interstitial blocks of telomere sequence that result from unsuitable fusion to double-strand breaks (telomere-DSB fusion), measuring the rate of mitotic recombination at telomeres through counting telomeric-sister chromatid exchanges (T-SCEs) and replication timing (controlling) of mammalian telomeres during the S-phase (Bailey *et al.* 2010). Thus, the main difference between the CO-FISH and standard FISH is in

the capacity of CO-FISH to produce signals only in single chromatids as can be seen in (Figure 2.2).

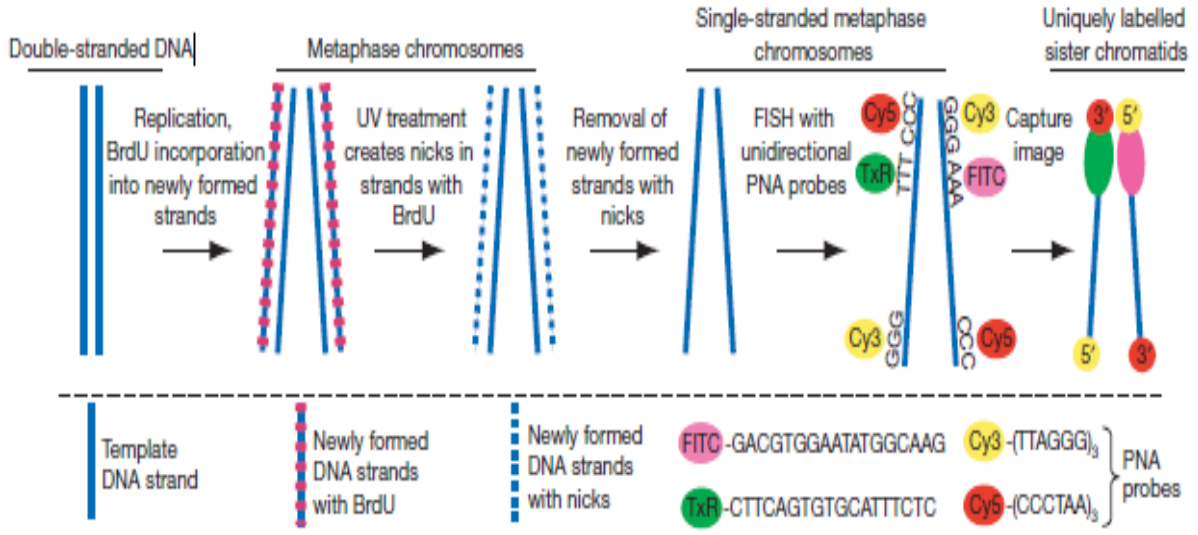

Figure 2.2 - The CO-FISH procedure according to (Falconer *et al.* 2010). In our protocol we used only a 5' probe resulting in only one signal/pair of sister chromatids.

After sub-culturing, cells were incubated for 20 hours with 3µl of 5‟-bromo-2-deoxyuridine at the concentration of 1x10-5M (Sigma Co.). This was followed by metaphase preparation as mentioned above. In the next step the slides were made and were aged overnight at 54°C in order to fix the chromosomes and making their structure resistance to the subsequent DNA denaturing.

2.4.1 - Washing, digestion and fixation

The slides were washed with PBS for 15 minutes and then stained with 2.5 µl of Hoescht 33258 (0.5 µl/ml) which was mixed gently with standard saline citrate (2x SSC) for 15 minutes. After exposing the slides to 365 nm UV light for 30 min, 100 µl of Exonuclease III (Promega Co.) (1.5 µl Exonuclease III + 10 µl buffer + 88.5 µl H2O) was added to each slide

and covered with cover slip at room temperature for 10 minutes. Samples were then washed twice with PBS for 5 minutes on the shaker. Subsequently, the slides were treated with the Ethanol series for about 5 minutes for dehydration (70%, 90%, 100% ethanol respectively) and left to dry at room temperature.

2.4.2 - Hybridization

A total of 20 µl of the PNA probe specific for the telomeric DNA sequence $(CCCTAA)_3$, and labeled with Cy3, was added on the slides followed by transfer to the heating block for about 2 minutes at 70-75°C. The slides were placed for 2 hours in darkness at room temperature to allow for hybridization.

2.4.3 - Post hybridization wash

The slides were washed twice with 70% formamide dissolved in the SSC buffer in a coupling jar, protected against light by foil, for 15 minutes. The slides were then washed three times with PBS and dehydrated in ethanol series (70%, 90%, and 100% respectively) for 5 minutes each. A total of 15 µl of vecta-shield anti-fade (DAPI) was added to each slide and covered with a cover-slip. The cover slips were sealed with a nail varnish.

2.4.4 - Image analysis

Digital images were acquired using a Zeiss fluorescence microscope equipped with a CCD camera and the ISIS captures software (in *situ* imaging system "ISIS", Meta Systems, Altlussheim, Germany)

2.5 - Immunocytochemistry (γ-H2AX assay)

DNA damage in cells can be detected by different methods. One of the most popular methods is the γ-H2AX assay which detects sites of DNA damage in interphase nuclei using a monoclonal antibody against the above protein. All adherent cells were grown on poly-prep slides (Sigma-Aldrich) for 24 hours before fixation in 4% formaldehyde in PBS for 15 minutes. Cells were then permeabilized in 0.5**%** Triton-X 100 (Sigma-Aldrich) for 10 minutes at 4°C. Cells are then blocked with 0.5% BSA (Bovine Serum Albumin) in PBS for 30 minutes and covered in parafilm in humid containers. Primary antibody (γ-H2AX; Milipore) is added at the relevant concentration (1:500), for 1 hour in humid containers covered with parafilm. Slides were washed twice for five minutes each in TBST. Secondary antibody was added at relevant concentrations (1:1000) for one hour in a dark and humid container. Finally slides were washed in TBST for five minutes three times and dehydrated with serial ethanol as previously mentioned. The DAPI vectashield mounting medium was added and cover slides are sealed with nail varnish.

2.6 - γ-H2AX assay using the Imagestream

DNA damage in non-adherent cells, like lymphoblastoid cells, cannot be measured using the above protocol. In order to detect DNA damage in lymphoblastoid cell lines we used the Imagestream apparatus (Amnis, Seattle) which is capable of analysing fluorescence in all cells types grown in suspension.

For each individual sample seven flasks of cells grown to confluence were labelled as follows

- Untreated Control
- 30 minutes after irradiation

- 5 hours after irradiation
- 24 hours after irradiation
- 48 hours after irradiation
- PE Compensation (Phycoerythin)
- Draq 5 Compensation

The PE compensation samples will only be stained with the primary antibody (γ-H2AX) and secondary antibody (Phcoerythyrin), while the Draq 5 compensation sample will only be stained with the Draq-5 nuclear stain whilst all other samples will be stained with both markers. This will allow the analysis software to compensate for any signal overlap of the two markers.

When required samples were rinsed with 10mL of PBS and the cells detached with 1mL of Trpysin, Cells were then washed in 10mL of PBS twice and centrifuged at 1500rpm for 5 minutes in a table top centrifuge (Haraeus, GMBH) between each wash. Cells were then fixed in 1mL of Methanol: Acetone (50:50 v/v) and transferred to Eppendorf tubes. They were incubated at 4^{o}C overnight. All samples were centrifuged at 5000 rpm for 2 minutes. The fixative was aspirated and the cell pellet was resuspended in 1mL of permeabilisation buffer [0.5% Triton X-100 (Sigma Aldrich) in PBS]. This allows the cell membrane to become permeable, making antibody staining more effective. Samples were left on the shaking platform for 5 minutes at room temperature. Samples were centrifuged at 5000rpm for 2 minutes. The permeabilisation buffer was aspirated and the cell pellet was resuspended in 1mL of blocking buffer (0.2% non fat milk powder) (Premier International Food Ltd, Spalding Licolnshire UK), 0.1% Triton X-100 in PBS)). The samples were left on the rotary wheel for 1 hour at room temperature.

Samples were centrifuged at 5000 rpm for 2 minutes. The blocking buffer was aspirated and the cell pellet was resuspended in 1mL of γ-H2AX antibody (Millipore UK Ltd, Hampshire UK). The Draq-5 compensation sample was resuspended in 500µL of blocking buffer. The samples were incubated at 4^{o}C overnight.

The following day, the samples were washed 3 times in wash buffer; centrifuged at 5000 rpm for 2 minutes in between each wash. The cell pellet was resuspended in 100µL of secondary antibody (Phcoerythyrin, Sigma Aldrich) for all samples apart from the Draq 5 comp sample, which was resuspended in 500µL of blocking buffer. They were placed on the rotary wheel for 1 hour, which was covered in foil to prevent degradation of the fluorescent signal.

They were washed twice in wash buffer; centrifuged at 5000 rpm for 2 minutes in between each wash. The cell pellet was resuspended in 150µL of Accumax flow cytometry buffer (PAA). 0.5µL of Draq-5 nuclear stain (Biostatus Ltd, Leicestershire UK) was added to all samples with the exception of the PE compensation sample. Samples were incubated in a water bath at 37^{o}C for 30 minutes. Samples were then kept at 4^{o}C until processing on the Imagestream took place.

2.6.1 - Imagestream analysis

The Imagestream is a multispectral imaging flow cytometer, which counts cells and enables visualisation of each individual cell. It can take up to 6 simultaneous images of every cell including

- Brightfield which provides information about cell size, structure and morphology
- Darkfield which measures the light scattered by the cell
- Fluorescence is detected by a 488nM laser, which locates and measures the level of signal being emitted by the biomarker of interest.

There are four different channels that can be used for fluorescent markers at different wavelength. In this experiment:

- Channel 3 was used for the detection of the Phcoerythrin staining
- Channel 5 was used for the detection of the Draq-5 staining

Samples were processed using the Inspire™ software (Figure 2.3). Individual images of cells were captured using Brightfield to determine morphology and a 488nm laser set at 100mv to ascertain localisation and intensity of Phycoerythin and Draq-5. Cells were counted at an approximate rate of 30 -70 cells per second. A total of 10000 cells were counted per sample.

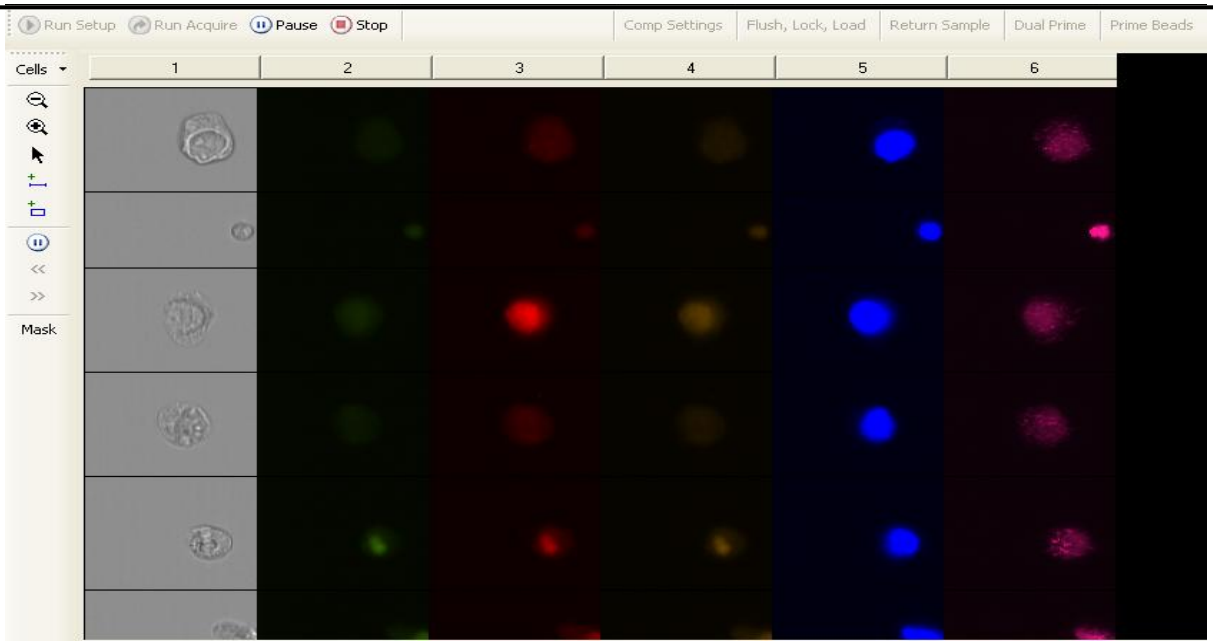

Figure 2.3 - A screenshot image of the Inspire software, showing each individual cell in Brightfield (Ch 1), PE staining (Ch 3), Draq-5 staining (Ch 5) and side scatter (Ch 6).

The images captured on the Inspire software were analysed using the IDEAS™ software (Figure 2.4). The analysis comprises a multi-step process and it is initiated by pre-defined "building blocks". Once all unwanted images such as debris, doublet cells and unfocussed images have been excluded from the population of cells being analysed (Figure 2.5), a series of masks are created. This defines regions of interest and directs the software to the area of the cell you are interested in (in this case the nucleus). Finally, based on the masks created, histograms are generated to provide statistical information such as the average number of foci in a cell and the average intensity of signal generated in a particular sample.

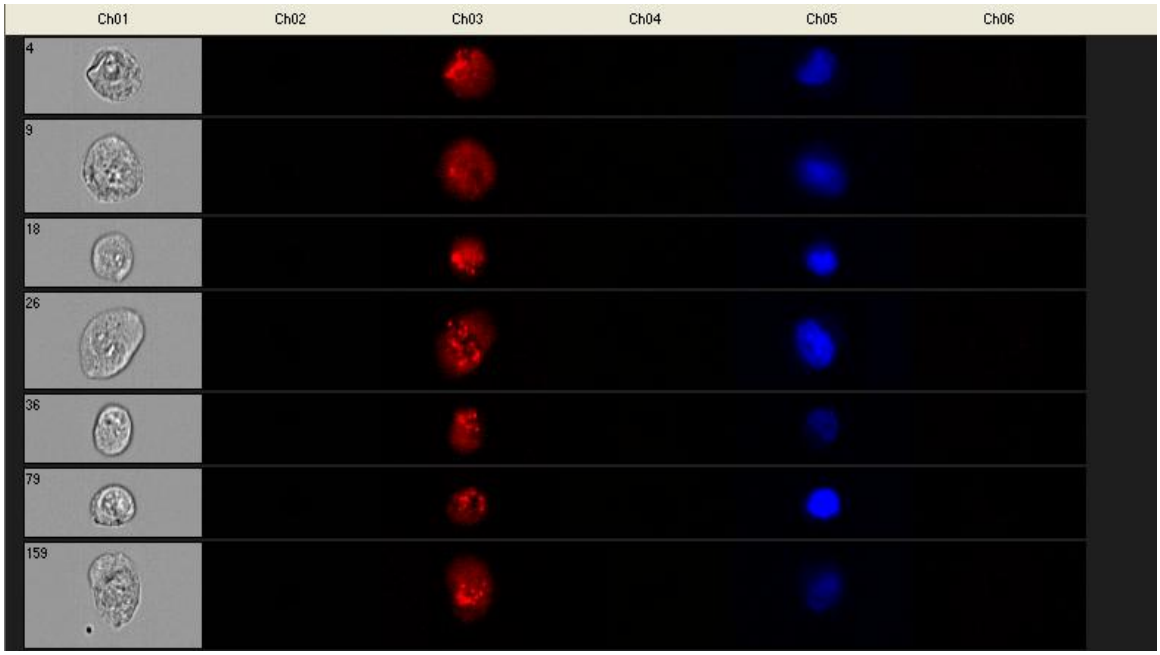

Figure 2.4 - Individual images of all cells captured as seen in the IDEAS software.

2.6.2 - Cell gating

The raw data was first sorted using the 'building blocks' provided with the software. The images were gated for a number of parameters as described below.

1) Single cells

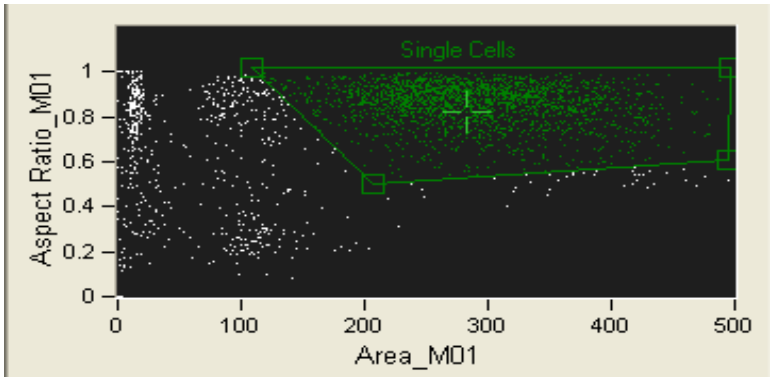

Figure 2.5 - Single cells are gated within the entire population that was counted. This is done to ensure only single cells are used in the analysis and eliminates debris as well as doublet cells.

2) Cells in focus

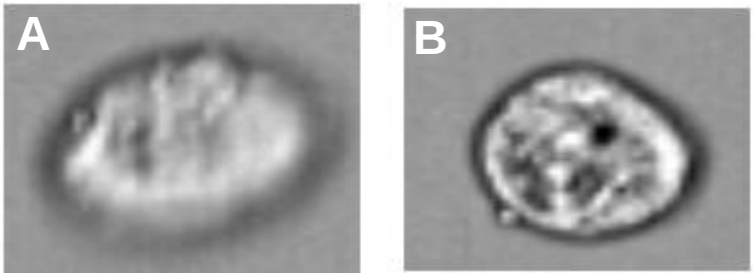

Figure 2.6 - The single cell population (Figure 2.5) is then sorted to remove cells that are out of focus (A) as it is not possible to determine the number of foci accurately unless cells are in focus (B).

3) Cells that have been stained with both secondary antibody and Draq 5

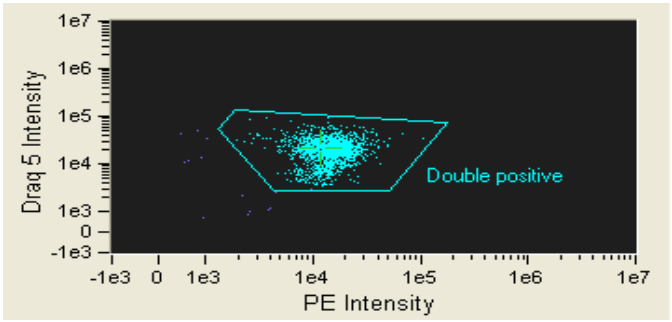

Figure 2.7 - Cells that are double stained will usually form a cluster as seen above. Only double stain cells including in analysis.

2.6.3 - Creating Masks

The next step entailed creating a series of masks to allow for quantification of γ-H2AX foci. A mask defines a region of interest within the cell. Initially a nuclear morphology mask (Figure 2.6) was created which identified the nucleus of each individual cell. This enables to direct the ensuing masks that are created to focus only on the nucleus. This is done as γ-H2AX foci will only appear in the nucleus and thereby eliminates false or cytoplasmic staining.

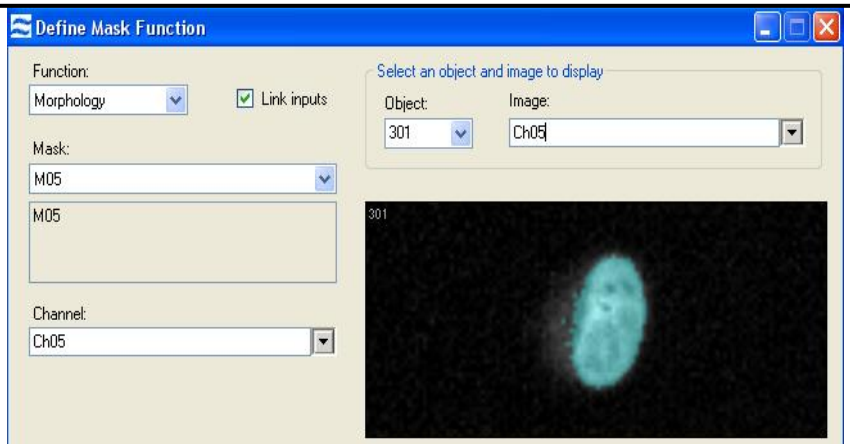

Figure 2.8 - Creating morphology mask using the Mask wizard.

An intensity mask was then created to determine overall PE intensity in the nucleus and therefore overall levels of DNA damage. When creating this mask, the Morphology mask created earlier was used to define the region that the Intensity mask will analyse (Figure 2.8). This mask was then applied to all cells that fell within the parameters set out earlier.

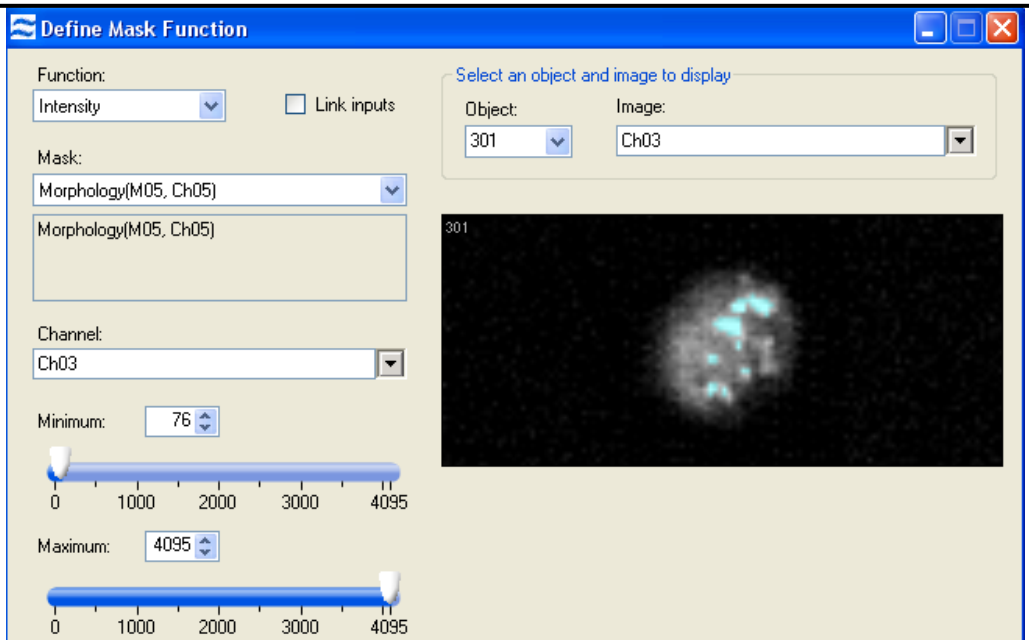

Figure 2.9 - Creating intensity mask using the Mask wizard.

A spot mask was also created to allow accurate quantification of the number of foci formed in each individual cell.

In order to create a spot mask, first a truth population of cells was selected. This population only contains images in which the number of foci can be clearly visualised and cells with a range of foci numbers are selected. The spot mask was then created (Figure 2.9) using these images as validation to ensure that the parameters set for the spot mask accurately masked only the foci within the nucleus.

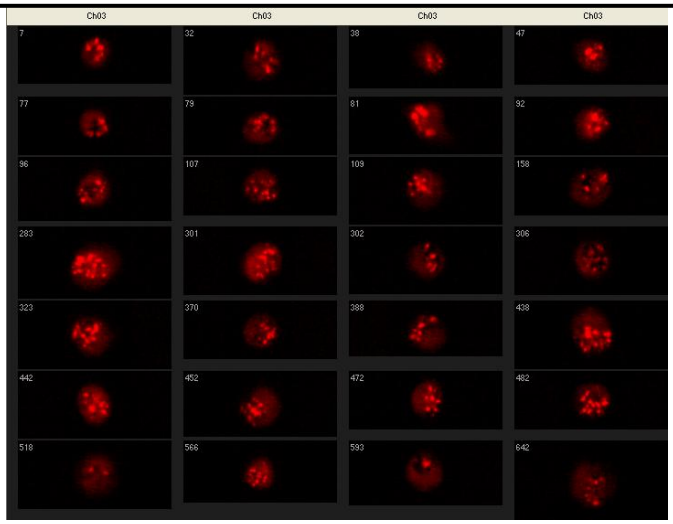

Figure 2.10 - Truth population shown in Ch03.

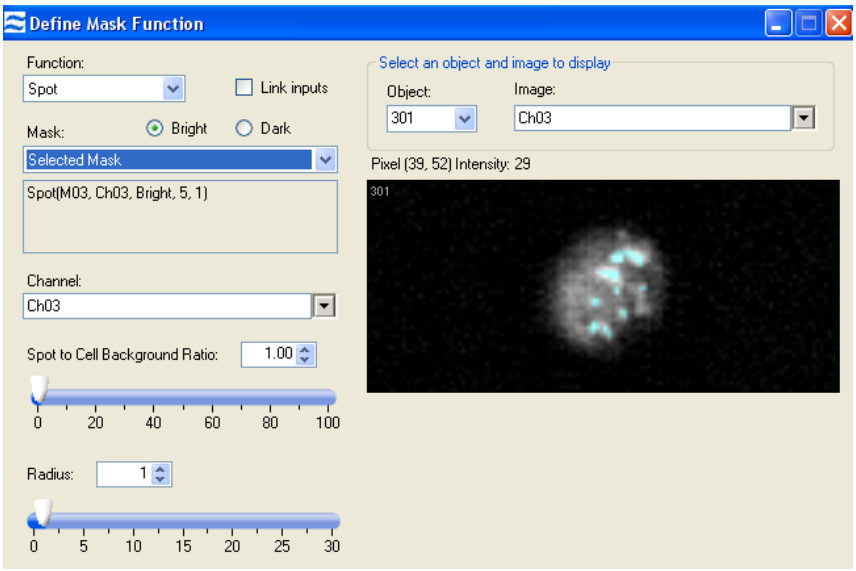

Figure 2.11 - Creating spot mask using the Mask Wizard.

In order to ascertain the accuracy of the mask created, a new feature is created using the spot mask (Figure 2.11) and a histogram was plotted using only the truth population (Figure 2.12). By clicking on the individual bins, it is possible to check whether the feature has accurately identified the number of foci in the cells as you are able to detect the number of foci visually.

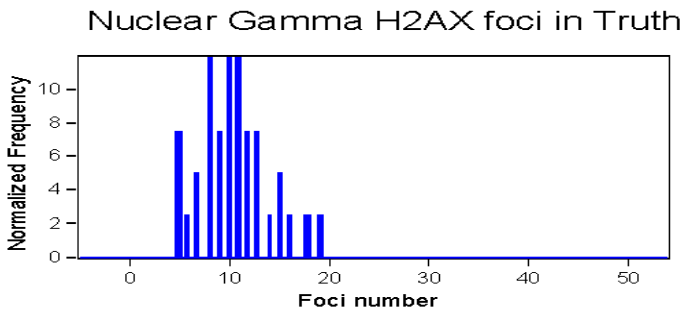

Figure 2.12 - Histogram generated to test the accuracy of the spot mask.

Once the accuracy of the spot mask feature was validated using the truth population, this was applied to the population of cells that fell within the criteria listed earlier.

2.7 - H2AX Assay using Cytospin

As an alternative method for the Imagestream analysis we used a simple cytospin procedure. This procedure spreads non-adherent cells onto microscope slides using gentle fixative reagents to allow subsequent immune-cytochemical analysis. Cells were grown in T25cm^2 flasks (Nunc) and attached to polyprep slides (Sigma-Aldrich) using a cytospin centrifuge at 1000 rpm for 5 min. All the procedures were performed at room temperature. Cells were fixed with 2% paraformaldehyde for 10 min, washed with PBS for 5 min, permeabilized with 0.2% Triton X-100 in PBS for 10 min, and washed with PBS for 5 min. At this point cells were ready for immunocytochemical staining as described in the section 2.5.

2.8 - Telomere dysfunction-induced foci (TIF) Assay

The TIF assay described here is based on the combination of antibody detection and hybridization with synthetic telomeric PNA. The original TIF technique was first described in 2003 by (Takai *et al.* 2003) in which co-localization between two antibodies was analyzed. One antibody binds to a DNA damage response protein such as 53BP1 and the second antibody binds to a telomere repeat binding protein (TRF1). A co-localization between the two antibodies was then detected and the site of co-localization represents DNA damage at a telomere and it is called a TIF. In our protocol detection of telomeres was performed through hybridization with telomeric PNA as described above. DNA damage was detected using the γ-H2AX antibody. This was essentially an immuno-FISH protocol which is described below.

Cells were seeded in tissue culture flasks two days prior to experiments and after cells reached 80-90 % confluence, they were trypsinized and 1ml of cell suspension (containing roughly 50,000 cells) was added onto poly-prep slides (Sigma-Aldrich) and placed inside a petri dish (to minimize the infection risk). Cells were left to grow for 24 hours at 37^{o}C in the atmosphere of 10% CO_2. If irradiation of cells was required 5 ml of pre-warmed medium was added into petri dishes before transferring the cells to the irradiation room. All of the procedure was done at room temperature unless stated otherwise. After cells were irradiated with the required dose, slides were incubated for between 30 minutes and 24h at 37^{o}C before further processing. After that slides were rinsed in PBS and fixed in 4% formaldehyde for 15 minutes. Cells were then permeabilized in 0.2%Triton-X in ddH_2O at +4.0^{o}C for 10 minutes followed by blocking with 0.5% BSA (Bovine Serum Albumin) in PBS for 30 minutes and covered with parafilm. One hundred µl of **γ**-H2AX antibody (Upstate)

solution was added (dilution of 1:500 with 0.5% BSA) for one hour in dark, damp conditions after which slides were washed with TBST (Tris-buffered saline tween-20) for 3 minutes twice on a shaker. Then, 100µl FITC secondary anti-mouse antibody was added (diluted 1:400 with 0.5% BSA) for one hour in dark, damp conditions and washed with TBST for five minutes, three times in a dark coplin jar and on an orbital shaker. Cells were fixed again with 4**%** formaldehyde for 20 minutes with no shaking in a dark place and this second fixation prevents bleaching of the fluorescence signals. At this point the slides can be analysed for the presence of γ-H2AX signals if necessary, or the protocol can be continued to detect telomeres. For telomere detection slides were dehydrated with an ethanol series (70%, 90% and 100% concentration) for five minutes each and then air dried. After this, slides were hybridized for two to three minutes at 70° C with PNA telomeric oligonucleotides (CCCTAA)3, labeled with Cy-3 (Applied Biosystems), and left for two hours in dark and damp conditions. Post hybridization washes were performed using 70% formamide for 10 minutes, twice, and then finally washed with TBST for 10 more minutes before adding 15µl Vecta-shield anti-fade DAPI mounting medium (Vector Laboratories). The slides were analysed using the computerized Axioskop 2 Zeiss fluorescence microscope equipped with a CCD camera and MetaSystems software.

2.9 - Reverse Transcriptase Polymerase Chain Reaction (RT-PCR) Analysis

2.9.1 - RNA extraction

RNA extraction was performed using an RNeasy Plus kit (QIAGEN), which provided fast processing and effective purification of RNA from cells. The procedure was carried out according to the manufacturer's instructions (Fig. 2.13 summarises the process). Briefly, approximately 80% confluent cells were trypsinized and collected as a pellet prior to lysis. Cells were disrupted by adding the RLT buffer (guanidium thiocyanate lysis buffer), followed by homogenisation. The homogenised lysate was transferred to a gDNA elimination spin column and centrifuged for 30 second at 1000rpm. One volume of 70% RNA free ethanol was added to the flow-through. The sample was transferred to an RNeasy spin column and centrifuged for 15 second at 1000rpm.

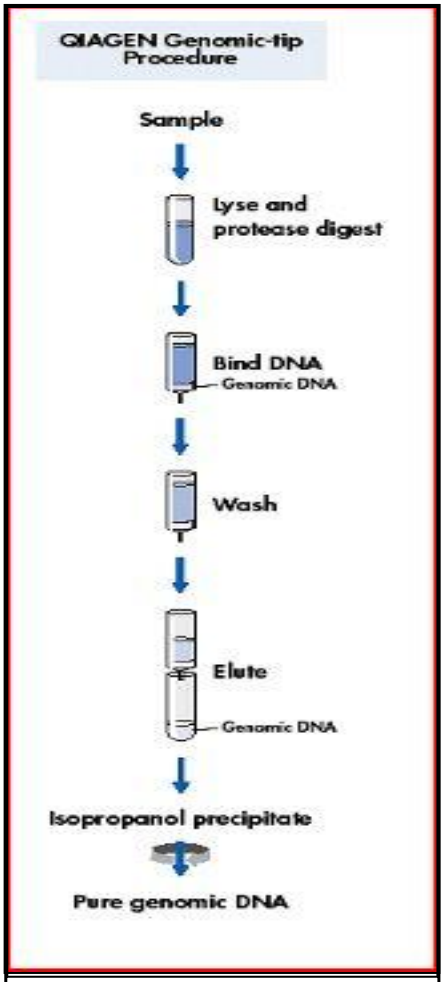

Figure 2.13 - RNA extraction procedure.

Different buffers were added while centrifuging after each addition and discarding the flow-through. Finally, 30µl of RNA-free water was added to the spin column membrane that was centrifuged for 1 minute at 1000rpm. The RNA quantity was measured using the spectrophotometer NanoDrop 2000C (Thermo Fisher Scientific), which enables measuring of 0.5 - 2 µl samples with high accuracy and reproducibility.

The spectrophotometer was blanked using the reference RNA free solution that was placed onto the measurement pedestal, and a reading was taken at 260nm wavelength. The measurement of RNA absorbance took place afterwards. The following table (Table 2.2) demonstrates an example of the reading from the total RNA extraction of one of the experiments.

Table 2.2 - Sample reading from total RNA extraction

Cell line	A260/280 nm ratio	A260/230 ratio	RNA concentration (ng/µl)
HeLa	2.06	2.20	2056.1
U2OS	2.03	2.15	594.1

2.9.2 - First-strand cDNA synthesis with SuperScript III (life technolodgy)

The following components were added to a nuclease-free microcentrifuge tube:

1µg of total RNA (0.49 µl for Hela and 1.68 µl for U2OS)

1µl 0f DNAse I reaction buffer

1 µl of DNAse I Amp grade

RNA-free water (7.51 µl for Hela and 6.32 µl for U2OS)

Final volume 10µL reaction mix

The final mixture volume was incubated at room temperature for 15 minutes. A total of 1 µl of EDTA was added to each sample. The final mixture volume (11 µl) was heated to 65˚C for 10 minutes using a thermal cycler (PTC-225 Peltier). One µl of Random primer and 1 µl of dNTP were added for each sample and the final mixture volume (13 µl) was heated for 5 minutes at 65˚C.

The following components were added to the collected 13 µl reaction mix:

4µl of 5x first strand buffer

1µl of 0.1 M DTT (Dithiothreitol)

1µl of RNAseOUTTM Recombinant RNase Inhibitor (40 units/µl)

1µl of superScriptTM III RT (200 units/µl)

Final volume 20µl reaction mix

The 20µl reaction mix was mixed gently and was heated at 25˚C for 5 minutes. This was followed by incubation for 60 minutes at 50˚C for random primer, followed by 15 minutes at 70˚C to inactivate the reaction. The cDNA sample is now ready to be used as a template for amplification by PCR.

2.9.3 - Primer Design

The DKC1 primers (Table 2.3) were designed using NCBI primer blast software. The GAPDH primers (Table 2.3) were kindly provided by Dr.Mark Pook, Brunel University.

Table 2.3 - Primer sequences for RT-PCR and real-time PCR

Gene Name	Sequence (5' - 3')	Product length
DKC1 (Forward)	GGCGAGTTGTTTACCCTTTGG	102 bp
DKC1 (Reverse)	GCATAATCTTGGCCCCATAGC	
GAPDH (Forward)	GAAGGTGAAGGTCGGAGT	226 bp
GAPDH (Reverse)	GAAGATGGTGATGGGATTTC	

2.9.4 - RT- PCR

Optimizing primer concentration

Conventional PCR reaction was used in order to test the specificity of the primers. Three different concentrations (10µM, 5µM and 2.5µM) of forward and reverse primers were tested to find the optimized primer concentration.

One to 5 µl of cDNA can be used for PCR amplification using PCR Master Mix (Thermo Scientific) (consisting of 15Mm MgCl2). For 21µl reaction the following reagents were added:

1µl of cDNA

1µl of forward primers according to the gene of interest

1µl of Reverse primers according to the gene of interest

18µl of Master Mix

Final volume 21µl

The sample was gently mixed and was placed into a thermal cycler PCR machine that was configured with the following program (Table 2.4):

Table 2.4 - PCR cycle temperature

	Temperature (˚c)	Time	Cycles number
Denaturation	94	2 minutes	1 cycle
Denaturation	94	30 seconds	35 cycles
Annealing	61	30 seconds	
Extention	72	30 seconds	
Extention	72	10 minutes	1 cycle

2.9.5 - Agarose gel electrophoresis

Two percent agarose gel was made using agarose dissolved in 1x Tris acetate EDTA (TAE) buffer solution (Sigma-Aldrich). Before setting the moltened gel into an agarose gel electrophoresis tank, 5µl ethidium bromide (10 mg/ml) was added. The gel was covered with 1x TAE and the PCR samples were loaded into the gel wells. In order to determine the PCR product size accurately, a 1kb ladder was used. The gel was run at 65 V for approximately 1.5 hours. To visualise the PCR results, An Alphaimager under U.V. light was used.

2.9.6 - Real-Time quantitative RT-PCR (Real-Time qRT –PCR)

After the RT-PCR primer optimization was completed, the next step was to test the primer concentration using qRT-PCR. This technique is used to amplify cDNA and simultaneously quantify the cDNA products by utilising the SYBR Green I dye. SYBR Green binds directly to double stranded DNA. Therefore, it is possible to measure the fluorescence emission of the DNA-dye complex and quantify the amount of DNA produced.

The optimal concentration yields the lowest threshold cycle (Ct), determined by the intersection between the amplification curve and the threshold line, and maximum Rn, which is the reported signal of normalised fluorescence. Both Hela and U2OS cell lines were used to test for *DKC1* optimal primers. Three different primer concentrations were examined: 10µM, 5µM and 2.5µM. (Figure 2.14) shows the results obtained while testing the primers optimal concentrations.

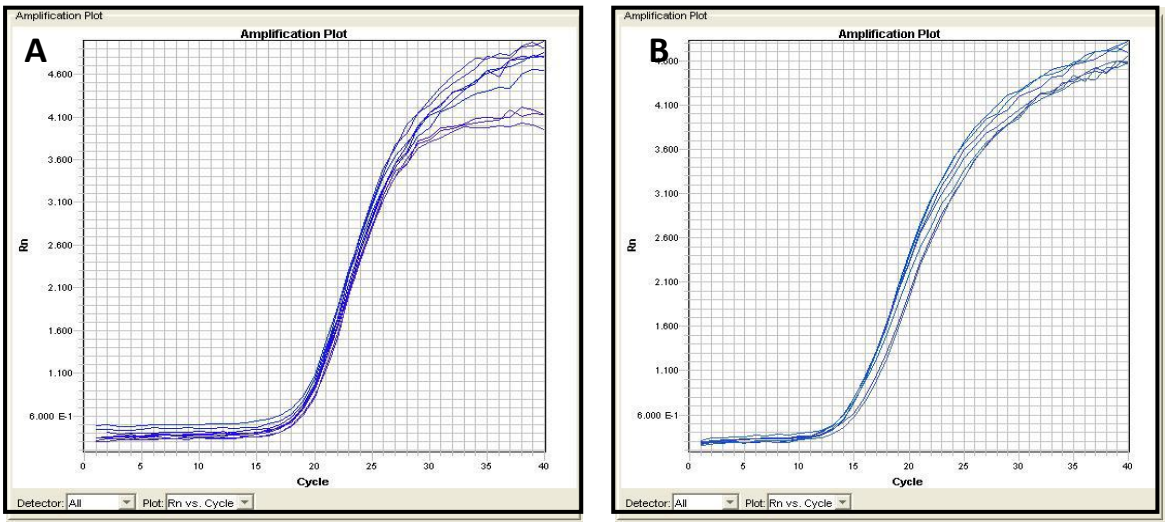

Figure 2.14 - Optimisation of *DKC1* and *GAPDH* primers concentration. The graphs show the amplification curves obtained at three concentrations of DKC1 primers: 10µM, 5µM and 2.5µM (A) Amplification curve for *DKC1* primers at three concentrations 10µM, 5µM and 2.5µM using U2OS cell line. (B) Amplification curve for *GAPDH* primers at 10µM, 5µM and 2.5µM using U2OS cell line.

2.10 - Small interfering RNA (siRNA)

Small interfering RNA (SiRNA) also known as short interfering RNA is a class of double-stranded RNA molecules that interferes with the expression of a specific gene. Since the discovery of RNAi (RNA interference) in 1998 by Fire and Mello using C. Elegans (Fire *et al.* 1998), a whole range of small RNA molecules have been identified including microRNA (miRNA), (siRNA), and Piwi-interacting RNA (piRNA) (Ghildiyal and Zamore 2009). Each class of these RNAs differ in their modes of target regulation, their biogeneses, and in the biological pathways they regulate. RNAi was described by Fire and Mello to be a form of post-transcriptional gene silencing, whereby a ds (double stranded) RNA induces the degradation of homologous endogenous transcript, either reducing or totally inactivating the mRNA transcript of a specific gene (Fire *et al.* 1998). This method of post-transcriptional

gene silencing is transient and the expression of the specific mRNA will revert back to normal in human cells within 7 to 10 days post transfection.

2.10.1 - Effective controls for RNAi Experiment

The selection of the proper controls in any RNAi experiment with an analysis of loss of function (LOF) of a target gene is key to the reliability and effectiveness of the specific RNAi experiment (Huppi *et al.* 2005). There are several criteria that should be met for an acceptable LOF analysis through RNAi experiment for publication that editors of Nature Cell Biology suggested in 2003.

In short these criteria are as follows:

1. Mismatched or scrambled RNA (Also known as non-targeting siRNA)
2. Basic controls: Reduction in the expression level must be measured at the mRNA and protein levels, as well as the functional read outs whenever possible.
3. Quantitative control: A titration of siRNA is recommended to detect the lowest minimal concentration of siRNA for the required effect.
4. Multiplicity control: To be confident in the RNAi data is to demonstrate that the desired effect can be achieved with two or more siRNAs targeted to different sites in the message (mRNA) under study (Hannon 2002; Chen and Xie 2012).

2.10.2 - Re-suspension of siRNA

The siRNA oligonucleotides were purchased from Dharmacon (Thermo Scientific) and were re-suspended according to the manufacturer's recommended protocol. All siRNA

oligonucleotides were delivered in a dry powder form and re-suspended in a siRNA re-suspension buffer provided by the manufacturer (Table 2.5).

Table 2.5 - Summary of controls in RNA Inhibition experiments

Control Type	Function	Product Used
Positive Control	Optimizes and monitors efficiency of siRNA delivery into cells	ON-TARGET GAPDH Control Pool (Silencing GAPDH)
Negative Control	Distinguish between sequence-specific silencing to non-specific effect	None-Targeting (Scrambled RNA)
Untreated Control	Determine the base level of gene expression, as well as viability and phenotype	Cells cultured without any siRNA treatment

All siRNAs were briefly centrifuged in a tube to collect the siRNA pellet at the bottom. According to the amount of siRNA, all the siRNA stock was diluted to a final concentration of 5µM/µl in 5x siRNA re-suspension buffer (Dharmacon), containing 20mMKCl, 6mM HEPES-pH 7.5, and 0.2 mM MgCl2, diluted down to a 1x siRNA buffer with RNase free water (Dharmacon). A total of 1000 µl of 1x siRNA buffer was added to 5nmol siRNA tube to give a final concentration of 5 µm/µl. The solution was resuspended with a pipette three to five times to avoid introducing any bubbles. The solution was left on an orbital shaker set at 200rpm/minute for 30 minutes at RT. Then the solution was briefly centrifuged and the SiRNA concentration was verified using the spectrophotometer

NanoDrop 2000C (Thermo Fisher Scientific). (Table 2.6) summarizes the purity, quality, and total concentration of all siRNAs used in our experiments.

Table 2.6 - Summary of short interfering RNA used in RNAi experiments

siRNA	Company	Stock Quantity Concentration	Working Quantity	A260/280 (>2.0 is pure)
GAPDH	Dharmacon	5 µM	5 nM	2.19
None-Target (Scrambled)	Dharmacon	5 µM	5 nM	2.29
DKC1	Dharmacon	5 µM	5 nM	2.19

2.10.3 - Procedure

U2OS and Hela adherent cells were seeded in T25 flasks. A total of 400,000 cells were added to each flask containing 5ml medium. U2OS and HeLa cells were seeded for 24 hours prior to SiRNA addition. After 24 hours, the medium was replaced. Cells were harvested 48 hrs, 72hrs, 96hrs and 7 days after treatment. This was followed by RNA extraction, cDNA synthesis and knockdown measurement using real-time qRT –PCR. When *DKC1* expression was at its lowest level, H2AX and TIF assay was performed. The schematic below (Figure 2.15) represent the exact experimental procedure used in all siRNA experiments.

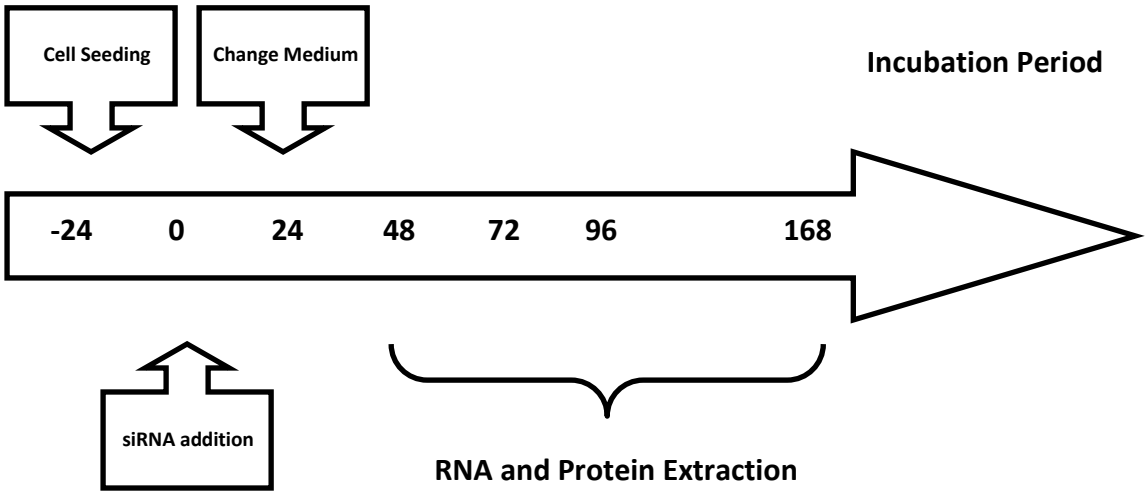

Figure 2.15 - Summary of experimental plan. The long line represents time in hours.

2.11 - Western Blot

Western blot is a technique used to specifically detect and quantify protein from a tissue or cell samples. It uses gel electrophoresis to separate proteins according to size and mobility. Proteins are then transferred to a Polyvinylidene Fluoride (PVDF) membrane in a wet blot conditions. An appropriate primary antibody is used to detect a specific target. Enhanced Chemiluminescent dye is used to detect the Horseradish peroxidase (HRP) conjugated secondary antibody that is bound to the specific primary antibody and the protein of interest is detected on an X-ray film.

2.11.1 - Protein Sample Preparation

Cells were grown to 80-90 percent confluence and the plate was rinsed six times with cold PBS. All the excess liquid was removed and 200µl of RIPA buffer

(Radioimmunoprecipitation assay buffer) and 10µl of 25x protease inhibitor were added for at least 5 minutes onto the plate. Samples were thawed and mechanically sheared ten times using a 1ml syringe and a 23g needle. Samples were collected into Eppendorf tubes and spun at 13,000rpm for 15 minutes. The supernatant was aliquoted and transferred to clean Eppendorf tubes and stored at -20°C.

2.11.2 - Protein Quantification

Each protein in the sample was quantified using a Pierce® BCA Protein Assay Kit (Thermo scientific). Pierce BCA Protein Assay is a detergent-compatible formulation based on bicinchoninic acid (BCA) for the colorimetric detection and quantitation of total protein. The assay was performed according to manufacturer's recommended protocol (Table 2.7). In short, a serial dilution of 0.025mg/ml – 1.5mg/ml of protein standard was made using bovine serum albumin (BSA). This was used to construct a standard curve (Figure 2.16), where all unknown sample protein concentrations were measured against the standard curve.

Table 2.7 - Preparation of diluted BSA standards for BCA analysis

Tube	Volume of dH2O	Volume of BSA	Final BSA concentration
A	**10µl**	**30µl**	**1500µg/ml**
B	**20µl**	**20µl**	**1000µg/ml**
C	**20µl**	**20µl of A**	**750µg/ml**
D	**20µl**	**20µl of B**	**500µg/ml**
E	**20µl**	**20µl of D**	**250µg/ml**
F	**20µl**	**20µl of E**	**125µg/ml**
G	**30µl**	**10µl of E**	**25µg/ml**
H	**40µl**	**–**	**0µg/ml**

A total of 200µl of Working Reagent (BCA protein assay reagent A/B diluted 1:49) was prepared for each sample/standard and added to a new eppendorf tube. A total of 10µl of protein lysate, diluted 1:20 with dH2O, was added to the tubes, followed by a gentle mix. The plate was incubated at 37° C for 30min in an incubator and then allowed to cool at room temperature. The A562 of the standards and protein lysates was then measured using a plate reader (BP800, BioHit). A standard curve was prepared by plotting the blank-corrected measurement for each BSA standard against its concentration. The standard curve was then used to determine the protein concentration of each study sample.

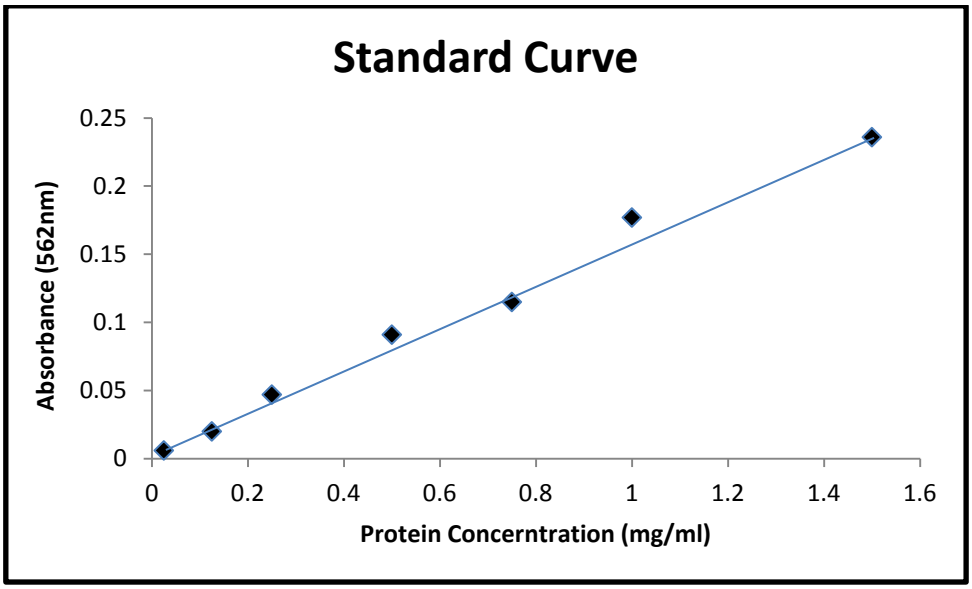

Figure 2.16 - Standard curve used in protein quantification.

2.11.3 - Protein Gel Electrophoresis

Protein lysates were prepared from Hela and U2OS cell lines and the protein concentration determined using BCA assay as previously described. For each sample, approximately 40µg of protein was prepared in 1x working sample buffer to a total volume of 20µl. The lid of the eppendurf tube was pierced and samples were placed at 100°C for 10min to denature the globular structure of the proteins and then put on ice.

Twenty µl of the prepared samples and 10µl of a Precision plus Protein™ standard (Bio-Rad) were added to each well of a ready-made 10**%** precast gel (Bio-Rad). The lower the molecular weight of a protein of interest, the higher the percentage of gel that is required. For example, a 10% gel will be sufficient for the separation of protein of 250 KDalton (kDa) or less. The gel was bought ready-made or was made using the following ingredients:

-3.3ml distilled water (DW)

-4.0ml 30 percent acrylamide mix (protogel EC890)

-2.5ml 1.5M Tris pH 8.8 (36.3g Tris/200ml)

-100µl 10 percent SDS

-100µl 10 percent ammonium persulphate (APS) freshly made

-4.0µl TEMED

The above formula will give a 12**%** gel that is poured into the gel tank plate. The gel tank plate was set up following the manufacturer's protocol. The above gel was loaded immediately onto the gel plate, topped with water for even distribution, and left for 30 minutes to set. The stacking gel was then made with the following reagents:

-1.4ml DW

-330µl 30 percent Acrylamide mix

-250µl 1M Tris pH 6.8 (24.2g Tris/200ml)

-20µl 10 percent SDS

-20µl 10 percent APS

-2µl TEMED

The stacking gel was poured onto the gel (the excess water was blotted off first) and left to set for at least 15 minutes with a separation comb in place. Eventually the comb was removed and 20µl of prepared protein sample was loaded carefully onto each well. The protein marker was normally loaded on the first and last wells. The interior and exterior of the tank was filled with 1x running buffer made with 3.0g (w/v) of tris base, 14.4g (w/v) of glycine, 1g of SDS, and distilled water to 1 litter. The samples were initially run at 100V until proteins were evenly located in the gel and the power was switched to 150V for approximately 45 minutes. The samples were checked regularly to prevent running off of the protein samples.

2.11.4 - Blotting and transfer

Once proteins were separated in the gel based on their size and mobility (heavier proteins move slower and hence were at the top of the gel, whereas smaller proteins move faster and were found near the bottom of the gel), proteins were transferred onto a blotting paper. Polyvinylidine fluoride (PVDF) is a non-reactive membrane that has a non-specific affinity to amino acids. PVDF was activated by soaking in 100**%** methanol for 10 seconds. A sandwich of filter pad, 3mm filter paper, activated PVDF membrane, gel, 3mm filter paper, and filter pad was assembled according to the manufacturer's protocol (Bio-Rad). A small magnetic stirrer was placed in the tank, topped with 1x transfer buffer made with 11.25g (w/v) of glycine, 2.42g (w/v) of tris base, 200ml (v/v) of methanol and distilled water to 1 liter. The blotter was placed inside the tank and the tank was run at 60V for 45 minutes on a magnetic stirrer to create an even distribution of the electrolysis. An ice pack was also placed inside the tank to prevent overheating of the buffer solution.

2.11.5 - Blocking and antibody incubation

Once the transfer of protein from gel onto the PVDF membrane was complete the proteins were blocked with 5% blocking reagent containing 5g (w/v) of semi-skimmed milk (Marvel) in 100ml of Tris buffer saline-Tween (TBST) made with 16g (w/v) of NaCl, 0.2g (w/v) KCl, 3g (w/v) of Tris base, 0.1% (v/v) Tween-20 added to 800ml of distilled water adjusted pH to 7.6, and distilled water added to 1 liter. The membrane was left in 30ml of blocking solution for about one hour on a shaker at room temperature. The milk mixture blocks the unspecific binding of an antibody with the membrane. After one hour of blocking, the membrane was rinsed with TSBT and the primary antibody was added. The primary

antibody was diluted down according to the manufacturer's recommendation and was further optimized by the user. (Table 2.8) below shows all antibodies used in our experiment with optimized dilution ranges.

Table 2.8 - Primary and secondary antibodies used in western blot experiments

Antibody	Manufacturer	Source	Clonality	Dilution
DKC1 Primary	Abcam	Rabbit	Polyclonal	1:1000
DKC1 Secondary	DAKO	Rabbit	Polyclonal	1:2000
Beta-actin Primary	SIGMA	Rabbit	Polyclonal	1:1000
Beta-actin Secondary	DAKO	Rabbit	Polyclonal	1:2000

Primary antibodies were diluted in one in five dilutions in 5% blocking buffer in 1x TBST and added to the membrane overnight on a shaker set at medium pace (200rpm/minute) at 4°C. The following day the membrane was washed four times with 1x TBST for 15 minutes each and incubated with a secondary antibody diluted in one in five dilutions of 5 % blocking buffer on a shaker at RT for a minimum of one hour.

2.11.6 - Protein detection with chemiluminescence

After 1 hour incubation with a secondary antibody the membrane was washed four times in 1x TBST for 15 minutes. Meanwhile ECL plus (Enhanced chemiluminescence) kit (GE Healthcare) was taken out of the fridge and left at RT to warm up. The amount of ECL required for detection was based on the size of the membrane and was recommended by the manufacturer to be of a final volume of 0.125m/cm2 of membrane. The manufacturer's

protocol was consulted for the exact mixture of chemical A and chemical B. As a rule of thumb, 2ml of reagent A was mixed with 50µl of reagent B. That is 1 part of reagent A mixed with 40 parts of reagent B. The ECL mixture was added onto the membrane and covered with Saran wrap for 5 minutes in a dark room. The excess of the ECL was tipped off onto a paper towel, wrapped in the membrane facing down onto a piece of clean Saran wrap and placed in an x-ray cassette.

Unexposed ECL plus hyperfilm (GE healthcare) was put on top of the membrane and the cassette closed and left for exposure for 5 minutes. The x-ray films were developed using an automatic machine (Xograph). The exposure time was assessed accordingly depending on the size of the exposed bands. If the protein bands were faint and could not be visualized then a second film was exposed for a longer period. The ECL chemiluminescence was active for at least one hour.

2.12 - Statistical Analysis

Basic statistical analysis such as descriptive measurements and graphical display were done using Microsoft Excel 2007 software. All t-tests were done at 95 percent significance with α set at 0.05.

Chapter 3 - Interphase Q-FISH

3.1 - Introduction

Mammalian chromosomes are complex structures, which require specialized functional elements for their accurate segregation. One such essential element is the telomere (Blackburn 2000). Telomeres consist of conserved DNA sequences (TTAGGG) and specific proteins. Telomeric DNA sequence and telomeric proteins form a unique structure at the chromosome end that helps preserving chromosomes as single entities. Therefore, all eukaryotes must have appropriate mechanisms to maintain functional telomeres in both somatic and germ line cells (Wong and Slijepcevic 2004).

The main function of telomeres is to protect chromosome integrity and stability. Non-functional telomeres cause end-to-end chromosome fusion and subsequent breakage-fusion-bridge cycles leading to genomic instability (Slijepcevic *et al.* 1996). During the lifetime of a cell, telomeres undergo significant changes. The most important indicator of correct telomere function is telomere length maintenance within the range typical for each species. Telomere length regulation is a complex process that involves interaction of telomeric proteins with telomerase or telomerase-independent mechanisms to maintain telomere length at species-specific levels. Telomere function, which is governed by its structure, most likely requires a specific telomere length (Slijepcevic 2001). To fully understand mechanisms of telomere dynamics and the role of individual molecules that regulate this dynamics, it is necessary to be able to measure telomere length with a high degree of accuracy.

The first method used for telomere length measurements was based on southern blot analysis and it will be referred to as the classical method. The classical method is relatively crude and it can provide an estimate of average telomere length only (Harley

1991). The main uncertainty with measuring telomere length using the classical method comes from the fact that degenerate, telomere-like DNA sequences in the sub-telomeric regions of chromosomes hybridize with the telomeric DNA leading to inaccurate assessment of telomere length. Nevertheless, the classical method was sufficient to provide a rough assessment of average telomere length in the case of human chromosomes (Kipling and Cooke 1990). However, the classical method was non-informative in the case of mouse chromosomes due to large size of mouse telomeres (Blasco *et al.* 1997). Therefore, alternative methods for telomere length measurements had to be invented to overcome disadvantages of the classical analysis.

The best alternative method is quantitative fluorescence *in situ* hybridization (Q-FISH) and its modification based on flow cytometry, known as flow-FISH (Zijlmans *et al.* 1997; Rufer *et al.* 1998). The Q-FISH method uses peptide nucleic acid (PNA) telomeric oligonucleotides as a probe (O'Sullivan *et al.* 2004). PNA probes generate stronger and more specific hybridization signals than the same DNA probes thus eliminating the problem of non-specific hybridization (Zijlmans *et al.* 1997). Furthermore, Q-FISH provides accurate estimate of telomere length in individual chromosome, irrespective of species of origin, with the resolution of 200 bp, while the classical method can be used to estimate average telomere length in some species only. The flow FISH method uses the same principle as the Q-FISH but only measures telomere length in interphase cells and thus it provides an accurate assessment of average telomere length (Volpi and Bridger 2008).

While Q-FISH and flow FISH methods are accurate they have some disadvantages. Q-FISH requires metaphase cells for the analysis. This is not a problem for most cell lines which possess normal growth properties and have a good mitotic index that warrants sufficient

amount of good quality metaphase cells required for Q-FISH. However, cell lines derived from patients with defects in DNA damage response mechanisms show poor growth characteristics in *vitro* and have low mitotic indices which precludes use of Q-FISH for telomere length assessment. Furthermore, the dependence of Q-FISH on metaphase cells makes this method unsuitable for telomere length assessment in tissues. The main disadvantage of the flow-FISH method is associated with the problem of auto-fluorescence. During the flow cytometry analysis each cell type generates a specific degree of auto-fluorescence. This is negligible in the case of lymphocytes and flow-FISH works best with this cell type. All other cell types generate higher degrees of fluorescence, including fibroblasts and epithelial cells, thus complicating the telomere length estimate (Zimonjic *et al.* 2001). Finally, flow-FISH cannot be used for assessment of telomere length in tissue samples.

The easiest approach to eliminate the above problems would be to apply Q-FISH hybridization principles on interphase cells and use digital microscopy to assess telomere length. The use of interphase cells eliminates the Q-FISH metaphase cell requirement. The use of microscopy eliminates the problem of auto-fluorescence specific to flow-FISH. Furthermore, the method based on interphase cells would allow assessment of telomere length in tissues. In this chapter we describe development of our own method to assess telomere length in interphase cells. We will refer to this method as interphase Q-FISH (IQ-FISH). The primary motivation for development of IQ-FISH is the fact that this project is focused on the link between telomere maintenance and DNA damage response. Therefore, the project depends on the use of cell lines from individuals with defective DNA damage response (see next chapters). As indicated above, neither Q-FISH nor flow-FISH can be used for assessment of telomere length in such cell lines. In order to be able to accurately assess telomere length in the above lines, development of IQ-FISH is essential.

3.2 - Results

3.2.1 - Description of cell lines for IQ-FISH development and the rationale

The key requirement for development of IQ-FISH is the availability of cell lines with well defined telomere lengths that can serve as calibration standards. Dr Slijepcevic's group has previously described two mouse cell lines with well defined telomere lengths: L5178Y (LY-R) and L5178Y-S (LY-S) (McIlrath *et al.* 2001). Both cell lines are lymphoblastoid in origin. The LY-R cell line is the parental cell line and it has telomere length of 49 kb as assessed by Q-FISH (McIlrath *et al.* 2001). The LY-S cell line was derived from the LY-R cell line after prolonged in vitro culturing and it shows sensitivity to ionizing radiation due to an unknown molecular defect. Telomere length in the LY-S cell line is estimated by Q-FISH to be in the region of 7 kb (McIlrath *et al.* 2001). Typical metaphase LY-R and LY-S cells after hybridization with telomeric PNA oligonucleotides are shown in (Figure 3.1).

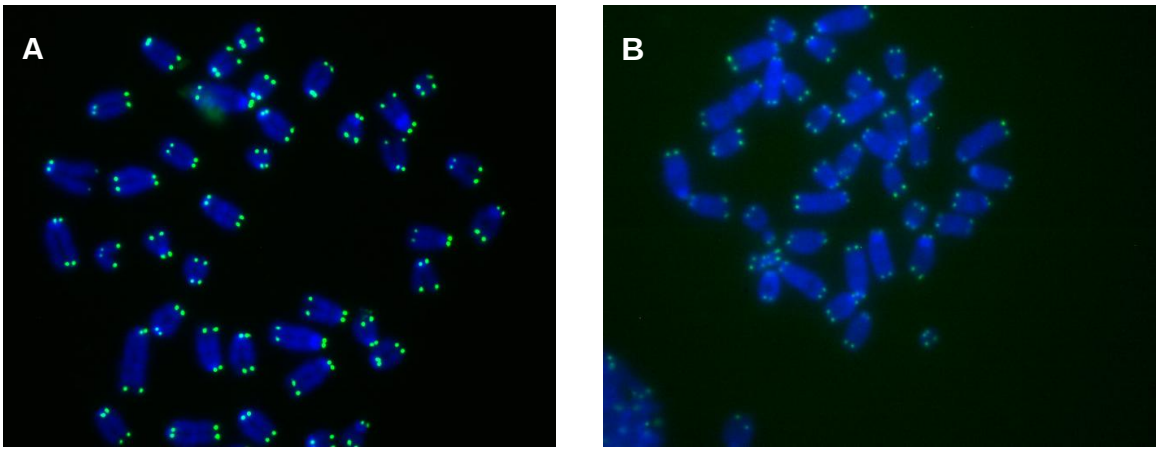

Figure 3.1 - Digital images of metaphase cells derived from mouse cell lines LY-R (A) and LY-S (B) after hybridization with telomeric PNA oligonucleotides.

Dr Slijepcevic's group has previously described a modified Q-FISH protocol for assessment of telomere length using these two cell lines as calibration standards (Wong and Slijepcevic 2004). Q-FISH typically requires the calibration procedure in order to ensure reproducibility of results. The main variables in Q-FISH experiments include variability in microscope fluorescence bulb intensity which changes over time and the length of exposure time required to acquire images of telomeric signals which will be subject to fluorescence intensity measurement using appropriate software packages. To be able to control these variables the originally described Q-FISH protocol used fluorescence beads of defined size as internal calibration standards for each microscopy session (Zijlmans *et al.* 1997). Instead of fluorescence beads LY-R and LY-S cell lines were used as calibration standards (Wong and Slijepcevic 2004). Fluorescence intensity of LY-R and LY-S telomeres were measured on five different dates and statistically analysed to test for reproducibility of measurements. The resulting data-set constituted historical telomere fluorescence values for the calibration protocol. Each time telomere fluorescence was measured in a new sample, telomere fluorescence in LY-R and LY-S cells were also measured and compared the resulting LY-R/LY-S values against LY-R/LY-S historical values to generate correction factors. These correction factors were applied to the values of telomere fluorescence intensity of samples under investigation (Wong and Slijepcevic 2004). It has been shown that this approach works well using different cell lines (Wong and Slijepcevic 2004). Therefore, we reasoned that a similar approach, based on the LY-R/LY-S interphase cell ratios as calibration standards may be appropriate for developing the IQ-FISH protocol.

The rationale for development of IQ-FISH, consisting of 4 tasks, is shown in Figure 3.2. In brief, the starting point is identification of the suitable software package for telomere fluorescence intensity measurement in interphase cells (Task 1), followed by comparison of

this software against the already verified software for metaphase Q-FISH (TFL TELO) (Task 2) and extensive measurement of telomere fluorescence using LY-R and LY-S cells to determine optimal conditions and calibration correction factors (Task 3). Finally, the software will be tested using a set of human and mouse cell lines with known telomere length (Task 4). Each task is described in detail below.

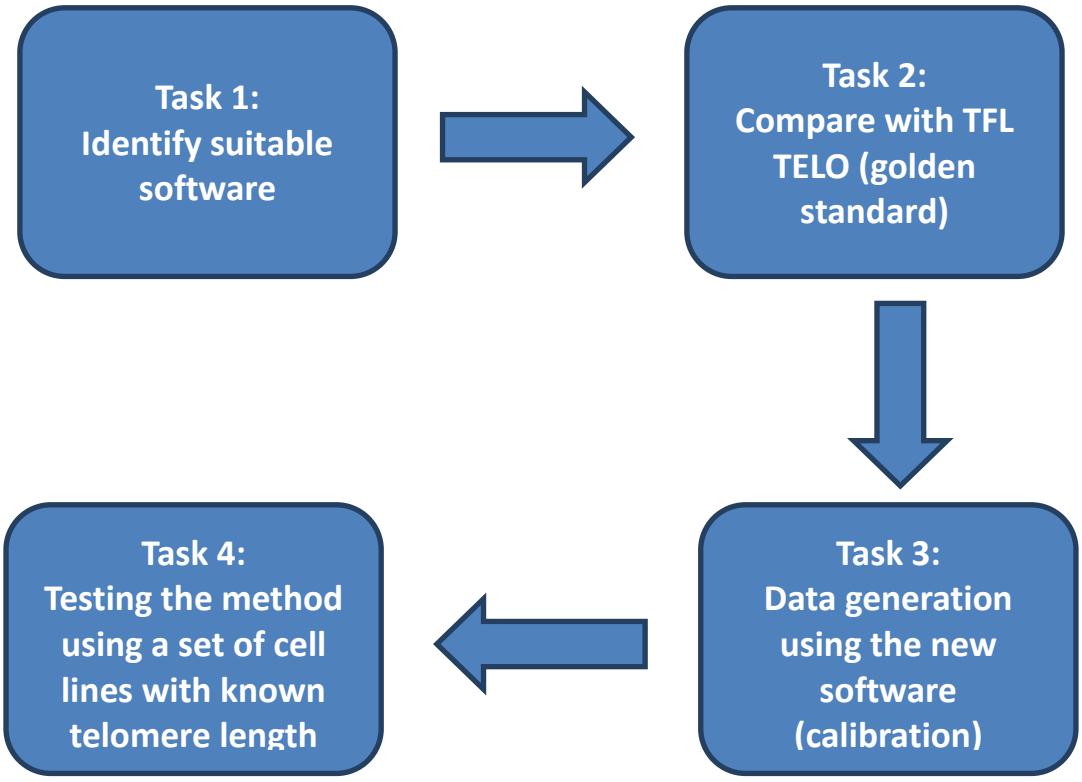

Figure 3.2 - The rationale for development of IQ-FISH.

3.2.2 - Task 1: Identify suitable software

The aim of Task 1 was to identify a suitable software package that can accurately measure telomere fluorescence intensity in interphase cells. This was a major task and we could not do this without external help. In order to fulfil this task we approached Mr

Michael Elis from Digital Scientific, Cambridge, UK. This company has a track record in developing software packages for various FISH applications. Mr Elis recommended the IPLab software package, which has extensive analysis and measurement options and provided basic instructions as to how to measure fluorescence intensity in interphase cells. We then carried out extensive testing of various functions of this software to confirm that it is suitable for our purpose.

We started with testing the so called “image segmentation” function. This function defines the area of the image in which fluorescence intensity will be measured. In practice this means selecting exclusively cell nuclei as areas of interest and ignoring the rest of the image. A typical segmented image with cell nuclei stained in green is shown in (Figure 3.3).

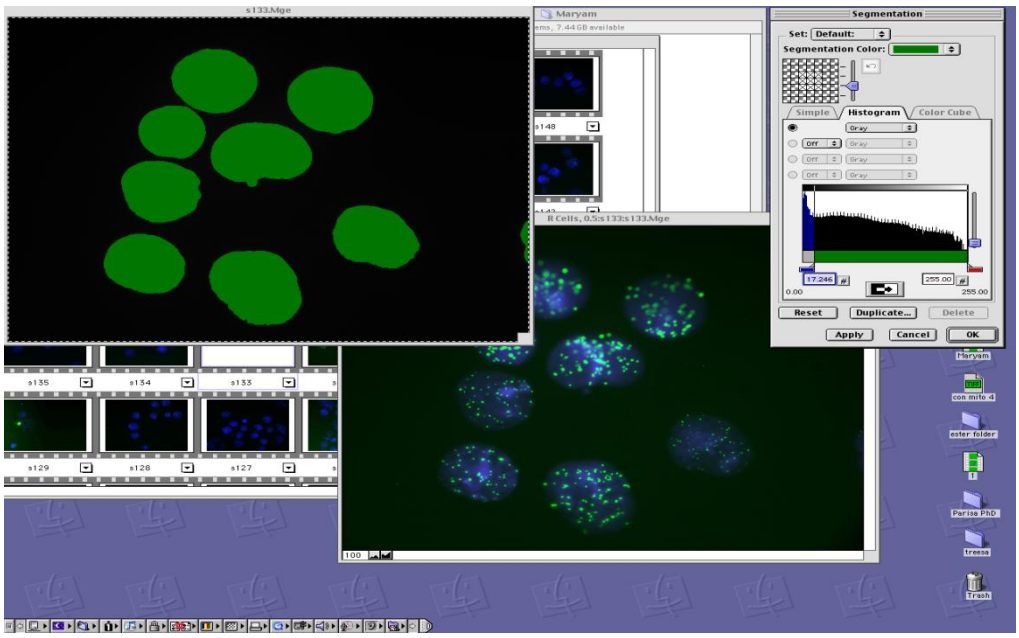

Figure 3.3 - A typical segmented image with cell nuclei stained in green.

This analysis has shown that the "segmentation function" is appropriate and that it always accurately selects the cell nuclei as areas of interests. The selection tool is adjustable and it allows a precise definition of area of interest.

We assessed other functions of the software including the "background removal" option, "measurement" options and display of results. The "background removal" option is important as it allows subtracting the fluorescence background noise from the actual fluorescence values. This function is performed using the so called "Pixel arithmetic" procedure which is shown below (Figure 3.4). Our analysis has shown that the "Pixel arithmetic" option shows a good degree of reliability and reproducibility.

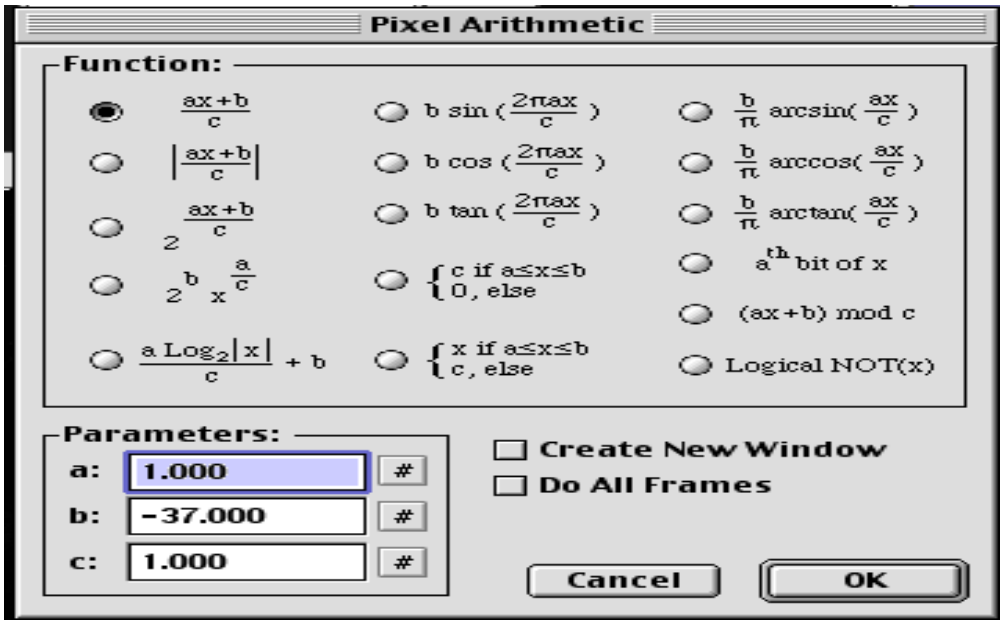

Figure 3.4 - A snapshot of the mathematical manipulations behind the process of telomere fluorescence intensity measurement.

Finally, we examined the "measurement" function and whether results of fluorescence intensity measurements are presented in an appropriate manner. The

software option called “Set Measurements”, which is shown below (Figure 3.5), provides a range of statistical parameters that completely describe results. Signal intensity measurement in most software packages is carried out through densitometry analysis. IP-Lab provides this analysis (see Figure 3.7) in the form of “mean” values or “sum” values. The “mean” value represents an average telomere fluorescence intensity value for each analysed cell, whereas “sum” values represent the sum of all pixels due to telomeric signals in a single cell. For our purpose the “mean” values are probably most suitable as this is equivalent to average telomere length. The “sum” values cannot distinguish between diploid and polyploidy cells. Nevertheless, in the analysis below (see Task 3) we will provide values for both “mean” and “sum”. Therefore, the assessment of various options within the IP-Lab software indicates that this software package is suitable for IQ-FISH.

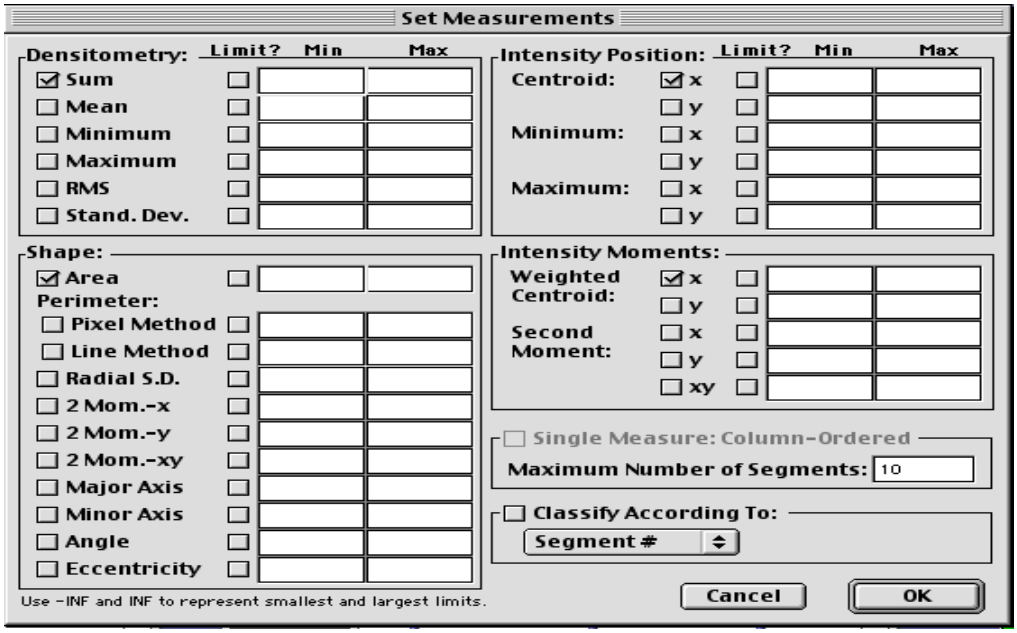

Figure 3.5 - Snap shot of the software option called set measurements, which provides a range of statistical parameters that completely describe results**.**

3.2.3 - Task 2: Compare with TFL TELO (Golden Standard)

The next task (see Figure 3.2) was to compare the accuracy of fluorescence intensity measurement using the IP-LAB software against the software that can be considered "the golden standard" for Q-FISH. The software in question is TFL-TELO developed by Prof. Peter Lansdorp and his colleagues (Zijlmans *et al.* 1997). This is the most extensively used piece of software for metaphase Q-FISH. Using this software and the classical Q-FISH calibration procedure relying on fluorescence beads, Dr Slijepcevic's group estimated that telomeres in LY-R cells are 7 times longer than in LY-S cells (49 kb and 7 kb respectively) (McIlrath *et al.* 2001). Furthermore, using a calibration protocol relying on LY-R/S cells, Dr Slijepcevic's group estimated that the difference in telomere fluorescence intensity between the same cell lines is 6.9 times (Wong and Slijepcevic 2004) which is in good agreement with the initial measurement.

In order to determine whether the IP-Lab software shows a similar resolution we used two approaches. The first approach aimed to analyse telomere fluorescence intensity in LY-R and LY-S cells using the IP-LAB software and compare the resulting LY-R/LY-S ratio against ratios already published by us using the TFL TELO software for these cell lines (McIlrath *et al.* 2001; Wong and Slijepcevic 2004). The second approach aimed to analyse telomere fluorescence using the IP-LAB software in a set of human fibroblast cell samples from Fanconi anemia patients and corresponding control patients. A previous study indicated that cells from Fanconi anemia patients show significantly shorter telomeres than cells from corresponding control patients when analyzed by the TFL TELO software (Callen *et al.* 2002), suggesting that this could be a good test for the accuracy of the IP-LAB software.

In both approaches, that will be described below, we used a single exposure time of 0.5 sec and analysed telomere fluorescence intensity in a single microscopy session for LY-R/LY-S cells and human fibroblast samples respectively to reduce the chances of microscope lamp variability. On recommendation of Mr Michael Elis we used a 63 X objective for acquiring images of interphase cells. This objective was used throughout the course of this project for the purpose of telomere fluorescence intensity measurements. Telomere fluorescence was expressed as unmodified fluorescence. The term "unmodified fluorescence" refers to the fact that no internal control was used to correct for variations associated with fluorescence microscopy. The proper procedure for internal controls and calibration will be described in Task 4. It is important to stress that if the measurements are carried out in a single microscopy session variations between samples due to microscope lamp variability will be negligible.

Representative images of LY-R and LY-S interphase cells are shown in (Figure 3.6). As can be seen below there is a clear difference in the strength of fluorescence signals between LY-R and LY-S cells.

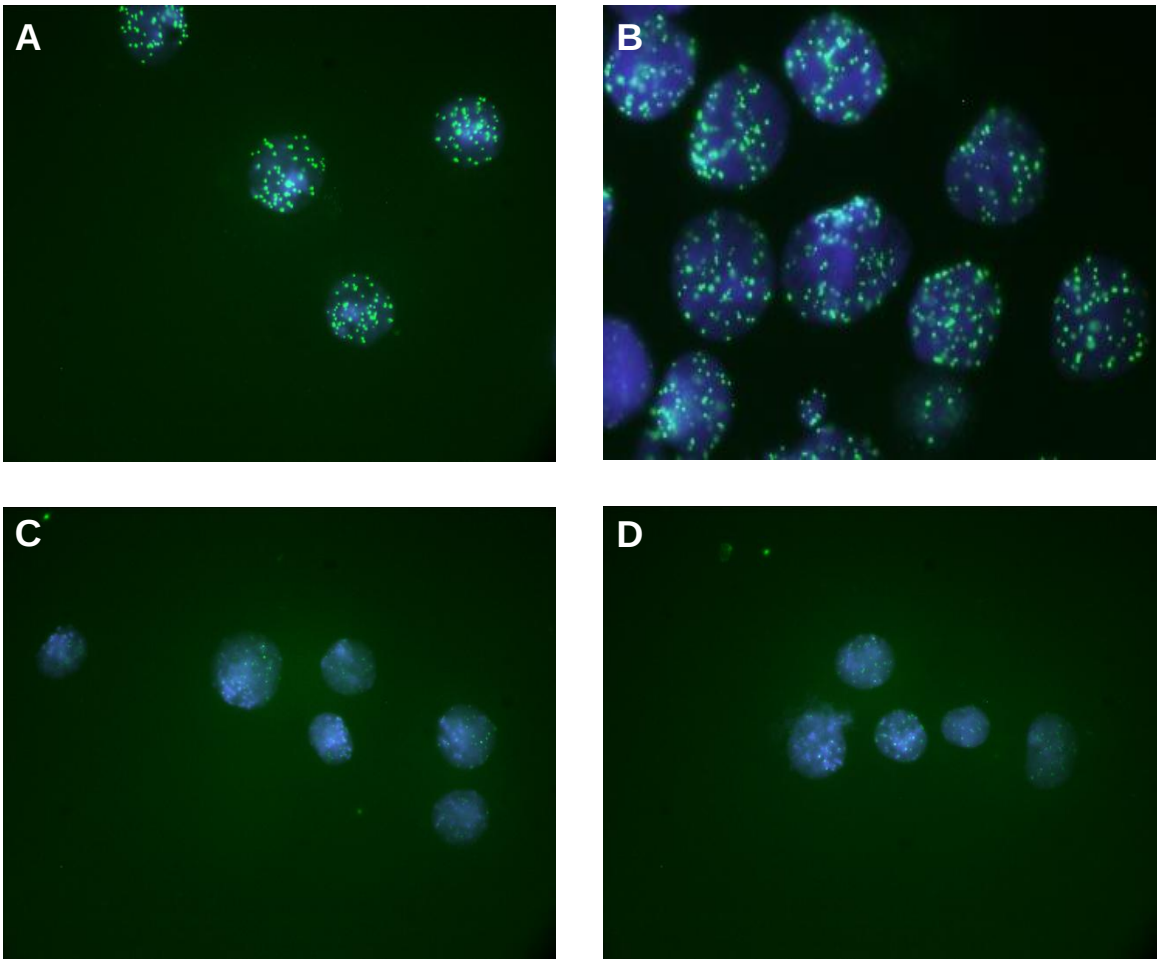

Figure 3.6 - Digital images of LY-R (A, B) and LY-S (C, D) interphase cells after hybridization with telomeric PNA oligonucleotides.

Results of the telomere fluorescence intensity measurement in LY-R and LY-S cell lines using the IP-LAB software are shown in (Figure 3.7).

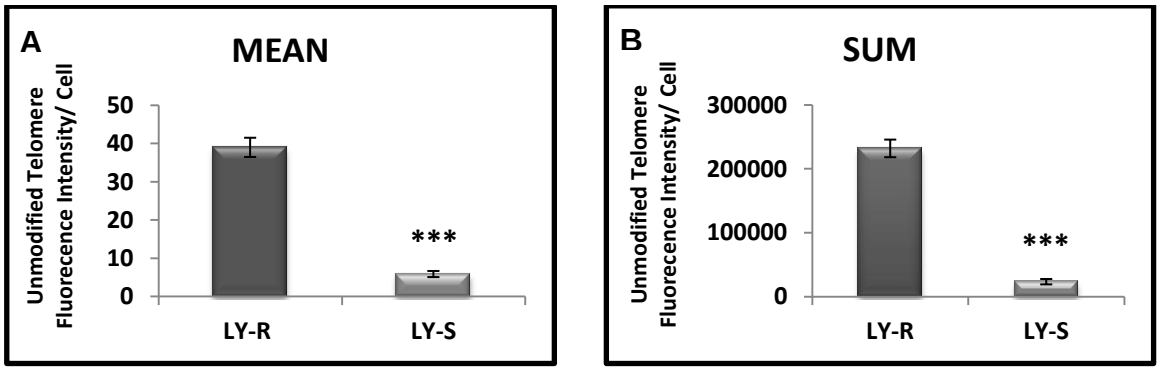

Figure 3.7 - Mean Unmodified Telomere Fluorescence Intensity measurements in LY-R and LY-S per cell (A). SUM Telomere Fluorescence Intensity measurements in LY-R and LY-S per cell. ***=P<0.001, Error bars represent SEM.

Our analysis revealed that the average telomere fluorescence, expressed as the mean unmodified fluorescence in IP LAB is 6.6 times greater in LY-R than in LY-S cells (Figure 3.7 A). This is in good agreement with the ratios of 6.9 and 7 observed earlier for these cell lines using the TFL TELO software (McIlrath *et al.* 2001; Wong and Slijepcevic 2004). As stated above, we have also analyzed the sum unmodified fluorescence in both cell lines. This analysis revealed that LY-R cells have 9.9 times greater fluorescence than LY-S cells (Fig 3.7 B). This was expected as the "sum" measurement option cannot distinguish between diploid and polyploid cells and therefore resulting fluorescence represents an overestimate in comparison with the results generated using the "mean" measurement option.

We next analyzed telomere fluorescence in samples from Fanconi anemia which is a rare, inherited blood disorder that lead to bone marrow failure and control patients. Samples represented fibroblast cell cultures and they were provided by Dr Gordana Joksic, Vinca Institute, Belgrade, Serbia. Fanconi anemia samples were from 4 children diagnosed with Fanconi anemia, complementation group D2 (FANCD2) with average age 8±5 years. Samples from healthy age-matched children were used as controls (Joksic *et al.* 2012).

Analysis of individual samples revealed a tendency of control samples to show greater telomere fluorescence than Fanconi anemia samples (Figure 3.8). When the average fluorescence for each group of patients was calculated it was clear that cells from Fanconi anemia patients showed lower telomere fluorescence (21.20) than cells from control individuals (40.70). Thus, our results are in line with the previous study employing the TFL TELO software (Callen *et al.* 2002).

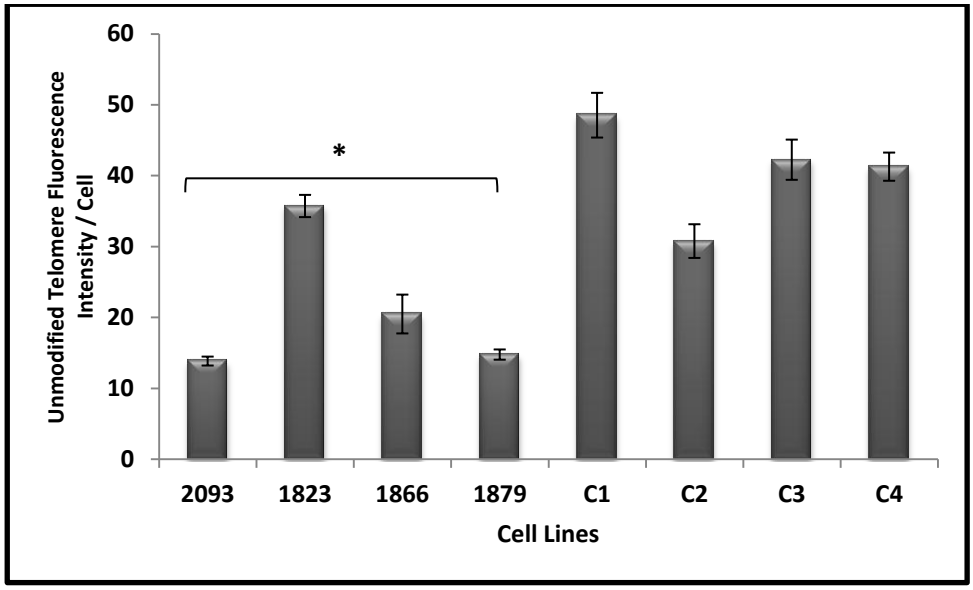

Figure 3.8 - Telomere fluorescence in control and Fanconi anemia patient cells. C1-4 are samples representing control patients. Samples 2093, 1823, 1866 and 1879 are cells from children diagnosed with Fanconi anemia FANCD2 complementation group (Joksic *et al.* 2012). *=P<0.05, Error bars represent SEM.

Therefore, based on the above two approaches, we conclude that the IP-Lab software shows a similar resolution as the TFL-TELO software and that we can proceed to Task 3 in development of the IQ-FISH protocol.

3.2.4 - Task 3: Data generation using the new software (calibration)

The next task was to determine the optimal conditions for measuring telomere fluorescence intensity in interphase cells and generate a data-set of measurements which will serve as the basis for creating correction factors. These factors will provide the basis of our calibration procedure the purpose of which is to ensure consistency of fluorescence intensity measurements.

Since the major variable in measuring telomere fluorescence by microscopy is exposure time during image acquisition, we selected three exposure times including 0.1, 0.2 and 0.5 sec, in order to determine which exposure time will give us the difference between the two cell lines, LY-R and LY-S, that is closest to the difference between the same cell lines obtained by the TFL-TELO software (McIlrath *et al.* 2001; Wong and Slijepcevic 2004). Furthermore, we performed measurements on 5 different occasions in order to ensure reproducibility of results. Each measurement was done in a single microscopy session lasting no longer than 1 h. Results of this analysis are shown in (Figure 3.9). As explained above, we measured 2 parameters: the “mean” and the “sum”.

MEAN **SUM**

A: Session 1

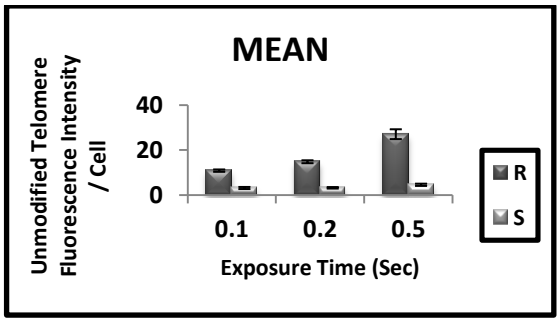

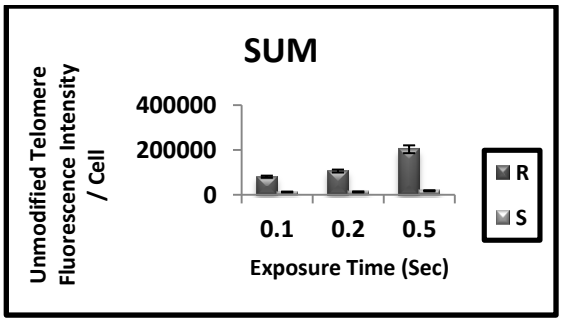

B: Session 2

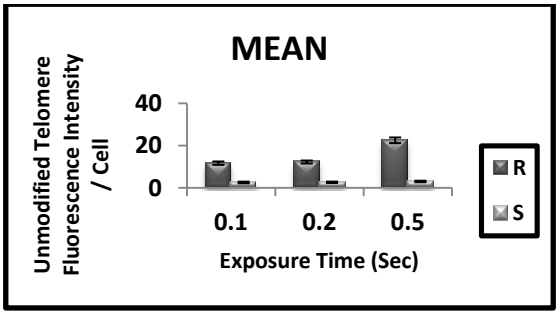

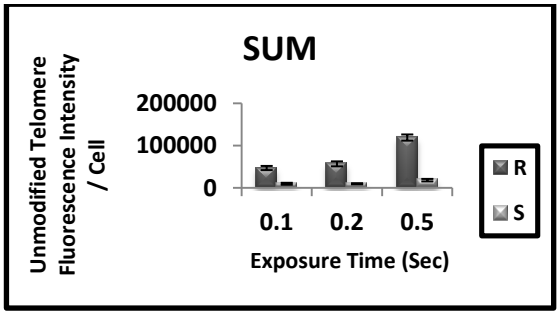

C: Session 3

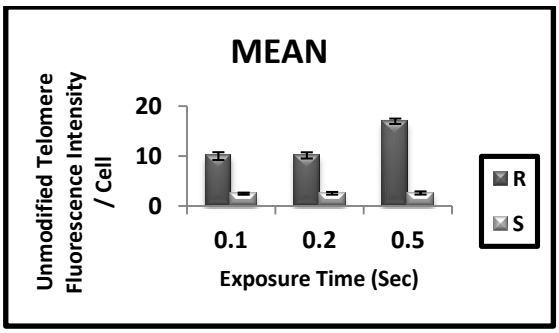

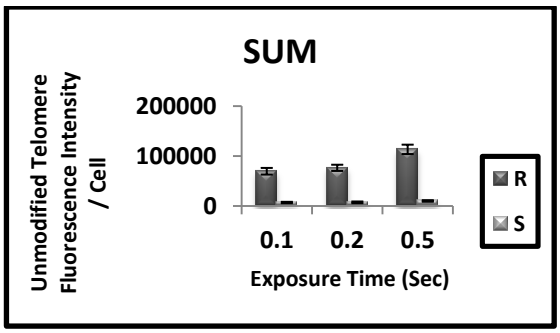

D: Session 4

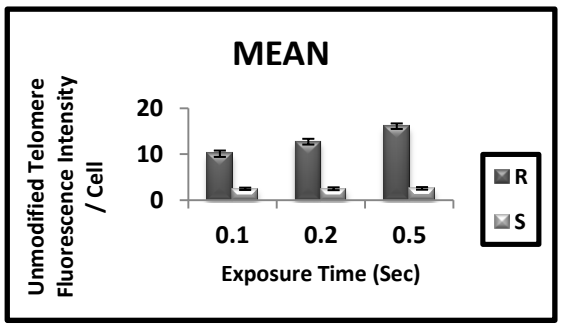

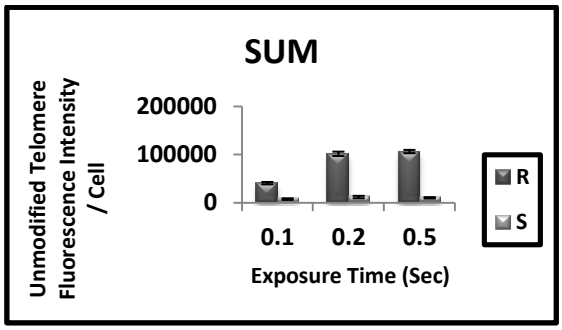

E: Session 5

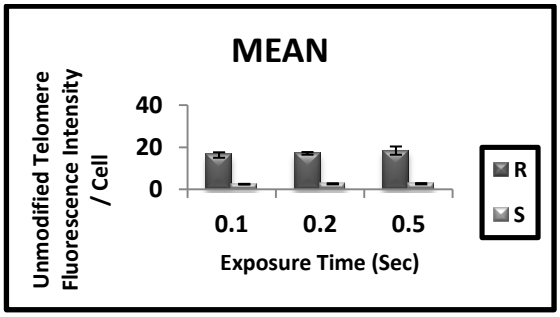

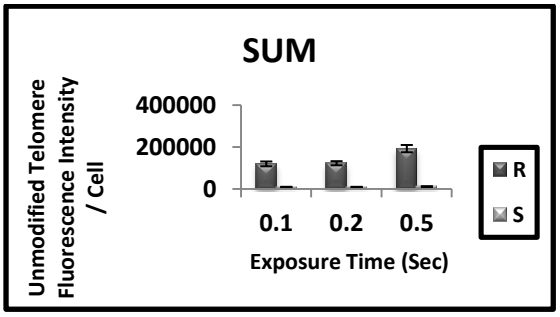

F: Average

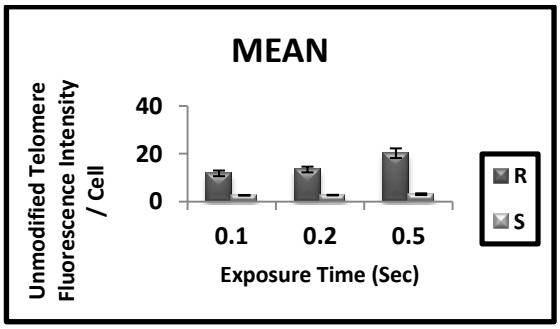

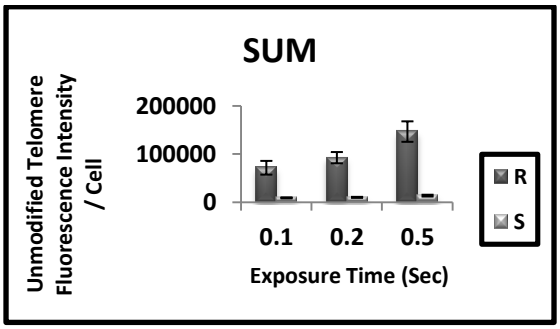

Figure 3.9 - (A–E) Unmodified Telomere fluorescence in mouse lymphoma LY-R and LY-S cells observed at five different sessions. (**F**) Unmodified Mean and Sum telomere fluorescence values in LY-R and LY-S cells at five different sessions.

As can been seen from (Figure 3.9) the fluorescence intensity generally increases with the length of exposure time. This is an additional confirmation of the IP-Lab accuracy as the good quality software is expected to detect the dependence between the fluorescence signal intensity and the length of exposure time.

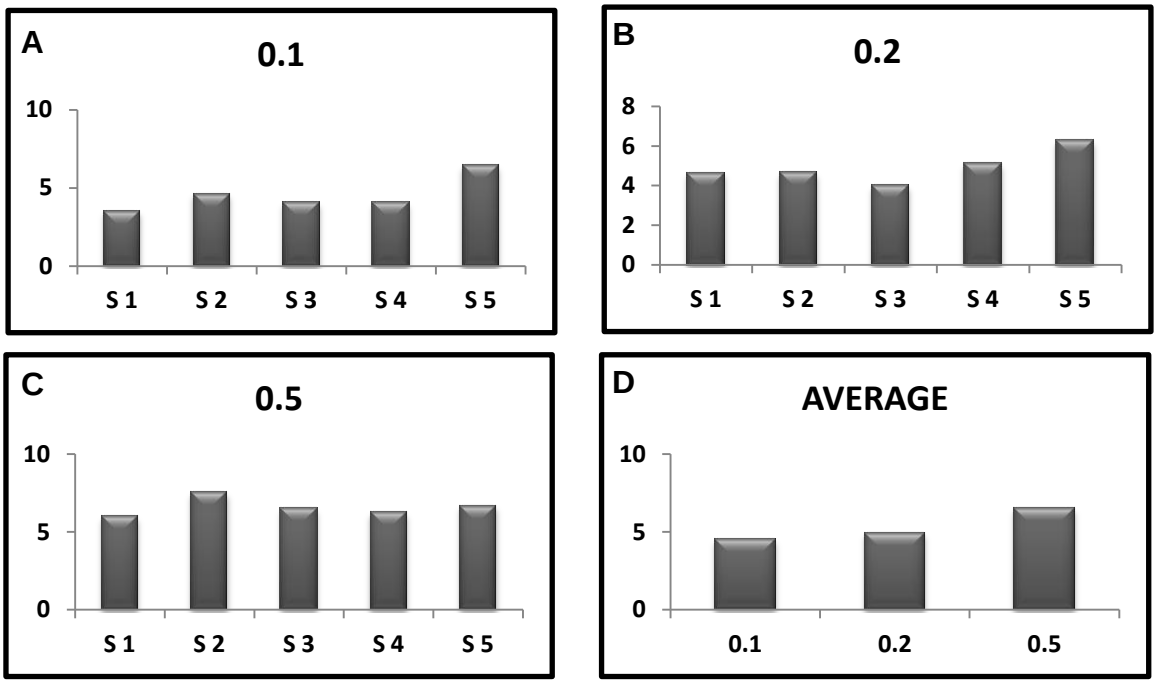

Figure 3.10 - Ratios between telomere fluorescence in LY-R and LY-S cells at 0.1(A), 0.2 (B), 0.5(C) exposure time and total average (D).

Analysis of ratios between telomere fluorescence in LY-R and LY-S cells at each exposure time is shown in (Figure 3.10). The lowest ratio was observed at the exposure time of 0.1 second (A) and the highest ratio at the exposure time of 0.5 sec (C). The ratio of 6.5 observed at the exposure time of 0.5 sec (D) corresponds well with the published ratios of 6.6 and 7 generated using metaphase Q-FISH based on the TFL-TELO software. Therefore, we conclude that the optimal exposure time for IQ-FISH is 0.5 sec and this exposure time will be used in all future experiments.

To provide information about variability of telomere fluorescence between individual cells a histogram is presented in (Figure 3.11). This histogram indicates a greater degree of variation in LY-R cells relative to LY-S cells which is in line with published information (Cabuy *et al.* 2005), thus further indicating the accuracy of the IP-LAB software.

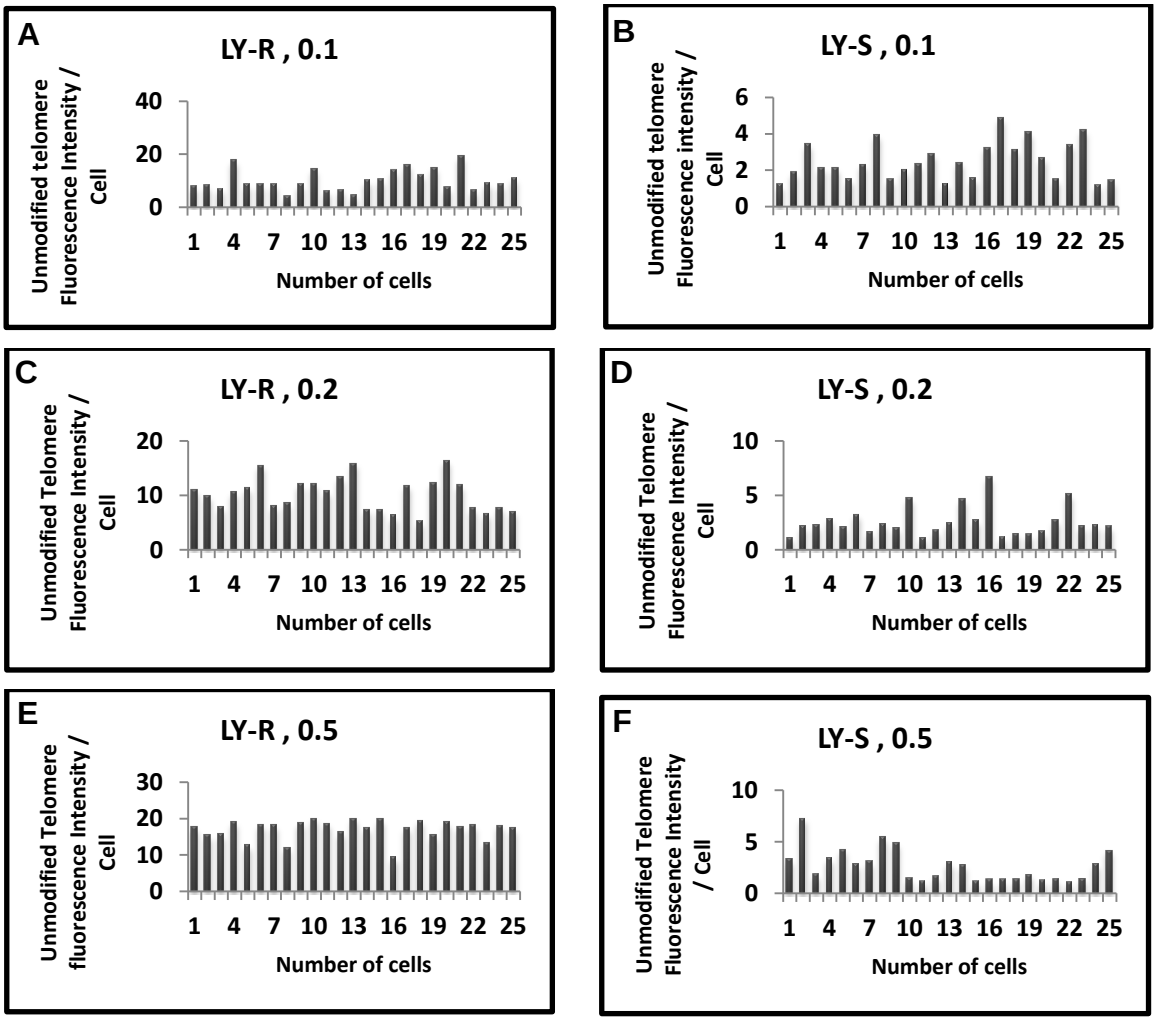

Figure 3.11 - Histogram indicates a greater degree of variation in LY-R cells relative to LY-S cells.

Having established the optimal exposure time for IQ-FISH based on 5 measurement sessions the next step was to established criteria for the calibration procedure. As indicated above, Q-FISH requires internal standards as a basis for correcting variations in microscope

lamp intensity. We thought that correction factors based on ratios between fluorescence intensity observed in LY-R and LY-S cells will serve our purpose well. The basic idea is to use the 5 measurements presented in (Figure 3.9) as a standard against which all measurements will be compared. For example, each time a new sample is analyzed by Q-FISH, fluorescence intensity of LY-R and LY-S cells will be measured again and compared against the standard based on 5 measurements presented in (Figure 3.9). This will generate correction factors that will be applied on unmodified fluorescence of the sample under investigation. The full procedure for generating correction factors is outlined below.

The values of telomere fluorescence in LY-R and LY-S cells generated during the 5 measurement sessions, which represent the standard for generating correction factors (CFs), are labelled $FL_{LY\text{-}R}$ and $FL_{LY\text{-}S}$. Each time a new sample is analysed images of at least 25 LY-R and LY-S cells will be acquired in order to obtain internal controls and these are labelled $FL_{LY\text{-}R(exp)}$ and $FL_{LY\text{-}S(exp)}$. The correction factors will be generated using the following formulas:

$CF1 = FL_{LY\text{-}R} / FL_{LY\text{-}R(exp)}$

$CF2 = FL_{LY\text{-}S} / FL_{LY\text{-}S(exp)}$.

The final correction factor, CF, is the mean of CF1 and CF2. To express telomere fluorescence of a sample under investigation we will use the following formula:

$CCFL = CF \times FL_X$.

In this formula CCFL represents Corrected Calibrated FLuorescence and FL_X represents unmodified fluorescence of the sample under investigation.

3.2.5 - Task 4: Testing the method using a set of cell lines with known telomere lenght

Having established the accuracy of the IP-LAB software (Task 2), the optimal exposure time and calibration procedure including the procedure for generating CFs (Task 3), we next tested the above protocol on 4 cell lines with relatively well characterized telomere length.

First, we used two human cell lines: HeLa and U2OS. HeLa is a frequently used cell line and it is originating from the cervical carcinoma (Van Simaeys *et al.* 2010). It is known that the HeLa cell line has the robust telomerase activity (Harrington *et al.* 1997). The U2OS cell line is also a cancer cell line originating from a sarcoma. The U2OS cell line belongs to a group of cell lines that lack telomerase activity and maintains telomere length by the alternative mechanisms also known as ALT (Alternative Lengthtening of Telomeres) most likely based on recombination (Zhu *et al.* 2004). Telomerase positive cancer cell lines like HeLa usually have stable average telomere length that is significantly shorter than the average telomere length in the ALT positive cell lines like U2OS (Fan *et al.* 2009). ALT positive cell lines are characterized by a highly variable telomere length with some chromosomes showing almost complete lack of telomeric DNA sequences but other chromosomes having unusually long telomeres, significantly exceeding the maximum telomere length observed in human cells (Cesare and Reddel 2008).

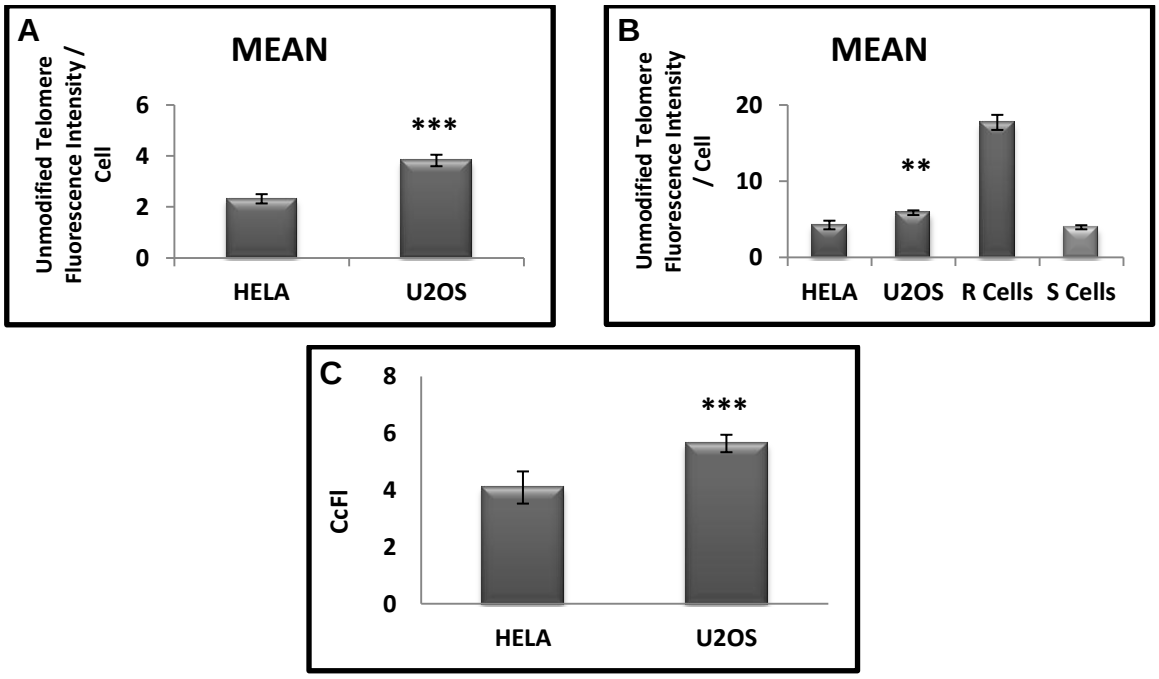

Figure 3.12 - Telomere length analysis of Hela and U2OS cell lines (A) Unmodified fluorescence observed in HeLa and U2OS cells (B) Unmodified fluorescence relative to LY-R and LY-S internal controls ($FL_{LY\text{-}R(exp)}$ and $FL_{LY\text{-}S(exp)}$) (C) CCFL for the Hela and U2OS cell lines**.** **=P<0.01, ***=P<0.001, Error bars represent SEM.

Results of this analysis are presented in (Figure 3.12). (Figure 3.12A) shows unmodified fluorescence observed in HeLa and U2OS cells, (Figure 3.12B) shows this unmodified fluorescence relative to LY-R and LY-S internal controls ($FL_{LY\text{-}R(exp)}$ and $FL_{LY\text{-}S(exp)}$) and (Figure 3.12C) shows CCFL for the two cell lines. As expected, U2OS cells showed significantly greater telomere fluorescence than HeLa cells. It is interesting to note that LY-S cells, previously estimated to have telomere length of 7 kb (McIlrath *et al.* 2001), have almost exactly the same unmodified fluorescence as HeLa cells (Figure 3.12B). Telomere length of 7 kb is a typical average telomere length for a human cell line (McIlrath *et al.* 2001). Therefore, these results are in line with published observations. Furthermore, U2OS cells show approximately 60% greater telomere fluorescence than HeLa cells (Figure 3.12B),

which is again in line with published information indicating that ALT cells have significantly longer telomeres than telomerase positive cells (Cerone *et al.* 2001).

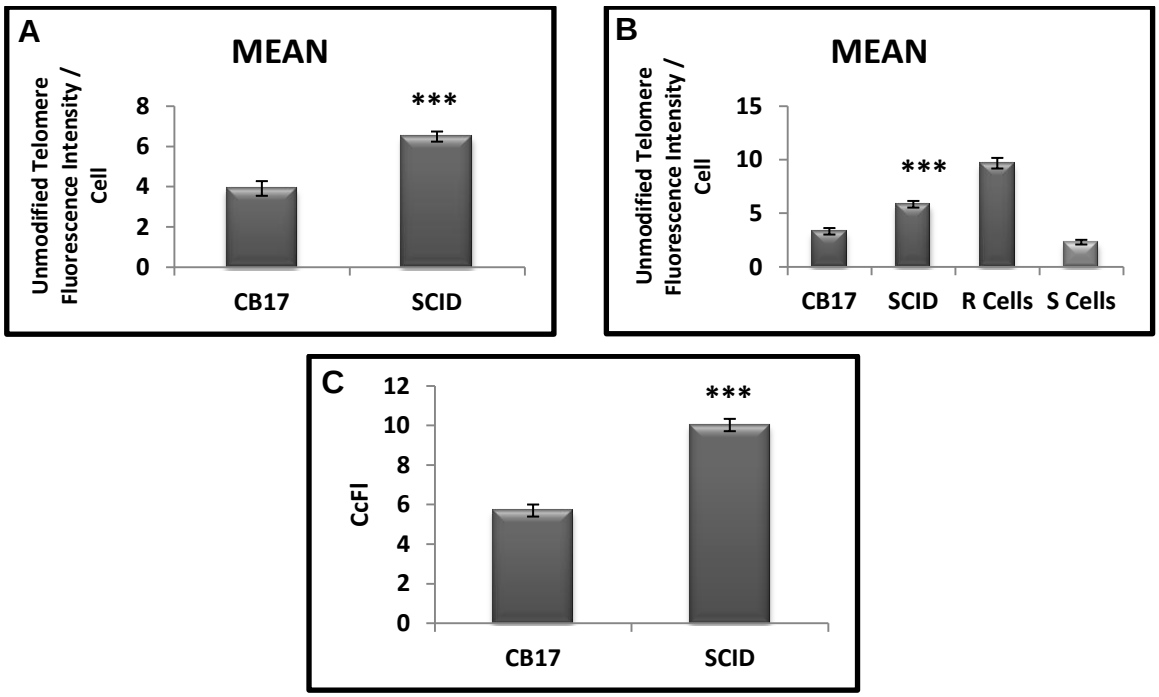

Figure 3.13 - Telomere length analysis of CB17 and SCID cell lines (A) unmodified telomere fluorescence in the CB17 and SCID ell lines (B) Unmodified fluorescence relative to LY-R and LY-S internal controls ($FL_{LY\text{-}R(exp)}$ and $FL_{LY\text{-}S(exp)}$) (C) CCFL for the CB17 and SCID cell lines. ***=P<0.001, Error bars represent SEM.

We also measured telomere length in two mouse cell lines CB17 and SCID (Figure 3.13). The SCID cell line has been shown previously to have ~ 2 times longer telomeres than the CB17 cell line (Wong and Slijepcevic 2004). In line with this, our results show that the unmodified telomere fluorescence in the SCID cell line is ~ 1.65 greater than the same in the CB17 cell line (Figure 3.13A). After applying the calibration procedure, as shown in (Figure 3.13B) and (Figure 3.13C), it is clear that both cell lines have telomere lengths in a range typical of mouse cells i.e. greater than the LY-S cell line which is probably a minimum telomere length for a mouse cell line and far greater than telomere fluorescence observed in human cell lines HeLa and U2OS (Figure 3.12). Taken together, these results indicate that

our IQ-FISH protocol based on the use of the IP-LAB software and the described calibration procedure shows a resolution and consistency comparable to the classical Q-FISH protocol.

3.3 - Discussion

Telomere replication and chromosome end protection are crucial for maintenance of genome integrity (Blackburn 1991; van Heek *et al.* 2002). Telomere maintenance is closely linked with cellular and organismal ageing and it appears to be a key determinant of the replicative capacity in vertebrate somatic cells. In addition, evidence exists to show that telomere shortening is an early contributor to human tumorigenesis. (O'Sullivan *et al.* 2002). This is consistent with the hypothesis that telomere dysfunction provokes chromosomal instability which in turn promotes carcinogenesis (Artandi *et al.* 2000; Hackett *et al.* 2001). Finally, there is increasing evidence that telomere maintenance is linked with DNA damage response mechanisms (Yasaei and Slijepcevic 2010). In order to understand the role of telomeres played in these three biological processes, namely ageing, carcinogenesis and DNA damage response, it is essential to develop accurate methods for measuring telomere length, as this is a robust indicator of telomere function. A number of methods for measuring telomere length have been described including Southern blot, Q-FISH, Flow-FISH, q-PCR and STELA (single telomere length analysis) (Lansdorp *et al.* 1996; Oexle 1998; Rufer *et al.* 1998).

Of all these methods Q-FISH is probably the most sensitive technique for measuring telomere length. Q-FISH explores the advantage of PNA based probes in terms of hybridization efficiency over their DNA equivalents. As a result, Q-FISH can measure telomeres in each individual chromosome with the resolution of 200 bp (Zijlmans et al.,

1997), something that cannot be achieved by any other technique. The most common protocol for Q-FISH is based on the calibration procedure employing plasmids, which carry variable numbers of telomeric TTAGGG repeats and fluorescence beads of specific size (Zijlmans *et al.* 1997; Samper *et al.* 2000; Goytisolo *et al.* 2001; McIlrath *et al.* 2001). In this protocol telomere fluorescence is expressed in telomere fluorescence units (TFUs) where each unit corresponds to approximately 1 kb of telomeric DNA. It has been shown previously that telomere length in LY-R and LY-S cells is ~ 48 and ~ 7 kb, respectively as measured by the above Q-FISH protocol (McIlrath *et al.* 2001).

The aim of this project is to investigate the link between telomere maintenance and DNA damage response. In order to achieve this it is essential to use human or mouse cell lines with defective DNA damage response pathways. Such cell lines usually have defective proliferative potential and are characterized by various problems in cell cycle regulation leading to a poor mitotic index which precludes the use of Q-FISH as a way of measuring telomeres in these cell lines. The alternative would be to use Flow-FISH, a modified Q-FISH method based on flow cytometry that measures average telomere length in interphase cells. However, Flow-FISH works poorly with all types of adherent cells such as fibroblasts or epithelial cells because of the problem associated with auto-fluorescence in these cell lines (Baerlocher *et al.* 2006). It is important to note that most DNA damage response defective cell lines used in this project are adherent cell lines. Therefore, we needed to develop a protocol for telomere length measurement in DNA damage response defective cell lines that will not be affected by their poor proliferative potential. We could not rely on other methods such as q-PCR or STELA (only measures telomeres in one chromosome at a time).

We reasoned that a microscopy-based method capable of accurately measuring telomere fluorescence, which is equivalent to telomere length, in interphase cells would be

a suitable solution. This would eliminate (a) the problem associated with the poor mitotic index in DNA damage response defective cell lines which precludes the use of Q-FISH and (b) the problem of auto-fluorescence in adherent cell lines which precludes the use of Flow FISH. We call this method IQ-FISH. The method only requires a small number of virtually any cell type (<100) and it has the resolution typical of Q-FISH i.e. it is able to detect as little as 200 bp of telomeric DNA repeat sequence.

We have developed and verified the IQ-FISH techniques in 4 steps described earlier (see Figure 3.2). The initial tests using two mouse lymphoma cell lines, LY-R and LY-S, have shown that IQ-FISH is able to detect the difference in average telomere length between these lines to a similar degree as the conventional Q-FISH method (Figure 3.7). The difference in telomere length reported for these two cell lines was either 6.9 or 7 times depending on the Q-FISH calibration method used (McIlrath *et al.* 2001; Wong and Slijepcevic 2004). Our IQ-FISH method generated the difference of 6.6 times between the lines which is in good agreement with Q-FISH results (Figure 3.7). It is important to stress that telomere lengths in LY-R and LY-S cells vary to a certain degree, typically 5-10%, with each cell cycle (Cabuy *et al.* 2004). Therefore, the small difference between Q-FISH and IQ-FISH results is expected. Furthermore, we have shown that IQ-FISH is capable of detecting subtle differences in telomere length between fibroblast cell lines originating from Fanconi anemia and control patients (Figure 3.8) that was reported in an earlier study (Callen *et al.* 2002). This is probably the best criterion for accuracy of our IQ-FISH method as the differences between individual human cells lines are much subtler than between mouse cell lines.

In these two initial verification steps we have not used any calibration method. The FISH based fluorescence intensity measurements require calibration in order to ensure

reproducibility of results over time. For example, the microscope fluorescence bulb, which typically has a 200 h lifespan, will generate much higher telomere fluorescence values when fresh installed than when it reaches the end of its operational time. The difference can be in the region of 50% or more (Slijepcevic, unpublished observations). However, the relative difference between telomere fluorescence of, for example, LY-R and LY-S cell lines remains the same. Therefore, calibration serves to eliminate differences in measurements over time. In the original Q-FISH protocol calibration was performed using fluorescence beads of constant size (Zijlmans *et al.* 1997). Alternatively, Wong and Slijepcevic (2004) used LY-R and LY-S cells as calibration standards as these cell lines show reproducible differences in their telomere fluorescence intensities over time (Cabuy *et al.* 2005). We have decided to use LY-R and LY-S cell lines for our calibration method in the same way as reported by Wong and Slijepcevic (2004). Using this method we have also determined the optimal exposure time for IQ-FISH which was 0.5 sec (Figure 3.10). Overall, this procedure allowed us to generate CCFL for each sample and ensured that results of telomere fluorescence measurements will be the same irrespective of the age of microscope fluorescence bulb owing to the fact that LY-R and LY-S cells are measured simultaneously with each sample and generated values for these lines corrected against historical values typical for these lines (see pages 20-21 for details).

In the last verification step (Figure 3.12 and Figure 3.13) we have put our IQ-FISH method to the full test using 2 human cell lines and 2 mouse cell lines that had known relative telomere lengths, including the above calibration protocol (Figures 3.12 and Figure 3.13). The human HeLa cell line has telomere length typical of human carcinoma cell lines which is in the region of 2-3 kb (Zhu *et al.* 2004). On the other hand, the U2OS cell line, which is a human osteosarcoma cell line that maintains telomere length by the ALT mechanism (as opposed to

telomerase in HeLa cells) shows, on average, longer telomeres than typical human carcinoma cell lines (Jegou *et al.* 2009). This difference is clearly identifiable by IQ-FISH (Fig 3.12). Furthermore, the difference between the two mouse cell lines, CB17 and SCID, observed by IQ-FISH (Fig 3.13) is similar to the published difference between these lines which is approximately 40% (Wang and Slijepcevic 2004).

Another test that can be used to assess the accuracy of IQ-FISH is the comparison between human and mouse cell lines. The CB17 mouse cell line has telomere length typical of human cells i.e. in the region of <10 kb (Wong and Slijepcevic 2004). This is clearly the case as evidenced by similarity in telomere fluorescence between the CB17 and HeLa cell lines which differ only by 20% (Figs 3.12 and 3.13). Similarly, mouse LY-S cells have telomere length typical of human cells lines (McIlrath *et al.* 2001). This is clearly evident in Figs 3.12 and 3.13 in which LY-S cells show telomere fluorescence similar to HeLa and CB17 cell lines.

In conclusion, we have developed a method, termed IQ-FISH, for accurate identification of average telomere length in interphase cells. This method requires a small number of cells (<100) and it is a method of choice for estimating telomere length in cell lines with a poor proliferative capacity as explained above.

Chapter 4 - Effects of BRCA2 on telomere maintenance

4.1 - Introduction

In the previous chapter we have described development of IQ-FISH method with a view of studying the interplay between telomere maintenance and DNA damage response. There is a strong body of evidence suggesting that telomere maintenance mechanisms and DNA damage response mechanisms are functionally related. At least 17 proteins involved in DNA damage response have been reported to affect telomere maintenance either through effects on telomere length or function (for review see Slijepcevic 2006). Selected examples include proteins such as Ku and DNA-PKcs involved in DNA double strand break (DSB) repair by non-homologous end joining (NHEJ) (Bailey *et al.* 1999), a protein involved DNA damage signalling, ATM (Hande *et al.* 2001), the MRN complex consisting of MRE11, RAD50 and NBS proteins responsible for DSB sensing (Zhu *et al.* 2000) and the ERCC1/XPF protein responsible for nucleotide excision repair (NER) (Zhu *et al.* 2003). It is essential to understand the interplay between telomere maintenance and DNA damage response as this may be helpful for understanding the role of telomeres played in clinically relevant processes such as carcinogenesis and ageing (Aubert and Lansdorp 2008). The key to this is the analysis of human or murine cell lines that have specific defects in DNA damage response genes. In general, any such cell line will show some sort of defect related to the cell cycle regulation that eventually lead to an altered proliferative potential in comparison with relevant normal control cell lines. Assessing telomere length, as one of the key marker of telomere function, by techniques such as Q-FISH, which requires a reasonable mitotic index for high quality metaphase preparation essential for this technique, is practically impossible because of the altered cell cycle regulation in DNA damage response defective cells. Therefore, development of IQ-FISH was essential for this project as this enables us to

assess average telomere length, quickly and accurately, even in the cell lines with the most severe growth delays. Other advantages of IQ-FISH from the perspective of this project are discussed in the previous chapter.

Having established a method for an accurate assessment of telomere length in DNA damage response defective cells (Chapter 3) we are now in the position to combine this analysis with the analysis of DNA damage response mechanisms in the same cell lines with a view of assessing the degree of functional interplay between telomere maintenance and DNA damage response. In this project DNA damage response in any cell line will be analysed using a well established DNA damage marker, a phosphorylated form of histone H2AX or γ-H2AX (Yuan *et al.* 2010). Furthermore, a technique called TIF (Telomere dysfunction Induced Foci) assay enables the direct assessment of DNA damage at telomeres by combining simultaneous visualization of sites of DNA damage (through γ-H2AX) and telomeres (through either telomeric PNA sequence or an antibody that binds telomeric proteins) in interphase cells. This technique will also be combined with IQ-FISH and the classical γ-H2AX assay to examined telomere maintenance in DNA damage response defective cells.

The aim of this chapter is to focus on BRCA2, a DNA damage response protein involved in the HR (homologous recombination) pathway (Venkitaraman 2001). Interestingly, recent studies have revealed that BRCA2 affects telomere maintenance (Badie *et al.* 2010; Sapir *et al.* 2011; Bodvarsdottir *et al.* 2012). BRCA2 interacts with telomeres during S and G2 phases of the cell cycle and this mediates access of RAD51, an HR protein, to telomeres (Badie *et al.* 2010). An array of telomere dysfunction phenotypes was noted in the presence of defective BRCA2. This includes telomere shortening, telomere fragility, TIFs and increased frequencies of T-SCEs (Telomere Sister Chromatid Exchanges) (Badie *et al.* 2010; Bodvarsdottir *et al.* 2012). Therefore, BRCA2 is probably the first major protein that

has a direct involvement in human cancer with a clear role in telomere maintenance. This could be relevant for understanding the role of BRCA2 in breast tumorigenesis and also developing novel therapeutic approaches.

BRCA2 and telomere dysfunction are both associated with chromosome instability and cancer susceptibility. Cells which carry mutated BRCA2 protein are genetically unstable, display structural chromosome abnormalities such as triradials and quadriradials and show poor proliferative potential (Yu *et al.* 2000; Desmaze *et al.* 2003). This point effectively illustrates the validity of the approach to develop a technique that can effectively measure telomere length in poorly proliferating cells i.e. IQ-FISH (Chapter 3).

We analysed telomere length and function, as well as DNA damage response, in lymphoblastoid cell lines originating from *BRCA2* carriers (+/-) and also a single fibroblast cell line from a patient with bi-allelic mutations in *BRCA2* (-/-). Our results show lack of correlation between DNA damage response and telomere maintenance in heterozygous cell lines but a clear positive correlation in the homozygous cell line.

4.2 - Results

4.2.1 - Interphase Quantitative Fluorescent in situ hybridization (I-QFISH) analysis of normal and heterozygous *BRCA2* cell lines

We started by analysing telomere length in lymphoblastoid cell lines from two *BRCA2* mutation carriers. Both cell lines were purchased from the Coriell Cell Repository.

The GM14622 cell line was from a patient with a constitutive *BRCA2* mutation (frameshift mutation 6503delTT in exon 11), leading to a truncation at codon 2099 (Coriell

2009). The GM14170 cell line was from a patient with a constitutive *BRCA2* mutation (1bp deletion at nucleotide 6174 in exon 11) resulting in a frameshift beginning at codon 1982 and terminating at codon 2003 (Coriell 2009). The GM0893 lymphoblastoid cell line from a normal individual was used as a control. A total of 50 interphase cells per cell line were analysed by IQ-FISH to determine the mean telomere length of each cell line as described in the previous chapter. Our analysis revealed that both *BRCA2* defective cell lines (GM14622 and GM14170) showed shorter telomeres than the control cell line (GM00893) (Figure 4.1). GM14622 cells showed ~ 1.5x shorter telomeres relative to the control cell line (P=0.13) and GM14170 cells showed ~ 3x shorter telomere (P<0.001) compared to the control cell line. The GM14170 cell line had shortest telomeres (Figure 4.1).

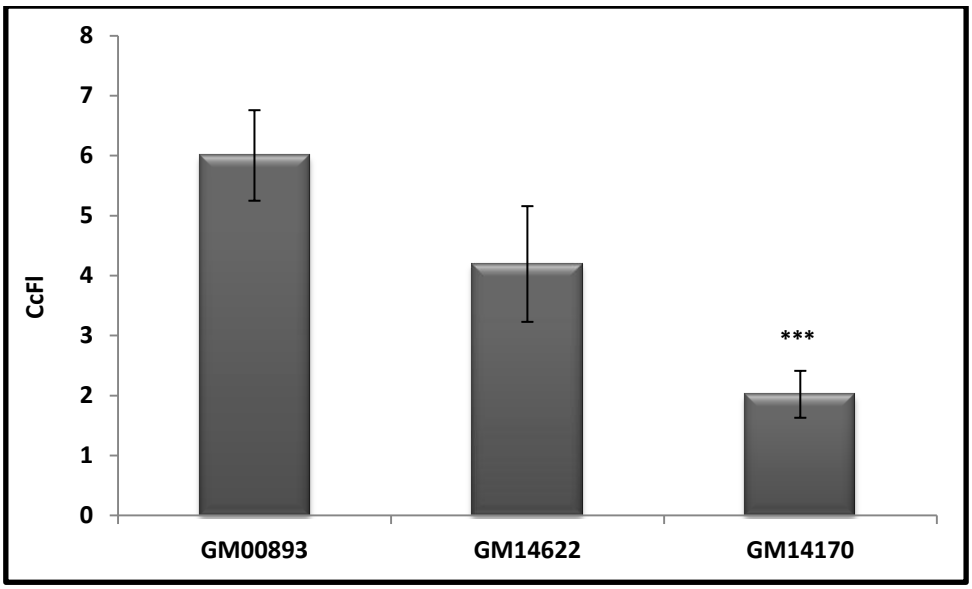

Figure 4.1 - Corrected calibrated fluorescence (CcFl) in *BRCA2* defective cell lines relative to the control cell line. *** = P<0.001, Error bars represent SEM.

4.2.2 - DNA damage kinetics in normal and heterozygous *BRCA2* cell lines using Image stream

Given the significantly shorter telomeres in cell lines from two *BRCA2* carriers relative to the control cell line (Figure 4.1) there is a chance that this could affect telomere function and thus indirectly affect DNA damage response in these cell lines. Therefore, we next analysed DNA damage response mechanisms in the above three cell lines with a view of assessing whether any potential DNA damage response defect could be related to telomere dysfunction.

DNA damage can be assessed by a variety of methods in mammalian cells. The most commonly used method for this purpose in our laboratory is the γ-H2AX test. Phosphorylated H2AX (γ-H2AX) facilitates recognition and repair of DNA double strand breaks (DSBs) which occur as a result of exposure to DNA damaging agents such as ionizing radiation. Staining of irradiated cells by the γ-H2AX specific antibody reveals nuclear foci that are readily observable microscopically in a dose response manner. This test requires adherent cells which are typically grown on coated microscope slides prior to induction of DNA damage. Induced DNA damage is then assessed by immunocytochemical analysis over time to construct DNA repair kinetics curves. However, lymphoblastoid cell lines grow in suspension and they are not suitable for the classical γ-H2AX test. Instead, we used a relatively new approach to analyse DNA repair kinetics in these cell lines based on the ImageStraem apparatus (for details see Material and methods). The Amnis ImageStraem is essentially an apparatus that combines features of a flow cytometer and a low power fluorescence microscope. Amnis' imaging flow cytometry automatically and objectively accumulates high number of individual cell images (in their thousands), quantifies the foci

due to DNA damage detectable by the γ-H2AX-specific antibody in these cells and determines dose response kinetics faster and easier than the conventional microscopy (Bourton *et al.* 2012).

Irradiated cells were analysed by ImageStream using advanced masking techniques that identify the punctate staining of DNA damage foci. Morphological measurements involved in this analysis include object shape, size, and punctate fluorescence spot counting emphasizing the advantages of quantitative multiparametric image analysis on large numbers of cells provided with the ImageStream.

A Control

Double Positive

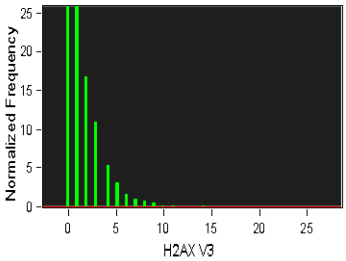

Population Statistics

Population	Count	%Gated
Double Positive & Focus & Single Cells	2690	100

H2AX V3

Population	Mean
Double Positive & Focus & Single Cells	1.65

B 30 Min

Double Positive

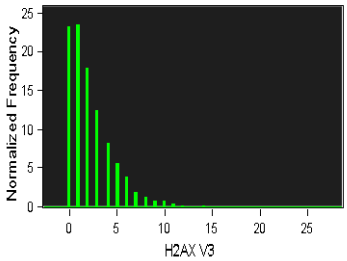

Population Statistics

Population	Count	%Gated
Double Positive & Focus & Single Cells	5377	100

H2AX V3

Population	Mean
Double Positive & Focus & Single Cells	2.29

C 5 hrs

Double Positive

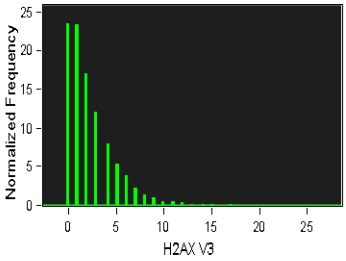

Population Statistics

Population	Count	%Gated
Double Positive & Focus & Single Cells	8449	100

H2AX V3

Population	Mean
Double Positive & Focus & Single Cells	2.37

D 24hrs

Double Positive

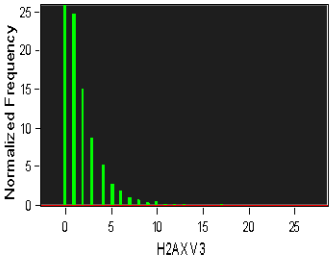

Population Statistics

Population	Count	%Gated
Double Positive & Focus & Single Cells	7891	100

H2AX V3

Population	Mean
Double Positive & Focus & Single Cells	1.63

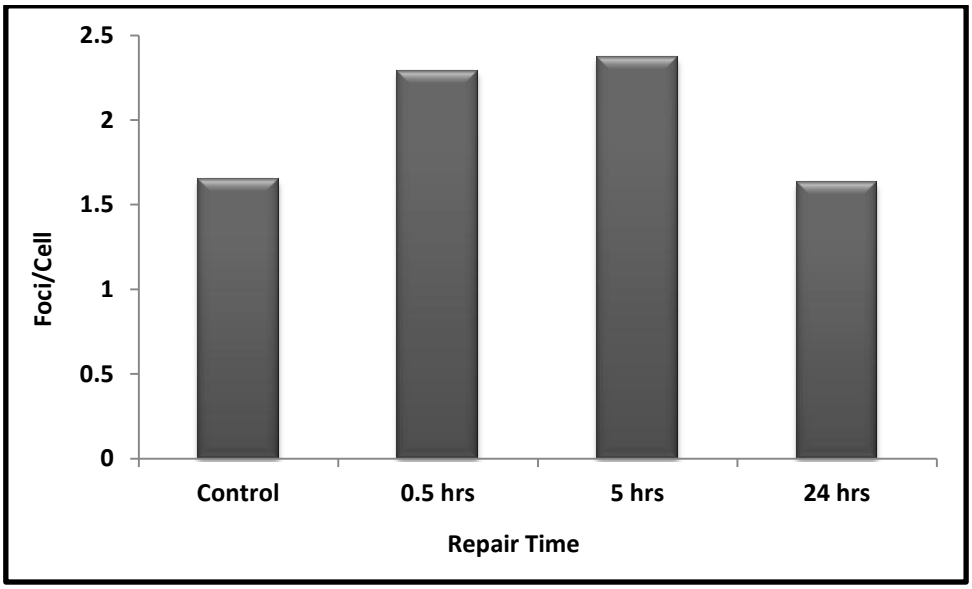

Figure 4.2 - Histograms and graph generated by Inspire software ™ using the Spot Mask feature on the GM00893 cell line.

(Figure 4.2) shows results generated using the Spot Mask software on the control GM00893 cell line. Following irradiation with 1.0 Gy these cells have been analysed 30 min, 5 hrs and 24 hrs later in order to generate a DNA repair kinetics curve. The 30 min and 5 hrs samples seen in (Figure 4.2 B & C), show a small shift to the right in comparison to the control sample shown in (Figure 4.2 A). This represents an increase in the number of DNA damage foci and it is indicative of the induction of DNA damage. At the 24 hrs point, the number of foci is at similar levels to the untreated control, thereby indicating that the DNA repair process has been completed (Figure 4.2 D). The same analysis performed with the Inspire software is shown in (Figure 4.3).

A Control

Nuclear Foci

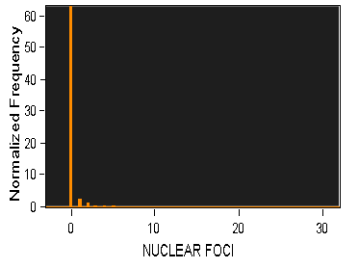

Population Statistics

Population	Count	%Gated
Double positive & Focus & Single cells	6339	100

NUCLEAR FOCI

Population	Mean
Double positive & Focus & Single cells	0.16

B 30 Min

Nuclear Foci

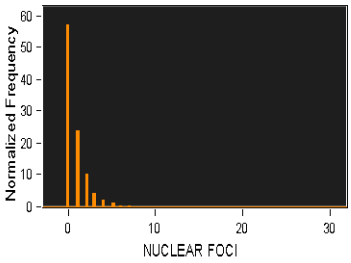

Population Statistics

Population	Count	%Gated
Double positive & Focus & Single cells	8151	100

NUCLEAR FOCI

Population	Mean
Double positive & Focus & Single cells	0.84

C 5 hrs

Nuclear Foci

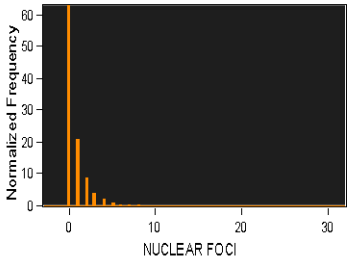

Population Statistics

Population	Count	%Gated
Double positive & Focus & Single cells	7100	100

NUCLEAR FOCI

Population	Mean
Double positive & Focus & Single cells	0.74

D 24 hrs

Nuclear Foci

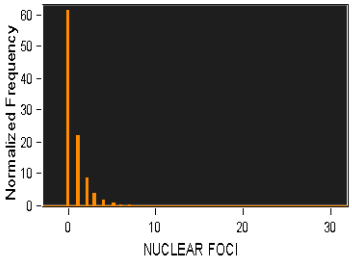

Population Statistics

Population	Count	%Gated
Double positive & Focus & Single cells	7653	100

NUCLEAR FOCI

Population	Mean
Double positive & Focus & Single cells	0.74

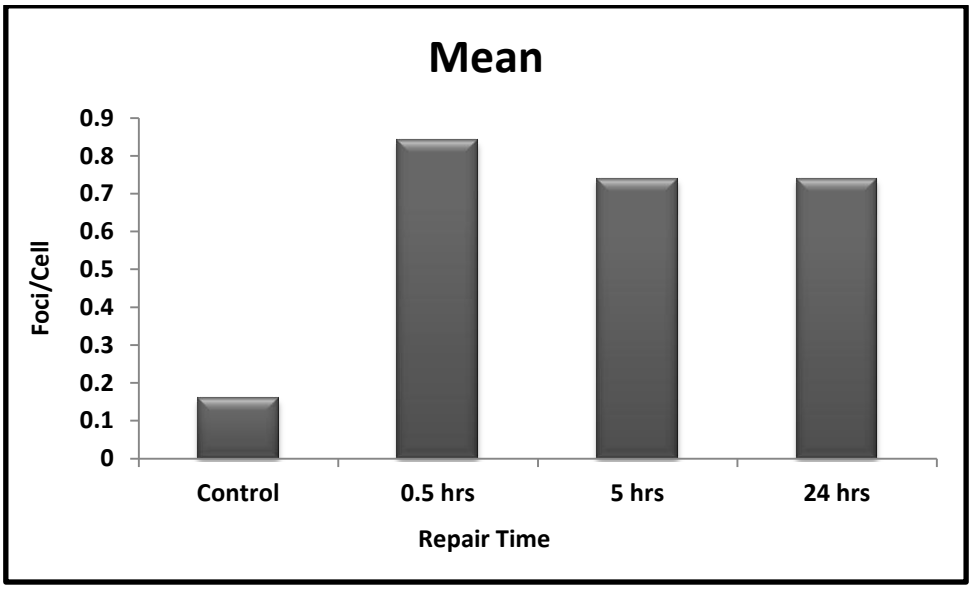

Figure 4.3 – Histograms and graph generated by Inspire software ™ using the Spot Mask feature on the GM14622 cell line.

However, the ImageStream analysis was associated with significant problems. Firstly, the cell count was too low in order to do a type of analysis recommended by the manufacturer of the apparatus. We only managed to analyse ~ 5000 cells in the majority of samples in a time-span of 20 minutes. The ImageStream can typically process up to 1000 cells/second according to the manufacturer website (Bourton *et al.* 2012). It is likely that the steps required for the preparation of cell for the analysis contributed to significant cell loss as our starting cell population was in line with the recommended protocol.

Secondly, the morphology of cells changed significantly after preparatory treatment. This treatment involved incubation of cells with a number of agents (see Material and methods) that could alter the cell morphology unless the protocol has been carefully optimized. Cells contained physical damage that could be easily identified on brightfield images (Figure 4.4).

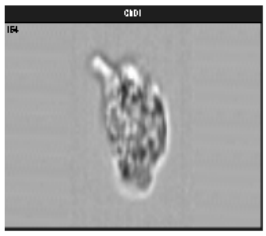

Figure 4.4 - An individual cell with physical damage. Image generated by the Inspire software.

This also questions reliability of results given the fact that some forms of this damage probably cannot be distinguished from IR-induced DNA damage. Furthermore, IR treated cells without the ImageStream preparatory steps looked fine morphologically under the microscope.

Thirdly, the problem persisted after several attempts suggesting that a lot of work dedicated to method development and optimisation would have to be involved in order for us to be able to produce reliable results from this analysis. Furthermore, even though ImageStream can analyse DNA damage quickly the fact remains that preparatory steps for the analysis are time consuming and on the whole there is not much difference in time required to analyse DNA damage kinetics by ImageStream and the conventional microscopy-based γ-H2AX assay. The final problem was that ImageStream was frequently out of action as a result of various hardware and software problems. Therefore, we decided to analyse DNA damage in lymphoblastoid cells by an alternative method. One such method is a simple and non-expensive cytospin based spreading of lymhoblastoid cells onto microscope slides which then can be used for immunocytochemical analysis such as the γ-H2AX assay.

4.2.3 - DNA damage kinetics in normal and heterozygous *BRCA2* cell lines using a cytospin-based method

Spreading cells on to a microscope slide by the Cytospin machine (Shandon) is an uncomplicated technique by which a single layer of cells is deposited onto a clearly defined part of a glass microscope slide. The design of the slide allows the filter card to absorb the excess fluid from the cells. This technique deposits the cells onto slides in a way that physical damage is minimal as evidenced by a subsequent microscope analysis. In order to exclude the possibility that the cytospin procedure induces DNA damage in centrifuged cells we have performed a series of tests which also served to adapt the γ-H2AX assay for this technique (not shown). Typical images of cells after the cytospin procedure are shown in (Figure 4.5). Well-preserved cell morphology is evident and the fluorescence signal produced by the γ-H2AX antibody is comparable to that produced by the classical γ-H2AX assay that we use for adherent cells.

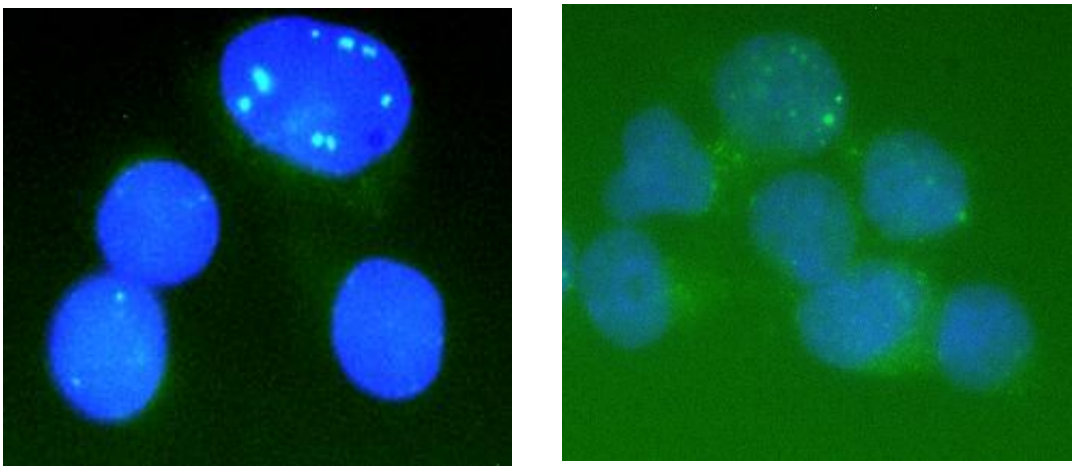

Figure 4.4 - Examples of images of cells after immunocytochemical procedure using cytospin. Green fluorescence represents DNA damage foci.

These results indicate that imunocytochemistery procedure using cytospin does not (i) affect cell morphology and (ii) induce DNA damage in investigated cells.

Having established that the cytospin-based protocol is suitable for our purpose we exposed the above 3 cell lines to 1.0 Gy of IR (gamma rays) and monitored frequencies of γ-H2AX foci 30 min, 5 hrs, 24 hrs and 48 hrs post-irradiation. Results of this analysis are shown in (Figure 4.6). It is important to note that we have done statistical analysis in two ways. First we compared two *BRCA2* defective cell lines against the control cell line at each individual point (control, 0.5 hrs, 5 hrs, 24 hrs and 48 hrs) and the result of this analysis are represented by stars placed immediately above bars in (Figure 4.6). The table incorporated in (Figure 4.6) contains results of the statistical comparison between control (spontaneous) frequencies of DNA damage foci and their counterparts at each time point post-irradiation (0.5 hrs, 5 hrs, 24 hrs and 48 hrs) for each individual cell line. For example, in most cases frequencies of DNA damage foci 0.5 hrs and 5 hrs after exposure will be significantly higher relative to spontaneous frequencies as these time intervals are insufficient for the repair processes to remove large amounts of induced DNA damage. However, significant differences between frequencies of DNA damage foci 24 hrs and 48 hrs post-exposure relative to spontaneous frequencies in the same cell line is indicative of unrepaired DNA damage and therefore it could represent a DNA damage defect. We have considered a cell line defective in DNA damage response if it showed a significant difference between frequencies of spontaneous DNA damage foci and those observed 48 hrs post-exposure. The general format of the (Figure 4.6) regarding the results of statistical analysis was used throughout this thesis.

The control GM00893 cell line had a significantly lower spontaneous frequency of γ-H2AX foci than two *BRCA2* defective cell lines (Figure 4.6). Analysis of repair kinetics after IR

revealed that both cell lines from *BRCA2* carriers repaired DNA damage effectively judging by the lack of statistical differences between DNA damage 48 hrs after exposure and spontaneous DNA damage (Figure 4.6). Surprisingly, the normal cell line showed statistical difference in this regard (Figure 4.6) but this is likely to be a chance event judging by its repair proficiency observed in later experiments (see Figures 4.7 and 4.8). These results suggest that shorter telomeres observed in two cell lines from *BRCA2* carriers do not lead to a defective DNA damage response.

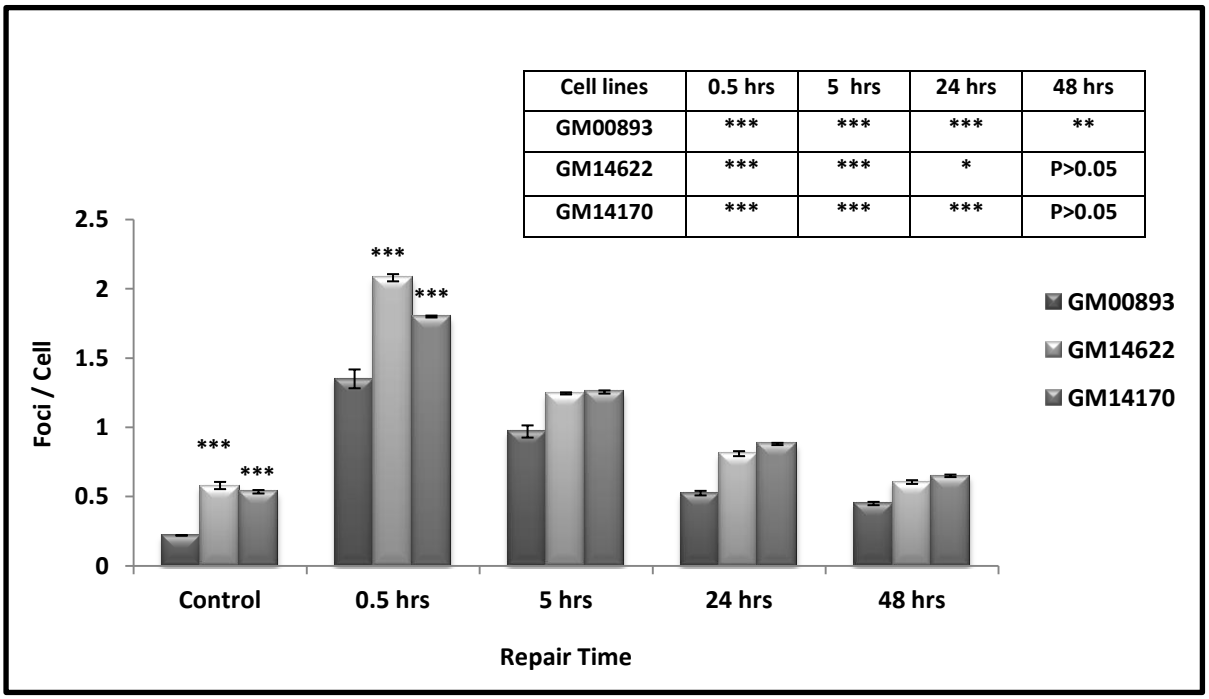

Figure 4.5 – Frequencies of DNA damage foci in normal and *BRCA2* defective cell lines after exposure to 1.0 Gy of gamma rays. Statistical analysis is explained in the text. *=P<0.05, **=P<0.01, ***=P<0.001, Error bars represent SEM.

We next analysed responses of the above cell lines to additional DNA damaging agents including Mitomycin C (MMC) and Bleomycin (BLM). MMC is an antibiotic isolated from Streptomyces caespitosus (Lee *et al.* 2006). It is classified as an alkylating agent

capable of covalently binding DNA and inducing inter- and intra-strand cross-links. The presence of such cross-links results in inhibition of DNA synthesis primarily during late G1 and S phases, although it is not cell-cycle specific (Kopp and Seregard 2004). All cell lines were treated with 60 ng/mL of MMC for 2 hours and DNA damage repair kinetics followed as above. Our analysis revealed that, with the exception of a weak significance observed in the case of the GM14170 cell line (Figure 4.7), there were no significant differences between spontaneous γ-H2AX foci and those observed 48 hrs after treatment (P>0.05) (Figure 4.7).

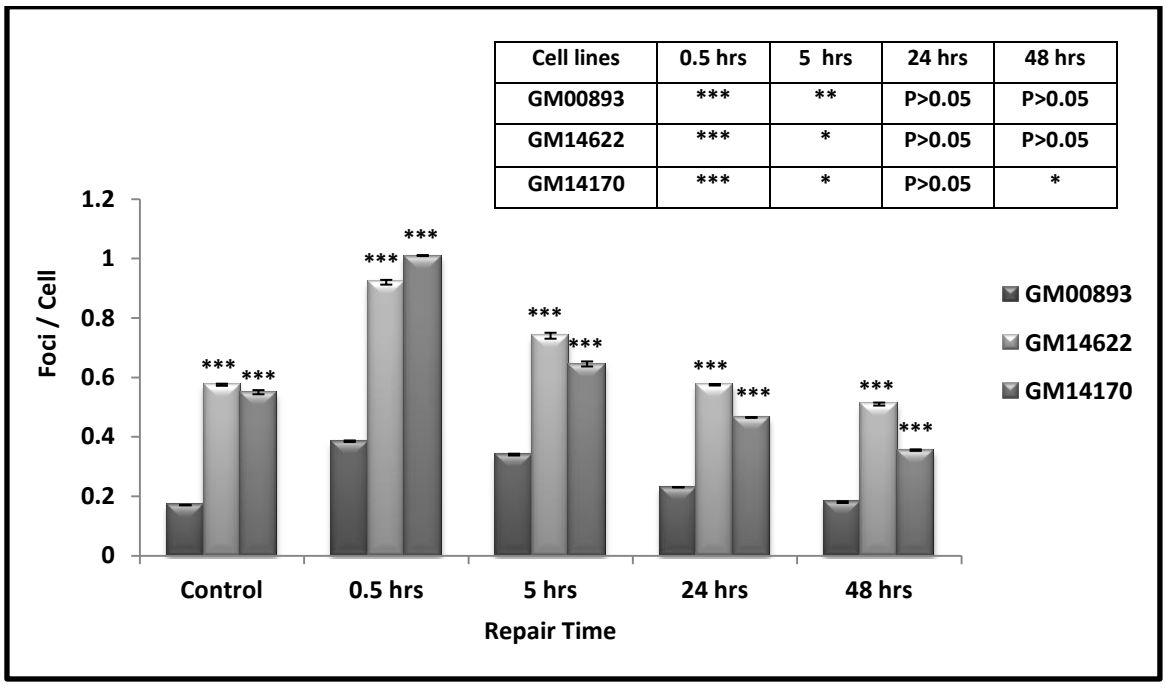

Figure 4.6 – Frequencies of DNA damage foci in normal and *BRCA2* defective cell lines after MMC treatment. *=P<0.05, **=P<0.01, ***=P<0.001, Error bars represent SEM.

Next, we used BLM to induce DNA damage in the above cell lines and compared frequencies of γ-H2AX foci up to 48 hrs after treatment. BLM is a radiomimetic drug which efficiently induces DSBs in treated cells (Tomilin *et al.* 2001). Briefly, confluent cells were

treated with 8µg/ml of BLM for 1 hour and frequencies of γ-H2AX foci counted. Our results revealed that all cell lines repair DNA damage effectively, further supporting the notion that short telomeres observed in cell lines from *BRCA2* carriers do not cause defective DNA damage responses (Figure 4.8).

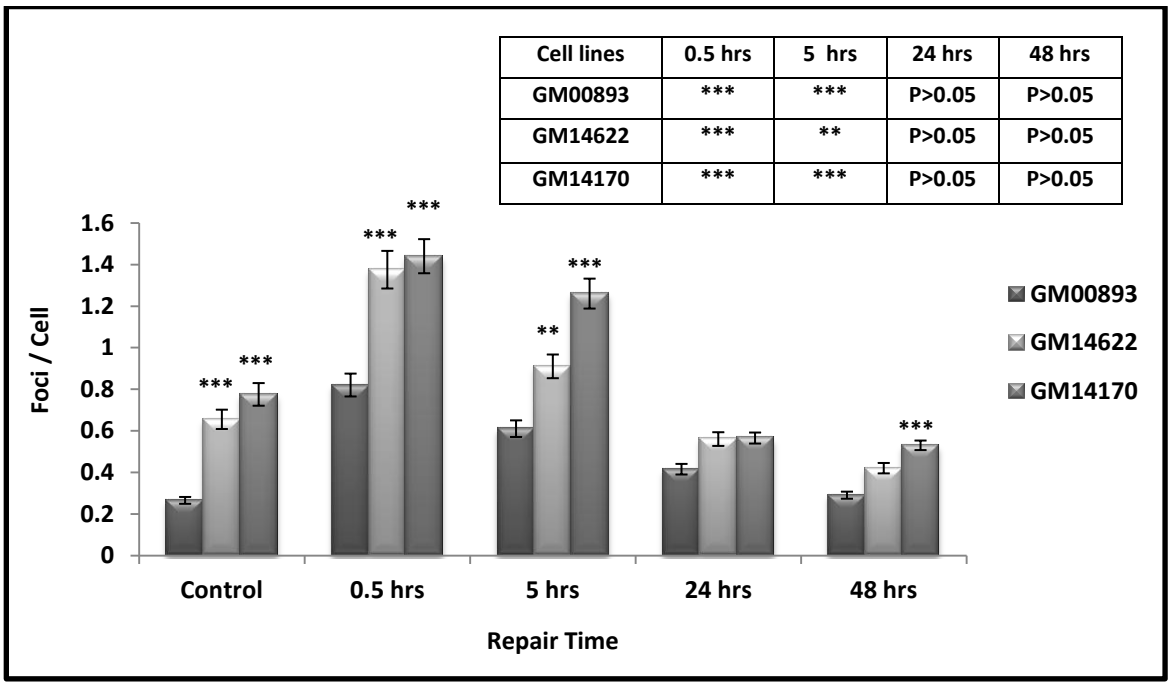

Figure 4.7 - H2AX analysis between normal and *BRCA2* defective cell lines after BLM treatment. **=P<0.01, ***=P<0.001, Error bars represent SEM.

4.2.4 - Telomere dysfunction-induced foci (TIF) Assay analysis in normal and heterozygous *BRCA2* cell lines

Next, we used the TIF assay to assess whether induced DNA damage localizes within telomeric sequences. As indicated earlier DNA damage occurring within telomeric DNA can be visualized using the TIF assay. Markers of DSBs, γ-H2AX or 53BP1 (Wang *et al.* 2002),

colocalize with damaged telomeres and constitute telomere dysfunction-induced foci (TIFs) (Takai *et al.* 2003). The presence of these TIFs is the signature of telomere dysfunction in cells. A representative example of a TIF observed in the cell line from a *BRCA2* carrier is shown in (Figure 4.9).

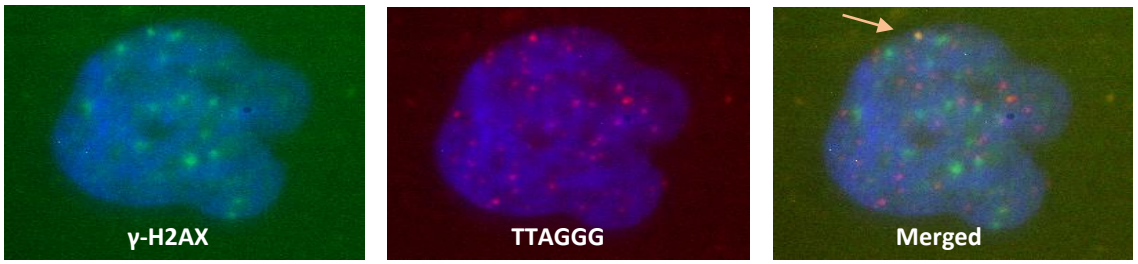

Figure 4.8 – An example of a TIF indicated by an arrow.

Our analysis revealed that *BRCA2* defective cells showed higher spontaneous frequencies of TIFs compared to normal cells (Figures 4.10 - 4.12). However, after treatment with IR frequencies of TIFs returned to spontaneous levels as there were no significant differences between control values and values of TIFs observed 48 hrs after IR. A very similar situation was encountered after treatment of cells with MMC and BLM (Figures 4.11 and 4.12). Taken together these results suggest that telomere function in the above cell lines is normal in spite of shorter telomeres observed in *BRCA2* defective cell lines.

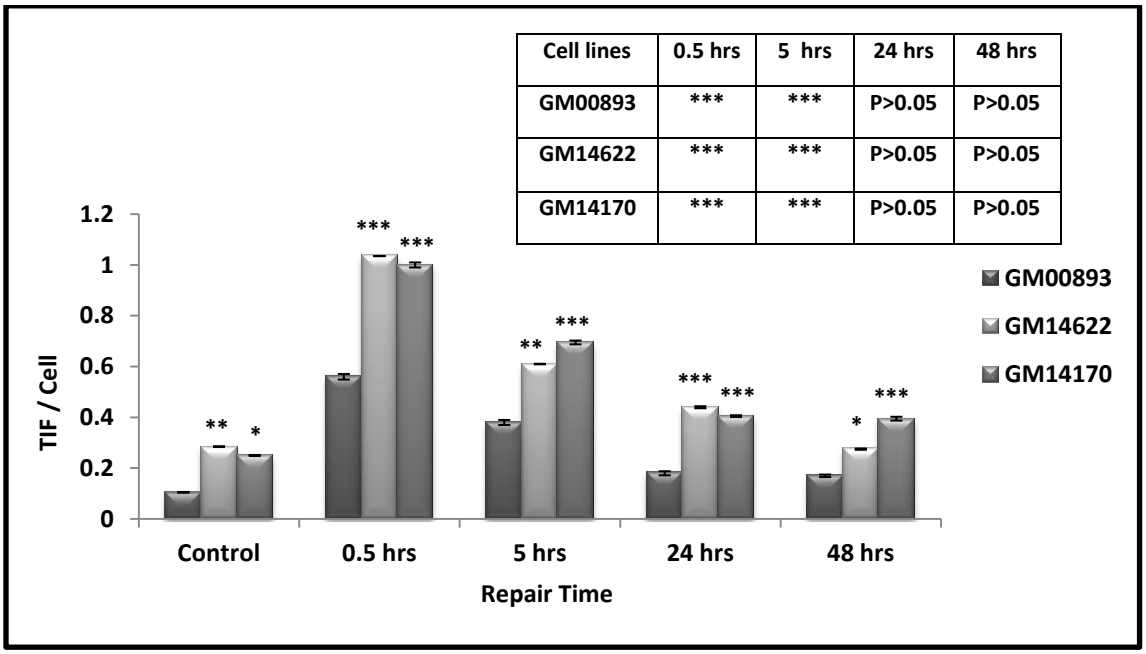

Figure 4.9 - Average number of TIF per cell in irradiated cell lines after 30 minutes, 5 hrs, 24 hrs and 48 hours post irradiation. *=P<0.05, **=P<0.01, ***=P<0.001, Error bars represent SEM.

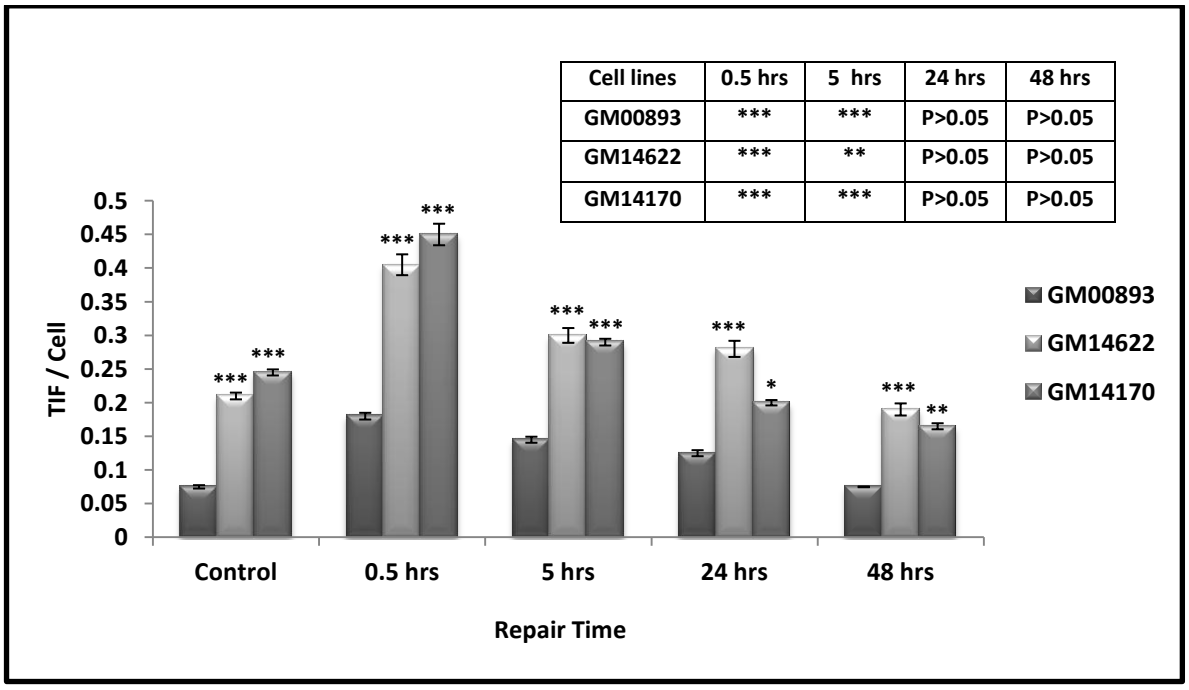

Figure 4.10 - Average number of TIF per cell in irradiated cell lines after MMC treatment. . *=P<0.05, **=P<0.01, ***=P<0.001, Error bars represent SEM.

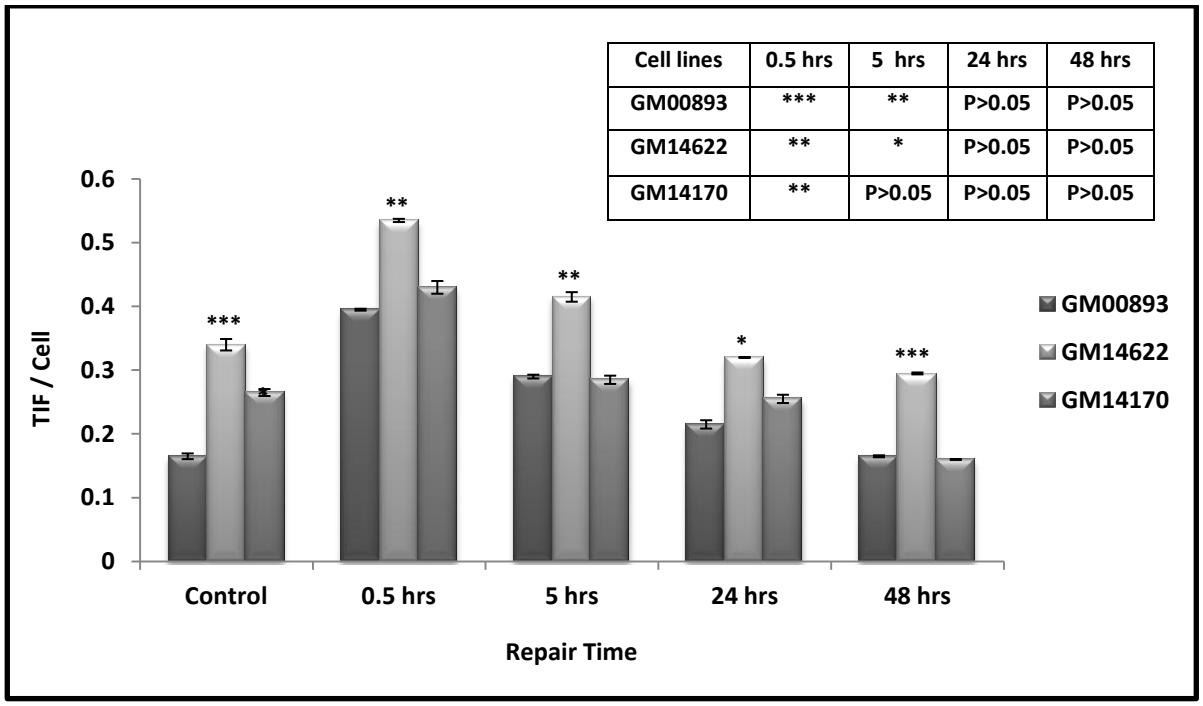

Figure 4.11 - Average number of TIF per cell in irradiated cell lines after BLM treatment. *=P<0.05, **=P<0.01, ***=P<0.001, Error bars represent SEM.

4.2.5 - Analysis of telomere length in cells from a patient with bi-allelic mutations in *BRCA2*

The fact that cell lines from *BRCA2* carriers have a functional copy of *BRCA2* suggests that this copy is sufficient to provide a functional DNA damage response. Therefore, it is possible that if mutations affect both copies of *BRCA2* cells would have a more severe DNA damage response defects and this would allow us to assess more critically contribution of telomeres to such defects. To explore this possibility we used the primary fibroblast cell line from a patient diagnosed with Fanconi anaemia, VU0423-F, who had bi-allelic mutations in the *FANCD1* gene, which is in fact the *BRCA2* gene (Howlett *et al.* 2002). We started by analysing telomere length in the VU0423-F cell lines and the corresponding control cell line

(primary fibroblast) GM08399. This analysis revealed that VU0423-F cells had significantly shorter telomeres than control cells (Figure 4.13).

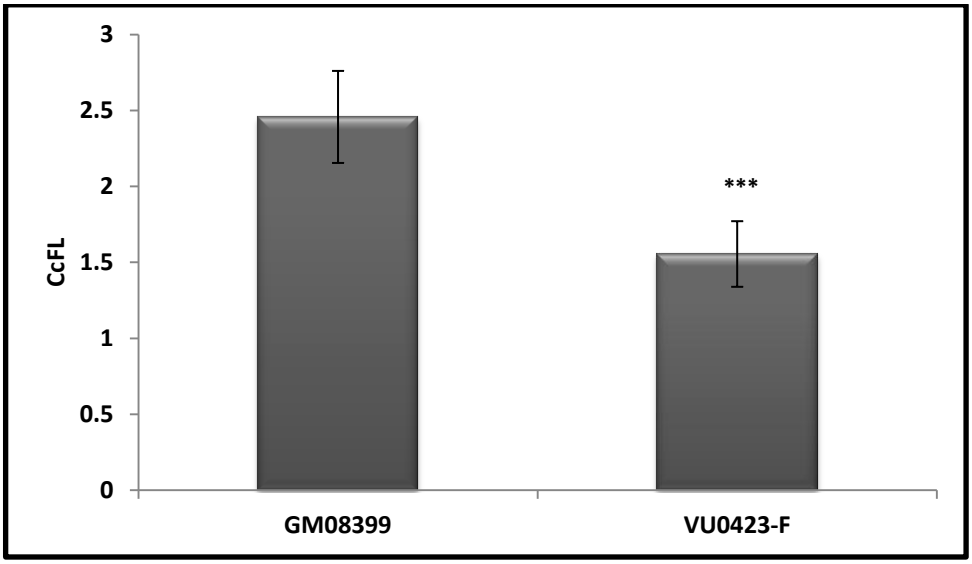

Figure 4.12 - Corrected calibrated fluorescence (CcFl) in normal and cells with homozygous *BRCA2* mutations. *** = P<0.001, Error bars represent SEM.

4.2.6 - DNA repair kinetics in the cell line with bi-allelic mutations in *BRCA2*

We next analysed DNA repair kinetics in GM08399 and VU0423-F cell lines in the same way as in lymphoblastoid cell lines with the only exception that the current two cell lines were adherent cell lines and we did not need the cytospin-based protocol. Cells were irradiated with 1.0 Gy of gamma rays and harvested 0.5 hrs, 5hrs, 24 hrs and 48hrs after irradiation. Representative examples of images of cells after immunocytochemical procedure designed to detect γ-H2AX are given in (Figure 4.14).

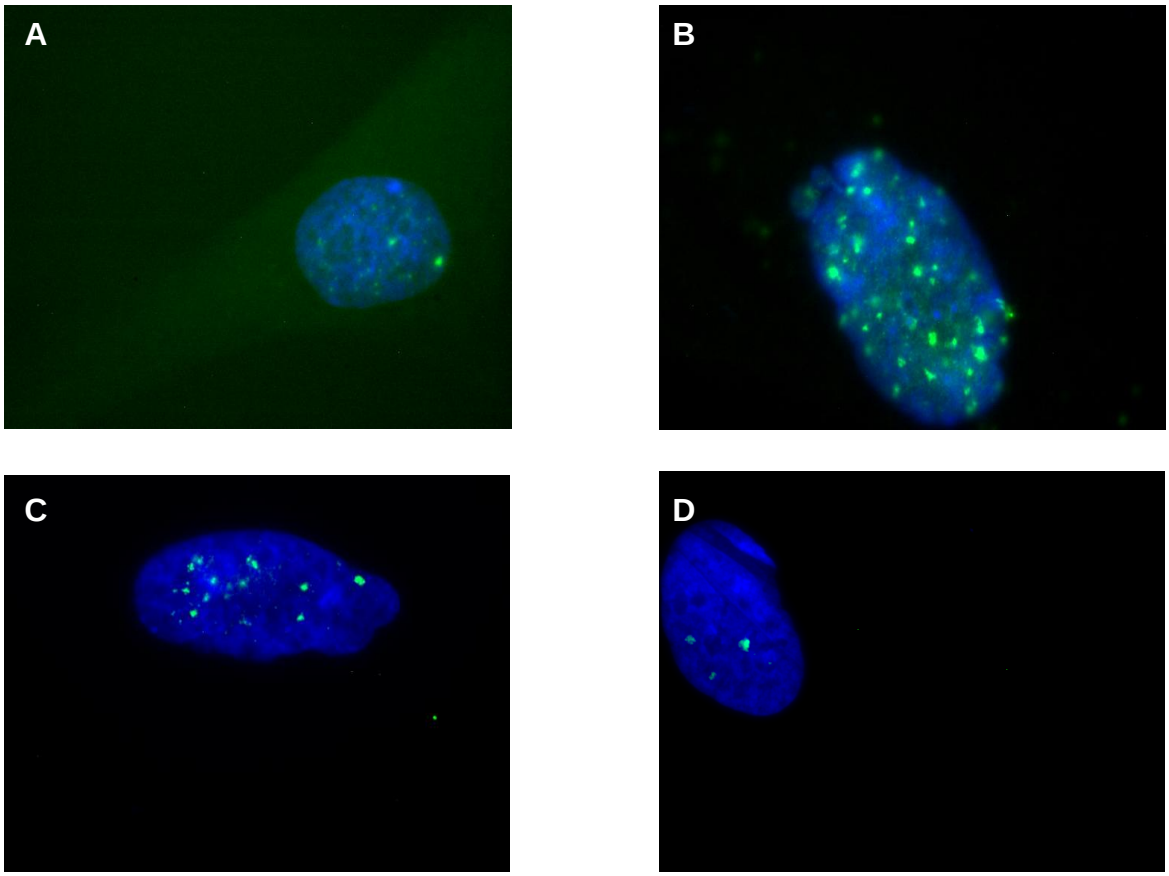

Figure 4.13 - H2AX foci images after 0 (A), 30 min (B), 5 hrs (C) and 48 hours post irradiation in *BRCA2* defective cells.

Frequencies of H2AX foci in untreated GM08399 and VU0423-F cell lines revealed that GM08399 cells have lower spontaneous frequency of DNA damage. Spontaneous frequencies of H2AX foci usually tend to go up with cell age (Medvedeva *et al.* 2007). However, both cell lines underwent similar population doublings and the possibility that endogenous DNA damage in VU0423-F cells is higher because of cells age can be excluded.

Analysis of repair kinetics after IR revealed that VU0423-F cells show much higher level of H2AX foci / cell than GM08399 cells 48 hrs after IR (Figure 4.15). This finding is consistent with the view that VU0423-F cells show abnormal repair kinetics after IR because both copies of BRCA2 are mutant. While normal cells repair almost all DNA damage 48 hrs after IR, as indicated by the presence of only ~ 0.4 H2AX foci / cell ($P>0.05$), VU0423-F cells

show persistence of DNA damage 48 hrs after IR as indicated by the observed ~3 / foci per cell 48 hrs after IR (Figure 4.15). The statistical analysis revealed that these differences are significant (P<0.001) (see table in Figure 4.15). These results clearly show a defective DNA damage response in the cell line with dysfunctional copies of *BRCA2* alleles in contrast to the situation in cells from *BRCA2* carriers. The next task for us was to determine contribution of dysfunctional telomeres to this phenotype.

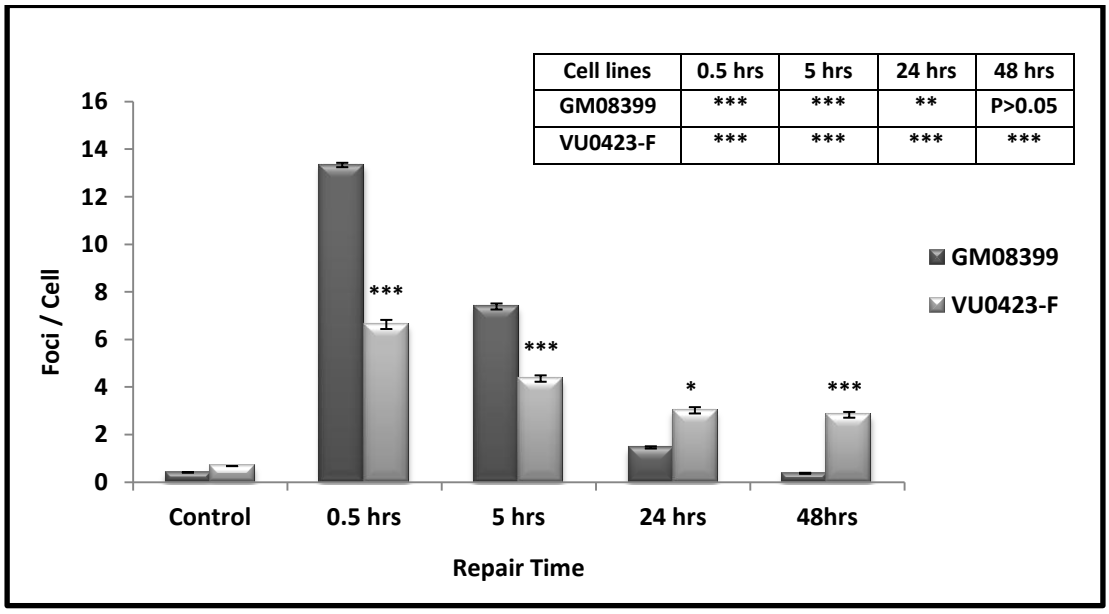

Figure 4.14 - Frequencies of γH2AX foci in GM08399 and VU0423-F cell lines. *=P<0.05, **=P<0.01, *** = P < 0.001, Error bars represent SEM.

4.2.7 - TIF Assay analysis of cells with bi-allelic mutations in *BRCA2*

Next, we employed the TIF assay to assess whether DNA damage accumulates preferentially at telomeres. Our analysis revealed that VU0423-F cells showed slightly higher spontaneous frequencies of TIFs compared to normal cells (Figure 4.16). However, this difference was not statistically significant (P=0.35). IR induced some TIFs in both cell lines as evidenced by the increase in their values 30 min after exposure. However, these values have

fallen to the normal levels in both cell lines 48 hrs after exposure. Based on these results we conclude that dysfunctional telomeres do not contribute to dysfunctional DNA damage response in cells with homozygous mutations in *BRCA2*, at least using the TIF assay as a method of assessment.

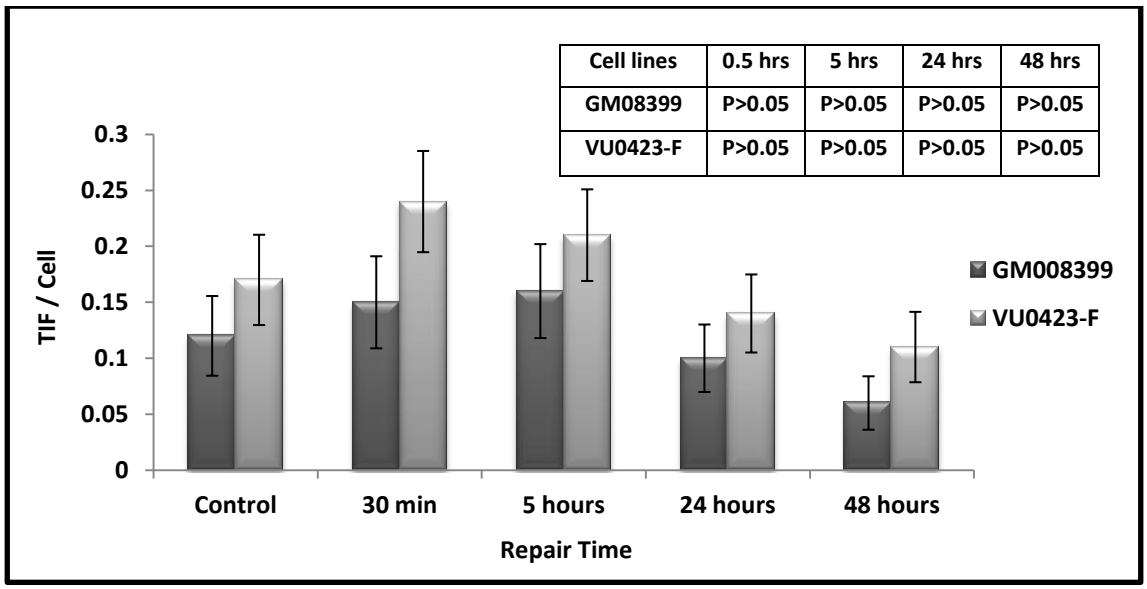

Figure 4.15 - Average number of TIF per cell in normal and homozygous BRCA2 cell lines after 30 minutes, 5, and 24 and 48 hours post irradiation. P>0.05, Error bars represent SEM.

4.2.8 - Chromosome Orientation Fluorescence in situ Hybridization (CO-FISH) analysis of normal and homozygous *BRCA2* cell lines

It is possible that TIF values may be normal in affected cells but telomeres still may show dysfunction due to factors that do not involve H2AX. One possibility is that recombination rates at telomeres may be altered in *BRCA2* defective cells given its role in HR. To investigate effects of *BRCA2* dysfunction on recombination at telomeres we analysed T-SCE frequencies in the VU-0423-F cell line containing bi-allelic mutations in *BRCA2* and the control primary fibroblast cell line from a normal individuals, GM08399, using CO-FISH. A

total of 30 metaphase cells per cell line were analyzed by CO-FISH to delineate frequencies of T-SCEs in each cell line. Examples of T-SCEs are shown in (Figure 4.17).

The difference was statistically significant (P<0.001), showing increased T-SCE levels in the VU0423-F cell line relative to the control cell line (Figure 4.18). Normal, control cell line showed 0.9 T-SCE/cell. In contrast, VU0423-F cells had 4.6 T-SCEs/cell which is a five-fold increase.

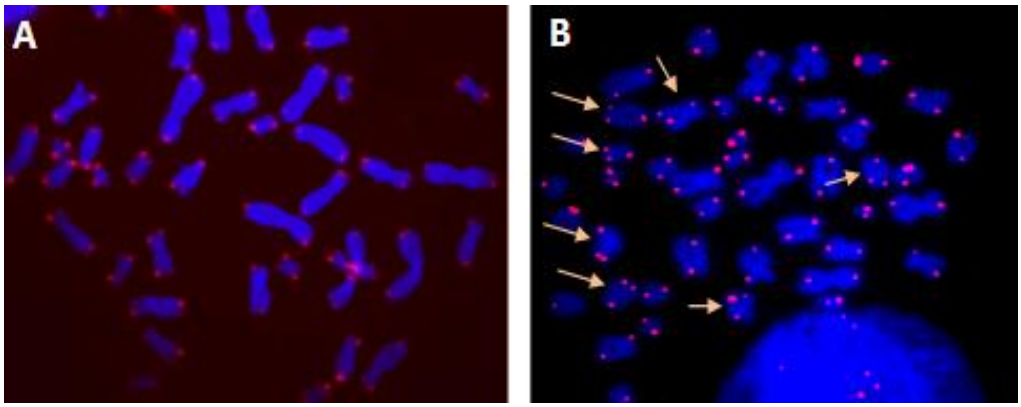

Figure 4.16 - T-SCE detected by CO-FISH. T-SCE events as observed through a fluorescence microscope (Olympus BX41) using the SmartCapture image acquisition software. A) In GM08399 cells T-SCE is a very rare event (No T-SCEs). B) VU0423-F cells showed multiple T-SCEs events indicated by arrows. For details of CO-FISH and how T-SCEs are detected see Materials and methods.

These results suggest that the *BRCA2* defect affects recombination rates at telomeres and therefore this could be a contributory factor to the defective DNA damage response observed in these cells. However, this hypothesis is difficult to test because IR, as the most commonly used experimental DNA damaging agent in our laboratory, is a weak inducer of recombination events as evidenced by its inability to induce sister chromatid exchanges (Gutierrez *et al.* 1999).

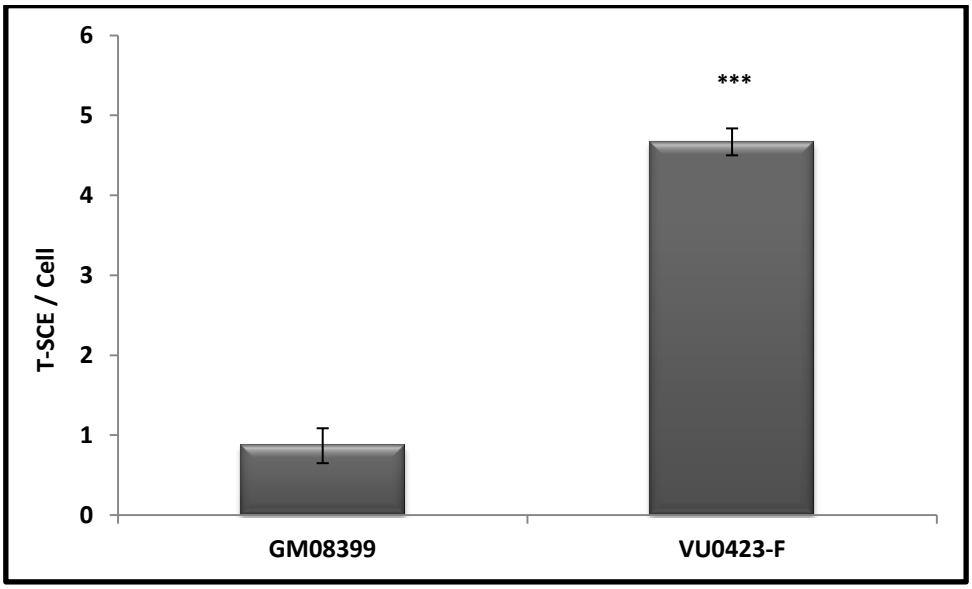

Figure 4.17 - Frequencies of T-SCEs (event/metaphase) in GM08399 and VU0423-F cell lines. Error bars represent SEM. *** = P<0.001.

4.2.9 - Anaphase Bridges analysis in normal and homozygous BRCA2 cell lines

In order to test if dysfunctional telomere maintenance contributes to defective DNA damage response in the VU0423-F cell line more directly we needed a method that can detect induction of DNA damage at telomeres in this cell line other than TIF. One possibility would be to test chromosome aberrations induced by IR in this cell line and determine whether they localize at telomeres preferentially or not. However, the problem with this approach is that the VU0423-F cell line grows extremely poorly as a result of *BRCA2* mutations, especially when exposed to IR. The result is an extremely low mitotic index and almost complete lack of good quality metaphase spreads after exposure to IR. During the analysis of mitotic index in these cells we noticed that when large numbers of cells are scanned (virtually thousands) then one can identify a relatively reasonable number of

mitotic cells in these preparations without the conventional chromosome preparation procedure. Even though these cells show poor chromosome morphology that precludes an accurate analysis of chromosome aberrations we were able to identify clearly anaphase cells containing so called anaphase bridges. These bridges represent rearranged chromosomes including those resulting from IR induced chromosome breakage such as dicentric chromosomes. Some of these rearranged chromosomes may occur as a result of chromosome rearrangements resulting from dysfunctional telomeres (Gilson and Londono-Vallejo 2007). Anapahse bridges due to dysfunctional telomeres can easily be identified by applying the telomeric PNA probe which will then identify telomeric DNA within the chromatin bridge, a clear indication of telomere dysfunction. We therefore decided to scan large number of VU0423-F and control cells after exposure to IR and focus exclusively on anaphase cells with a view of identifying anaphase bridges indicative of dysfunctional telomeres. An example of an anaphase bridge due to dysfunctional telomeres is shown in (Figure 4.19). Interestingly, telomeric signals within the anaphase bridges did not colocalize with H2AX (Figure 4.19). This is in line with the observed lack of TIFs (Figure 4.16) thus suggesting that telomere dysfunction in *BRCA2* defective cells manifests in a TIF independent manner.

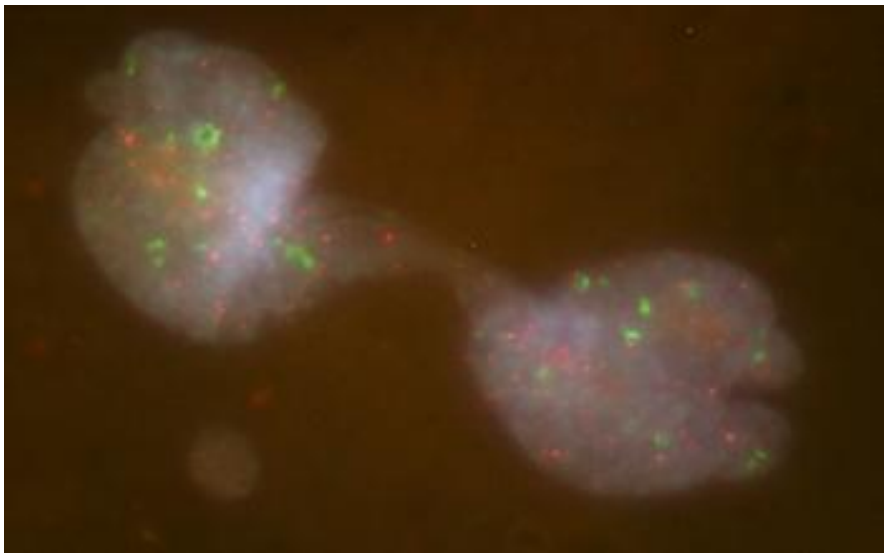

Figure 4.18 – An anaphase bridges in the VU0423-F cell line. Note the presence of red fluorescence within the chromatin bridge. Red fluorescence represents telomeres. Green fluorescence is due to H2AX.

It was clear from this analysis (Figure 4.20) that VU0423-F cells show significantly elevated frequencies of anaphase bridges due to dysfunctional telomeres relative to control cells ($P<0.001$). While there was no statistically significant difference between frequencies of anaphase bridges due to dysfunctional telomeres in control untreated and IR exposed cells, the VU0423-F cells showed statistically significant difference between untreated samples and IR exposed samples at all observation points (0.5 hrs, 5 hrs and 24 hrs after IR) (Figure 4.20). Based on these results we can conclude that dysfunctional telomeres directly contribute to a defective DNA damage response observed in VU0423-F cells as anaphase bridges due to dysfunctional telomeres are clearly inducible by IR in this cell line but not in the control cell line.

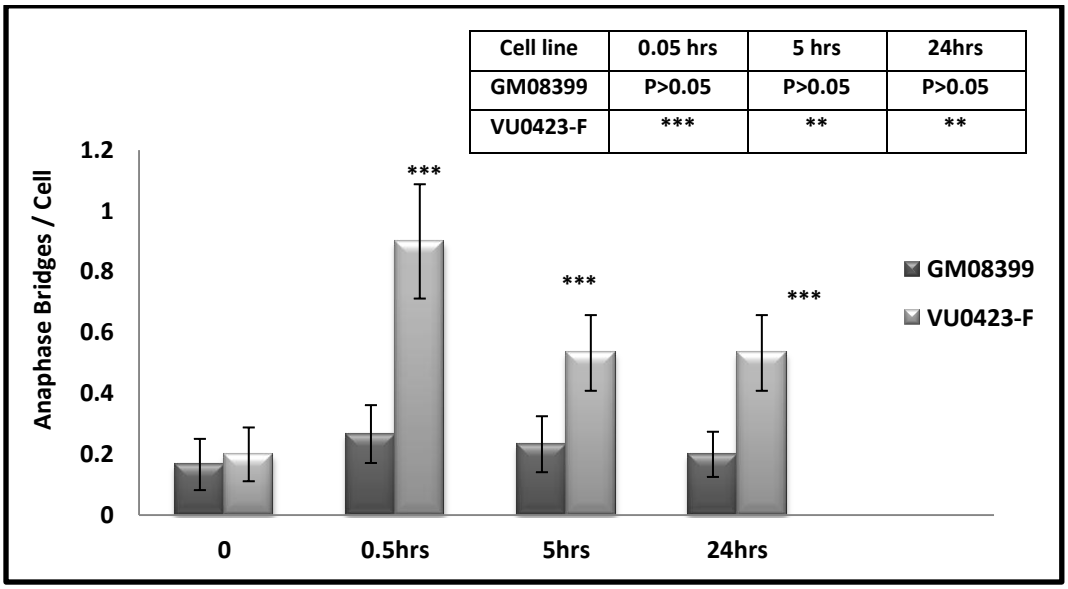

Figure 4.19 - Analysis of anaphase bridges in *BRCA2* defective and control cells. **=P<0.01, ***= P<0.001. Error bars represent SEM.

4.3 - Discussion

There is increasing evidence that telomere maintenance is functionally linked with DNA damage response mechanisms (Slijepcevic 2006). Based on numerous observations of dysfunctional telomeres in DNA damage response defective cells due to mutations in many relevant genes it has been hypothesized that telomere maintenance may be an integral part of DNA damage response mechanisms (see Slijepcevic 2006). With a view of testing this hypothesis further, in this chapter we focused on a well-known protein, BRCA2, that plays an important role in DNA damage response. Interestingly, several recent studies (Badie *et al.* 2010; Sapir *et al.* 2011; Bodvarsdottir *et al.* 2012) showed that BRCA2 affects telomere maintenance. Of particular interest to us is the observation that BRCA2 directly interacts with telomeres and helps another DNA damage response protein, RAD51 access telomeres (Badie *et al.* 2010). This is directly in line with the hypothesis that telomeres are directly

involved in DNA damage response (Slijepcevic 2006) as at least two proteins, BRCA2 and RAD51, involved in HR, a key pathway for repair of DNA DSBs, directly interact with telomeres (Badie *et al.* 2010). The observed telomere dysfunction phenotype in BRCA2 defective cells was consistent with the involvement of telomeres in HR. For example, it has been shown that BRCA2 defective cells have increased frequencies of T-SCEs; events indicative of elevated recombination at telomeres (Sapir *et al.* 2011; Bodvarsdottir *et al.* 2012). In addition to this finding, it was shown that BRCA2 defective cells exhibit other telomere maintenance defects including abnormal telomere length regulation.

Our results clearly confirm above findings. We observed a several-fold increase in the frequency of T-SCEs in the VU0423-F cell line relative to the control cell line (Figure 4.18). Furthermore, we observed significantly shorter telomeres in VU0423-F cells relative to control cells (Figure 4.13) suggesting alterations of telomere length regulation resulting from dysfunctional BRCA2. It is important to address that we have used only one control cell line (GM00893) in the case of our lymphoblastoid experiments as GM00893 cells were only control that were growing well without any problem. However, in our experiments we were more concerned with the heterozygoys vs. homozygoys mutations. So we had BRCA1 or BRCA2 +/+ (normal control), BRCA1 or BRCA2 +/- (heterozygous) and BRCA2-/- homzigous and this covers whole spectrum.

However, our main aim was to examine whether dysfunctional telomere maintenance contributes to the defective DNA damage response observed in BRCA2 deficient cells. Interestingly, in our result we have shown that haploinsufficiency cells showed defective repair. Based on our results we can conclude that when one copy of BRCA2 is functional in human cells, these cells do not show altered DNA damage response

(Figures 4.6-4.8). This is not in line with some published studies, which suggest that even cells from BRCA2 carriers show somewhat defective DNA damage response. Some of these studies used a different method for assessing DNA damage from ours and the difference could be due to this. Because of the observed lack of defective DNA damage response in cells from BRCA2 carriers we could not examine the possibility that telomeres directly contribute to dysfunctional DNA damage response in cells with heterozygous mutations in BRCA2 (Figures 4.10-4.12). Nevertheless, we have shown that cells from BRCA2 carriers have significantly shorter telomeres than control cells (Figure 4.1). This is in line with a previous study (Martinez-Delgado *et al.* 2011). However, this finding suggests two possibilities. First, even though telomeres are shorter in cells from BRCA2 carriers than in control cells (Figure 4.1) they might not be critically short to cause the dysfunction phenotype that could contribute to defective DNA damage response. Second, even if there is a telomere dysfunction in these cells directly caused by telomere shortening, such a dysfunction is not able to alter the overall DNA damage response in cells with heterozygous mutations in BRCA2. We cannot specifically exclude either of these possibilities, as we have not directly tested them. Based on TIF results (Figure 4.10-4.12), the later option seems plausible, but there are some problems with interpretation of TIF results that will be explained below.

However, it is clear from our results that when both copies of BRCA2 are dysfunctional, as in the case of VU0423-F cells, this leads to both dysfunctional DNA damage response (Figure 4.15) and dysfunctional telomere maintenance (Figure 4.16). This scenario allows us to test whether dysfunctional telomeres contribute to the defective DNA damage response observed in BRCA2 defective cells. The main problem in testing for this possibility was the poor proliferative potential of VU0423-F cells. This was probably the slowest

growing primary fibroblast cell line that we had in our laboratory. The easiest test to assess contribution of telomeres to dysfunctional DNA damage response in these cells, chromosome aberration analysis after exposure to IR, could not be performed in this cell line because of extremely poor proliferative potential. A good quality chromosome preparation requires a reasonable mitotic index. We thought we could rely on the TIF assay to assess contribution of telomeres to dysfunctional DNA damage response. The TIF assay does not depend on the mitotic index and can be performed on slow growing cells. After exposure to IR we did observed some increase in TIF frequencies in both cell lines 30 min and 5hrs post exposure even though this was not statistically significant (Figure 4.15) suggesting that IR can induce TIFs. However, the problem was a very low frequency of TIFs observed – maximum of 0.25/cell (Figure 4.15). Given that TIFs are identified in interphase cells by the overlap of staining between telomeric PNA and the H2AX positive signal (Figure 4.8) a low frequency of events in this situation is always associated with the chance finding. Therefore, we could not reasonably rely on TIF analysis to test for the above possibility.

Instead, we explored the fact that when large numbers of cells are scanned (virtually thousands) even slow growing cells such as VU0423-F cells will yield some mitotic cells that can be analysed microscopically. We focused exclusively on anaphase cells identified in this way and applied FISH with the telomeric PNA probe to identify anaphase bridges that contain telomeric signals (Figure 4.20). The presence of telomeric signals within anaphase bridges is an indication that either two dysfunctional telomeres fused together or that one dysfunctional telomere fused with a non-telomeric DSB. The fact that frequencies of anaphase bridges due to dysfunctional telomeres were inducible by IR in VU0423-F cells but not in control cells (Figure 4.19) leads us to conclude that dysfunctional telomeres directly contribute to dysfunctional DNA damage response observed in these cells. However, to

substantiate this conclusion further, faster growing cell lines with dysfunctional copies of both BRCA2 alleles are required. It is interesting to mention in this regard that an earlier study using murine BRCA2-/- cells have identified numerous chromosomal aberrations after exposure to genotoxic stress (Yu *et al.* 2000). Some of these aberrations resembled chromosome aberrations due to dysfunctional telomeres (chromosome end-to-end fusions) (Yu *et al.* 2000). However, no telomeric FISH was used in the study and this possibility should be tested directly in the future.

In conclusion, our results show that cells from a patient with bi-allelic mutations in BRCA2 show telomere dysfunction abnormalities including alterations in telomere length regulation and elevated frequencies of recombination at telomeres. Following exposure of these cells to IR, the observed telomere dysfunction contributed to defective DNA damage response observed in these cells in the form of elevated frequencies of anaphase bridges involving dysfunctional telomeres.

Chapter 5 - Effects of BRCA1 on telomere maintenance

5.1 - Introduction

In the previous chapter we have shown that the BRCA2 protein affects telomere maintenance and that dysfunctional telomeres resulting from mutations in both copies of *BRCA2* contribute to a defective DNA damage response observed in affected cells. These results are consistent with the view that telomere maintenance is functionally linked with DNA damage response mechanisms (Slijepcevic 2006). The aim of this chapter is to focus on the BRCA1 protein and probe its role in this functional link.

Mutations in the breast cancer susceptibility gene, *BRCA1*, confer genetic predisposition to early-onset familial breast and ovarian cancer (Welcsh *et al.* 2000). Even though the BRCA1 protein has been shown to play a role in the maintenance of genome integrity, transcriptional regulation and chromatin remodelling, the precise mechanism underlying its tumour suppressor function remains unknown (Welcsh *et al.* 2000; Starita and Parvin 2003). It is interesting that telomere maintenance mechanisms also act as a tumor suppression mechanism (Cesare and Reddel 2008). Therefore, analysis of telomere maintenance in cells with mutant BRCA1 could potentially shed light on how this protein exerts its tumour suppression properties. It is interesting that BRCA1 co-localizes with numerous DNA damage response factors and there is a likelihood that this protein participates in DNA double strand break (DSB) repair through homologous recombination (Powell and Kachnic 2003). Cells from carriers of BRCA1 mutations show sensitivity to ionizing radiation (IR), which suggests that genomic instability could be triggered even when a single copy of BRCA1 is mutated (Foray *et al.* 1999; Trenz *et al.* 2002).

It has been shown previously by Dr Slijepcevic's group that BRCA1 affects telomere maintenance (Cabuy *et al.* 2008). The expression of BRCA1 was knocked down by RNAi in

the breast epithelial cell line MCF10 and the breast adenocarcinoma cell line MCF7 (Cabuy *et al.* 2008). The affected cell lines exhibited increase in anaphase bridge frequencies due to dysfunctional telomeres, but no changes in telomere length (Cabuy *et al.* 2008). Two additional studies have confirmed that BRCA1 plays a role in telomere maintenance. (French *et al.* 2006) demonstrated that the expression of a dominant negative mutation in BRCA1 in breast epithelial cells leads to changes in telomere length (elongation) and increase in chromatin bridges in anaphase. Using mouse *Brca1*-/- cells (McPherson *et al.* 2006) demonstrated accelerated telomere loss and increased frequencies of telomeric fusion in these cells relative to control cells. Earlier observations that BRCA1 acts as a negative regulator of telomerase (Xiong *et al.* 2003) and that BRCA1 interacts with APB (ALT [Alternative lengthening of telomeres]) Promyelocytic leukemia Bodies) in ALT positive cells (Wu *et al.* 2003) also strongly indicate the role of BRCA1 in telomere maintenance.

The aim of this chapter was to examine the contribution of dysfunctional telomeres due to mutations in BRCA1, either in human or mouse cell lines, to dysfunctional DNA damage response in these cells. We have carried out similar experiments like in the previous chapter, namely analysis of telomere length by IQ-FISH, analysis of DNA damage response by the γ-H2AX assay and analysis of telomere function by the TIF assay. Furthermore, we carried out, in some cases, chromosomal aberration analysis after exposure of cells to IR.

5.2 - Results

5.2.1 - IQ-FISH analysis of cell lines from *BRCA1* carriers

We started by analysing telomere length in two lymphoblastoid cell lines established from carriers of different *BRCA1* mutations. Both cell lines have been purchased from Coriell Cell Repositories. The GM13705 cell line had the 3875del4 mutation in exon 11 (Castilla *et al.* 1994) and the GM14090 cell line had the 185delAG mutation in exon 2 causing a premature termination codon at position 39 (Struewing *et al.* 1995). As a control we used the lymphoblastoid GM00893 cell line established from a normal individual. The analysis of telomere length by IQ-FISH revealed that the GM14090 cell line had, on average, the shortest telomeres (Figure 5.1). For example, GM14090 cells showed ~ 1.9x shorter telomeres ($P<0.001$) than normal control cells (Figure 5.1). The GM13705 cell line showed ~ 1.4x shorter telomeres relative to the control cell line ($P<0.001$) (Figure 5.1). These results suggest that cells from *BRCA1* carriers show alterations in telomere length regulation in comparison to control cells. Alterations in telomere length regulation could potentially lead to telomere dysfunction.

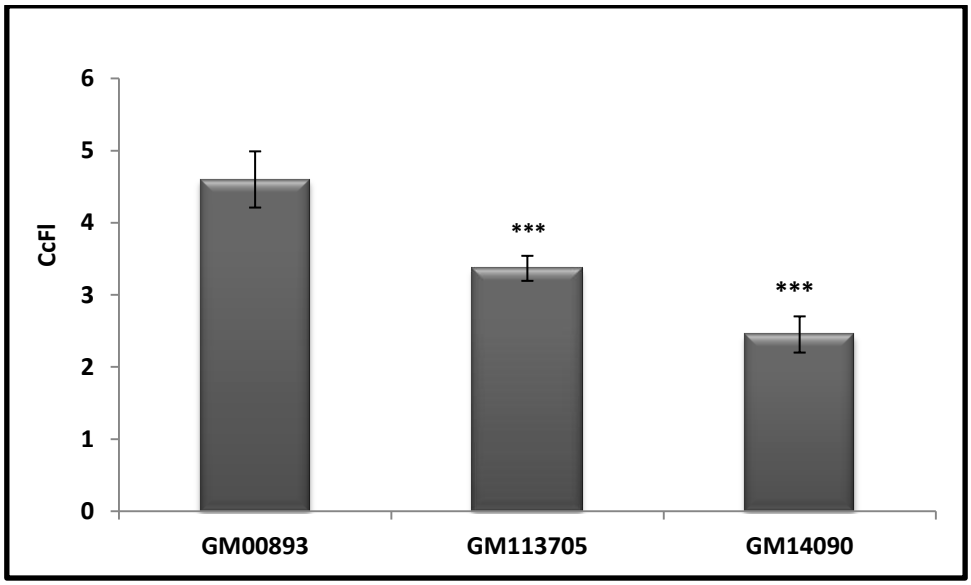

Figure 5.1 - Corrected calibrated fluorescence (CcFl) in *BRCA1* defective cell lines relative to the control. ***=P<0.001, Error bars represent SEM.

5.2.2 - DNA damage kinetics in cell lines from *BRCA1* carriers

Next, we analysed DNA damage response in the above cell lines using the γ-H2AX assay in combination with cytospin as in the previous chapter. Examples of DNA damage foci observed in the above cell lines using the cytospin-based protocol for cell spreading are shown in Figure 5.2. Results of DNA damage response analysis are shown in Figure 5.3. All cell lines showed some spontaneous DNA damage, which was significantly higher in *BRCA1* defective cell lines (Figure 5.2). In GM00893 and GM13705 cell lines repair of DNA damage was efficient as no difference in frequencies of γ-H2AX positive cells was observed between spontaneous values and values observed 24 hrs and 48 hrs after exposure to 1.0 Gy of gamma rays (Figure 5.3). In contrast, the GM14090 cell line showed some residual DNA damage (significantly higher relative to spontaneous values in this cell line; P<0.001) 24 hrs

and 48 hrs after exposure to IR (Figure 5.3). This suggests that DNA damage response in the GM14090 cell line is defective.

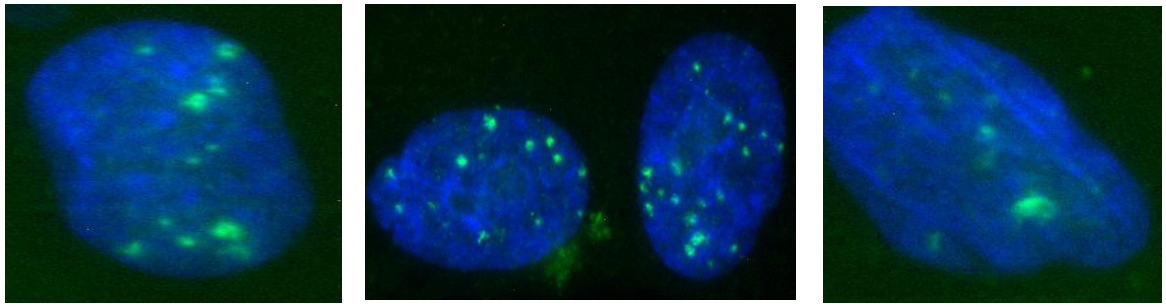

Figure 5.2 - Examples of DNA damage foci observed in *BRCA1* carriers using the cytospin-based protocol for cell spreading.

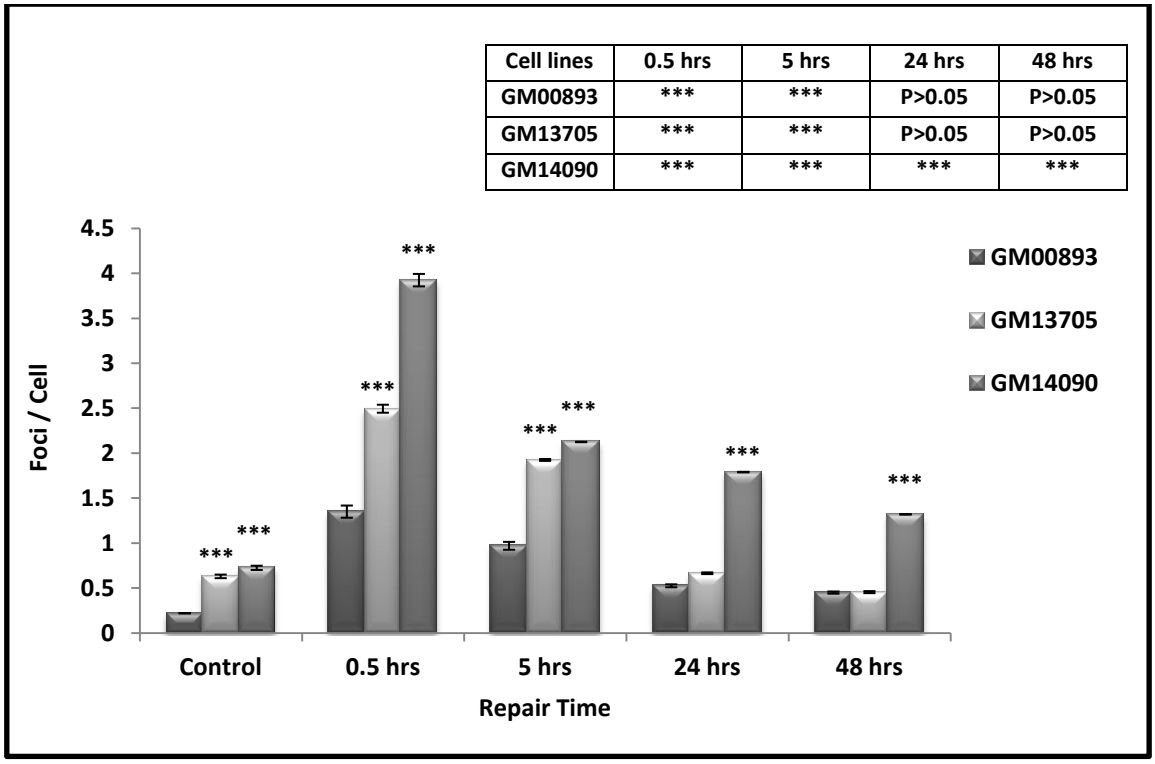

Figure 5.3 - H2AX analysis in normal and *BRCA1* defective cell lines after 1.0 Gy. ***=P<0.001, Error bars represent SEM.

We also exposed the above cell lines to other DNA damage inducing agents including MMC and BLM. Results of this analysis are shown in (Figures 5.4 and 5.5). Interestingly, all cell lines have shown normal response to MMC as the differences in frequencies of γ-H2AX positive cells were not statistically significant 24 hrs and 48 hrs after exposure, relative to control values, in any of the cell lines used (Figure 5.4). However, it was surprising that a similar response was observed after treatment of cells with BLM (Figure 5.5). BLM is a radiomimetic agent and the expectation was that the GM14090 cell line will show some residual DNA damage 24 hrs and 48 hrs as in the case of IR exposure (Figure 5.3). The only explanation we can offer is that the dose of BLM used was not sufficient to induce enough DNA damage that could lead to the defective response becoming obvious. This view is supported by the fact that immediately after the exposure (30 min) IR treated GM14090 cells showed approx. 4 DNA damage spots/cell (Figure 5.3) whereas BLM treated GM14090 cells showed approx. 1.5 DNA damage spots/cell (Figure 5.5) which is a 2.5-fold difference.

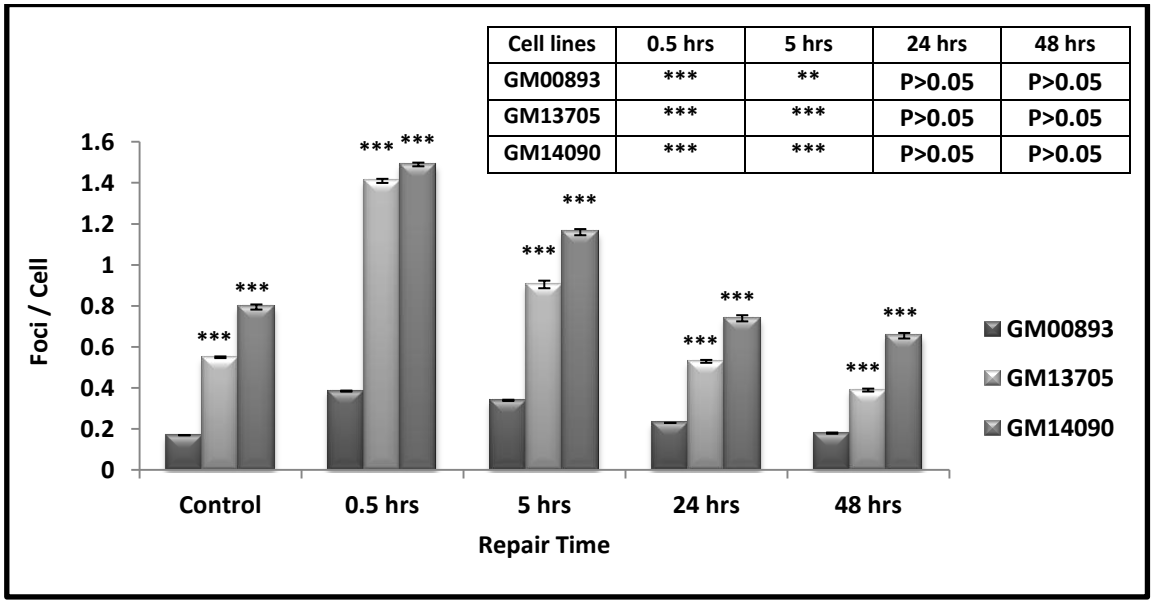

Figure 5.4 - H2AX analysis in normal and *BRCA1* defective cell lines after MMC treatment. ***=P<0.001, Error bars represent SEM.

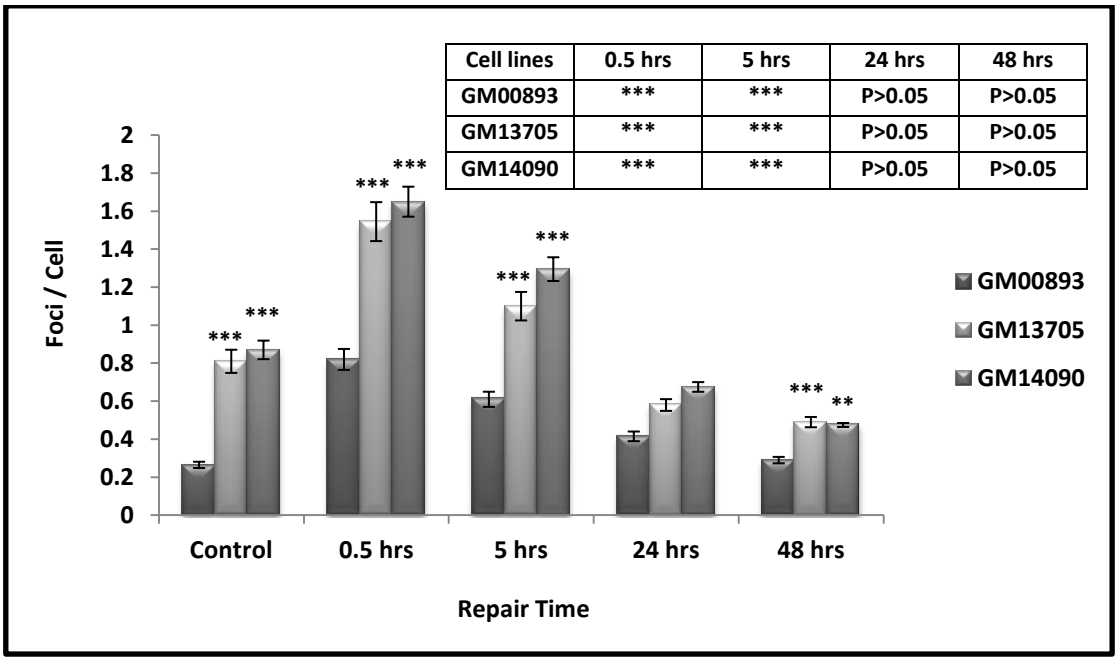

Figure 5.5 - H2AX analysis in normal and *BRCA1* defective cell lines after BLM treatment. **=P<0.01, ***=P<0.001, Error bars represent SEM.

5.2.3 - Telomere dysfunction-induced foci (TIF) Assay analysis in normal and heterozygous *BRCA1* cell lines

We next wanted to establish whether telomere dysfunction, due to changes in telomere length regulation in cells from *BRCA1* carriers (Figure 5.1), contributes to the defective DNA damage response observed in one of the cell lines (GM14090) (Figure 5.3). In order to achieve this we used the TIF assay. Examples of TIFs observed during this analysis are shown in (Figure 5.6). All cell lines showed some spontaneous TIFs with the frequencies being higher in *BRCA1* defective cells relative to control cells (Figure 5.7). As expected, the only cell line that showed residual TIFs was GM14090 (Figure 5.7). At all time-points investigated these cells showed higher TIF values relative to their untreated counterparts (Figure 5.7). It was particularly indicative that 24 hrs and 48 hrs after exposure TIF values remained higher in these cells relative to untreated control cells even though the difference

was not significant at the 48 hrs point (Figure 5.7). The other two cell lines, GM00893 and GM13705, showed higher TIF values, relative to untreated controls, only immediately after exposure (30 min) (Figure 5.7). These results suggest that dysfunctional telomeres contribute to the dysfunctional DNA damage response observed in the GM14090 cell line. To further support this view we compared (Figure 5.3) and (Figure 5.7) to determine the approximate contribution of dysfunctional telomeres to this defective DNA damage response. From (Figure 5.3) it is clear that frequencies of γ-H2AX foci in the GM14090 cell line were as follows:

30 min after exposure – 3.9 / cell

5 hrs after exposure – 2.1 / cell

24 hrs after exposure – 1.79 /cell

48 hrs after exposure – 1.32 / cell

On the other hand, frequencies of TIFs (Figure 5.7) were as follows:

30 min after exposure – 2.2 / cell

5 hrs after exposure – 1.2 / cell

24 hrs after exposure – 0.9 / cell

48 hrs after exposure – 0.6 / cell

When the values representing γ-H2AX/cell are compared with values representing TIF/cell then it is clear that TIFs contribute 50% to total DNA damage sites represented by γ-H2AX foci in the GM14090 cell line. If the figure of 50% γ-H2AX foci/cell is taken away from

each post-exposure point in the case of GM14090 cells, this would bring the GM14090 in line with the other two cell lines that showed a normal DNA damage response. From this brief analysis one can conclude that dysfunctional telomeres directly cause a dysfunction in DNA damage response observed in the GM14090 cell line.

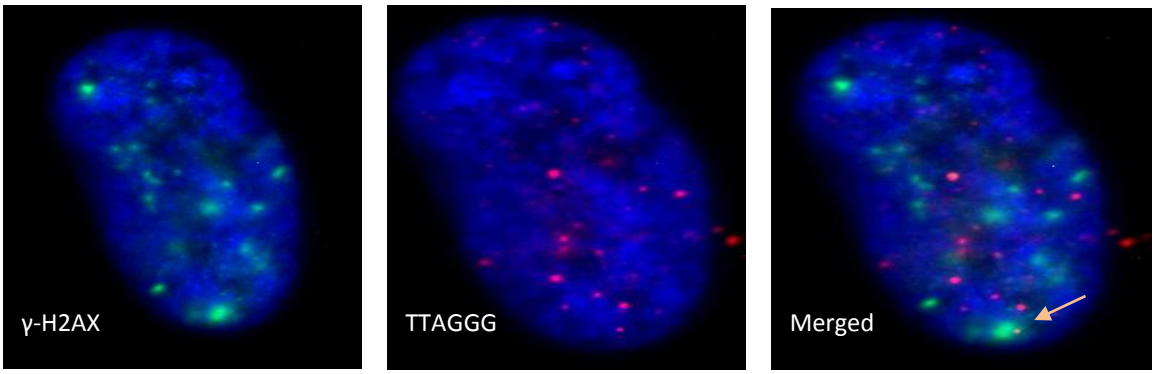

Figure 5.6 - Examples of TIFs observed In *BRCA1* Carriers.

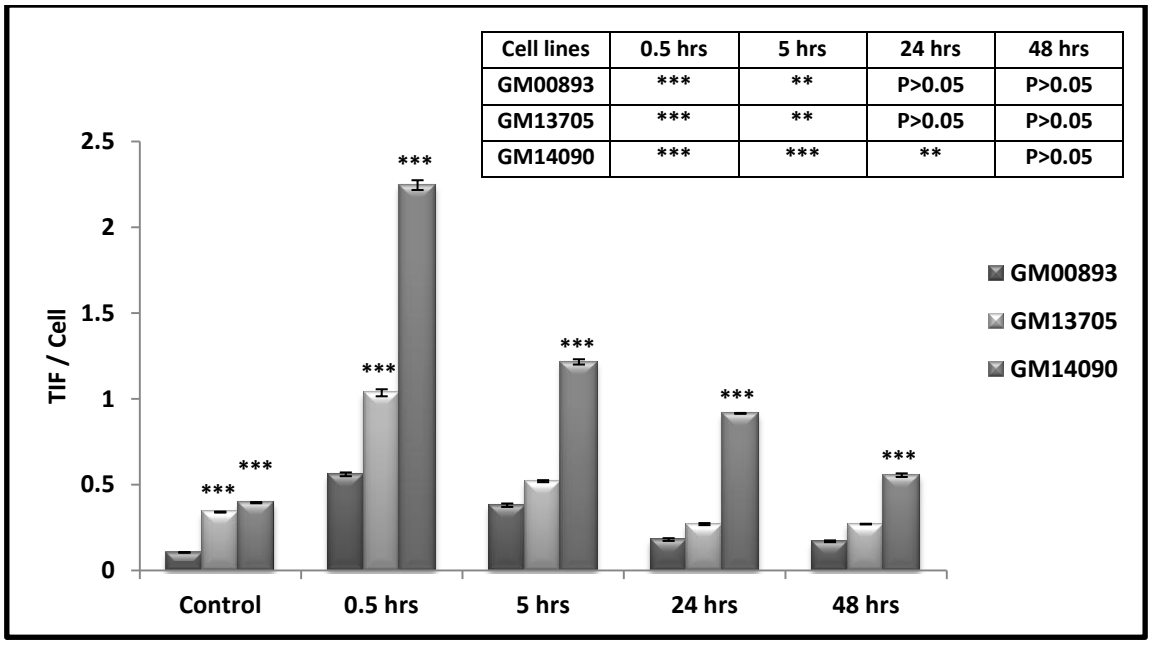

Figure 5.7 - Average number of TIF per cell in irradiated cell lines after 30 minutes, 5 hrs, 24 hrs and 48 hours post irradiation. ***=P<0.001, Error bars represent SEM.

We also exposed lymphoblastoid cell lines to other DNA damaging agents including MMC and BLM (Figures 5.8 and 5.9). However, these results were not as clear-cut as those obtained in the case of exposing cells to IR. The MMC exposed cells showed no difference in TIF frequencies between control values and values observed at 24 hrs and 48 hrs after exposure in any of the cell lines analysed (Figure 5.8). Similarly, the exposure of cells to BLM resulted in no difference between spontaneous and post-exposure TIF values at most points apart from marginal (but not significant) difference observed in the case of the GM14090 cell line at 48 hrs post-exposure (Figure 5.9). Therefore, we can conclude that the GM14090 cell line shows a defective DNA damage response when exposed to IR and that telomere dysfunction contributes significantly to this defective response (Figures 5.3 and 5.7).

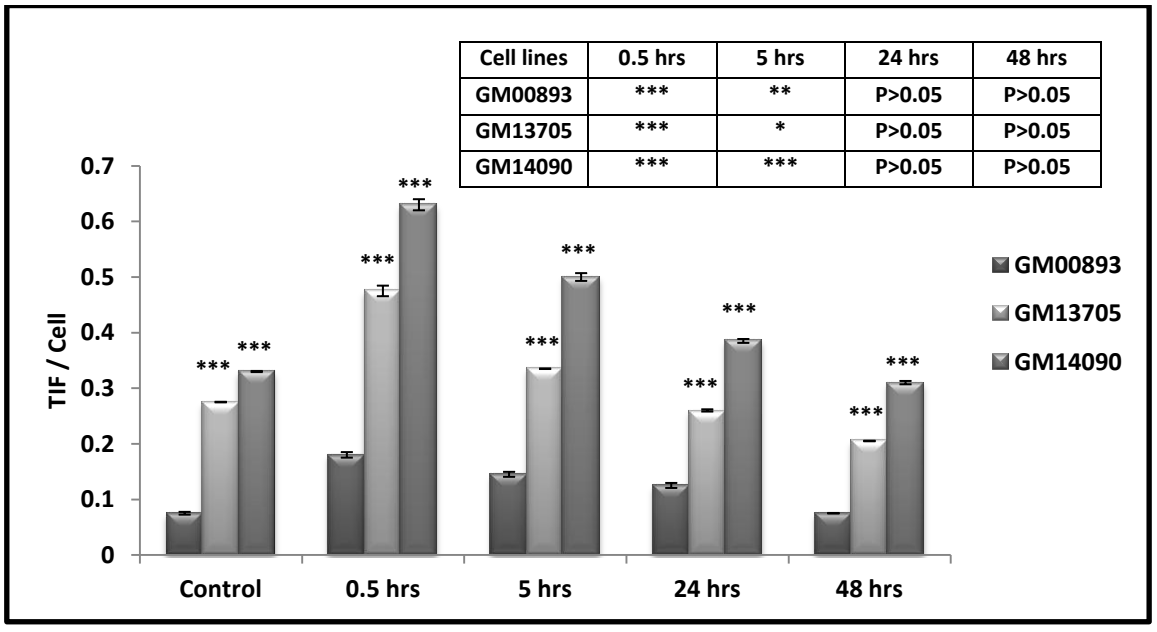

Figure 5.8 - Average number of TIF per cell after MMC treatment. ***=P<0.001, Error bars represent SEM.

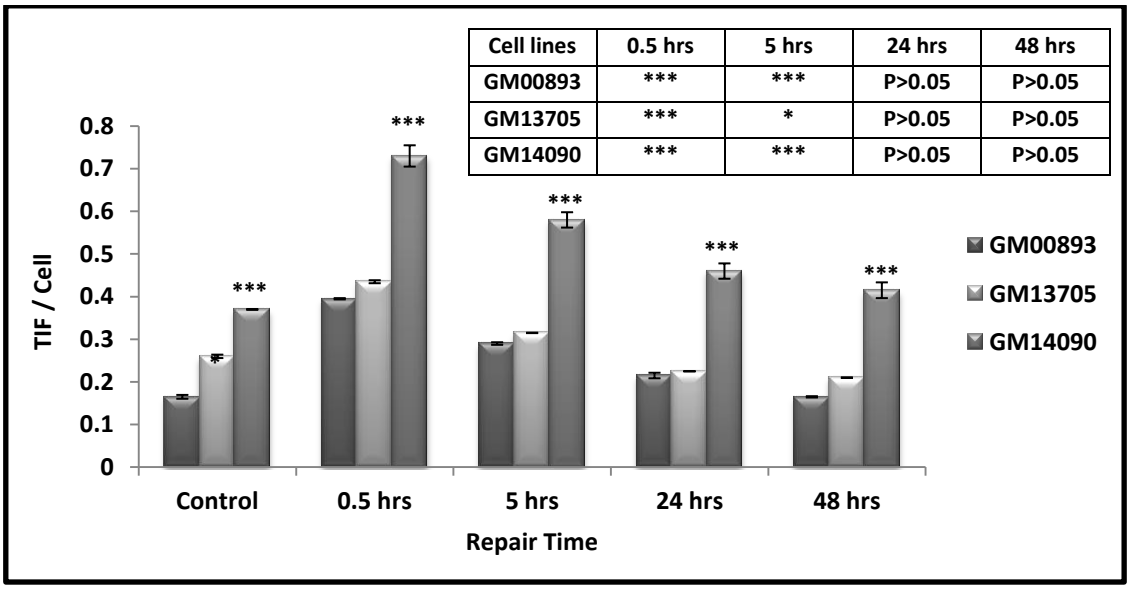

Figure 5.9 - Average number of TIF per cell after BLM treatment. *=P<0.05, ***=P<0.001, Error bars represent SEM.

5.2.4 - Interphase Quantitative Fluorescent *in situ* hybridization (I-QFISH) Analysis of Normal and Mouse Embryonic Stem Cells

In order to further substantiate the above conclusion we wanted to analyse cell lines with mutations in both *BRCA1* alleles. In contrast to *BRCA2*, no bi-allelic *BRCA1* mutations have been identified in human patients. Therefore, we resorted to mouse cell lines that have both copies of *Brca1* affected. We used mouse embryonic stem cells in which both copies of *Brca1* were disrupted by gene targeting and a corresponding control embryonic stem cell line. These cell lines were obtained from Dr Beverly Koller (University of North Carolina) and their generation has been described previously (Snouwaert *et al.* 1999). Mouse *Brca1*$^{+/+}$ embryonic stem cells (E14), as well as *Brca1*$^{-/-}$ mouse embryonic stem cells (408), were grown under tissue culture condition required for stem cells (see Material and methods) and their telomere lengths were measured by IQ-FISH (Figure 5.10). Our result revealed that *Brca1*$^{-/-}$ cells (408) exhibited significantly (P<0.05) shorter telomere length

compared to the control *Brca1*$^{+/+}$ cells (E14). Therefore, these results are similar to those observed in cell lines from *BRCA1* carriers (Figure 5.1).

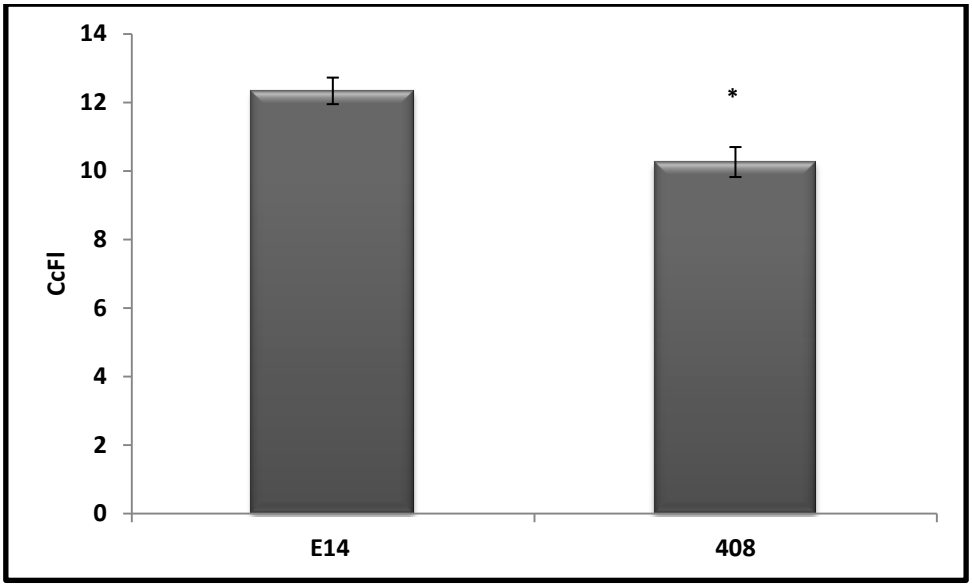

Figure 5.10 - Corrected calibrated fluorescence (CcFl) in mouse embryonic stem cell lines.*=P<0.05, Error bars represent SEM.

5.2.5 - DNA damage kinetics in normal and mouse embryonic stem cell lines

We have also analysed DNA damage response in mouse embryonic stem cells, with and without functional *Brca1* using the γ-H2AX assay. Representative examples of DNA damage foci in these cells after exposure to 1.0 Gy of IR are shown in (Figure 5.11). It is important to note that mouse embryonic stem cells were different from the rest of cell lines used in terms of fluorescence signal quality. As can be seen from Fig 5.11 the fluorescence background was high and sometime this complicated the analysis. The high fluorescence background in these cells is most likely caused by specific tissue culture conditions required by these cells. It is well documented that these cells grow in clumps and form 3 D structure

in which cells are positioned on top of each other. In spite of changes in washing conditions after antibody staining the fluorescence background remained high. Therefore, we used various options in the image acquisition software to remove non-specific background in order to make sure that only true DNA damage sites are taken into account.

Frequencies of γ-H2AX foci in untreated mouse embryonic stem cell lines revealed that *Brca1*$^{+/+}$ cells have a lower spontaneous frequency of γ-H2AX foci than *Brca1*$^{-/-}$ cells (Figure 5.12). Analysis of repair kinetics after IR exposure (1.0 Gy) revealed that *Brca1*$^{-/-}$ cells show significantly higher frequencies of γ-H2AX foci/cell than their untreated counterparts 24 hrs and 48 hrs after exposure to IR ($P<0.001$) (Figure 5.12). In the case of *Brca1*$^{+/+}$ cells the difference between γ-H2AX foci in untreated cells and treated cells at 24 hrs and 48 hrs post-treatment points was not statistically significant ($P=0.10$) (Figure 5.12). Therefore, these results show that mouse *Brca1*$^{-/-}$ embryonic stem cells show dysfunctional DNA damage response.

As above, we next wanted to establish potential contribution of dysfunctional telomeres to this defective response. However, in spite of several attempts the TIF assay in mouse embryonic stem cells did not work. We believe that specific conditions under which embryonic stem cells grow in culture have contributed to this. These cells typically form "islands" in which they do not grow in a single layer but rather form a 3 D shape in which some cells are on top of each other. This has made even the γ-H2AX assay difficult (see above), but we resorted to analysing exclusively cells on the edges of these islands that clearly had a 2 D shape. The problem with TIF was an extremely high degree of fluorescence background when both required fluorochromes (red and green) were applied. This made TIFs non-specific and completely prevented any meaningful analysis. The use of high

stringency washing after hybridization, or application of similar measures, did not improve the protocol. Therefore, we had to rely on different methods to assess contribution of telomeres to dysfunctional DNA damage response in mouse *Brca1* $^{-/-}$ cells. Since these cells grew relatively well in culture we thought that a cytological analysis of chromosome end-to-end fusions, events indicative of telomere dysfunction, would be a suitable method for this purpose.

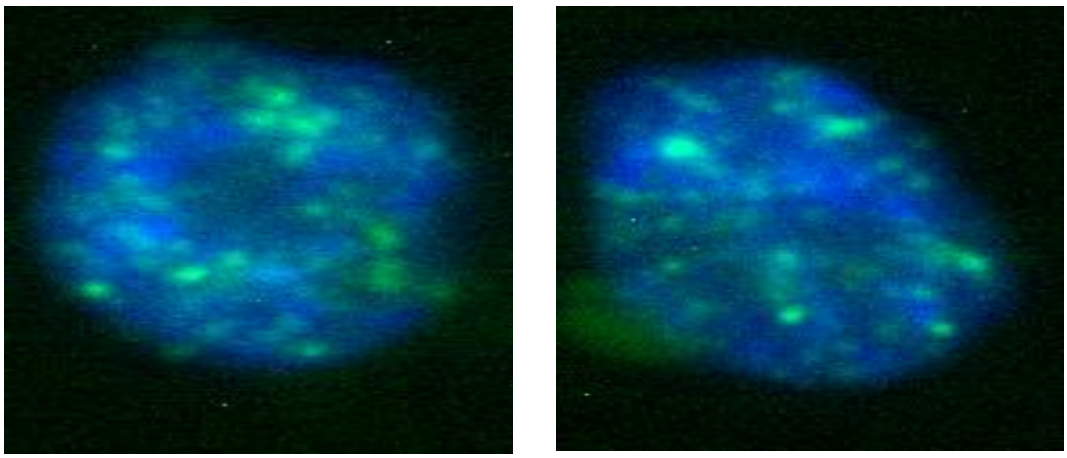

Figure 5.11 - Examples of DNA damage foci in mouse embryonic stem cells after exposure to IR.

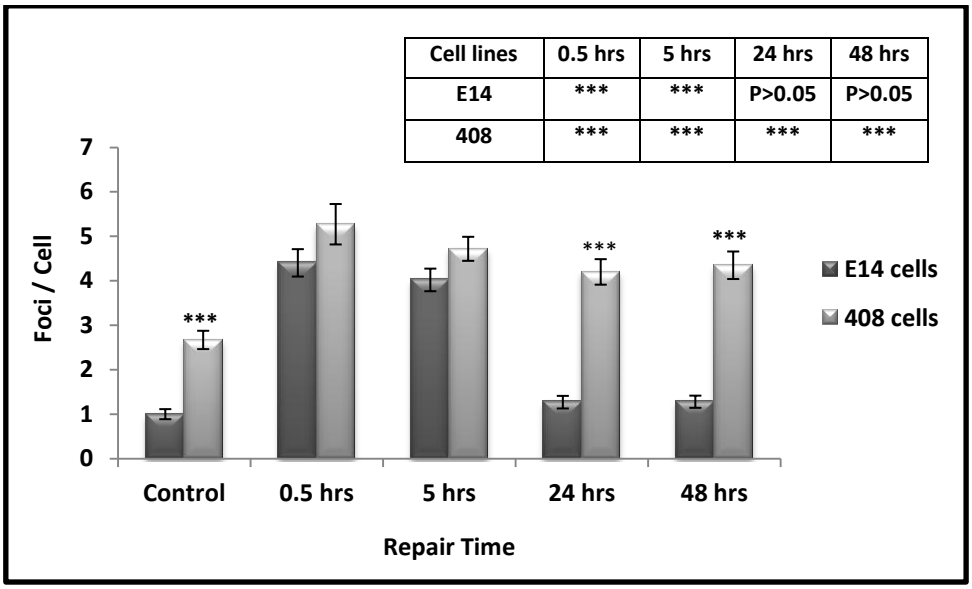

Figure 5.12 - Frequencies of γH2AX foci in mouse embryonic stem cells after 1.0 Gy of gamma rays. ***=P<0.001, Error bars represent SEM.

5.2.6 - Analysis of chromosome end-to-end fusions in mouse embryonic stem cells

Next, we irradiated mouse embryonic stem cell lines with 2.0 Gy of gamma rays and analysed exclusively end-to-end chromosome fusions after FISH with the telomeric PNA probe in irradiated and control cells. Examples of end-to-end chromosome fusions are shown in (Figure 5.13). It is important to note that we have only counted end-to-end chromosome fusions that showed the presence of telomeric signal at the fusion points.

Results of our analysis are shown in (Figure 5.14). Mouse *Brca1-/-* cells had higher spontaneous frequencies of chromosome end-to-end fusions relative to control cells. Interestingly, we have also observed a significantly higher frequency of γ-H2AX foci in these cells relative to control cells (Figure 5.12). The dose of 2.0 Gy of gamma rays was not able to induce end-to-end chromosome fusions in control cells as evidenced by the lack of statistical difference in frequencies of end-to-end chromosome fusions in irradiated and non-irradiated control cells (Figure 5.14). In contrast, *Brca1-/-* cells showed a statistically

significant difference between frequencies of end-to-end chromosome fusions in treated and untreated cells (Figure 5.14). It is therefore likely that some of the DNA damage foci observed in *Brca1-/-* cells after the γ-H2AX assay are due to dysfunctional telomeres. Unfortunately, we have not been able to quantify contribution of dysfunctional telomeres to the global DNA damage response in this cell line due to problems with the TIF assay.

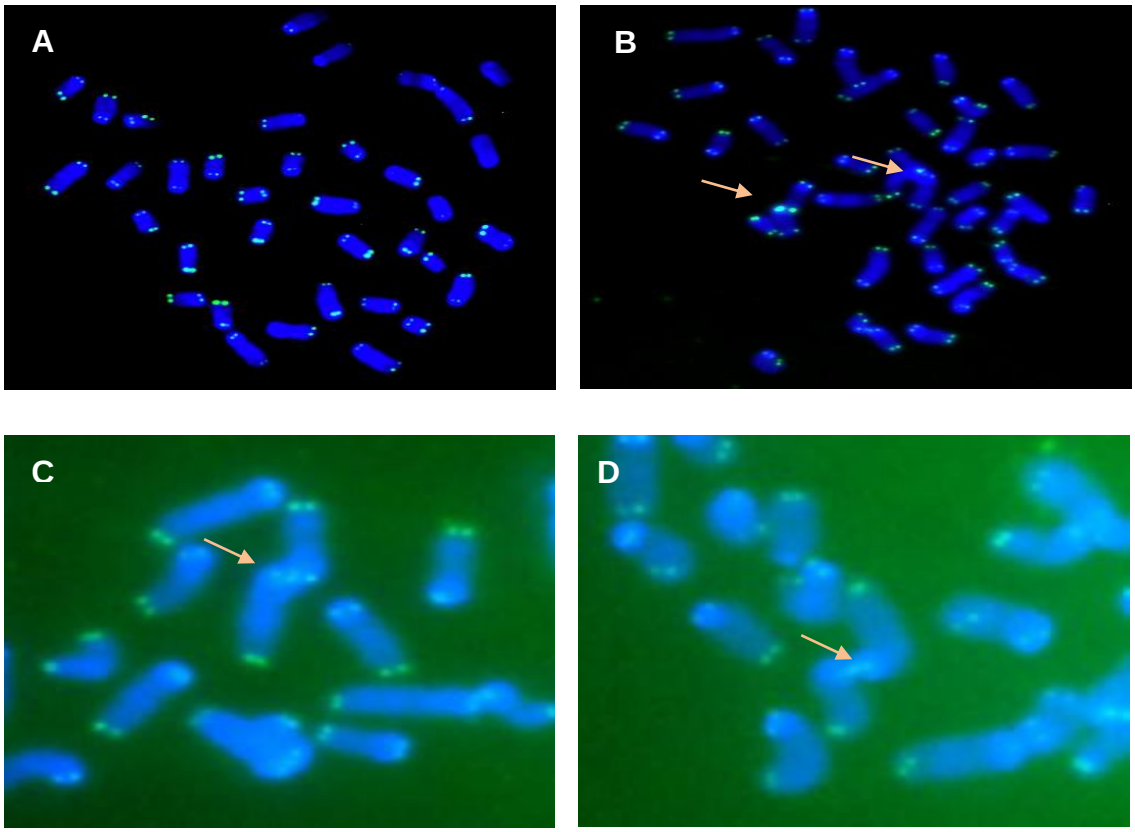

Figure 5.13 - Examples of telomeric fusions in mouse embryonic stem cells. (A) Untreated cells with no telomeric fusions. (B,C,D) Telomeric fusion in treated cells indicated by arrows.

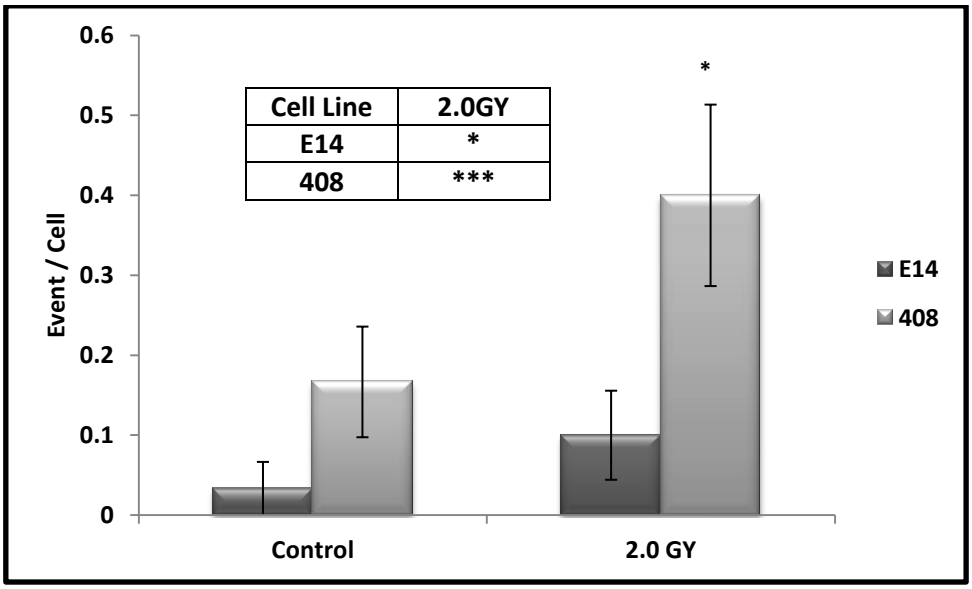

Figure 5.14 - Chromosome fusion analysis in mouse embryonic stem cells. *=P<0.05, ***=P<0.001, Error bars represent SEM.

5.3 - Discussion

Results presented in this chapter indicate that a dysfunctional copy of the *BRCA1* gene in a human cell line (GM14090) and both dysfunctional *Brca1* alleles in a mouse embryonic stem cell line (408) cause alterations in telomere length regulation as evidenced by shorter telomeres in these cell lines relative to appropriate control cell lines, and render these cells dysfunctional in terms of response to IR relative to control cells (Figsure 5.3 and 5.12). In the case of the human GM14090 cell line, established from a *BRCA1* mutation carrier (*BRCA1+/-*) we have been able to clearly establish that dysfunctional telomeres critically contribute to the defective DNA damage response in these cells. For example, when we examined frequencies of total DNA damage positive foci induced by IR in these cells relative to DNA damage foci that are located at telomeres and therefore caused by dysfunctional telomeres, we observed that the difference between GM14090 cells and the other two cell lines used in the study (one of which also originated from a BRCA1 carrier),

was due to those DNA damage foci located at telomeres (see page 146). Also, an examination of DNA damage kinetics suggested that damage at telomeres, in forms of TIFs, was significantly higher at all time points (5 hrs, 24 hrs and 48 hrs) post-exposure in the GM14090 cell line than in the other two cell lines (Figure 5.5).

In the case of mouse Brca1-/- we observed a similar but less clear-cut situation mainly because we have not been able to carry out the TIF assay as a result of problems specific to embryonic stem cells (see above). Nevertheless, we have been able to show that mouse Brca1-/- cells (i) possess shorter telomeres than control cells (Figure 5.10), (ii) have unrepaired DNA damage up to 48 hrs after induction (Figure 5.12) and (iii) have increased frequencies of spontaneous and radiation induced end-to-end chromosome fusions (Figure 5.14). Taken together, these results argue that telomere dysfunction mediated by dysfunctional Brca1 also contributes to defects in the global DNA damage response in these cells.

There are several potential mechanisms through which BRCA1 can exert its effects on telomeres and through this on DNA damage response. It was shown that BRCA1 participates in the regulation of telomerase activity (Xiong *et al.* 2003). It is therefore possible that dysfunctional BRCA1 may alter the normal telomerase function and lead to telomere shortening similar to that observed in (Figure 5.1 and 5.10). Alternatively, BRCA1 may affect telomeres independently of telomerase. A recent study suggests that BRCA1 interacts with components of shelterin, TRF1 and TRF2, and that another DNA damage response protein, RAD50, is required for this interaction (Ballal *et al.* 2009). Furthermore, BRCA1 regulates the length of single strand 3’ telomeric overhang with the help of RAD50 (Ballal *et al.* 2009). From these observations it is clear that BRCA1 exerts its effects on

telomeres via its role in DNA damage response, thus providing further evidence for the hypothesis that DNA damage response and telomere maintenance are functionally linked. Another potential mechanism through which BRCA1 could affect telomere maintenance is through its interaction with the protein involved in the ALT mediated maintenance of telomeres (Wu *et al.* 2003). However, this possibility seems least likely because only a very small proportion of tumour cells maintain their telomeres by ALT.

The obvious involvement of BRCA1 in telomere maintenance is interesting from the cancer treatment perspective. A tumour suppressor role of BRCA1 is well documented (Zhu *et al.* 2011). Telomere maintenance is also considered a tumour suppressor mechanism (Hahn 2003). When telomeres become critically short, typically in cells that come to the end of their proliferative lifespan, DNA damage response is activated in affected cells and they are usually eliminated from tissues by apoptosis (Gu *et al.* 2008). Thus, telomere length acts as a regulator of tissue homeostasis and it constitutes a powerful tumour suppressor mechanism. Given that both BRCA1 and telomeres are involved in two different tumour suppressor pathways the question is whether this scenario could be exploited for clinical interventions in the case of cancer therapy. One strategy would be to manipulate BRCA1 in order to make telomeres dysfunctional in tumour cells and at the same time inhibit telomerase activity in the same cells by one of the well-publicized telomerase inhibitors, which are currently under clinical testing (Xiong *et al.* 2003). This targeting of two tumour suppressor pathways via the link that the both share, namely the role in telomere metabolism, could potentially deprive tumour cells from the pathway, which essentially makes them immortalized. Such cells, once unable to maintain telomeres through the conventional telomerase-mediated mechanisms, would resort to alternative pathways such as ALT. However, given the documented role of BRCA1 in the ALT pathway it is possible that

this pathway could also be manipulated in order to fully achieve the aim of completely depriving tumour cells from a vital mechanism that provides unlimited proliferative capacity for them, namely telomere maintenance. One of the points for future research would be to examine in more detail the role of BRCA1 in ALT with a view of exploiting this pathway for cancer therapeutics.

Chapter 6 - DNA damage response in Dyskeratosis congenita cells

6.1 - Introduction

In previous chapters we have shown that defects in BRCA1 and BRCA2 proteins cause alterations in telomere maintenance and that, in some cases, these alterations contribute directly to defects in DNA damage response in affected cells. This is in line with the hypothesis that DNA damage mechanisms and telomere maintenance mechanisms are functionally linked (Slijepcevic 2006).

In order to test this hypothesis we have, so far, relied on using cell lines with defective DNA damage response genes such as *BRCA1* and *BRCA2* with a view of assessing their effects on telomere maintenance and also when such effects exist, whether they exert effects on the global DNA damage response. For example, in the case of a cell line from a carrier of a *BRCA1* mutation we have been able to show that the defective DNA damage response observed is exclusively due to dysfunctional telomeres (see page 146).

Another way of testing the functional link between telomeres and DNA damage response would be to probe the efficiency of DNA damage response mechanisms in cells in which telomeres are dysfunctional, but all DNA damage response genes are normal. A human disease DC is a rare progressive heritable disorder that is caused by mutations in genes that regulate telomere maintenance (Bessler *et al.* 2010). At least seven different genes are affected in this disease including genes associated with telomerase and RNA processing, as well as genes that encode some telomere binding proteins. These include: *DKC1* (Knight *et al.* 1999), *TERC* (Vulliamy *et al.* 2004), *TERT* (Vulliamy *et al.* 2005; Marrone *et al.* 2007), *TINF2* (Savage *et al.* 2008), *NHP2* (Vulliamy *et al.* 2008), *NOP10* (Walne *et al.* 2007), and *WRAP53* (Zhong *et al.* 2011). As a result, DC patients show shorter telomeres than age matched control individuals and measurement of telomere length is used to

confirm DC diagnosis in some laboratories (Vulliamy *et al.* 2001). Therefore, in order to test the functional link between telomeres and DNA damage response further, cells from DC patients can be used as a suitable model for assessing the efficiency of DNA damage response in the context of dysfunctional telomeres.

A number of studies published in the past have examined the response of cells from DC patients to genotoxic agents including IR. For example, (DeBauche *et al.* 1990) showed that DC fibroblasts had several times higher frequencies of radiation-induced chromatid breaks than control cells. In addition, lymphocytes from a Hoyeraal-Hreidarsson patient, the most severe form of X-linked DC, showed sensitivity to radiation and alkylating agents (M'Kacher *et al.* 2003). It was also reported independently that a DC patient showed hypersensitivity to radiation therapy (Cengiz *et al.* 2004). However, a recent study suggested that DC cells have a normal DNA damage response (Kirwan *et al.* 2011). This view was based on a simple comparison of etoposide-induced γ-H2AX foci in lymphocytes from DC and control patients immediately after the exposure, which resulted in similar frequencies of DNA damage foci in both cell types (Kirwan *et al.* 2011). Crucially, no repair of DNA damage was analysed after the exposure in the study by (Kirwan *et al.* 2011). This type of analysis is the standard procedure in our experiments. For example, we normally monitor DNA damage frequencies 30 min, 5 hrs, 24 hrs and 48 hrs following treatment with genotoxic agents (see previous chapters). Defective DNA damage response will become apparent only if non-repaired DNA damage persists long time after its induction. Therefore, the conclusion of the (Kirwan *et al.* 2011) study that DC cells have a normal DNA damage response, is somewhat weak in light of their failure to analyse DNA damage kinetics. Another weakness of this study is that no other DNA damaging agent apart from etoposide was used in spite of published studies indicating sensitivity of DC cells to ionizing radiation (see above).

Importantly, (Kirwan *et al.* 2011) showed that DC cells have increased apoptosis, cell cycle abnormalities and increased spontaneous TIF frequencies in lymphocytes and increased spontaneous γ-H2AX frequencies in fibroblasts. All these phenotypic features can potentially cause defects in DNA damage response mechanisms. Interestingly, a mouse study contradicts (Kirwan *et al.* 2011) conclusines. Pathological *Dkc1* mutations in mouse cause defective DNA damage response after exposure to etoposide (Gu *et al.* 2008).

In this chapter we examined DNA damage response in cells from DC patients belonging to the X-linked subtype using the γ-H2AX and TIF assays. This genetic subtype of DC is characterized by mutations in the gene encoding Dyskerin (DKC1), an integral component of telomerase (Gardano *et al.* 2012). Furthermore, we carried out RNAi to knock-down the expression of *DKC1* in two different human cell lines. Our results indicate that DC cells show a defective response to ionizing radiation.

6.2 - Results

6.2.1 - Telomere length analysis in DC cell lines

We started by measuring telomere length in fibroblast cell lines from DC patients that have defective *DKC1*. One cell line originated from a DC patient with a heterozygous *DKC1* mutation, and the other cell line originated from a DC patient with homozygous *DKC1* mutations. The third cell line was used as a control and it originated from a normal individual. The analysis was performed before we finalized our IQ-FISH protocol and as a result telomere fluorescence values shown in (Figure 6.1) represent unmodified telomere fluorescence. In line with numerous published studies (see above) DC cells showed significantly shorter telomeres than control cells (Figure 6.1). It was also clear that the rate of telomere shortening was more dramatic in DC cells with a heterozygous mutation than in

control cells judging by the slope of curve representing telomere loss over time (Figure 6.1). For example, we calculated that normal cells lose 0.5 fluorescence units due to telomeric DNA/cell passage, whereas DC cells with a heterozygous *DKC1* mutation lose 2.5 fluorescence units due to telomeric DNA/cell passage. DC cells with homozygous mutations grew slowly and we only managed 4 tissue culture passages (Figure 6.1). This precluded a meaningful calculation of telomere loss that was calculated in other cell lines over a period of 12 passages (Figure 6.1). Overall, these results confirm telomere shortening in DC cells relative to control cells.

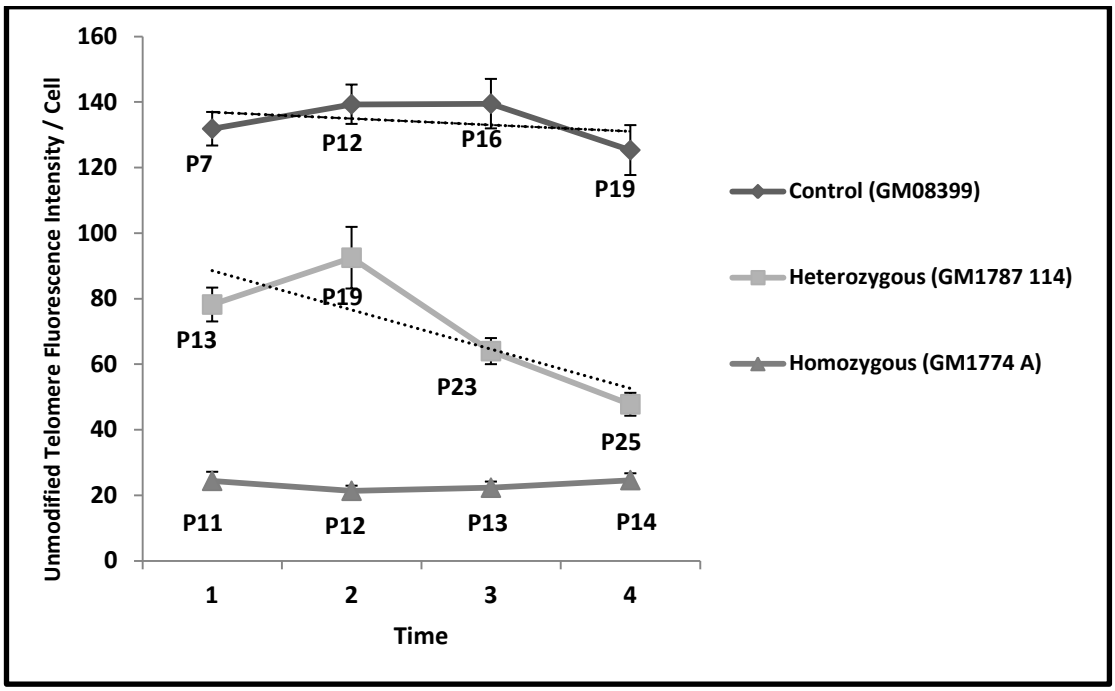

Figure 6.1 - Average telomere length in normal and DC cell lines. Error bars represent SEM.

6.2.2 - DNA damage kinetics in DC cell lines

Next, we monitored DNA damage response in DC cells after exposure to IR using the γ-H2AX assay. Results of this analysis are shown in (Figure 6.2). Both DC cell lines showed elevated spontaneous frequencies of γ-H2AX foci relative to control cells (Figure 6.2).

Interestingly, 30 min and 5 hrs after the exposure to 1.0 Gy of gamma rays there was no difference in frequencies of DNA damage foci between cell lines (Figure 6.2). However, the cell line with the homozygous *DKC1* mutation showed persistence of DNA damage 24 and 48 hrs post-exposure with the levels of γ-H2AX foci significantly higher than in control non-exposed cells (P<0.001), or control exposed cells with normal *DKC1* (P<0.001) (Figure 6.2). The presence of unrepaired DNA damage in DC cells with homozygous *DKC1* mutations 24 hrs and 48 hrs after induction is indicative of a defective DNA damage response. While in normal cells and cells with a heterozygous *DKC1* mutation frequencies of γ-H2AX foci return virtually to the level observed before exposure, at 24 hrs and 48 hrs points, DC cells with homozygous mutations showed approximately 2-fold frequencies of γ-H2AX foci in comparison to the same cells before exposure (Figure 6.2).

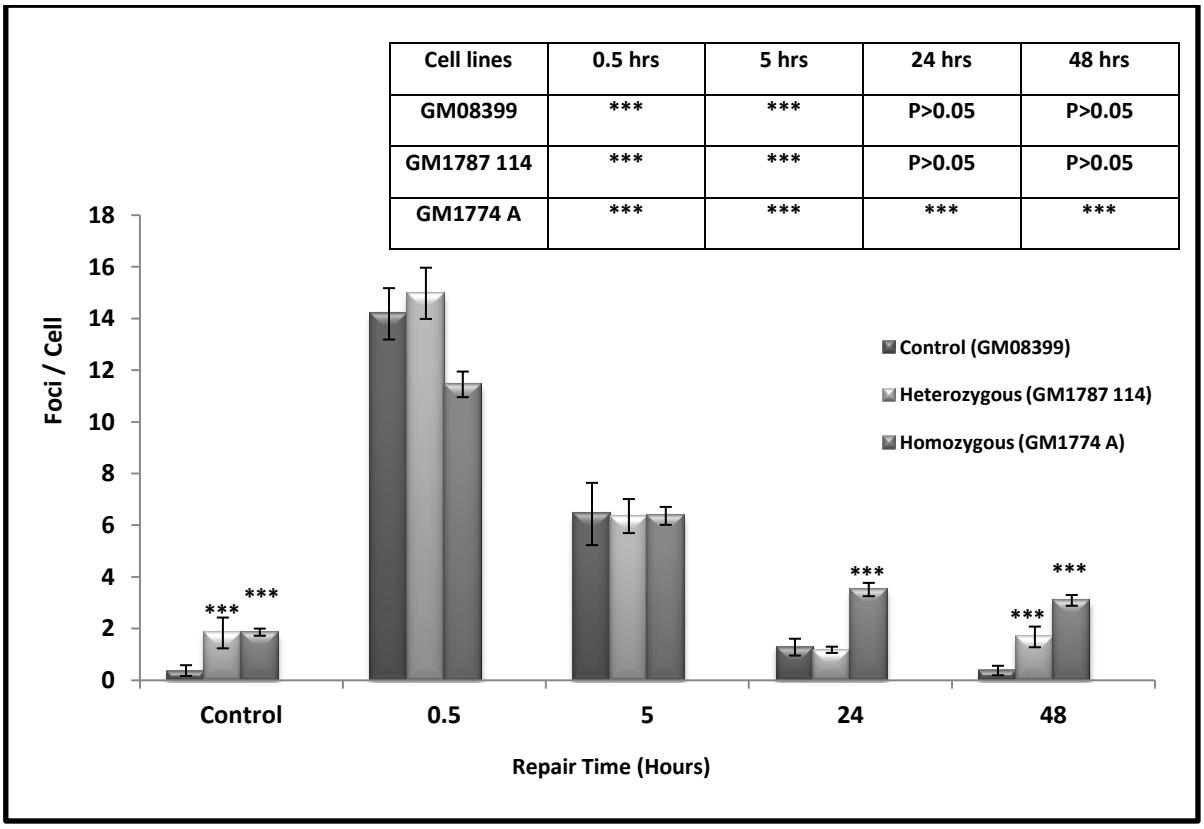

Figure 6.2 - H2AX analysis in normal and DC cell lines after 1.0 Gy of gamma rays. *** = P<0.001. Error bars represent SEM.

6.2.3 - Telomere dysfunction-induced foci (TIF) Assay analysis in Fibroblast DC cell lines

Next, we carried out TIF analysis in the above three cell lines. Our analysis revealed that DC cells showed higher spontaneous frequencies of TIFs compared to normal cells (Figure 6.3). However, there were no significant differences between control values and values of TIFs observed at any point after exposure to IR. The TIF values were low like in the case of *BRCA2* defective cells (see Chapter 4) suggesting that assays other than TIF should be employed to investigate whether dysfunctional telomeres contribute to the observed defective DNA damage response in the GM1774A cells.

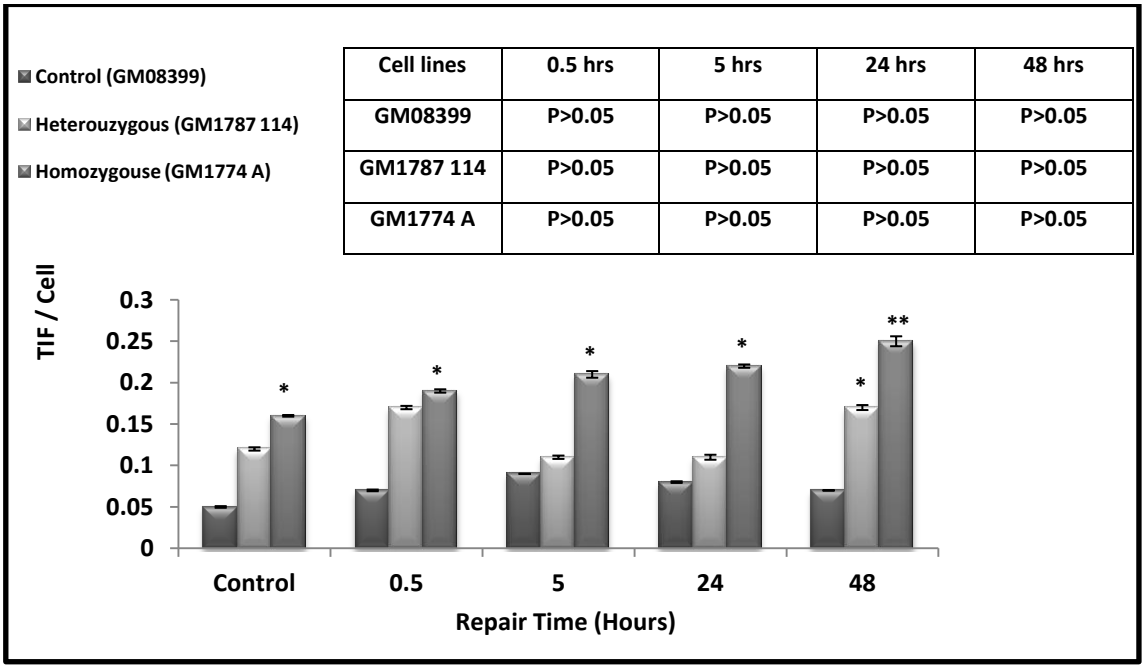

Cell lines	0.5 hrs	5 hrs	24 hrs	48 hrs
GM08399	P>0.05	P>0.05	P>0.05	P>0.05
GM1787 114	P>0.05	P>0.05	P>0.05	P>0.05
GM1774 A	P>0.05	P>0.05	P>0.05	P>0.05

Figure 6.3 - Average number of TIF per cell in irradiated cell lines after 30 minutes, 5, and 24 and 48 hours post irradiation. *=P<0.05, **=P<0.01, Error bars represent SEM.

6.2.4 - Analysis of chromosomal aberrations in DC cell lines

We have attempted to analyse radiation induced chromosomal aberrations in DC and control cells. Unfortunately, the GM1774A cell line, originating from a patient with homozygous *DKC1* mutations showed a too low mitotic index in order to allow preparation of good quality metaphases. So, we have been able to analyse only two remaining cell lines. These analyses have shown no difference in frequencies of radiation induced chromosome aberrations between the cell lines (Figure 6.4).

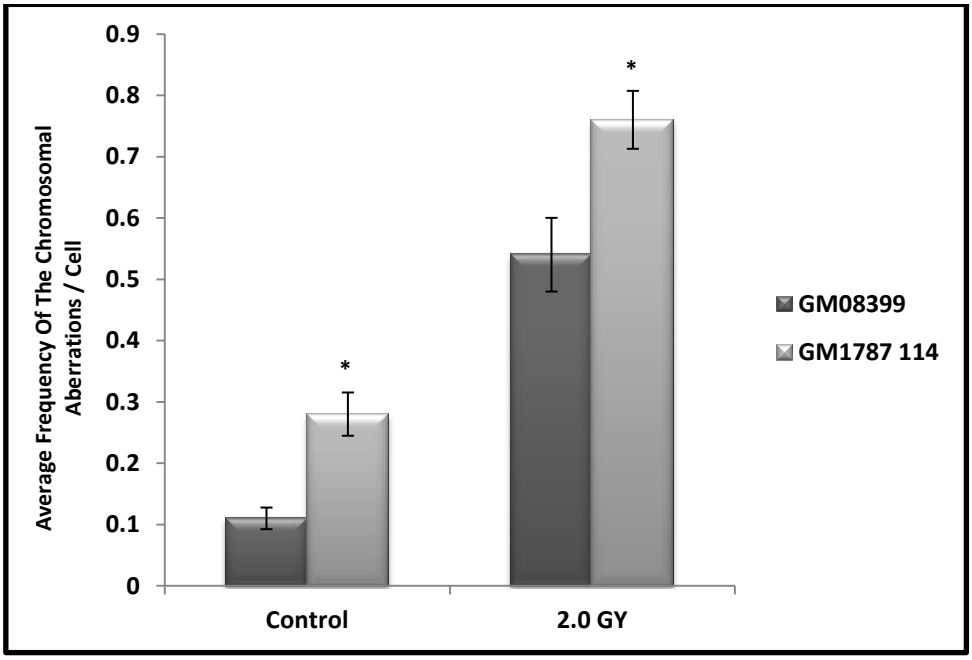

Figure 6.4 - Chromosomal aberration analysis in control (GM08399) and DC heterozygous (GM1787 114) cells. *=P<0.05. Error bars represent SEM.

6.2.5 - Anaphase Bridges analysis in Fibroblast DC cell lines

We have also attempted to analyse anaphase bridge frequencies in the above cell lines. Similarly to the situation encountered with the analysis of chromosome aberrations,

we have not been able to observe enough GM1774A mitotic cells to have sufficient number of cells in anaphase to satisfy a minimal requirement for the statistical analysis. Results of anaphase bridge analysis for the remaining two cell lines are presented in (Figure 6.5). Overall, we could not find any statistical differences between control and IR, MMC or BLM treated cells (Figure 6.5). Differences between cell lines were inconsistent. For example, frequencies of spontaneous anaphase bridges/cell in the GM08399 ranged from 0.045-0.09 (Figure 6.5). In the case of treatment the variation was between 0.09-0.155 (Figure 6.5). Similarly, spontaneous anaphase bridges/cell in the GM1787114 cell line ranged from 0.09 – 0.19 (Figure 6.5). In the case of treatment the range was 0.135 – 0.205 anaphase bridges/cell (Figure 6.5). Because of the clear overlap between spontaneous anaphase bridge/cell values and those observed after treatment the statistical analysis did not result in significant differences with the exception of BLM treatment (Figure 6.5 C).

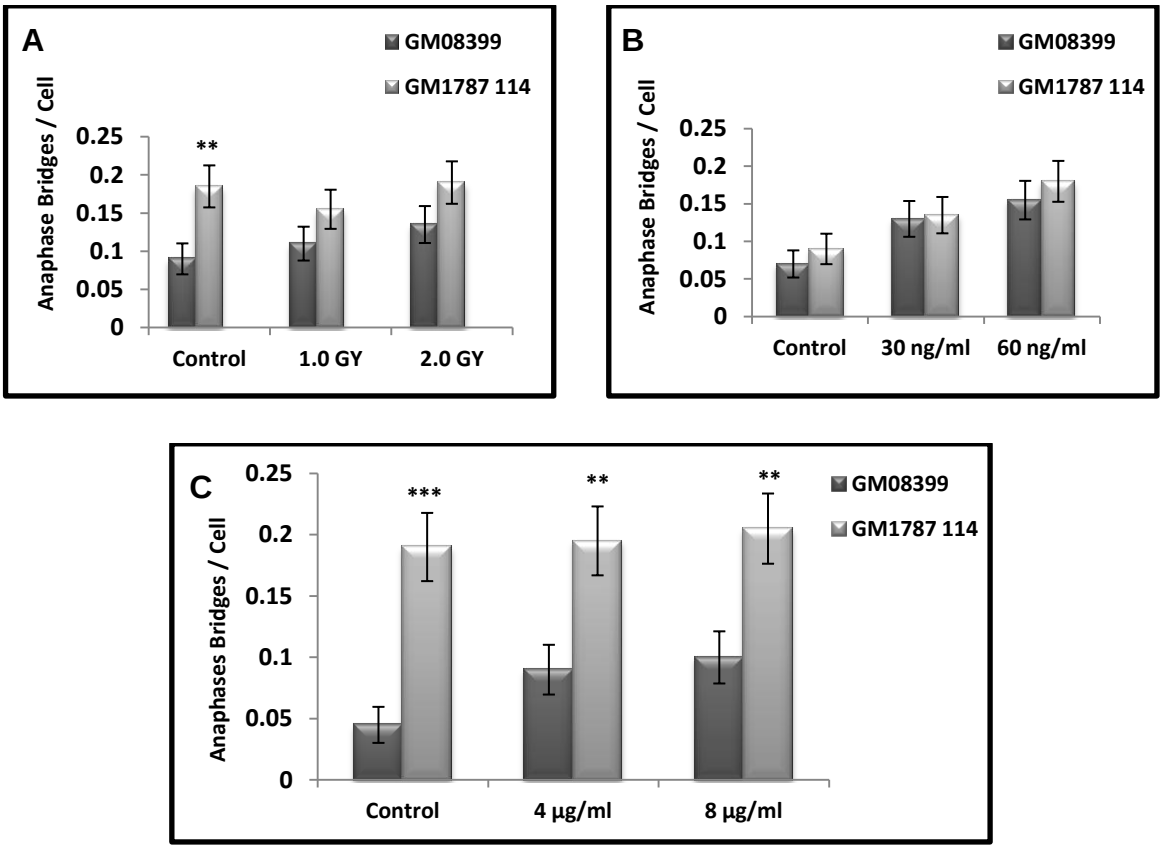

Figure 6.5 - Analysis of anaphase bridges between DC and control cells after exposure to IR (A), MMC (B) and BLM (C). ** = P<0.01, *** = P<0.001. Error bars represent SEM.

6.2.6 - Knock-down of *DKC1* in Hela and U2OS through siRNA

The presence of unrepaired DNA damage 24 hrs and 48 hrs after irradiation in DC cells with homozygous *DKC1* mutations and its absence in control cells, or cells with a heterozygous *DKC1* mutation (Figure 6.2) suggests that dysfunctional *DKC1*, which eventually leads to telomere shortening and loss of telomere function, also leads to a dysfunctional DNA damage response. To test this hypothesis, we decided to knock-down the expression of *DKC1* in two immortalized human cell lines and examine their DNA damage response mechanisms. We used the HeLa cell line that maintains telomeres by telomerase and the U2OS cell line that maintains telomeres by the ALT (Alternative Lengthening of

Telomeres) pathway. The reasoning behind this choice of cell lines was that the knock-down of *DKC1* will not have any phenotypic effects on ALT positive cells which usually lack telomerase activity (Grobelny *et al.* 2001). As indicated earlier, *DKC1* is an integral component of telomerase.

To carry out the knock-down experiments we used the Dharmacon Smart Pool siRNA approach as this approach worked well before in our laboratory. The complete protocol for knock-down has been described fully in chapter 2. Details of four siRNA oligonucleotides within the Smart Pool specific for the *DKC1* gene are listed in (Table 6.1).

Table 6.1 - All four sequences of siRNA used in knock-down of DKC1 gene

Dharmacon Smart Pool siRNA	Target Sequence
Human DKC1 Sequence 1	CAAGGUGACUGGUUGUUUA
Human DKC1 Sequence 2	GCAGGUAGUUGCCGAAGCA
Human DKC1 Sequence 3	UCUCAUAAACGGCUGGUUA
Human DKC1 Sequence 4	GGACAGGUUUCAUUAAUCU

Before the actual knock-down experiments, we needed to carry out some important quality control steps in order to ensure that the verification of the RNAi procedure is robust enough. These included optimization of primers for *DKC1* and the control *GAPDH* gene by conventional PCR and optimization of primer concentrations for quantitative RT-PCR and

establishment of dissociation curves. The results of primer optimization for *DKC1* and *GAPDH* genes are shown in (Figure 6.6). A typical dissociation curve showing clear amplification products without non-specific amplification is shown in (Figure 6.7)

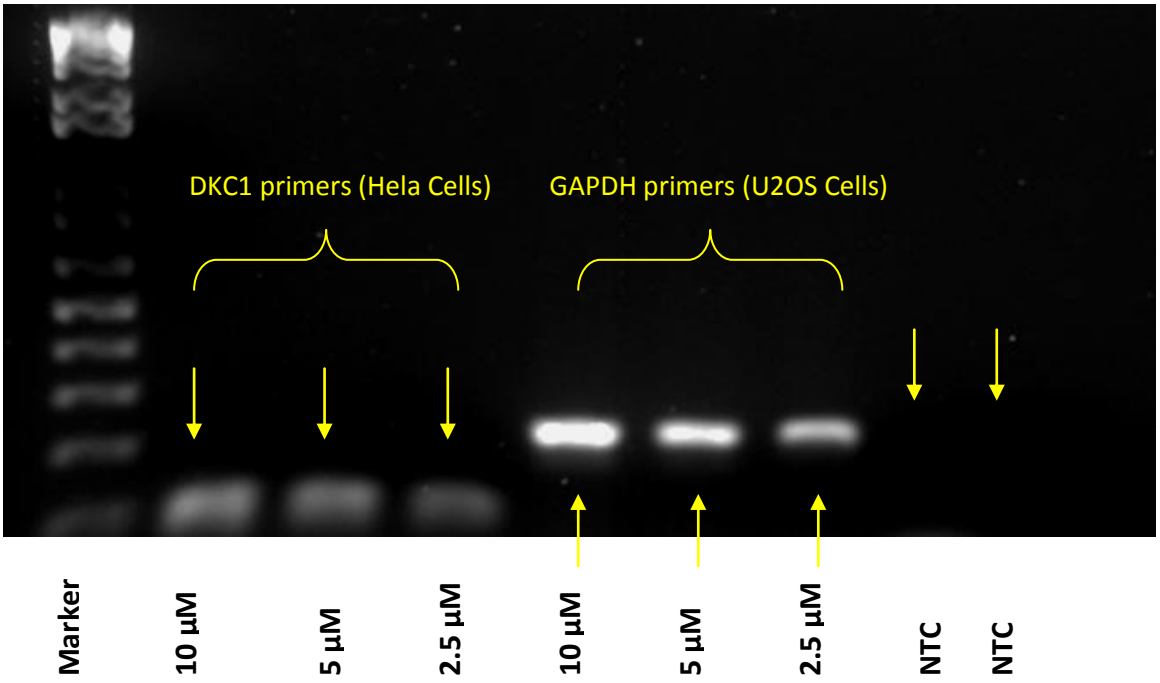

Figure 6.6 – Primer optimization. Lane 1 is a molecular weight marker. Lane (2-4) shows the *DKC1* (dyskerin) gene product in the Hela cell line. Lane (5-7) shows the *GAPDH* gene product in the U2OS cell line. Lane 8 and 9 are negative controls.

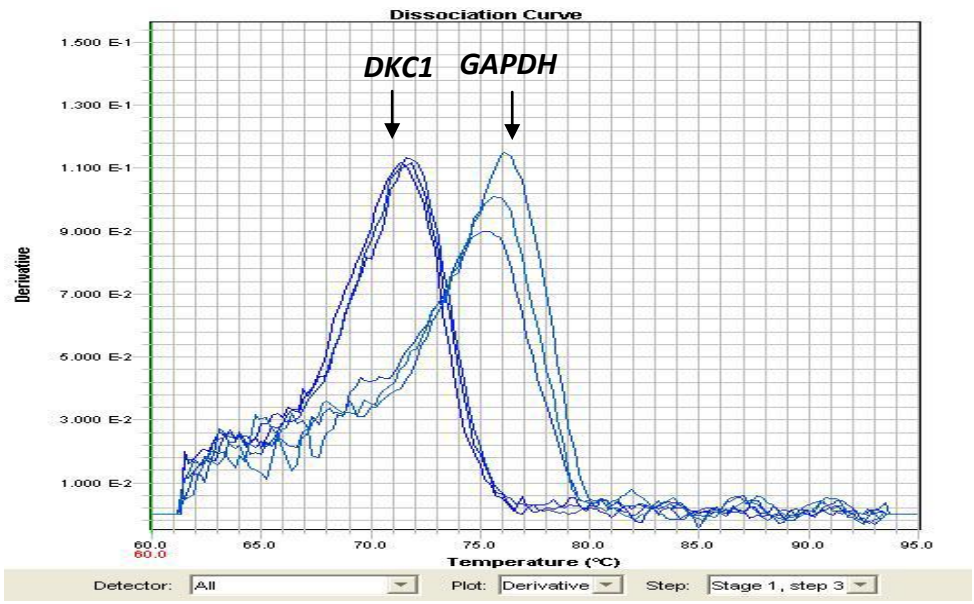

Figure 6.7 - Dissociation curve analysis confirms only one amplification product without any non-specific amplification or primer dimmer.

Having completed important preparatory steps we started the knock-down protocol with the control *GAPDH* gene. Choosing proper controls is an important feature of any study design. One important control that ensures an efficient delivery of the siRNA oligonucleotides into the cells was the knock-down of the housekeeping gene *GAPDH*. Results of the *GAPDH* knock-down are shown in (Figure 6.8). It is clear that the knock-down was efficient as the expression of *GAPDH* was reduced to between 20% and 40% and the effect lasted up to 72 hrs depending on the cell line (Figure 6.8).

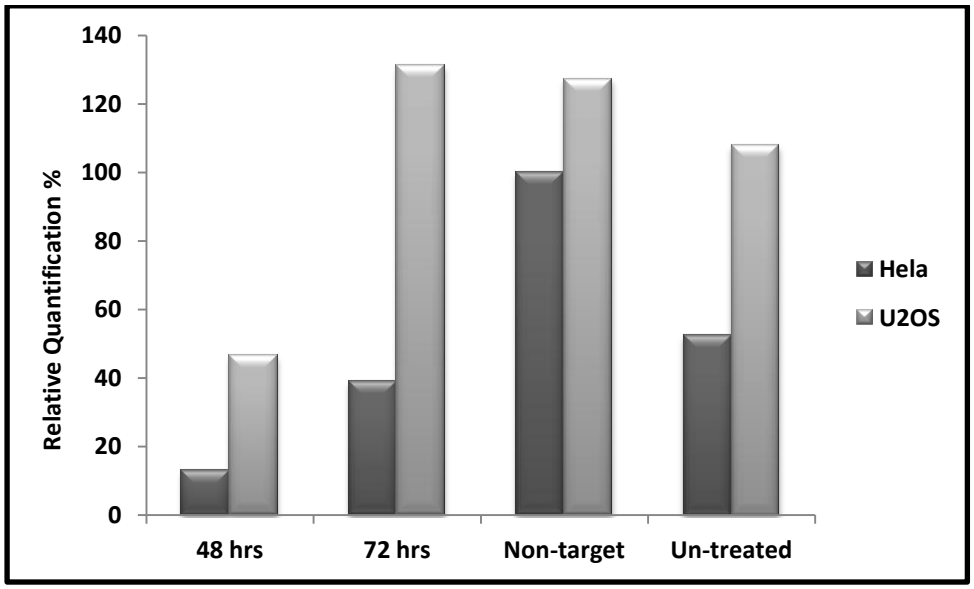

Figure 6.8 - Knock-down of the *GAPDH* gene in Hela and U2OS human cell lines.

We then focused on knocking-down *DKC1*. The RT-PCR results show that this procedure resulted in 50% *DKC1* knockdown 48hrs and 72hrs after transfection depending on the cell line (Figure 6.9). This knock-down efficiency was somewhat lower than in the case of *GAPDH*. A similar pattern was observed by Western blot, which showed a clear reduction in the *DKC1* specific signal 48 hrs after transfection in the U2OS cell line and 48 and 72 hrs after transfection in the HeLa cell line (Figure 6.10).

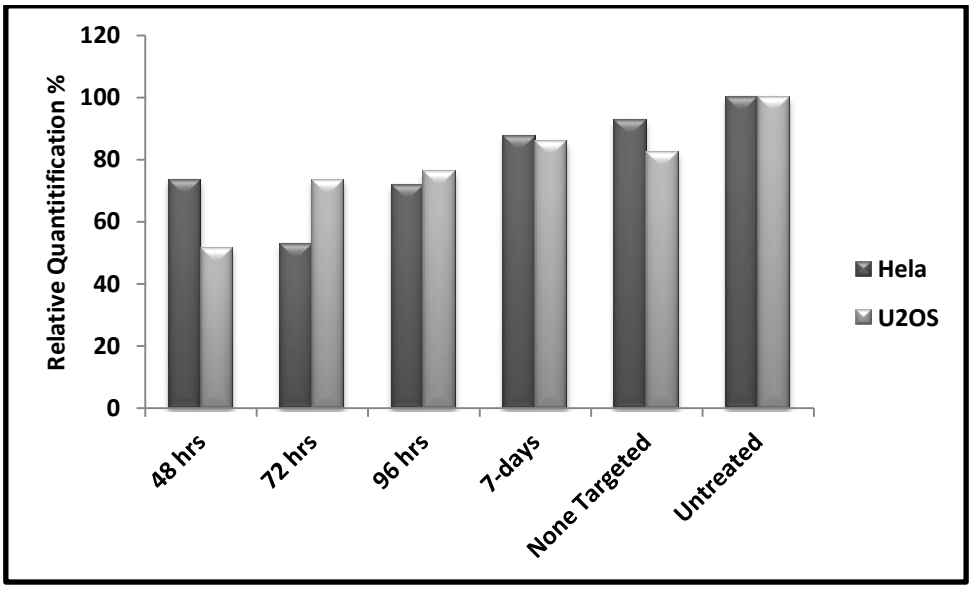

Figure 6.9 - Knock-down of the *DKC1* gene in Hela and U2OS human cell lines. Graph showing relative percentage of *DKC1* mRNA in the two cell lines. A 52 % knock-down was achieved in the Hela cell line (72 hrs after transfection) and 51 % in the U2OS cell line (48 hrs after transfection).

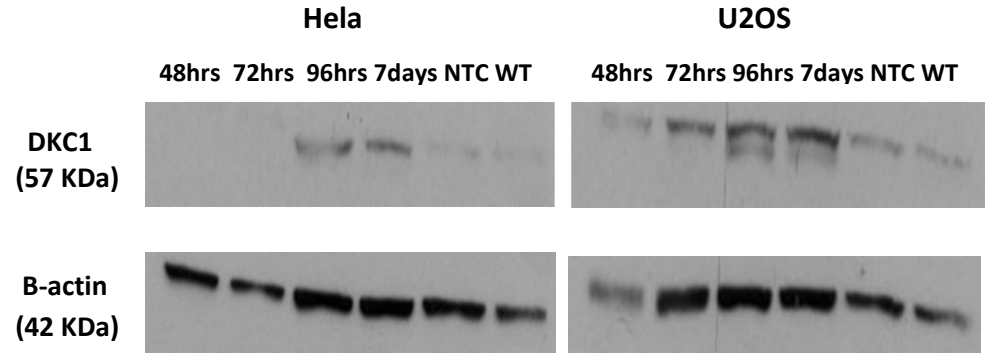

Figure 6.10 - Western blot analysis of *DKC1* expression following transfection with siRNA oligonucleotides.

The next step for us was to check the DNA damage response phenotype in both cell lines at post-transfection points that showed the lowest expression of *DKC1*. In the case of HeLa cells the lowest expression was 52% and this expression was observed 72 hrs after transfection with siRNA oligonucleotides (Figure 6.9). In the case of U2OS cells the lowest expression was 51% and it was observed 48 h after transfection (Figure 6.9). We have selected exclusively the above time points in each cell line respectively and examined DNA damage response using γ-H2AX and TIF assays. Since we observed unrepaired DNA damage in DC cells 48 hrs after irradiation (Figure 6.2) which is potentially indicative of a defective DNA damage response we decided to plan the experiment to take into account this point. The outline of the experimental plan is presented in (Figure 6.11) and examples of cell images with DNA damage foci observed are shown in (Figure 6.12). In brief, we transfected cells with siRNA oligonucleotides and waited for 48 hrs (U20S) or 72 hrs (Hela) at which point we have irradiated these cells with 1.0 Gy of gamma rays. Exactly 48 hrs after irradiation we carried out γ-H2AX and TIF assays. The controls included (i) unexposed HeLa and U2OS cells, (ii) HeLa and U2OS cells transfected with scrambled oligonucleotides and (iii) irradiated HeLa and U2OS cells without any transfection analysed for the presence of DNA damage 48 hrs after exposure to radiation (see Figures 6.11).

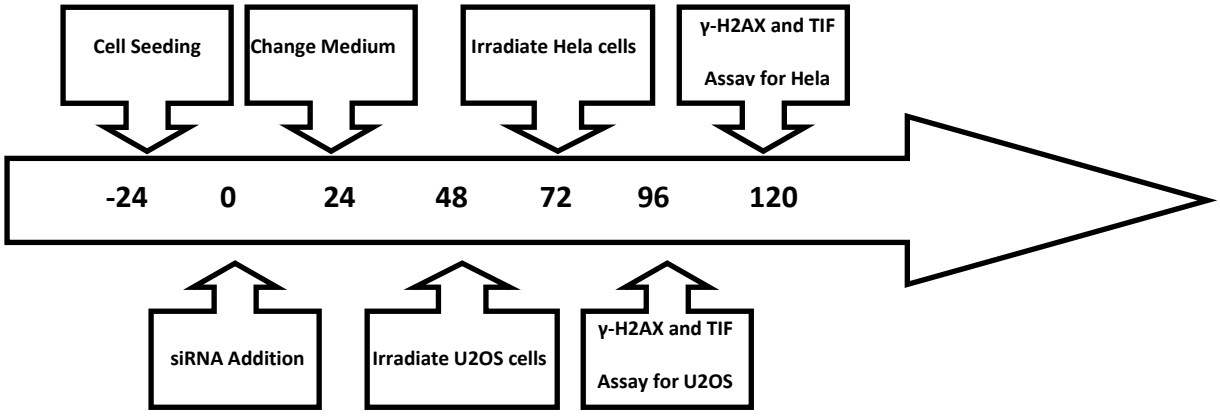

Figure 6.11 - The outline of the experimental plan in order to check the DNA damage response phenotype in Hela and U2OS cell lines at post-transfection points.

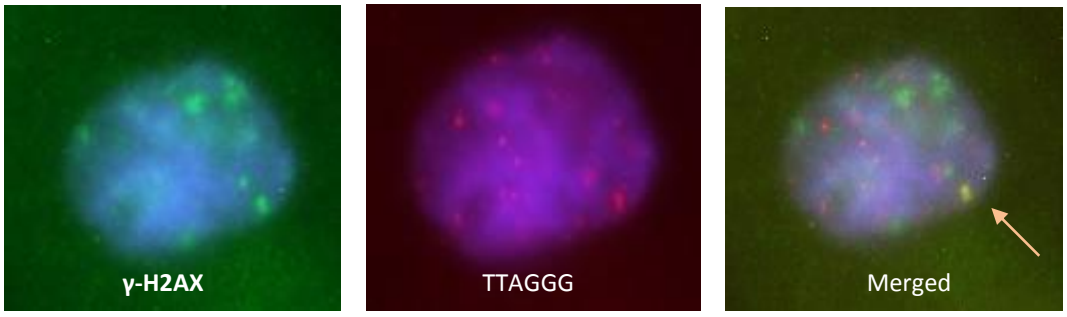

Figure 6.12 - Examples of cell images with DNA damage foci and TIF post transfection.

Results of our analysis are shown in (Figures 6.13 and Figure 6.14). Both cell lines have shown some residual DNA damage 48 hrs after exposure to IR which was marginally significant (see table, second column, in Figure 6.13). Cells transfected with scrambled oligonucleotides showed similar levels of γ-H2AX foci as control non-exposed cells (Figure 6.13). Most importantly, HeLa and U2OS cells transfected with *DKC1* specific siRNA oligonucleotides and exposed to radiation at relevant time points (see Figure 6.13) showed

higher frequencies of γ-H2AX foci relative to all three controls used, some of which have yielded significant differences (Figure 6.13). This suggests that, even though the *DKC1* expression was only reduced by 50%, DNA damage response was affected in both cell lines. Unexpectedly, U2OS cells with reduced *DKC1* expression showed unrepaired DNA damage 48 hrs after irradiation (Figure 6.13) suggesting that *DKC1* may affect DNA damage independently of its role in telomerase. However, we would like to note that the experiment described above needs to be sufficiently repeated before we draw any definitive conclusion. Because of time constrains the DNA damage analysis described above was performed only once and should be considered preliminary.

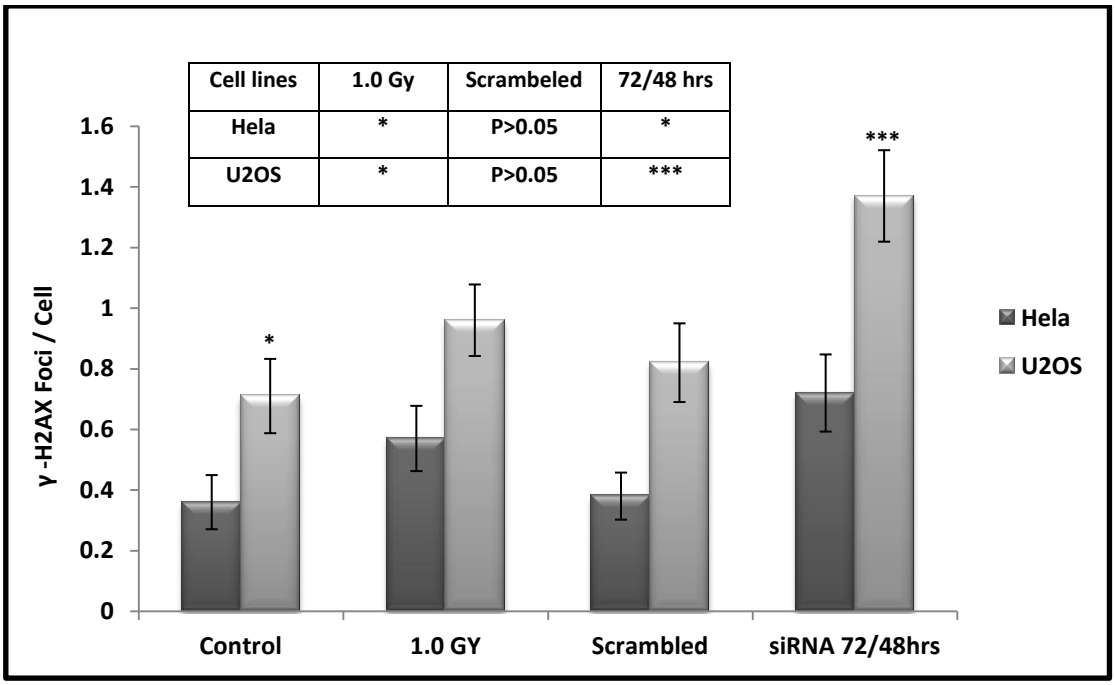

Figure 6.13 - Frequencies of γ-H2AX foci/cell in Hela and U2OS cells before and after *DKC1* knock-down.*=P<0.05, *** = P < 0.001, Error bars represent SEM.

Similarly, TIF frequencies were significantly higher in U2OS and HeLa cells 48 hrs and 72hrs after exposure to radiation relative to control samples suggesting that dysfunctional

telomeres potentially contribute to defects in DNA damage response (Figure 6.14). As stated above these results need to be repeated before the conclusion that elevated TIF frequencies observed contribute to defects in DNA damage response can stand.

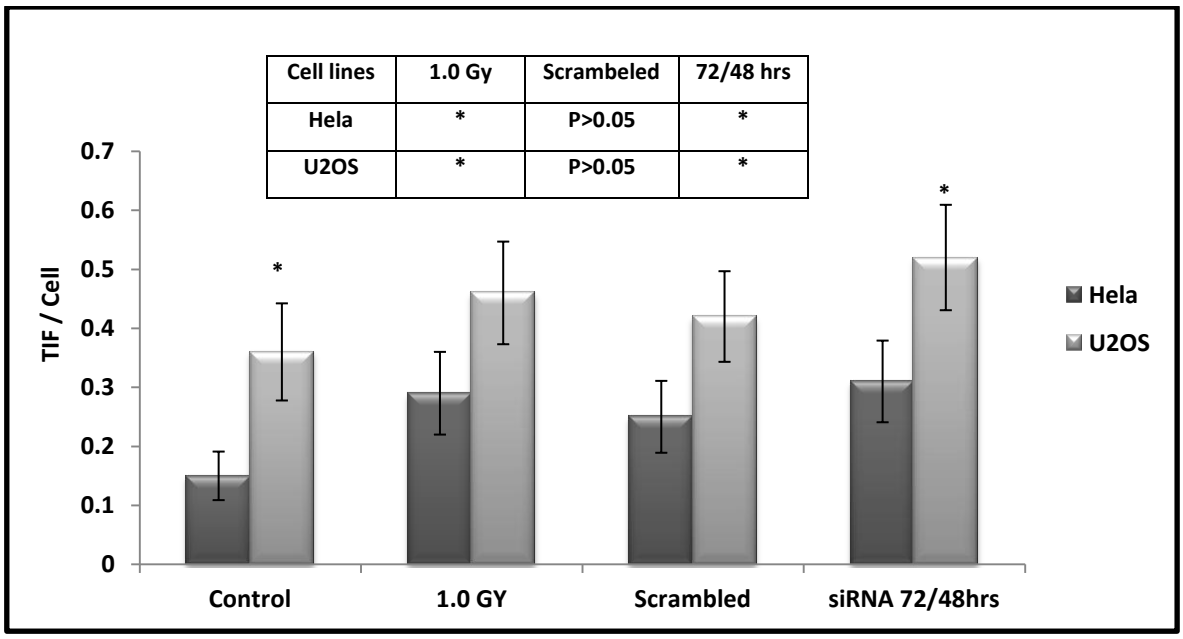

Figure 6.14 - Frequencies of TIF foci per cell in Hela and U2OS cell lines. * = P<0.05, Error bars represent SEM.

6.3 - Discussion

Results presented in this chapter indicate that DC cells show a defective DNA damage response. Cells from a DC patient with homozygous mutations in *DKC1* showed unrepaired DNA damage 24 hrs and 48 hrs after exposure relative to control cells and cells from a DC patient with a heterozygous *DKC1* mutation (Figure 6.2). The presence of unrepaired DNA damage in affected cells long time after induction of genotoxic stress is consistent with a defective DNA damage response. To test this possibility further we knocked-down *DKC1* in a telomerase positive cell line (HeLa) and in an ALT positive cell line

(U2OS) and examined their DNA damage response. Our preliminary experiments suggest that *DKC1* knock-down causes a defective DNA damage response in both cell lines (Figure 6.11) thus providing further support for the possibility that DC cells may have a defective DNA damage response.

Taken together our results argue against conclusion of a recent study that DC cells have a normal DNA damage response (Kirwan *et al.* 2011). As stated in the introductory section for this chapter the study by (Kirwan *et al.* 2011) had, in our view, a significant weakness. They only compared frequencies of etoposide-induced γ-H2AX foci immediately after treatment and observed essentially similar values of DNA damage foci in DC and control cells (Kirwan *et al.* 2011). This is clearly in line with our results. At the time points 30 min and 5 hrs after exposure to radiation we have not observed significant differences in frequencies of γ-H2AX foci between control and DC cells (Figure 6.2). Differences in γ-H2AX foci frequencies between DC cells with homozygous mutations in *DKC1* on one sides and normal control cells and cells with a heterozygous mutation in *DKC1* become apparent 24 hrs and 48 hrs after exposure (Figure 6.2). (Kirwan *et al.* 2011) have not analysed DNA damage in their samples beyond the single time point and because of this we think that their conclusion in order to be valid requires a full study of DNA damage kinetics beyond that single point. Furthermore, conclusion by (Kirwan *et al.* 2011) that DC cells have a normal DNA damage response is contradicted by a mouse study. (Gu *et al.* 2008) used a mouse DC model to analyse DNA damage response. They copied a 2 kb deletion mutation found in an X-linked DC family into the mouse genome. This mutation removes the last exon (exon 15) from the *DKC1* gene. This mouse model exhibited phenotypic features similar to DC patients including telomere shortening (Gu *et al.* 2008). Furthermore, (Gu *et al.* 2008) showed that DNA damage induced by etoposide in mouse embryonic fibroblasts (MEFs)

with the above *Dkc1* mutation was significantly higher than in control cells. Similarly to (Kirwan *et al.* 2011) no DNA damage repair kinetics in these cells was carried out (Gu *et al.* 2008) and this is a potential weakness of the study. However, given that several other published studies indicate that DC cells may have a dysfunctional DNA damage response, in particular the response to ionizing radiation we believe that the conclusion by (Kirwan *et al.* 2011) cannot be justified unless results of DNA damage kinetics are carried out in the same samples.

The most interesting question for us is why Dyskerin affects ALT cells? Even though our results presented in (Figures 6.10 and 6.11) are still preliminary and require further validation we are tempted to speculate that, if these results are upheld, Dyskerin may have a role in DNA damage response independently of telomerase. It is well established that most ALT positive cells lack detectable telomerase activity (Zhu *et al.* 2004) and we assume that the U2OS cell line follows this pattern. However, to be on the safe side it is important to verify this and one of the points for future studies is to assess the status of telomerase activity in U2OS cells. In rare cases it happens that ALT cells may also have detectable telomerase activity (Grobelny *et al.* 2001) and it is essential to clarify this point. If, after all clarification steps, turns out that Dyskerin is indeed involved in DNA damage response independently of telomerase mechanisms of its action need to be identified. It is interesting in this context that some other components of telomere metabolism have roles that deviate from their expected roles. For example, telomerase plays a role in processes other than telomere length regulation (Greider 1993). One of the shelterin components, a telomere binding proteins TRF2, plays a direct role in DNA damage response independently of its role in telomere stability maintenance or telomere length regulation (Huda *et al.* 2009).

In conclusion, based on our results we believe that DC cells have a dysfunctional DNA damage response. Our *DKC1* knock-down experiments require further validation as discussed earlier and this is project is continued by another PhD student.

Chapter 7 - General discussion

7.1 - General discussion

In the last 10-15 years a substantial body of evidence has emerged to suggest a link between dysfunctional maintenance of telomeres and defective DNA damage response. The first clear indication for this link was the observation of dysfunctional telomere maintenance in the human syndrome Ataxia telangiectasia (AT) characterized by a defective DNA damage response due to mutations in the *ATM* (AT mutated) gene (Metcalfe *et al.* 1996). This observation has been taken further over the years and numerous human cell lines or mouse models characterized by a variety of DNA damage response defects have been examined for the presence of abnormalities in telomere maintenance. At least 17 genes involved in DNA damage response have been shown to affect telomere maintenance so far (Slijepcevic 2006) thus providing supporting evidence for the functional interplay between these two pathways, namely telomere maintenance and DNA damage response. A strong proof for this functional interplay comes from a study that a telomere binding protein, TRF2, which has not been assigned any role in DNA damage processing before, actually interacts with photo-induced DNA DSBs immediately after their induction (Bradshaw *et al.* 2005). The work presented in this thesis was aimed at probing the above further. It is essential to understand the interplay between telomere maintenance and DNA damage response as this may be helpful for understanding the role of telomeres played in clinically relevant processes such as carcinogenesis and ageing (Aubert and Lansdorp 2008).

This thesis generated three novel sets of results. Firstly, we developed a new method for measuring telomere length in interphase cells, termed IQ-FISH (Chapter 3). The method is essential for measuring telomere length in cell lines that have poor proliferative potential as a result of defects in various DNA damage response genes. Secondly, we have shown that

defects in BRCA1 and BRCA2 proteins cause alterations in telomere maintenance and these alterations, in some cases, contribute directly to defects in DNA damage response in affected cells (Chapters 4 and 5). Thirdly, we have shown that cells from a DC patient, with homozygous mutations in the *DKC1* gene, have a dysfunctional DNA damage response (Chapter 6).

As previously mentioned telomere maintenance is closely linked with cellular and organismal ageing and it appears to be a key determinant of replicative capacity in vertebrate somatic cells. Additionally, evidence shows that telomere shortening is an early contributor to human tumorigenesis (O'Sullivan *et al.* 2002). Therefore, our results are useful for understanding details of telomere maintenance mechanisms in the context of ageing and tumorigenesis.

It was essential to develop an accurate method for measuring telomere length in poorly proliferating cells. A number of methods for measuring telomere length have been described including Southern blot, Q-FISH, Flow-FISH, q-PCR and STELA (single telomere length analysis) (Lansdorp *et al.* 1996; Oexle 1998; Rufer *et al.* 1998) Of all these methods Q-FISH is probably the most sensitive technique for measuring telomere length. However, Q-FISH requires a good mitotic index, typical of rapidly proliferating cells, for high quality metaphase preparation which is essential for this technique. In the past we have attempted to measure telomere length by Q-FISH in DC cells described in Chapter 6, VU0423 cells described in Chapter 3 and some other cells characterized by a dysfunctional response to DNA damage. However, the mitotic index in all cell lines was low thus precludeing metaphase cell preparation. This was the key reason we have resorted to development of IQ-FISH in the context of this project. Based on the analysis of cells lines with defective DNA

damage response (Chapters 4-6) we can conclude that the IQ-FISH method is a fast and accurate method for assessing telomere length in any sample with low cell numbers. We believe that >100 cells are sufficient to obtain accurate telomere length information in any sample. No other telomere length measuring technique can compete with IQ-FISH in this sense. Q-FISH is inferior for the reasons discussed in Chapter 3. Southern blot, RT-PCR and STELA rely on extraction of DNA from samples and the quantity of cells required is likely to be in the region of thousands at least, if not a degree of magnitude higher as DNA extraction procedure usually results in the significant loss of the DNA (Svenson *et al.* 2011). Flow-FISH also requires a significant number of cells/sample, probably in the region of 100,000, and it is inferior to IQ-FISH (Slijepcevic 2001) in terms of cell numbers required to complete the analysis.

The IQ-FISH technique allowed us to focus on cells with defective DNA damage response genes, such as *BRCA1* and *BRCA2*, with a view of assessing their effects on telomere maintenance. Several recent studies (Badie *et al.* 2010; Sapir *et al.* 2011; Bodvarsdottir *et al.* 2012) showed that *BRCA2* affects telomere maintenance. In this thesis we have been able to link the DNA damage response defect in the cell line from a patient with bi-allelic mutations in *BRCA2* with defects in rates of telomere recombination (Chapter 4). The observed telomere dysfunction phenotype in *BRCA2* defective cells was consistent with the involvement of telomeres in HR. These results are consistent with the view that telomere maintenance is functionally linked with DNA damage response mechanisms. However, we have also shown lack of correlation between DNA damage response and telomere maintenance in cell lines from *BRCA2* mutation carriers (+/-) (Chapter 4) suggesting that a single functional copy of *BRCA2* is sufficient to provide an efficient DNA damage response in human cells.

We have also examined the role of BRCA1, either in human or mouse cell lines, and have shown that even the presence of a heterozygous mutation in human lymphoblastoid cells is able to confer dysfunctional DNA damage response which is caused by dysfunctional telomere maintenance (Chapter 5). We have also been able to show the effect of homozygous Brca1 mutations on DNA damage response and telomeres in mouse embryonic stem cells (Chapter 5).

Perhaps the most interesting result in this thesis is demonstration of a DNA damage response defect in *DKC1-/-* cells from a DC patient (Chapter 6). Cells from this patient show unrepaired DNA damage 24 and 48 hrs after its induction by IR whereas normal control cells are able to repair this damage efficiently. We have also carried out RNAi experiments to prove that *DKC1* is indeed responsible for this defective DNA damage response. Our preliminary results support the initial view (Chapter 6) but the experiments require further validation currently carried out by another PhD student.

7.2 - Future research

Overall, our results are supportive of the functional inter-dependence between the two pathways. One of the points for the future research would be to probe details of the mechanisms between this inter-dependence. The guiding principle here is perhaps the study by Bradshaw et al. (2005) which clearly demonstrated the involvement of TRF2, a telomeric protein without any formally assigned role in DNA damage response, in processing phot-induced DSBs in human cells. We believe that biochemical experiments aimed at probing the direct involvement of various telomere binding proteins or component of telomerase in DNA damage response may be justified. Telomerase is a complex enzyme consisting from many different components including *DKC1*. Given our demonstration that *DKC1* defective

cells have a dysfunctional response to DNA damage it may be appropriate to probe the potential role of this protein in DNA damage response. It is important to stress that telomerase activity is unregulated after many forms of DNA damage. For example, exposure of human cells to ionizing radiation leads to an observable increase in telomerase activity which is independent of telomere length regulation (Moriarty *et al.* 2002) suggesting the role of telomerase in DNA damage response.

Another point for future research would be the exploration of translational possibilities that stem from our research. Cancer therapy is an avenue that can be explored here. *BRCA1* and *BRCA2* are well characterized tumour suppressors (Lee and Muller 2010). Telomere maintenance is essentially a tumour suppressor pathway (Gu *et al.* 2005). Manipulating the inter-dependence between the protein players that are functionally linked through different pathways, namely DNA damage response and telomere maintenance, and play roles in both of them, may provide a strategy for better definition of these pathways in carcinogenesis and open some avenues for clinical intervention. One such possibility is briefly discussed on page 156 and recent publications (Sapir *et al.* 2011) provide further support for it.

References

Ahnesorg, P., P. Smith and S. P. Jackson (2006). "XLF interacts with the XRCC4-DNA ligase IV complex to promote DNA nonhomologous end-joining." Cell 124(2): 301-313.

Al-Wahiby, S. and P. Slijepcevic (2005). "Chromosomal aberrations involving telomeres in BRCA1 deficient human and mouse cell lines." Cytogenet Genome Res 109(4): 491-496.

Ame, J. C., C. Spenlehauer and G. de Murcia (2004). "The PARP superfamily." Bioessays 26(8): 882-893.

Armanios, M. and E. H. Blackburn (2012). "The telomere syndromes." Nat Rev Genet 13(10): 693-704.

Arngrimsson, R., I. Dokal, L. Luzzatto and J. M. Connor (1993). "Dyskeratosis congenita: three additional families show linkage to a locus in Xq28." J Med Genet 30(7): 618-619.

Artandi, S. E., S. Chang, S. L. Lee, S. Alson, G. J. Gottlieb, L. Chin and R. A. DePinho (2000). "Telomere dysfunction promotes non-reciprocal translocations and epithelial cancers in mice." Nature 406(6796): 641-645.

Aubert, G. and P. M. Lansdorp (2008). "Telomeres and aging." Physiol Rev 88(2): 557-579.

Badie, S., J. M. Escandell, P. Bouwman, A. R. Carlos, M. Thanasoula, M. M. Gallardo, A. Suram, I. Jaco, J. Benitez, U. Herbig, M. A. Blasco, J. Jonkers and M. Tarsounas (2010). "BRCA2 acts as a RAD51 loader to facilitate telomere replication and capping." Nat Struct Mol Biol 17(12): 1461-1469.

Baerlocher, G. M., I. Vulto, G. de Jong and P. M. Lansdorp (2006). "Flow cytometry and FISH to measure the average length of telomeres (flow FISH)." Nat Protoc 1(5): 2365-2376.

Bailey, S. M., M. N. Cornforth, A. Kurimasa, D. J. Chen and E. H. Goodwin (2001). "Strand-specific postreplicative processing of mammalian telomeres." Science 293(5539): 2462-2465.

Bailey, S. M. and E. H. Goodwin (2004). "DNA and telomeres: beginnings and endings." Cytogenet Genome Res 104(1-4): 109-115.

Bailey, S. M., J. Meyne, D. J. Chen, A. Kurimasa, G. C. Li, B. E. Lehnert and E. H. Goodwin (1999). "DNA double-strand break repair proteins are required to cap the ends of mammalian chromosomes." Proc Natl Acad Sci U S A 96(26): 14899-14904.

Bailey, S. M., E. S. Williams, M. N. Cornforth and E. H. Goodwin (2010). "Chromosome Orientation fluorescence in situ hybridization or strand-specific FISH." Methods Mol Biol 659: 173-183.

Bakkenist, C. J. and M. B. Kastan (2003). "DNA damage activates ATM through intermolecular autophosphorylation and dimer dissociation." Nature 421(6922): 499-506.

Ballal, R. D., T. Saha, S. Fan, B. R. Haddad and E. M. Rosen (2009). "BRCA1 localization to the telomere and its loss from the telomere in response to DNA damage." J Biol Chem 284(52): 36083-36098.

Bartek, J. and J. Lukas (2001). "Mammalian G1- and S-phase checkpoints in response to DNA damage." Curr Opin Cell Biol 13(6): 738-747.

Becker, M. M. and Z. Wang (1989). "Origin of ultraviolet damage in DNA." J Mol Biol 210(3): 429-438.

Bessler, M., D. B. Wilson and P. J. Mason (2010). "Dyskeratosis congenita." FEBS Lett 584(17): 3831-3838.

Blackburn, E. H. (1991). "Structure and function of telomeres." Nature 350(6319): 569-573.

Blackburn, E. H. (2000). "Telomere states and cell fates." Nature 408(6808): 53-56.

Blackburn, E. H. (2001). "Switching and signaling at the telomere." Cell 106(6): 661-673.

Blasco, M. A., H. W. Lee, M. P. Hande, E. Samper, P. M. Lansdorp, R. A. DePinho and C. W. Greider (1997). "Telomere shortening and tumor formation by mouse cells lacking telomerase RNA." Cell 91(1): 25-34.

Bodvarsdottir, S. K., M. Steinarsdottir, H. Bjarnason and J. E. Eyfjord (2012). "Dysfunctional telomeres in human BRCA2 mutated breast tumors and cell lines." Mutat Res 729(1-2): 90-99.

Boulton, S. J. (2006). "Cellular functions of the BRCA tumour-suppressor proteins." Biochem Soc Trans 34(Pt 5): 633-645.

Bourton, E. C., P. N. Plowman, S. A. Zahir, G. U. Senguloglu, H. Serrai, G. Bottley and C. N. Parris (2012). "Multispectral imaging flow cytometry reveals distinct frequencies of gamma-H2AX foci induction in DNA double strand break repair defective human cell lines." Cytometry A 81(2): 130-137.

Bradshaw, P. S., D. J. Stavropoulos and M. S. Meyn (2005). "Human telomeric protein TRF2 associates with genomic double-strand breaks as an early response to DNA damage." Nat Genet 37(2): 193-197.

Braig, M. and C. A. Schmitt (2006). "Oncogene-induced senescence: putting the brakes on tumor development." Cancer Res 66(6): 2881-2884.

Britt, A. B. (1996). "DNA Damage and Repair in Plants." Annu Rev Plant Physiol Plant Mol Biol 47: 75-100.

Brooks, P. J. (1997). "DNA damage, DNA repair, and alcohol toxicity--a review." Alcohol Clin Exp Res 21(6): 1073-1082.

Buck, D., L. Malivert, R. de Chasseval, A. Barraud, M. C. Fondaneche, O. Sanal, A. Plebani, J. L. Stephan, M. Hufnagel, F. le Deist, A. Fischer, A. Durandy, J. P. de Villartay and P. Revy

(2006). "Cernunnos, a novel nonhomologous end-joining factor, is mutated in human immunodeficiency with microcephaly." Cell 124(2): 287-299.

Buckingham, E. M. and A. J. Klingelhutz (2011). "The role of telomeres in the ageing of human skin." Exp Dermatol 20(4): 297-302.

Buisson, R., A. M. Dion-Cote, Y. Coulombe, H. Launay, H. Cai, A. Z. Stasiak, A. Stasiak, B. Xia and J. Y. Masson (2010). "Cooperation of breast cancer proteins PALB2 and piccolo BRCA2 in stimulating homologous recombination." Nat Struct Mol Biol 17(10): 1247-1254.

Cabuy, E., C. Newton, G. Joksic, L. Woodbine, B. Koller, P. A. Jeggo and P. Slijepcevic (2005). "Accelerated telomere shortening and telomere abnormalities in radiosensitive cell lines." Radiat Res 164(1): 53-62.

Cabuy, E., C. Newton, T. Roberts, R. Newbold and P. Slijepcevic (2004). "Identification of subpopulations of cells with differing telomere lengths in mouse and human cell lines by flow FISH." Cytometry A 62(2): 150-161.

Cabuy, E., C. Newton and P. Slijepcevic (2008). "BRCA1 knock-down causes telomere dysfunction in mammary epithelial cells." Cytogenet Genome Res 122(3-4): 336-342.

Callen, E., E. Samper, M. J. Ramirez, A. Creus, R. Marcos, J. J. Ortega, T. Olive, I. Badell, M. A. Blasco and J. Surralles (2002). "Breaks at telomeres and TRF2-independent end fusions in Fanconi anemia." Hum Mol Genet 11(4): 439-444.

Castilla, L. H., F. J. Couch, M. R. Erdos, K. F. Hoskins, K. Calzone, J. E. Garber, J. Boyd, M. B. Lubin, M. L. Deshano, L. C. Brody and et al. (1994). "Mutations in the BRCA1 gene in families with early-onset breast and ovarian cancer." Nat Genet 8(4): 387-391.

Cengiz, M., B. Celebioglu, E. Ozyar and I. L. Atahan (2004). "Unusual hypersensitivity to radiation therapy in a patient with dyskeratosis congenita syndrome." Oral Oncol 40(7): 758-759.

Cerone, M. A., J. A. Londono-Vallejo and S. Bacchetti (2001). "Telomere maintenance by telomerase and by recombination can coexist in human cells." Hum Mol Genet 10(18): 1945-1952.

Cesare, A. J. and R. R. Reddel (2008). "Telomere uncapping and alternative lengthening of telomeres." Mech Ageing Dev 129(1-2): 99-108.

Chen, J. and J. Xie (2012). "Progress on RNAi-based molecular medicines." Int J Nanomedicine 7: 3971-3980.

Chen, M. J., Y. T. Lin, H. B. Lieberman, G. Chen and E. Y. Lee (2001). "ATM-dependent phosphorylation of human Rad9 is required for ionizing radiation-induced checkpoint activation." J Biol Chem 276(19): 16580-16586.

Cohen, S. B., M. E. Graham, G. O. Lovrecz, N. Bache, P. J. Robinson and R. R. Reddel (2007). "Protein composition of catalytically active human telomerase from immortal cells." Science 315(5820): 1850-1853.

Connor, J. M., D. Gatherer, F. C. Gray, L. A. Pirrit and N. A. Affara (1986). "Assignment of the gene for dyskeratosis congenita to Xq28." Hum Genet 72(4): 348-351.

Coriell. (2009). Retrieved 20th Sep, 2012, from http://ccr.coriell.org/Sections/Search/Sample_Detail.aspx?Ref=GM14622&PgId=166.

Coulthard, S., A. Chase, J. Pickard, J. Goldman and I. Dokal (1998). "Chromosomal breakage analysis in dyskeratosis congenita peripheral blood lymphocytes." Br J Haematol 102(5): 1162-1164.

Crespan, E., A. Amoroso and G. Maga (2010). "DNA polymerases and mutagenesis in human cancers." Subcell Biochem 50: 165-188.

d'Adda di Fagagna, F., M. P. Hande, W. M. Tong, D. Roth, P. M. Lansdorp, Z. Q. Wang and S. P. Jackson (2001). "Effects of DNA nonhomologous end-joining factors on telomere length and chromosomal stability in mammalian cells." Curr Biol 11(15): 1192-1196.

D'Andrea, A. D. (2003). "The Fanconi Anemia/BRCA signaling pathway: disruption in cisplatin-sensitive ovarian cancers." Cell Cycle 2(4): 290-292.

Davidson, H. R. and J. M. Connor (1988). "Dyskeratosis congenita." J Med Genet 25(12): 843-846.

De Bont, R. and N. van Larebeke (2004). "Endogenous DNA damage in humans: a review of quantitative data." Mutagenesis 19(3): 169-185.

de Lange, T. (2004). "T-loops and the origin of telomeres." Nat Rev Mol Cell Biol 5(4): 323-329.

de Lange, T. (2005). "Shelterin: the protein complex that shapes and safeguards human telomeres." Genes Dev 19(18): 2100-2110.

DeBauche, D. M., G. S. Pai and W. S. Stanley (1990). "Enhanced G2 chromatid radiosensitivity in dyskeratosis congenita fibroblasts." Am J Hum Genet 46(2): 350-357.

Demuth, I., P. S. Bradshaw, A. Lindner, M. Anders, S. Heinrich, J. Kallenbach, K. Schmelz, M. Digweed, M. S. Meyn and P. Concannon (2008). "Endogenous hSNM1B/Apollo interacts with TRF2 and stimulates ATM in response to ionizing radiation." DNA Repair (Amst) 7(8): 1192-1201.

Deng, C. X. and R. H. Wang (2003). "Roles of BRCA1 in DNA damage repair: a link between development and cancer." Hum Mol Genet 12 Spec No 1: R113-123.

Desmaze, C., J. C. Soria, M. A. Freulet-Marriere, N. Mathieu and L. Sabatier (2003). "Telomere-driven genomic instability in cancer cells." Cancer Lett 194(2): 173-182.

Dokal, I. (2000). "Dyskeratosis congenita in all its forms." Br J Haematol 110(4): 768-779.

Durant, S. T. and J. A. Nickoloff (2005). "Good timing in the cell cycle for precise DNA repair by BRCA1." Cell Cycle 4(9): 1216-1222.

Enoch, T. and C. Norbury (1995). "Cellular responses to DNA damage: cell-cycle checkpoints, apoptosis and the roles of p53 and ATM." Trends Biochem Sci 20(10): 426-430.

Espejel, S. and M. A. Blasco (2002). "Identification of telomere-dependent "senescence-like" arrest in mouse embryonic fibroblasts." Exp Cell Res 276(2): 242-248.

Espejel, S., S. Franco, S. Rodriguez-Perales, S. D. Bouffler, J. C. Cigudosa and M. A. Blasco (2002). "Mammalian Ku86 mediates chromosomal fusions and apoptosis caused by critically short telomeres." EMBO J 21(9): 2207-2219.

Falconer, E., E. A. Chavez, A. Henderson, S. S. Poon, S. McKinney, L. Brown, D. G. Huntsman and P. M. Lansdorp (2010). "Identification of sister chromatids by DNA template strand sequences." Nature 463(7277): 93-97.

Fan, Q., F. Zhang, B. Barrett, K. Ren and P. R. Andreassen (2009). "A role for monoubiquitinated FANCD2 at telomeres in ALT cells." Nucleic Acids Res 37(6): 1740-1754.

Fire, A., S. Xu, M. K. Montgomery, S. A. Kostas, S. E. Driver and C. C. Mello (1998). "Potent and specific genetic interference by double-stranded RNA in Caenorhabditis elegans." Nature 391(6669): 806-811.

Foray, N., V. Randrianarison, D. Marot, M. Perricaudet, G. Lenoir and J. Feunteun (1999). "Gamma-rays-induced death of human cells carrying mutations of BRCA1 or BRCA2." Oncogene 18(51): 7334-7342.

Freibaum, B. D. and C. M. Counter (2006). "hSnm1B is a novel telomere-associated protein." J Biol Chem 281(22): 15033-15036.

French, J. D., J. Dunn, C. E. Smart, N. Manning and M. A. Brown (2006). "Disruption of BRCA1 function results in telomere lengthening and increased anaphase bridge formation in immortalized cell lines." Genes Chromosomes Cancer 45(3): 277-289.

Friedberg, E. C., G. C. Walker and W. Siede (1995). DNA Repair and Mutagenesis. Washington, DC, ASM Press.

Friedenson, B. (2007). "The BRCA1/2 pathway prevents hematologic cancers in addition to breast and ovarian cancers." BMC Cancer 7: 152.

Gardano, L., L. Holland, R. Oulton, T. Le Bihan and L. Harrington (2012). "Native gel electrophoresis of human telomerase distinguishes active complexes with or without dyskerin." Nucleic Acids Res 40(5): e36.

Genois, M. M., A. Mukherjee, J. M. Ubeda, R. Buisson, E. Paquet, G. Roy, M. Plourde, Y. Coulombe, M. Ouellette and J. Y. Masson (2012). "Interactions between BRCA2 and RAD51 for promoting homologous recombination in Leishmania infantum." Nucleic Acids Res 40(14): 6570-6584.

Ghildiyal, M. and P. D. Zamore (2009). "Small silencing RNAs: an expanding universe." Nat Rev Genet 10(2): 94-108.

Gilson, E. and A. Londono-Vallejo (2007). "Telomere length profiles in humans: all ends are not equal." Cell Cycle 6(20): 2486-2494.

Goytisolo, F. A., E. Samper, S. Edmonson, G. E. Taccioli and M. A. Blasco (2001). "The absence of the dna-dependent protein kinase catalytic subunit in mice results in anaphase bridges and in increased telomeric fusions with normal telomere length and G-strand overhang." Mol Cell Biol 21(11): 3642-3651.

Greider, C. W. (1993). "Telomerase and telomere-length regulation: lessons from small eukaryotes to mammals." Cold Spring Harb Symp Quant Biol 58: 719-723.

Greider, C. W. (1999). "Telomeres do D-loop-T-loop." Cell 97(4): 419-422.

Greider, C. W. and E. H. Blackburn (1985). "Identification of a specific telomere terminal transferase activity in Tetrahymena extracts." Cell 43(2 Pt 1): 405-413.

Griffin, C. S. and J. Thacker (2004). "The role of homologous recombination repair in the formation of chromosome aberrations." Cytogenet Genome Res 104(1-4): 21-27.

Grobelny, J. V., M. Kulp-McEliece and D. Broccoli (2001). "Effects of reconstitution of telomerase activity on telomere maintenance by the alternative lengthening of telomeres (ALT) pathway." Hum Mol Genet 10(18): 1953-1961.

Gu, B. W., M. Bessler and P. J. Mason (2008). "A pathogenic dyskerin mutation impairs proliferation and activates a DNA damage response independent of telomere length in mice." Proc Natl Acad Sci U S A 105(29): 10173-10178.

Gu, J., M. R. Spitz, H. Zhao, J. Lin, H. B. Grossman, C. P. Dinney and X. Wu (2005). "Roles of tumor suppressor and telomere maintenance genes in cancer and aging--an epidemiological study." Carcinogenesis 26(10): 1741-1747.

Gutierrez, S., E. Carbonell, P. Galofre, A. Creus and R. Marcos (1999). "Low sensitivity of the sister chromatid exchange assay to detect the genotoxic effects of radioiodine therapy." Mutagenesis 14(2): 221-226.

Hackett, J. A., D. M. Feldser and C. W. Greider (2001). "Telomere dysfunction increases mutation rate and genomic instability." Cell 106(3): 275-286.

Hahn, W. C. (2003). "Role of telomeres and telomerase in the pathogenesis of human cancer." J Clin Oncol 21(10): 2034-2043.

Hande, M. P., A. S. Balajee, A. Tchirkov, A. Wynshaw-Boris and P. M. Lansdorp (2001). "Extra-chromosomal telomeric DNA in cells from Atm(-/-) mice and patients with ataxia-telangiectasia." Hum Mol Genet 10(5): 519-528.

Hande, P., P. Slijepcevic, A. Silver, S. Bouffler, P. van Buul, P. Bryant and P. Lansdorp (1999). "Elongated telomeres in scid mice." Genomics 56(2): 221-223.

Hannon, G. J. (2002). "RNA interference." Nature 418(6894): 244-251.

Harley, C. B. (1991). "Telomere loss: mitotic clock or genetic time bomb?" Mutat Res 256(2-6): 271-282.

Harrington, L., W. Zhou, T. McPhail, R. Oulton, D. S. Yeung, V. Mar, M. B. Bass and M. O. Robinson (1997). "Human telomerase contains evolutionarily conserved catalytic and structural subunits." Genes Dev 11(23): 3109-3115.

Hartman, A. R. and J. M. Ford (2002). "BRCA1 induces DNA damage recognition factors and enhances nucleotide excision repair." Nat Genet 32(1): 180-184.

Heiss, N. S., S. W. Knight, T. J. Vulliamy, S. M. Klauck, S. Wiemann, P. J. Mason, A. Poustka and I. Dokal (1998). "X-linked dyskeratosis congenita is caused by mutations in a highly conserved gene with putative nucleolar functions." Nat Genet 19(1): 32-38.

Herceg, Z. and Z. Q. Wang (2001). "Functions of poly(ADP-ribose) polymerase (PARP) in DNA repair, genomic integrity and cell death." Mutat Res 477(1-2): 97-110.

Hoeijmakers, J. H. (2001). "Genome maintenance mechanisms for preventing cancer." Nature 411(6835): 366-374.

Hohensinner, P. J., J. J. Goronzy and C. M. Weyand (2011). "Telomere dysfunction, autoimmunity and aging." Aging Dis 2(6): 524-537.

Howlett, N. G., T. Taniguchi, S. Olson, B. Cox, Q. Waisfisz, C. De Die-Smulders, N. Persky, M. Grompe, H. Joenje, G. Pals, H. Ikeda, E. A. Fox and A. D. D'Andrea (2002). "Biallelic inactivation of BRCA2 in Fanconi anemia." Science 297(5581): 606-609.

Huda, N., H. Tanaka, M. S. Mendonca and D. Gilley (2009). "DNA damage-induced phosphorylation of TRF2 is required for the fast pathway of DNA double-strand break repair." Mol Cell Biol 29(13): 3597-3604.

Huppi, K., S. E. Martin and N. J. Caplen (2005). "Defining and assaying RNAi in mammalian cells." Mol Cell 17(1): 1-10.

Jegou, T., I. Chung, G. Heuvelman, M. Wachsmuth, S. M. Gorisch, K. M. Greulich-Bode, P. Boukamp, P. Lichter and K. Rippe (2009). "Dynamics of telomeres and promyelocytic leukemia nuclear bodies in a telomerase-negative human cell line." Mol Biol Cell 20(7): 2070-2082.

Joksic, I., D. Vujic, M. Guc-Scekic, A. Leskovac, S. Petrovic, M. Ojani, J. P. Trujillo, J. Surralles, M. Zivkovic, A. Stankovic, P. Slijepcevic and G. Joksic (2012). "Dysfunctional telomeres in primary cells from Fanconi anemia FANCD2 patients." Genome Integr 3(1): 6.

Ju, Z. and K. Lenhard Rudolph (2008). "Telomere dysfunction and stem cell ageing." Biochimie 90(1): 24-32.

Jyonouchi, S., L. Forbes, E. Ruchelli and K. E. Sullivan (2011). "Dyskeratosis congenita: a combined immunodeficiency with broad clinical spectrum--a single-center pediatric experience." Pediatr Allergy Immunol 22(3): 313-319.

Kim, T. K., T. Kim, T. Y. Kim, W. G. Lee and J. Yim (2000). "Chemotherapeutic DNA-damaging drugs activate interferon regulatory factor-7 by the mitogen-activated protein kinase kinase-4-cJun NH2-terminal kinase pathway." Cancer Res 60(5): 1153-1156.

Kimura, H. and A. Suzuki (2009). New Research on DNA Damage, Nova Science Publishers.

Kipling, D. and H. J. Cooke (1990). "Hypervariable ultra-long telomeres in mice." Nature 347(6291): 400-402.

Kirwan, M., R. Beswick, A. J. Walne, U. Hossain, C. Casimir, T. Vulliamy and I. Dokal (2011). "Dyskeratosis congenita and the DNA damage response." Br J Haematol 153(5): 634-643.

Knight, S. W., N. S. Heiss, T. J. Vulliamy, S. Greschner, G. Stavrides, G. S. Pai, G. Lestringant, N. Varma, P. J. Mason, I. Dokal and A. Poustka (1999). "X-linked dyskeratosis congenita is predominantly caused by missense mutations in the DKC1 gene." Am J Hum Genet 65(1): 50-58.

Kopp, E. D. and S. Seregard (2004). "Epiphora as a side effect of topical mitomycin C." Br J Ophthalmol 88(11): 1422-1424.

Lansdorp, P. M., N. P. Verwoerd, F. M. van de Rijke, V. Dragowska, M. T. Little, R. W. Dirks, A. K. Raap and H. J. Tanke (1996). "Heterogeneity in telomere length of human chromosomes." Hum Mol Genet 5(5): 685-691.

Lee, E. Y. and W. J. Muller (2010). "Oncogenes and tumor suppressor genes." Cold Spring Harb Perspect Biol 2(10): a003236.

Lee, J. Y., W. Stenzel, M. Lohr, H. Stutzer, R. I. Ernestus and N. Klug (2006). "The role of mitomycin C in reducing recurrence of epidural fibrosis after repeated operation in a laminectomy model in rats." J Neurosurg Spine 4(4): 329-333.

Lenain, C., S. Bauwens, S. Amiard, M. Brunori, M. J. Giraud-Panis and E. Gilson (2006). "The Apollo 5' exonuclease functions together with TRF2 to protect telomeres from DNA repair." Curr Biol 16(13): 1303-1310.

Li, S., J. Duan, D. Li, B. Yang, M. Dong and K. Ye (2011). "Reconstitution and structural analysis of the yeast box H/ACA RNA-guided pseudouridine synthase." Genes Dev 25(22): 2409-2421.

Lopes, M., C. Cotta-Ramusino, A. Pellicioli, G. Liberi, P. Plevani, M. Muzi-Falconi, C. S. Newlon and M. Foiani (2001). "The DNA replication checkpoint response stabilizes stalled replication forks." Nature 412(6846): 557-561.

Lord, C. J. and A. Ashworth (2012). "The DNA damage response and cancer therapy." Nature 481(7381): 287-294.

Lynch, M. D. (2006). "How does cellular senescence prevent cancer?" DNA Cell Biol 25(2): 69-78.

M'Kacher, R., V. Laithier, A. Valent, F. Delhommeau, D. Violot, E. Deutsch, J. Dossou, N. Beron-Gaillard, T. Girinsky, J. Bourhis, P. Carde, A. Bernheim and C. Parmentier (2003). "Sensitivity to radiation and alkylating agent of peripheral lymphocytes and fibroblasts in a Hoyeraal-Hreidarsson syndrome patient." Pediatr Hematol Oncol 20(8): 651-656.

Ma, Y., U. Pannicke, K. Schwarz and M. R. Lieber (2002). "Hairpin opening and overhang processing by an Artemis/DNA-dependent protein kinase complex in nonhomologous end joining and V(D)J recombination." Cell 108(6): 781-794.

Marrone, A., A. Walne, H. Tamary, Y. Masunari, M. Kirwan, R. Beswick, T. Vulliamy and I. Dokal (2007). "Telomerase reverse-transcriptase homozygous mutations in autosomal recessive dyskeratosis congenita and Hoyeraal-Hreidarsson syndrome." Blood 110(13): 4198-4205.

Martinez-Delgado, B., K. Yanowsky, L. Inglada-Perez, S. Domingo, M. Urioste, A. Osorio and J. Benitez (2011). "Genetic anticipation is associated with telomere shortening in hereditary breast cancer." PLoS Genet 7(7): e1002182.

Maser, R. S. and R. A. DePinho (2004). "Telomeres and the DNA damage response: why the fox is guarding the henhouse." DNA Repair (Amst) 3(8-9): 979-988.

McGlynn, P. and R. G. Lloyd (2002). "Recombinational repair and restart of damaged replication forks." Nat Rev Mol Cell Biol 3(11): 859-870.

McIlrath, J., S. D. Bouffler, E. Samper, A. Cuthbert, A. Wojcik, I. Szumiel, P. E. Bryant, A. C. Riches, A. Thompson, M. A. Blasco, R. F. Newbold and P. Slijepcevic (2001). "Telomere length abnormalities in mammalian radiosensitive cells." Cancer Res 61(3): 912-915.

McPherson, J. P., M. P. Hande, A. Poonepalli, B. Lemmers, E. Zablocki, E. Migon, A. Shehabeldin, A. Porras, J. Karaskova, B. Vukovic, J. Squire and R. Hakem (2006). "A role for Brca1 in chromosome end maintenance." Hum Mol Genet 15(6): 831-838.

McVey, M. and S. E. Lee (2008). "MMEJ repair of double-strand breaks (director's cut): deleted sequences and alternative endings." Trends Genet 24(11): 529-538.

Medvedeva, N. G., I. V. Panyutin, I. G. Panyutin and R. D. Neumann (2007). "Phosphorylation of histone H2AX in radiation-induced micronuclei." Radiat Res 168(4): 493-498.

Metcalfe, J. A., J. Parkhill, L. Campbell, M. Stacey, P. Biggs, P. J. Byrd and A. M. Taylor (1996). "Accelerated telomere shortening in ataxia telangiectasia." Nat Genet 13(3): 350-353.

Mikule, K., B. Delaval, P. Kaldis, A. Jurcyzk, P. Hergert and S. Doxsey (2007). "Loss of centrosome integrity induces p38-p53-p21-dependent G1-S arrest." Nat Cell Biol 9(2): 160-170.

Misri, S., S. Pandita, R. Kumar and T. K. Pandita (2008). "Telomeres, histone code, and DNA damage response." Cytogenet Genome Res 122(3-4): 297-307.

Moriarty, T. J., S. Dupuis and C. Autexier (2002). "Rapid upregulation of telomerase activity in human leukemia HL-60 cells treated with clinical doses of the DNA-damaging drug etoposide." Leukemia 16(6): 1112-1120.

Moynahan, M. E., J. W. Chiu, B. H. Koller and M. Jasin (1999). "Brca1 controls homology-directed DNA repair." Mol Cell 4(4): 511-518.

Nelson, N. D. and A. A. Bertuch (2012). "Dyskeratosis congenita as a disorder of telomere maintenance." Mutat Res 730(1-2): 43-51.

Nojima, K., H. Hochegger, A. Saberi, T. Fukushima, K. Kikuchi, M. Yoshimura, B. J. Orelli, D. K. Bishop, S. Hirano, M. Ohzeki, M. Ishiai, K. Yamamoto, M. Takata, H. Arakawa, J. M. Buerstedde, M. Yamazoe, T. Kawamoto, K. Araki, J. A. Takahashi, N. Hashimoto, S. Takeda and E. Sonoda (2005). "Multiple repair pathways mediate tolerance to chemotherapeutic cross-linking agents in vertebrate cells." Cancer Res 65(24): 11704-11711.

Noordzij, J. G., N. S. Verkaik, M. van der Burg, L. R. van Veelen, S. de Bruin-Versteeg, W. Wiegant, J. M. Vossen, C. M. Weemaes, R. de Groot, M. Z. Zdzienicka, D. C. van Gent and J. J. van Dongen (2003). "Radiosensitive SCID patients with Artemis gene mutations show a complete B-cell differentiation arrest at the pre-B-cell receptor checkpoint in bone marrow." Blood 101(4): 1446-1452.

O'Donovan, P. J. and D. M. Livingston (2010). "BRCA1 and BRCA2: breast/ovarian cancer susceptibility gene products and participants in DNA double-strand break repair." Carcinogenesis 31(6): 961-967.

O'Driscoll, M., A. R. Gennery, J. Seidel, P. Concannon and P. A. Jeggo (2004). "An overview of three new disorders associated with genetic instability: LIG4 syndrome, RS-SCID and ATR-Seckel syndrome." DNA Repair (Amst) 3(8-9): 1227-1235.

O'Driscoll, M. and P. A. Jeggo (2006). "The role of double-strand break repair - insights from human genetics." Nat Rev Genet 7(1): 45-54.

O'Sullivan, J. N., M. P. Bronner, T. A. Brentnall, J. C. Finley, W. T. Shen, S. Emerson, M. J. Emond, K. A. Gollahon, A. H. Moskovitz, D. A. Crispin, J. D. Potter and P. S. Rabinovitch (2002). "Chromosomal instability in ulcerative colitis is related to telomere shortening." Nat Genet 32(2): 280-284.

O'Sullivan, J. N., J. C. Finley, R. A. Risques, W. T. Shen, K. A. Gollahon, A. H. Moskovitz, S. Gryaznov, C. B. Harley and P. S. Rabinovitch (2004). "Telomere length assessment in tissue sections by quantitative FISH: image analysis algorithms." Cytometry A 58(2): 120-131.

Oexle, K. (1998). "Telomere length distribution and Southern blot analysis." J Theor Biol 190(4): 369-377.

Ohta, T., s. Tokishita, K. Mochizuki, J. Kawase, M. Sakahira and H. Yamagata (2006). "UV Sensitivity and Mutagenesis of the Extremely Thermophilic Eubacterium Thermus thermophilus, HB27." Genes and Environment Vol.28: 56–61.

Olovnikov, A. M. (1971). "[Principle of marginotomy in template synthesis of polynucleotides]." Dokl Akad Nauk SSSR 201(6): 1496-1499.

Paull, T. T., D. Cortez, B. Bowers, S. J. Elledge and M. Gellert (2001). "Direct DNA binding by Brca1." Proc Natl Acad Sci U S A 98(11): 6086-6091.

Piatyszek, M. A., N. W. Kim, S. L. Weinrich, K. Hiyama, E. Hiyama, W. E. Wright and J. W. Shay (1995). "Detection of telomerase activity in human cells and tumors

by a telomeric repeat amplification protocol (TRAP)." Methods in Cell Science Vol.17: 1-15,.

Powell, S. N. and L. A. Kachnic (2003). "Roles of BRCA1 and BRCA2 in homologous recombination, DNA replication fidelity and the cellular response to ionizing radiation." Oncogene 22(37): 5784-5791.

Reddel, R. R. (2000). "The role of senescence and immortalization in carcinogenesis." Carcinogenesis 21(3): 477-484.

Roos, W. P. and B. Kaina (2006). "DNA damage-induced cell death by apoptosis." Trends Mol Med 12(9): 440-450.

Roulston, A., R. C. Marcellus and P. E. Branton (1999). "Viruses and apoptosis." Annu Rev Microbiol 53: 577-628.

Rufer, N., W. Dragowska, G. Thornbury, E. Roosnek and P. M. Lansdorp (1998). "Telomere length dynamics in human lymphocyte subpopulations measured by flow cytometry." Nat Biotechnol 16(8): 743-747.

Samper, E., F. A. Goytisolo, P. Slijepcevic, P. P. van Buul and M. A. Blasco (2000). "Mammalian Ku86 protein prevents telomeric fusions independently of the length of TTAGGG repeats and the G-strand overhang." EMBO Rep 1(3): 244-252.

Sapir, E., Y. Gozaly-Chianea, S. Al-Wahiby, S. Ravindran, H. Yasaei and P. Slijepcevic (2011). "Effects of BRCA2 deficiency on telomere recombination in non-ALT and ALT cells." Genome Integr 2: 9.

Satyanarayana, A., R. A. Greenberg, S. Schaetzlein, J. Buer, K. Masutomi, W. C. Hahn, S. Zimmermann, U. Martens, M. P. Manns and K. L. Rudolph (2004). "Mitogen stimulation cooperates with telomere shortening to activate DNA damage responses and senescence signaling." Mol Cell Biol 24(12): 5459-5474.

Savage, S. A., N. Giri, G. M. Baerlocher, N. Orr, P. M. Lansdorp and B. P. Alter (2008). "TINF2, a component of the shelterin telomere protection complex, is mutated in dyskeratosis congenita." Am J Hum Genet 82(2): 501-509.

Sekiguchi, J. M. and D. O. Ferguson (2006). "DNA double-strand break repair: a relentless hunt uncovers new prey." Cell 124(2): 260-262.

Slijepcevic, P. (2001). "Telomere length measurement by Q-FISH." Methods Cell Sci 23(1-3): 17-22.

Slijepcevic, P. (2006). "The role of DNA damage response proteins at telomeres--an "integrative" model." DNA Repair (Amst) 5(11): 1299-1306.

Slijepcevic, P., Y. Xiao, I. Dominguez and A. T. Natarajan (1996). "Spontaneous and radiation-induced chromosomal breakage at interstitial telomeric sites." Chromosoma 104(8): 596-604.

Snouwaert, J. N., L. C. Gowen, A. M. Latour, A. R. Mohn, A. Xiao, L. DiBiase and B. H. Koller (1999). "BRCA1 deficient embryonic stem cells display a decreased homologous recombination frequency and an increased frequency of non-homologous recombination that is corrected by expression of a brca1 transgene." Oncogene 18(55): 7900-7907.

Starita, L. M. and J. D. Parvin (2003). "The multiple nuclear functions of BRCA1: transcription, ubiquitination and DNA repair." Curr Opin Cell Biol 15(3): 345-350.

Struewing, J. P., L. C. Brody, M. R. Erdos, R. G. Kase, T. R. Giambarresi, S. A. Smith, F. S. Collins and M. A. Tucker (1995). "Detection of eight BRCA1 mutations in 10 breast/ovarian cancer families, including 1 family with male breast cancer." Am J Hum Genet 57(1): 1-7.

Svenson, U., K. Nordfjall, D. Baird, L. Roger, P. Osterman, M. L. Hellenius and G. Roos (2011). "Blood cell telomere length is a dynamic feature." PLoS One 6(6): e21485.

T.A.Sciences. (2010-2012). "Telomere Science." Retrieved 17th Sep 2012, from http://www.tasciences.com/introduction-to-telomere-science/.

Takai, H., A. Smogorzewska and T. de Lange (2003). "DNA damage foci at dysfunctional telomeres." Curr Biol 13(17): 1549-1556.

Takata, M., M. S. Sasaki, E. Sonoda, C. Morrison, M. Hashimoto, H. Utsumi, Y. Yamaguchi-Iwai, A. Shinohara and S. Takeda (1998). "Homologous recombination and non-homologous end-joining pathways of DNA double-strand break repair have overlapping roles in the maintenance of chromosomal integrity in vertebrate cells." EMBO J 17(18): 5497-5508.

Thanbichler, M., P. H. Viollier and L. Shapiro (2005). "The structure and function of the bacterial chromosome." Curr Opin Genet Dev 15(2): 153-162.

Tomilin, N. V., L. V. Solovjeva, M. P. Svetlova, N. M. Pleskach, I. A. Zalenskaya, P. M. Yau and E. M. Bradbury (2001). "Visualization of focal nuclear sites of DNA repair synthesis induced by bleomycin in human cells." Radiat Res 156(4): 347-354.

Trenz, K., A. Rothfuss, P. Schutz and G. Speit (2002). "Mutagen sensitivity of peripheral blood from women carrying a BRCA1 or BRCA2 mutation." Mutat Res 500(1-2): 89-96.

van den Bosch, M., R. T. Bree and N. F. Lowndes (2003). "The MRN complex: coordinating and mediating the response to broken chromosomes." EMBO Rep 4(9): 844-849.

van Heek, N. T., A. K. Meeker, S. E. Kern, C. J. Yeo, K. D. Lillemoe, J. L. Cameron, G. J. Offerhaus, J. L. Hicks, R. E. Wilentz, M. G. Goggins, A. M. De Marzo, R. H. Hruban and A. Maitra (2002). "Telomere shortening is nearly universal in pancreatic intraepithelial neoplasia." Am J Pathol 161(5): 1541-1547.

van Overbeek, M. and T. de Lange (2006). "Apollo, an Artemis-related nuclease, interacts with TRF2 and protects human telomeres in S phase." Curr Biol 16(13): 1295-1302.

Van Simaeys, D., D. Lopez-Colon, K. Sefah, R. Sutphen, E. Jimenez and W. Tan (2010). "Study of the molecular recognition of aptamers selected through ovarian cancer cell-SELEX." PLoS One 5(11): e13770.

Venkitaraman, A. R. (2001). "Functions of BRCA1 and BRCA2 in the biological response to DNA damage." J Cell Sci 114(Pt 20): 3591-3598.

Viscardi, V., D. Bonetti, H. Cartagena-Lirola, G. Lucchini and M. P. Longhese (2007). "MRX-dependent DNA damage response to short telomeres." Mol Biol Cell 18(8): 3047-3058.

Volpi, E. V. and J. M. Bridger (2008). "FISH glossary: an overview of the fluorescence in situ hybridization technique." Biotechniques 45(4): 385-386, 388, 390 passim.

Vulliamy, T., R. Beswick, M. Kirwan, A. Marrone, M. Digweed, A. Walne and I. Dokal (2008). "Mutations in the telomerase component NHP2 cause the premature ageing syndrome dyskeratosis congenita." Proc Natl Acad Sci U S A 105(23): 8073-8078.

Vulliamy, T., A. Marrone, F. Goldman, A. Dearlove, M. Bessler, P. J. Mason and I. Dokal (2001). "The RNA component of telomerase is mutated in autosomal dominant dyskeratosis congenita." Nature 413(6854): 432-435.

Vulliamy, T., A. Marrone, R. Szydlo, A. Walne, P. J. Mason and I. Dokal (2004). "Disease anticipation is associated with progressive telomere shortening in families with dyskeratosis congenita due to mutations in TERC." Nat Genet 36(5): 447-449.

Vulliamy, T. J. and I. Dokal (2008). "Dyskeratosis congenita: the diverse clinical presentation of mutations in the telomerase complex." Biochimie 90(1): 122-130.

Vulliamy, T. J., S. W. Knight, P. J. Mason and I. Dokal (2001). "Very short telomeres in the peripheral blood of patients with X-linked and autosomal dyskeratosis congenita." Blood Cells Mol Dis 27(2): 353-357.

Vulliamy, T. J., A. Walne, A. Baskaradas, P. J. Mason, A. Marrone and I. Dokal (2005). "Mutations in the reverse transcriptase component of telomerase (TERT) in patients with bone marrow failure." Blood Cells Mol Dis 34(3): 257-263.

Walne, A. J. and I. Dokal (2004). "Telomerase dysfunction and dyskeratosis congenita." Cytotechnology 45(1-2): 13-22.

Walne, A. J., T. Vulliamy, A. Marrone, R. Beswick, M. Kirwan, Y. Masunari, F. H. Al-Qurashi, M. Aljurf and I. Dokal (2007). "Genetic heterogeneity in autosomal recessive dyskeratosis congenita with one subtype due to mutations in the telomerase-associated protein NOP10." Hum Mol Genet 16(13): 1619-1629.

Wang, B., S. Matsuoka, P. B. Carpenter and S. J. Elledge (2002). "53BP1, a mediator of the DNA damage checkpoint." Science 298(5597): 1435-1438.

Wang, Y., D. Cortez, P. Yazdi, N. Neff, S. J. Elledge and J. Qin (2000). "BASC, a super complex of BRCA1-associated proteins involved in the recognition and repair of aberrant DNA structures." Genes Dev 14(8): 927-939.

Ward, J. F. (1988). "DNA damage produced by ionizing radiation in mammalian cells: identities, mechanisms of formation, and reparability." Prog Nucleic Acid Res Mol Biol 35: 95-125.

Ward, J. F. (2000). "Complexity of damage produced by ionizing radiation." Cold Spring Harb Symp Quant Biol 65: 377-382.

Welcsh, P. L., K. N. Owens and M. C. King (2000). "Insights into the functions of BRCA1 and BRCA2." Trends Genet 16(2): 69-74.

Wong, H. P. and P. Slijepcevic (2004). "Telomere length measurement in mouse chromosomes by a modified Q-FISH method." Cytogenet Genome Res 105(2-4): 464-470.

Wong, J. M. and K. Collins (2006). "Telomerase RNA level limits telomere maintenance in X-linked dyskeratosis congenita." Genes Dev 20(20): 2848-2858.

Wood, R. D. (1997). "Nucleotide excision repair in mammalian cells." J Biol Chem 272(38): 23465-23468.

Wu, G., X. Jiang, W. H. Lee and P. L. Chen (2003). "Assembly of functional ALT-associated promyelocytic leukemia bodies requires Nijmegen Breakage Syndrome 1." Cancer Res 63(10): 2589-2595.

Xiong, J., S. Fan, Q. Meng, L. Schramm, C. Wang, B. Bouzahza, J. Zhou, B. Zafonte, I. D. Goldberg, B. R. Haddad, R. G. Pestell and E. M. Rosen (2003). "BRCA1 inhibition of telomerase activity in cultured cells." Mol Cell Biol 23(23): 8668-8690.

Yasaei, H. and P. Slijepcevic (2010). "Defective Artemis causes mild telomere dysfunction." Genome Integr 1(1): 3.

Ye, Q., Y. F. Hu, H. Zhong, A. C. Nye, A. S. Belmont and R. Li (2001). "BRCA1-induced large-scale chromatin unfolding and allele-specific effects of cancer-predisposing mutations." J Cell Biol 155(6): 911-921.

Yoo, H. Y., S. Y. Jeong and W. G. Dunphy (2006). "Site-specific phosphorylation of a checkpoint mediator protein controls its responses to different DNA structures." Genes Dev 20(7): 772-783.

Yu, V. P., M. Koehler, C. Steinlein, M. Schmid, L. A. Hanakahi, A. J. van Gool, S. C. West and A. R. Venkitaraman (2000). "Gross chromosomal rearrangements and genetic exchange between nonhomologous chromosomes following BRCA2 inactivation." Genes Dev 14(11): 1400-1406.

Yuan, J., R. Adamski and J. Chen (2010). "Focus on histone variant H2AX: to be or not to be." FEBS Lett 584(17): 3717-3724.

Zagorski, Z., B. Biziorek, E. Rakowska and D. Jedrzejewski (2001). "[Zinsser-Engman-Cole syndrome (dyskeratosis congenita) with severe sicca syndrome, panuveitis and corneal perforation--a case report]." Klin Monbl Augenheilkd 218(6): 455-458.

Zhang, J. and S. N. Powell (2005). "The role of the BRCA1 tumor suppressor in DNA double-strand break repair." Mol Cancer Res 3(10): 531-539.

Zhong, F., S. A. Savage, M. Shkreli, N. Giri, L. Jessop, T. Myers, R. Chen, B. P. Alter and S. E. Artandi (2011). "Disruption of telomerase trafficking by TCAB1 mutation causes dyskeratosis congenita." Genes Dev 25(1): 11-16.

Zhong, Q., C. F. Chen, P. L. Chen and W. H. Lee (2002). "BRCA1 facilitates microhomology-mediated end joining of DNA double strand breaks." J Biol Chem 277(32): 28641-28647.

Zhu, Q., G. M. Pao, A. M. Huynh, H. Suh, N. Tonnu, P. M. Nederlof, F. H. Gage and I. M. Verma (2011). "BRCA1 tumour suppression occurs via heterochromatin-mediated silencing." Nature 477(7363): 179-184.

Zhu, X. D., B. Kuster, M. Mann, J. H. Petrini and T. de Lange (2000). "Cell-cycle-regulated association of RAD50/MRE11/NBS1 with TRF2 and human telomeres." Nat Genet 25(3): 347-352.

Zhu, X. D., L. Niedernhofer, B. Kuster, M. Mann, J. H. Hoeijmakers and T. de Lange (2003). "ERCC1/XPF removes the 3' overhang from uncapped telomeres and represses formation of telomeric DNA-containing double minute chromosomes." Mol Cell 12(6): 1489-1498.

Zhu, Y., R. L. Tomlinson, A. A. Lukowiak, R. M. Terns and M. P. Terns (2004). "Telomerase RNA accumulates in Cajal bodies in human cancer cells." Mol Biol Cell 15(1): 81-90.

Zijlmans, J. M., U. M. Martens, S. S. Poon, A. K. Raap, H. J. Tanke, R. K. Ward and P. M. Lansdorp (1997). "Telomeres in the mouse have large inter-chromosomal variations in the number of T2AG3 repeats." Proc Natl Acad Sci U S A 94(14): 7423-7428.

Zimonjic, D., M. W. Brooks, N. Popescu, R. A. Weinberg and W. C. Hahn (2001). "Derivation of human tumor cells in vitro without widespread genomic instability." Cancer Res 61(24): 8838-8844.